2021

Polymer-Based Flexible Antennas and Chipless RFID Tags for General IoT Applications

Muhammad Usman Ali Khan
University of Wollongong

Polymer-Based Flexible Antennas and Chipless RFID Tags for General IoT Applications

Muhammad Usman Ali Khan

Supervisors:
A/Prof. Raad Raad
Prof. Chin, Kwan-Wu

This thesis is presented as part of the requirement for the conferral of the degree:
Doctor of Philosophy

University of Wollongong
School of Electrical, Computer and Telecommunication Engineering

03/2021

Abstract

The demand for flexible and wearable wireless systems is increasing exponentially in today's information-oriented society. Flexible electronic systems are equally beneficial and have wide applications in communication, medicine, military and radio frequency applications. Beginning with a detailed review of flexible materials which have been used during the last few decades, an overview of some abundantly used polymer substrates is provided, which compares their physical, electrical and mechanical properties. The polymers are highly resistant nonconductive materials made up of repeated subunits of hydrocarbons known as monomers. Polymers are widely used for different antennas and Radio Frequency Identifications (RFID) to facilitate bending and flexibility as a substrate such as polyimides (PI), polydimethylsiloxane (PDMS), polytetrafluoroethylene (PTFE), Rogers RT/ Duroid and Liquid Crystal Polymer (LCP). Flexible substrates have become essential to provide increased flexibility in wearable sensors, including polymers, plastic, paper, textiles and fabrics. This study is to comprehensively summarize the bending capabilities of flexible polymer substrate for general Internet of Things (IoT) applications. Various antennas, applicable for the frequency range between 2 GHz to 10 GHz by using different polymer substrates PI, PET, PDMS, PVC, and PTFE have been designed and fabricated with studies on the bending effects on the radiation performance of antenna designs that use the polymer substrates.

The RFID tags, based on polymers substrates, possess very enticing characteristics like high flexibility, crumpling and stretchability, lightweightedness, ease of processability, corrosion and humidity resistance, and most importantly a low cost with easy fabrication. A novel Flexible Bow Tie Chipless RFID tag is introduced on three flexible polymer substrates PET, PTFE Teflon and PVC, and its design, fabrication, testing and comparative analyses are presented in this research. The tag uses the Frequency Selective Surface (FSS) approach with a frequency ranging from 4 to 18 GHz by using CST studio and then fabricated through a laser etching technique on low-cost polymers. The results are obtained in an anechoic chamber by performing a series of comparative experiments for the Radar Cross Section (RCS) of the Bow Tie Chipless RFID tags. The bow tie design was compared to an Octagonal-shaped tag already published. Furthermore, the Singularity Expansion Method (SEM) based circuit modelling, the transient behaviour and the coupling coefficients of the Bow-Tie shaped tag are evaluated. The maximum read range is evaluated and the Bow Tie RFID tag is proved to be more robust and accurate with the variation of distance up to 1.8 m at 0 dBm, which is extendable to 2.14 m for higher input power. The bending capabilities of the tag are noted for radii curvature of 27 mm and 14 mm. The experimental result shows that the new Bow Tie RFID tag is more robust and accurate with the distance variation of up to 12 cm at 0 dBm power and can be used to encode a bit sequence.

The conductive textiles are extensively in use these days because they possess outstanding properties, such as extraordinary mechanical conformability, wearability comfort and brilliant biocompatibility. To corroborate the bending effects on RCS of wearable sensors, two embroidered Octagonal-shaped Chipless RFID tags on cotton fabric for wearable applications are

presented. The first tag is designed using silver-coated polyamide conductive fibre (HC12) and the second tag is embroidered using Vectran (LIBERATOR 40), a highly conductive multifilament yarn spun from LCP, on cotton fabrics. In contrast to the traditional RFID tag, the ID code is not saved in the memory of the chipless RFID tags, instead of using the physical features of the tag to send data. Using CST studio and precisely fabricated with the commercial ZSK Technical Embroidery System JCZA (0109-550), the proposed tag design uses an FSS technique for the frequency range of 8 to 18 GHz. Furthermore, with the experimental results for on-body RCS measurements and the bending effects on both tags down to 7 mm, despite the noticeable shift in resonant frequency and the signal degradation as compared to the reading of a non-bent reference tag, the |RCS| peaks are significantly retrievable. Hence, a successful bending analysis on both designs has proven their reliability in terms of bending for various stages of curvature. This embroidered Octagonal Chipless RFID tag is a fully textile design that is compact and can be deployed commercially in various IoT applications.

Acknowledgements

This research has been supported by the Higher Education Commission (HEC) of Pakistan and the Faculty of Engineering and Information Sciences - UOW.

I would like to express my deep gratitude to my supervisor A/Prof. Raad Raad for accepting me as a PhD student in early 2017. Since then, you have been patiently guiding me through my research on flexible antennas and chipless RFID tags using polymer substrates. Your insight and knowledge in the subject area have navigated me through this research archipelago.

I would like to thank Dr. Javad Foroughi, Senior Research Fellow at the Intelligent Polymer Research Intitute (IPRI), a research department of Australian Institute for Innovative Materials (AIIM) at UOW, from the bottom of my heart for helping me design and fabricate flexible antennas and Chipless RFID tags on various polymers, an atoll in the waters, your help has served me inexplicably well in my investigation and testing of the electrical, mechanical, thermal and physical properties of various polymers used in this research.

I also sincerely thank Dr. Muhammad Ali Qureshi, Associate Professor at The Islamia University of Bahawalpur, Pakistan for your orientating guidance through this research and my warmest thanks extends to all of my research fellows including, Ms. Maryam Haseeb, Dr. Muhammad Salman Raheel, Dr. Faisel Tubbal, Mr Panagiotis Ioannis Theoharis and Ms. Singing Liu for your great support, encouragement and priceless interest during this long journey.

I cannot end my acknowledgements without expressing my heartfelt gratitude to my family, especially my wife, for the support you have shown me throughout this research, I simply could not have done this without you; For my mother, my deepest gratitude I give to you for everything you have done for me throughout my life; and, for my brothers and friends, I thank you for your continuous support and encouragement.

Certification

I, Muhammad Usman Ali Khan, declare that this thesis submitted in fulfilment of the requirements for the conferral of the Doctor of Philosophy, from the University of Wollongong, is wholly my own work unless otherwise referenced or acknowledged. This document has not been submitted for qualifications at any other academic institution.

Muhammad Usman Ali Khan

23rd March, 2021

Abbreviations

a-Si:H/ITO	Hydrogenated Amorphous Silicon Indium Tin Oxide
AMLCD	Active-Matrix Liquid Crystal Display
BAN	Body Area Network
CLTE	Coefficient of Linear Thermal Expansion
CNRFID	Centre National de Reference RFID
CNR	Complex Natural Response
CP	Circularly Polarized
CPW	Coplanar Waveguide
CTE	Co-efficient of Resistance
EFIE	Electric Field Integral Equation
EM wave	ElectroMagnetic wave
EPC	Electronic Protocol Code
FES	Flexible Electronic System
FNBW	Full Null Beamwidth
FPC	Flexible Printed Circuits
FS	Frequency Shifts
FSS	Frequency Selective Surface
HPBW	Half Power Beamwidth
HS	Highest Shift
IC	Integrated Circuits
IDT	Interdigital Transducer
IGZO	Indium Gallium Zinc Oxide
IoT	Internet of Things
IPRI	Intelligent Polymer Research Institute
ISM	Industrial, Scientific and Medical
ISO	International Standard Organization
LCP	Liquid Crystal Polymer
LS	Lowest Shift
MFIE	Magnetic Field Integral Equation
MMW	Millimeter-Wave
MoM	Method of Moment
MRI	Microwave Radar Imaging
OP	Orthogonal Polarization
OLED	Organic Light-Emitting Diode
PANI	Polyaniline
PCB	Printed Circuit Board
PI	Polyimide

PEC	Perfectly Electric Conductor
PECVD	Plasma Enhanced Chemical Vapor Deposition
PET	Polyethylene Terephthalate
PDMS	Polydimethylsiloxane
PLF	Polarization Loss Factor
Poly-Si	Polycrystalline silicon
PP	Principal Polarization
PPM	Pulse Position Modulation
PTFE	Polytetrafluoroethylene
PCS	Personal Communication Systems
PVC	Polyvinylchloride
Q	Quality Factor
R	Radius
RCS	Radar Cross Section
REPs	Radiofrequency Encoded Particle
RFID	Radio Frequency Identification
SAW	Surface Acoustic Wave
SEM	Singularity Expansion Method
SIW	Substrate Integrated Waveguide
TCI	Transducer Connector Interface
TFT	Thin Film Transistor
TL	Transmission Line
UOW	University of Wollongong
ULS	Universal Laser Systems
UV	Ultraviolet
UWB	Ultra-Wide Band
VNA	Keysight Vector Network Analyzer
VR	Virtual Reality
VSWR	Voltage Standing Wave Ratio
WBAN	Wireless Body Area Network
WOLED	White OLED

List of Publications

Related to this Research (2017-2021)

I M. U. A. Khan, R. Raad, J. Foroughi, F. E. Tubbal, and J. Xi, "Novel Bow-Tie Chip-less RFID Tag for Wearable Applications," in *2019 19th International Symposium on Communications and Information Technologies (ISCIT)*, 2019: IEEE, pp. 10-13 [1].

II M. U. A. Khan, R. Raad, J. Foroughi, F. Tubbal, P. I. Theoharis, and M. S. Raheel, "Effects of Bending Bow-Tie Chipless RFID Tag for Different Polymer Substrates," in *2019 13th International Conference on Signal Processing and Communication Systems (ICSPCS)*, 2019: IEEE, pp. 1-4 [2].

III Muhammad Usman Ali Khan, Raad Raad, Javad Foroughi, "Transient Response & Electromagnetic Behaviour of Flexible Bow-Tie Shaped Chip-less RFID Tag for General IoT Applications," *Advances in Science, Technology and Engineering Systems Journal* 2020 [3].

IV Muhammad Usman Ali Khan, Raad Raad, Javad Foroughi, Panagiotis Ioannis Theoharis, Sining Liu, Jawad Masud, "A Silver-Coated Conductive Fibre HC12 Sewed Chipless RFID Tag on Cotton Fabric for Wearable Applications," *23rd IEEE International Multi Topic Conference 2020 (INMIC 2020),* 2020 [4].

V Muhammad Usman Ali Khan, Raad Raad, Javad Foroughi, "A Fibre Embroidered Chipless RFID Tag on Cotton Fabrics for Wearable Applications," *IEEE Global Communications Conference (GLOBECOM) SAC - Internet of Things & Smart Connected Communities,* 2020 [5].

VI Muhammad Usman Ali Khan, Raad Raad, Javad Foroughi, Muhammad Salman Raheel, Shadi Houshyar, "An Octagonal-Shaped Conductive HC12 & LIBERATOR-40 Thread Embroidered Chipless RFID for General IoT Applications," *ELSEVIER: Sensors & Actuators: A. Physical,* 2021 [6].

VII Muhammad Usman Ali Khan, Raad Raad, Javad Foroughi, Faisel Tubbal, Panagiotis Ioannis Theoharis, Sining Liu, "A Review: Flexible Antennas on Flexible Polymer Substrates and Bending Capabilities on Radiation Characteristics for Various Range of Frequencies," *MDPI Polymers,* 2021 [7].

Not Related to this Research (2017-2021)

VIII F. Tubbal, R. Raad, P. I. Theoharis, S. Iranmanesh, S. Abulgase, and M. U. A. Khan, "Dual Band Slot Antenna with F-Shaped Slits for C-band and X-band Applications," in *2019 13th International Conference on Signal Processing and Communication Systems (ICSPCS)*, 2019: IEEE, pp. 1-4 [8].

IX L. Sining, R. Raad, P. I. Theoharis, F. Tubbal, M. U. A. Khan, and F. H. Malik, "A Dual Band Loop Antenna with Metal Frame for CubeSat Communication," *23rd IEEE International Multi Topic Conference 2020 (INMIC 2020),* 2020 [9].

X P. I. Theoharis, R. Raad, F. Tubbal, M. U. A. Khan, and S. Liu, "Software Defined Radios for CubeSat Applications: A Brief Review and Methodology," *IEEE Journal on Miniaturization for Air and Space Systems,* pp 10-16, 2020 [10].

XI S. Abulgasem, F. Tubbal, R. Raad, P. I. Theoharis, S. Liu, and M. U. Ali Khan, "A Wideband Metal-Only Patch Antenna for CubeSat," *Electronics,* vol. 10, no. 1, p. 50, 2021 [11].

Table of Contents

List of Tables

List of Figures

Chapter 1: **Introduction**

1.1 Introduction and Motivation

Over the last few decades, the Flexible Electronic System (FES) known as flex circuits, have been growing rapidly in industries and organisations such as medical healthcare, energy and power, aerospace, industrial automation, military and defence, sports and entertainment where, now, the array of various devices are generally comprised of organic substances as a substrate. These substrates create flexible devices which are not only usually characterized by their flexibility, but also their lightweightedness, durability and energy efficiency and are, resultantly, becoming recognized for their huge relevance to healthcare and medical products as well as for defence and wearable electronics. According to a market survey by Research Nester, published in 'Global Flexible Electronic Market Overview', the flexible electronic market annual growth rate is anticipated to expand 19.7% over the period 2017-2024 [12] and is estimated to reach over 30 billion USD in 2028 [13]. For certain electronic and communication applications, the flexibility of different materials is of great importance with extensive use demonstrated in flexible displays, smart tags, wearable products and flexible antennas [14, 15]. Accordingly, researchers have incorporated a variety of materials for providing improved flexibility in electronic systems, including the application of polymers, plastics, paper, textiles and fabrics as substrates of these systems. Each of these materials has its own characteristics in terms of how efficiently it can be safely bent, twisted and/or crumpled [16]. The bendability and flexibility of these materials make them ideal for use in future FES development, including application in the Internet of Things (IoT). IoT is the pervasive presence of various objects around us, such as sensors, actuators, smartphones, smart computers, RFID tags, and smartwatches, which can communicate with each other. Given the recent focus on IoT and wearable flexible sensors, there is a new impetus for research into flexible electronics which can be bent or twisted so that they can be worn and mounted on various objects [17].

Over the last few decades, FES has become crucial for the progressive development in wearable devices which generally include flexible antennas, smart tags and sensors. The FES system covers various fields which depends on its specific applications, such as the development of Printed Circuit Boards (PCB), flexible displays, energy storage and generation, and devices applicable for Wireless Body Area Networks (WBAN), see Figure 1. The flexible PCBs, displays and energy storage devices are used extensively in healthcare, entertainment, business, military and space applications.

WBAN provides communications between body-worn devices and devices in the surroundings. These wearable devices include smart tags, such as Radio Frequency Identification (RFID) tags and flexible wearable antennas. The emergence of WBAN is evolving to combine FES and body-worn devices that can easily be mounted on the human body to allow humans to wear antennas and smart tags instead of carrying them. Research on the development of flexible wearable devices

such as antennas and smart tags on a flexible substrate is, therefore, a fascinating area in need of further investigation.

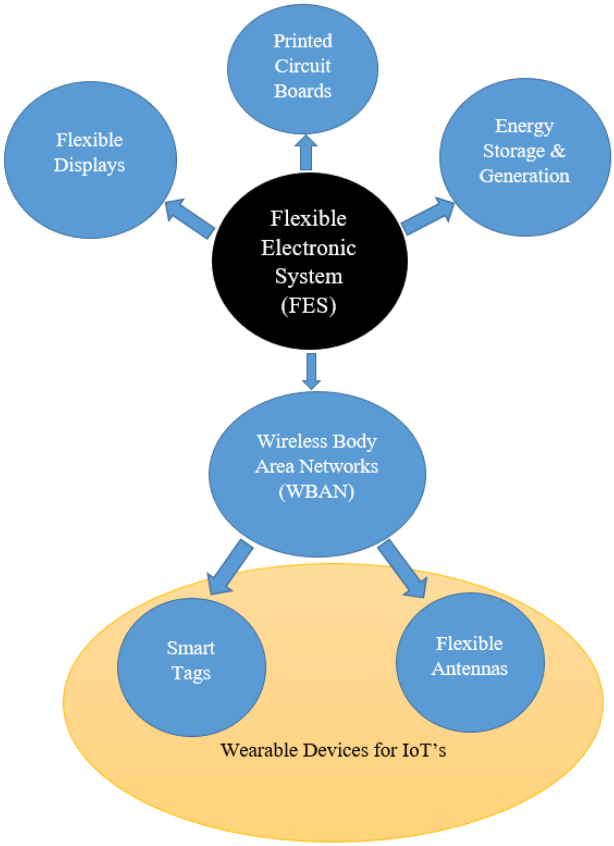

Figure 1. The Next Generation Flexible Electronic System (FES)

Presently, with the exponential development of these wearable sensors and devices, and the high demand of the flexible communication systems, various new challenges have arisen because of the unconventional performance requirements. The typical example, and the relevance to this thesis, includes wearable electronics with flexible antennas [18] and wearable RFID systems which incorporate a reader and an antenna integrated with a tag and body [19], so it is very important for the integrated RFID tag and the flexible antennas to be lightweight, small, durable, moisture and heat resistant, and most importantly highly flexible without distorting radiation characteristics. For this reason, this investigation focuses on the flexibility and seamless integrity of the antennas and the chipless RFID tags for wearable/IoT applications. Passive RFID tags, which have eliminated the requirement of any additional circuitry, are known as chipless RFID tags.

To achieve the aforementioned characteristics for flexible antennas and RFID tags, conventional conductors and substrate materials, such as metals and ceramics, are essentially inappropriate. This is because these materials are usually rigid, costly, and lack flexibility and mechanical resilience. A lot of research has already explored numerous materials which exhibit suitable properties as a substrate for conductive materials for antennas and RFID tags including conductive polymers [20-26], conductive threads [27-29] and conductive textiles [30-44]. For dielectric materials,

Polyimide (PI) [16, 21, 45-53], Polyethylene Terephthalate (PET) [1, 54-60], Polydimethylsiloxane (PDMS) [61-69], Polytetrafluoroethylene (PTFE) [2, 70-73], and Liquid Crystal polymers (LCP) [74-83] have been explored. The detailed review of these conductive and polymer-based substrate materials is presented in Chapter 2. As a substrate, these flexible dielectric material provide flexibility in the development of flexible wearable devices such as flexible antennas and smart tags which comprises of six stages as outlined in Figure 2.

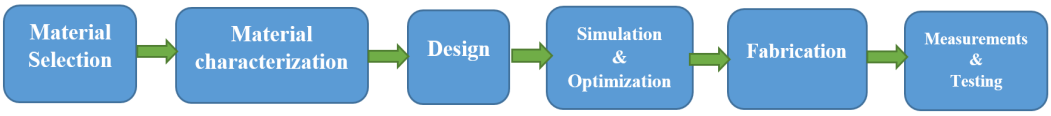

Figure 2. General Steps to Design Wearable Flexible Devices (Antennas & Smarts Tags)

Design development starts with the exploration of appropriate material for the conductive and dielectric part of the wearable devices. In the first step, the mechanical, electrical, thermal and chemical properties of the material are explored, as discussed in detail in section 2.4. The next step is the material characterization, in which material properties are tested or modified according to the requirements. The following step is to decide on the particular geometrical shape and mathematical design of the device, such as rectangular, circular, triangular or octagonal shapes. During this stage, the shape of the conducting plane, ground plane and the substrate will be determined. The process of designing a specific shape of the wearable device depends on the anticipated application and correlates to its frequency requirement. Mathematical modelling and the evaluation of the dimensional variables using parametric analysis form part of this process. After a suitable design implementation, the design moves on to be optimized and simulated using a 3D solver or simulator. Once appropriate simulation results are obtained, the device moves into the fifth stage of production, whether by printing or another appropriate fabrication technique. In the final stage, the radiation parameters, such as return loss, radiation pattern, gain, efficiency and Radar Cross Section (RCS), are measured in the anechoic chamber. Furthermore, performance tests to analyse aspects such as bending effects, durability, humidity and Specific Absorption Rate (SAR) can be conducted depending on the individual requirements and applications.

Nevertheless, for an appropriate design of the wearable flexible device, there are various additional challenges which must be met, such as being lightweight, low cost, bendable, durable, washable, thermally stable and integrable with the human body, as well as having low power consumption, in order to amalgamate the elements into a satisfactory combination. For instance, as all flexible non-conventional conductive materials and dielectrics possess different physical, chemical and mechanical properties, it is extremely critical that the etching and printing techniques in the fabrication process, achieve a high performance, for example, in the radiation efficiency and impedance matching of the flexible devices. For, the flexible dielectric materials like paper, textiles and polymers, while they are all commonly used in wearable applications, the polymer possesses various significant characteristics over its paper and conventional textiles counterparts, including its water and moisture resistance, low cost and power consumption and comparatively easy fabrication process. Additionally, yet another challenge is created from the distortion and

interruption in the radiation characteristics of flexible antennas and smart tags due to both their flexibility and their bendability. Consequently, investigation on these aspects is also in demand for flexible antennas and RFID designs based on a polymer substrate with a high level of flexibility and integrability with IoT.

With these considerations, this dissertation predominantly focuses on polymer-based wearable devices and investigates the bending impacts on radiation characteristics of wearable antennas and RFID tags by developing various designs of flexible antennas and smart tags on different flexible polymer substrates such as PET, PTFE Teflon, and Polyvinyl Chloride (PVC). In addition, chipless RFID smart tags, comprised of polymer-based conductive fibres on cotton, are investigated and their bending capabilities at a variety of levels of curvature are also analysed.

1.2 Objectives of the Thesis

There are three main objectives for this present study.

1.2.1 Investigation and Selection of Appropriate Flexible Polymer Substrate Material for Wearable Devices (Antennas and Smart Tags).

Since flexible dielectric substrates can be more mechanically robust and economical, can consume lower power and most importantly produce less distortion while undergoing certain levels of bending compared to conventional rigid dielectric substrates, one of the aims of this study is to investigate existing flexible polymer-substrate wearable devices such as flexible antennas and smart tags. Moreover, this study will provide a roadmap for future research for selecting an appropriate polymer substrate based on its mechanical, electrical and thermal properties for wearable applications. Also, the impact on the radiation characteristics, such as return loss and RCS of polymer-based substrate antennas and RFID tags, is studied for various frequency ranges.

1.2.2 Design, Fabrication and Testing of Polymer-based Substrate Wearable Devices (Antennas and Smart Tags) for High Range Frequencies (Up to 18 GHz)

According to various investigation and analytical studies on flexible polymer substrates, various wearable devices are fabricated on polymer substrates, such as PI, PET, PDMS, PTFE, LCP and polymers coated conductive fibres. The motivation for further investigations on these polymer materials stems from their significant properties under flex conditions with more than 90% of the literature on FES being focused on polymer-based applications and using these polymer substrates for wearable applications. Furthermore, Polymers as substrates for antennas and RFID tags can be more mechanically resilient, economical and environmentally friendly as compared to other non-conductive substrate materials. Additionally, flexible wearable devices taking advantage of mechanical flexibility are very limited in this literature, especially for the higher range of

frequencies above 4 GHz. In this context, one of the aims of this study is to design, fabricate and test flexible polymer-based antennas and chipless RFID tags for various frequency ranges and obtain radiation characteristics, such as return loss, radiation patterns, and RCS measurements. For wearable smart tags, the detection of the information or codes from a suitable distance, on-body efficient performance and the coupling coefficients between the resonators are very important for it to be suitable for IoT applications. In this context, one of the objectives is to perform mathematical modelling to evaluate coupling coefficients and to enhance the maximum read range for polymer-based chipless RFID tags. For this aim, a chipless RFID tag, based on FSS techniques, using a novel geometrical shape for the range of 4-18 GHz frequencies on a polymer substrate is proposed. Additionally, a polymer-coated conductive textile-based chipless RFID tag is proposed on cotton fabric for wearable applications.

1.2.3 The Impact of Bending on Radiation Characteristics of Polymer-based Substrate Wearable Devices (Antennas and Smart Tags)

The third and major aim of this study is to investigate the capability of wearable devices to flex and function properly under bending conditions. Where deformation of wearable devices implicates a significant change in radiation characteristics, such as the return loss of antennas, RCS of the smart tags and sensors, which result in a shift in the resonant frequency, the degradation of the signals is sometimes too high to receive appropriately at the receiving ends. In the case of flexible polymer-based antennas, the return loss is severely impacted when antennas undergo a certain level of bending. The level of degradation and distortion varies with various polymer substrates as it depends on the individual properties of the polymer substrate materials. Moreover, the impact of curvature is entirely diverse and changes with the operational frequency of the devices. Therefore, this study aims to categorise the flexible polymer-based antennas into various groups based on their operational frequencies, so that the impact of the change in return losses by the implication of certain bending can be observed. Similarly, the performance of the smart chipless RFID tags mainly depends on the successful reception of code words at the receiver in terms of RCS. The deformation of these tags reduces radiation efficiency and decreases signal strength at the receiver. Hence, the performance of the polymer-based chipless RFID tags is analysed under bent conditions and also on-body conditions. Testing is performed in an anechoic chamber to attain efficient results and to analyse the suitability of the devices for general wearable IoT applications.

1.3 Thesis Structure

This thesis is organized into six different chapters, the structure of which is illustrated in Figure 3. Chapter 1 provides an insight into the thesis outlines and introduction, the background of flexible electronics, motivation and challenges, flexible materials for wearable devices and their selection according to property suitability, and bending impacts on the radiation characteristics of wearable devices such as antennas and RFID tags. Flexible polymer-based antennas have been discussed in

Chapter 2 with a detailed history of flexible electronics. The basics of flexible wearable antennas for IoT applications, transmission line model, flexibility and bending capabilities and fabrication techniques for flexible antennas are also discussed. Furthermore, Chapter 2 gives a detailed introduction of the polymer-based flexible antennas, a comparative analysis of suitable polymer substrates for flexible antennas and RFID tags based on the physical, electrical and thermal properties of polymers, as well as deformational and bending impacts on radiation characteristics of antennas, such as their resonant frequency and reflection coefficients.

Figure 3. Thesis Structure and Chapter Distribution

Chapter 3 describes the design fabrication and testing of flexible polymer-based antennas for various ranges of frequencies and the bending impacts on the radiation characteristics of the flexible antennas. Flexible chipless RFID technology is analysed in Chapter 4 with a novel Bow Tie-shaped chipless RFID tag on PET substrate presented and compared with an Octagonal shaped chipless RFID tag on the same substrate. Bending analysis is performed on the Bow Tie tag for various bending levels inside the chamber. A fully textile, polymer-coated conductive thread-based chipless RFID tag embroidered over a cotton fabric is presented in Chapter 5 and tested for various bending cases. In this chapter, two octagonal-shaped chipless RFID tags are designed and embroidered on cotton. Bending analysis and the on-body RCS measurements are performed in the chamber and their electromagnetic behaviour, coupling coefficients and maximum read range

estimations are presented. Finally, the conclusion, original contribution and future work related to this study are described in Chapter 6.

1.4 Background

With the development of information and communication technology, flexible wearable devices have attracted significant attention due to their immense potential in the revolution of modern society. These flexible devices require seamless integration with the human and information network, self-configuring capabilities, and physical flexibility to withstand various flex conditions. This will lead towards a contribution to the IoT.

1.4.1 Internet of Things (IoT)

IoT is the pervasive presence of various objects around us such as sensors, actuators, smartphones, smart computers, flexible antennas, RFID tags, and smartwatches, which can communicate with each other. Given the recent focus on IoT and wearable flexible sensors, there is a new impetus for research into flexible electronics which can be bent or twisted so that they can be worn and mounted on various objects [17]. Flexible materials for some of these IoT applications require a high level of integrity of components and mechanical robustness with repeated rolling and bending capabilities, in particular, flexible smart fitness watches, RFID tags and wearable sensors are good examples of applications that use this flexible material. Besides this, the elasticity and stretch-ability of materials are key properties required by electronic devices that require large and reversible deformation. These bendable devices also need to be versatile and may require an ability to store energy, operate with low power, and integrate with other devices and IoT applications [84-86], see Figure 4.

While most IoT projects have focused on long-range connectivity and low power usage, there has been some significant work, mainly in sensing, for short-range and extremely low power applications. Example short-range sensing on flexible material applications in IoT include:

- Applications [87] that require continuous location updates are an integral part of IoT as this provides the basis to monitor the object in the IoT system. Indeed, wearable trackers are already used for tracking all manner of things, including human beings or animals [84, 88].
- RFID technology [87, 89], a unique identification system, is a prerequisite for deploying a smart device for sensing purpose.
- Energy harvesting technology [90, 91] is a technology that captures usable energy from the environment to power smart devices. The energy can be harnessed by the variation of temperature, radio signals and the speed of the wind and stored in the form of capacitors.
- Sensors [92, 93] are preliminary elements for IoT. Variables that can be sensed include body temperature, blood pressure and heartbeat monitoring [85, 94, 95]. Flexible IoT sensors have been proposed as a way of monitoring the healing of scars [96, 97], body tumour detection [98, 99], analysing metabolites in the body [100], wearable flexible signalling systems for

astronauts [101], and flexible gait tracking sensors and non-contact vital sensors [102].

An actuator [86, 91] is also an important element of IoT as it provides power to support movements in a system, such as controlling currents or the pressure of the liquid in the air. A piezoelectric actuator, which exhibits an electrical signal on the application of certain pressure onto it, is a typical example of this.

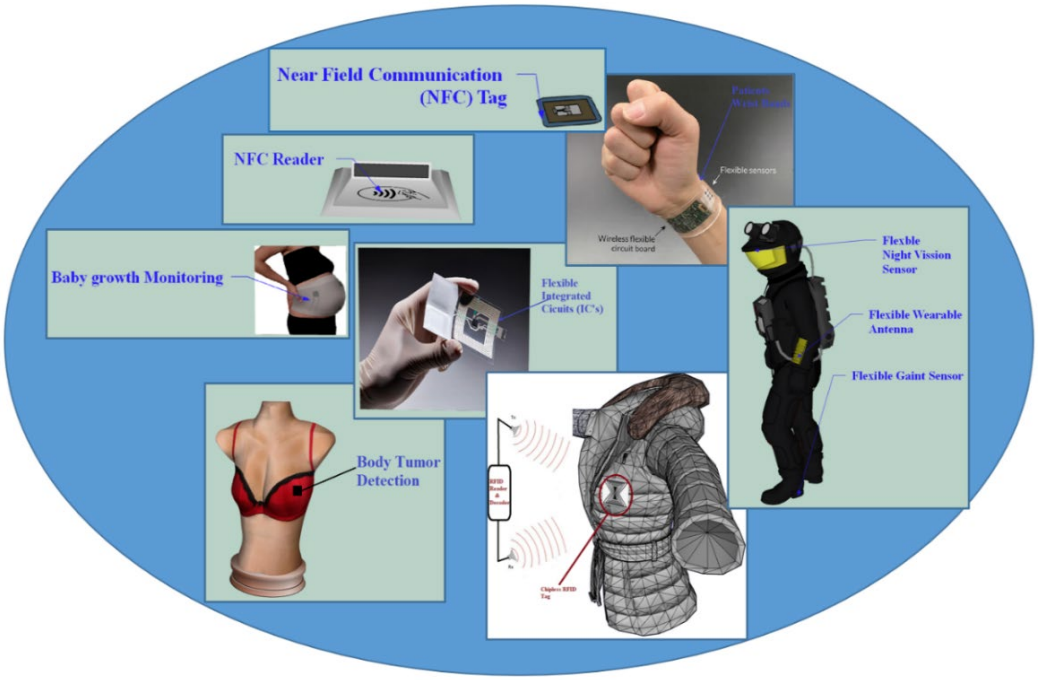

Figure 4. Flexible Internet of Things (IoT)

The interaction between objects through flexible IoT is illustrated in Figure 4. Although, IoT aim to connect everything to everything, the interface to this communication, the wearable sensor, needs to be as flexible and as easy to use as possible. While the basic structure is the same for the flexible antenna and the chipless RFID tags, both structure and the radiation parameters are discussed in this section.

1.4.2 Basics of the Flexible Antennas

Virtually all current mobile electronic devices communicate using passive antennas made up of a variety of materials. While rigid materials were conventionally used for antennas, flexible antennas, which can be designed as lightweight with a small thickness and a low profile [103], are gaining wider acceptance because of the many advantages they have over the traditional rigid antennas. Firstly, there is a significant 50-70% reduction in the size and weight of the flexible antennas compared to traditional antennas and this size can be further reduced, up to about 90% of its original size, for a specific frequency when the flexible substrate (e.g., polymer) is replaced by hard printed boards [104]. Secondly, flexible antennas are very robust yet lightweight and can withstand high mechanical strains [105-107]. The following sections form a tutorial on the flexible

antenna structure, basic parameters, bending capabilities and common flexible materials used for flexible electronics.

1.4.2.1 Basic Structure

Flexible antennas consist of a conductive layer and dielectric material backing. As shown in Figure 5, the basic flexible microstrip patch antenna is a layer of thin conductive strip placed on the top of a flexible substrate. This conductive patch must maintain adequate conductivity even when it is stretched or deformed [105].

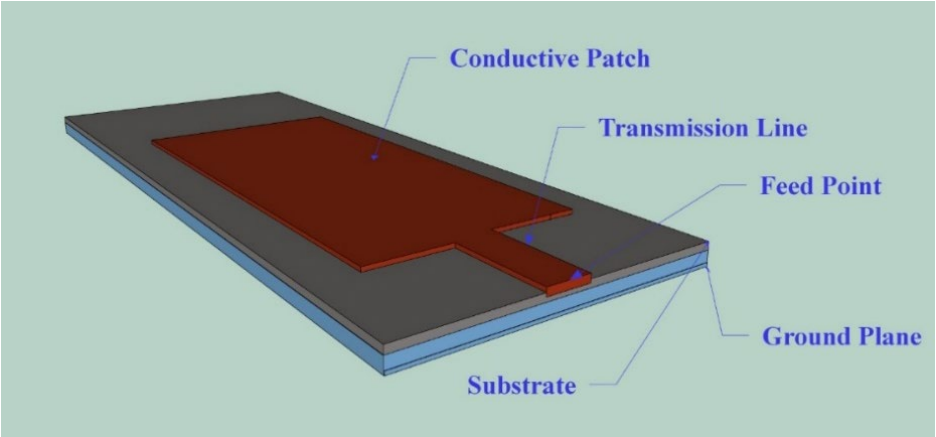

Figure 5. Microstrip Patch Antenna on Flexible Substrate

The property requirements of flexible antennas depend on their applications, required bendability and operating frequency. The different types of flexible materials which can be used as flexible substrates are analysed and compared later in this chapter.

1.4.2.2 Materials for Flexible Antennas

The essential structure of a flexible antenna is the same as a conventional antenna in that it has two major parts: a conductor and a dielectric. A conductive material is used as the radiating element or ground plane while a dielectric material acts as the substrate that supports the radiating element [101]. The general materials that can be used for the conductive layer, or *conductive patch* as illustrated with the basic parts of the flexible or wearable antenna in Figure 6, include pure metals, metals mixed with fabrics and conductive inks where copper, aluminium, silver are examples of intrinsic metals and conductive polyester is a metal mixed fabric. Silver nanoparticles are an example of a conductive ink that allows an antenna to be printed on a substrate. Polymers, paper, foam, plastics, textile fabrics and soft PCB are popular dielectric materials. Figure 6, shows a breakdown of the different material types and the following subsections detail the conductive and substrate materials used for flexible antennas.

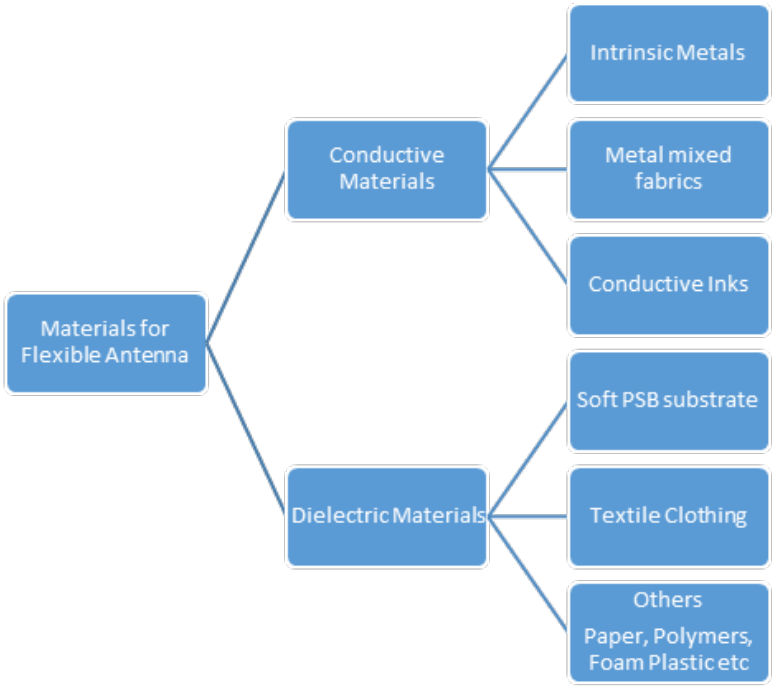

Figure 6. Materials for Flexible Antennas

1.4.2.2.1 Conductive Materials

Conductive materials are capable of transmitting electricity with little loss, or radiating energy, in the form of ElectroMagnetic (EM) waves. These materials must be endowed with bending properties or, more specifically, should have the capability of bending, crumpling and stretching without affecting the antenna performance when used in applications that require the flexing of the antenna from its nominal straight configuration, and should be resistant to material degradation. Moreover, the conductive material must be able to withstand repeated pressure, while low resistivity and high conductivity maintain high importance in the electrical properties of these conductors. Table 1 depicts some important conductive material properties required for flexible electronic systems in general and more specifically for flexible wearable devices, such as flexible antennas and RFID tags, where it is clear that conductive materials need a high level of conductivity, deformability and elasticity, as well as a high capacity for bending, adhesion and integration with textiles. They should simultaneously have a low level of resistivity, moisture and moisture absorption, see Table 1 for general requirements of conductors for flexible devices.

The materials used as the conductive or radiating part of an antenna can be categorized into three parts: i) pure or intrinsic metals; ii) metal mixed fabrics; and iii) conductive inks. Intrinsic metals [14, 78, 108-111], aluminium [73] and silver paste [112] have all been used extensively in flexible antenna fabrication. These materials are highly conductive, cost-effective and provide little complexity in the fabrication process. In wearable electronics, a metal-plated textile is commonly known as an E-Textile. These conductive fibres, or E-Textiles, are widely used as conductive materials where ductile materials such as Kevlar, nylon and Vectran are famous materials that can be coated with metals to form E-Fabrics with the benefit of being highly bendable and easy to sew [34, 113, 114]. The third category, the conductive inks, contain metallic particles such as carbon

and silver nanoparticles which can be printed on a flex substrate with a standard printing process, demonstrating that conductive inks are easy to fabricate and highly conductive. However, their limitations arise in high fabrication costs [16, 47, 74, 115].

Table 1. General Requirements of Conductive Materials for Flexible Devices

Properties	Level
Resistivity	Low
Conductivity	High
Deformability	High
Bending/Crumpling	High
Adhesion	High
Moisture absorption	Low
Elasticity	High
Environmental Degradation	Low
Integration with textiles	High
Fabrication complexity	Low

1.4.2.2.2 **Substrate Materials**

The conductive layer of an antenna is fabricated on a substrate which determines the flexibility of the antenna. Where flexible substrates are more likely to bend and less tolerant of temperature variation, this equivalates to being less dimensionally stable as compared to non-flexible substrates and it is the dimensional stability of the substrate which affects the tenacity and fabrication of the conductive layer. While there are further challenges, including deformability, high thermal and electrical stability, moisture sustainability, lightweightedness and fabrication complexity which needs to be addressed while selecting a substrate for a flexible antenna, the selection of the substrate properties typically depends on its target application. Table 2 illustrates the general properties of substrate materials required by flexible devices.

In addressing high radiation performance with respect to a high level of flexibility, it is the mechanical, electrical and thermal properties of substrate materials that are very important. While in general, flexible substrates in flexible electronic systems and flexible antennas are characterized by their energy efficiency, lightweightedness, reduced fabrication complexities, mechanical robustness and low manufacturing costs, the cost of the antenna may increase in chasing radiation perfection. Although it is the flexibility of a substrate that dictates the bendability of an antenna, antenna deformation not only affects radiation patterns but also its resonant frequency, matching level, bandwidth, directivity, radiation energy and efficiency [16, 74, 109]. For flexible substrates to form an excellent alternative to current traditional rigid substrates, not only compactness but desirable radiation characteristics are also required for high radiation efficiency to be achieved [52, 115, 116].

Table 2. General Requirements of Substrate Materials for Flexible Devices

Mechanical Properties	Elastic Modulus		Stiffness		Deformability	
	High		Low		High	
Electrical Properties	Electrical Insulation		Dissipation Factor		Electrical Stability	
	High		High		High	
Thermal Properties	Coefficient of Linear Thermal Expansion (CLTE)		Moisture Absorption		Thermal Stability	
	Low		Low		High	
Other Properties	Chemical Inertness	Weight	Fabrication Complexity	Surface Roughness	Opaqueness	Cost
	High	Low	Low	Depends on application	Depends on application	Low

1.4.3 Basic Parameters and Radiation Characteristics of Flexible Devices

Generally used to transmit and receive radio energy, an antenna is an essential component in communication systems [117] as it is the part of the communication system which is used to send and receive information [118], even efficiency and performance paradigms tend to be analysed by the parameters of the antenna. This section covers basic radian characteristics and parameters governed by a simple antenna [117, 119], where specific mathematical terminology has been assigned to different patterns and characteristics.

The antenna radiation spatial property is defined by a mathematical expression *Radiation Pattern*. This term can be subdivided into two more specific descriptive expressions as an *amplitude radiation pattern* and a *power radiation pattern*. When the electromagnetic field is obtained at a point with a constant radius, it is known as an *amplitude field pattern* and the spatial variation of power density at a particular point is called a *radiation power pattern*. Normalization is a method which limits the patterns on certain fixed values where both amplitude and power patterns are normalised to their maximum values and are usually called *normalised amplitude patterns* and *power radiation patterns,* respectively. Radiation patterns have certain tubulised portions known as *lobes*. The portion of the radiation pattern in the direction of maximum radiation is called a *major lobe* while the other portions bounded by weak radiations are called *minor lobes*. *Side lobes* are the kind of minor lobes which are not positioned in the intended direction while the minor lobe which is approximately 180° to the major lobe is called a *back lobe*, see Figure 7.

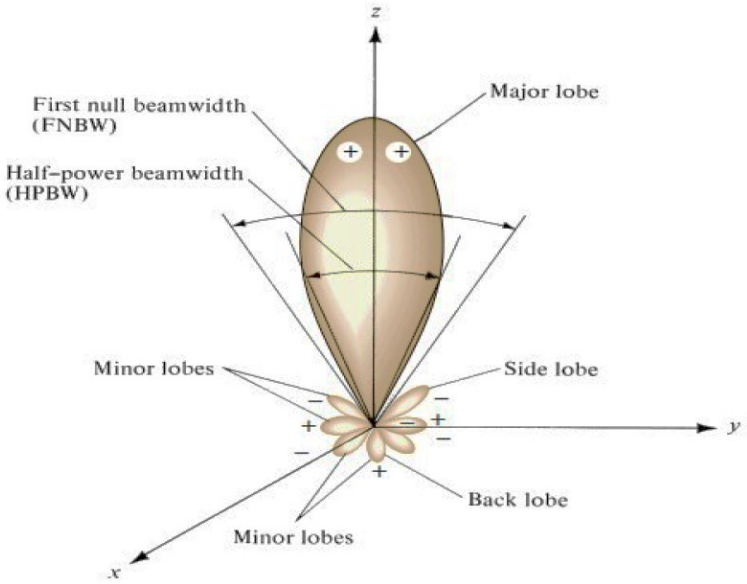

Figure 7. Radiation Pattern of Antenna [119]

Concerning antennas, an ideal antenna, which is radiated equally in all directions, carries the name of an *isotropic* antenna and the hypothetical pattern is called an *isotropic radiation pattern*. A *Directional antenna* radiates in one direction more efficiently than any other direction. There is another type of radiation pattern where an antenna, called an *Omni-directional antenna,* radiates directionally in one plane and remains constant in another plane, which is known as an *Omni-direction radiation pattern*.

An antenna is a source of electromagnetic radiation where this source is surrounded by areas that are divided into three regions: The *Reactive near-field region,* which immediately surrounds the radiating source where the reactive field predominates; The *Radiating near-field or Fresnel region,* which is the area between the reactive near-field and the far-field where the radiation intensity depends on the source or antenna; and the *Far-field region or Fraunhofer region*, the radiation field where the field distribution is independent of its distance from the source. For descriptive qualities to the shape of the radiation, 2D and 3D angles become relevant where the plane angle, having a vertex at the centre of a circle, is measured by *radian* and the solid angle, having its vertex at the centre of a sphere, and is called a *Ste-radian*. With regard to mathematical equations, the power radiation in a specific direction is described in terms of a *Poynting Vector W*, which is the product of Electric field intensity *E* and Magnetic field intensity *H*, where *W* is measured in W/m^2, i.e.,

$$W = E \times H. \tag{1}$$

Radiation intensity *U* is the power radiated from an antenna per unit in the solid angle, which can be evaluated from

$$U = r^2 W_{rad} \tag{2}$$

where W_{rad} is the radiation energy which is radiated from the antenna and r is the radius of the solid angle.

The intrinsic property of an antenna in relation to the angle of its radiation pattern is called its *beamwidth* and is the rangy separation between two similar but opposite points on a major lobe. The *Half Power Beamwidth (HPBW)* is a vital parameter in this regard as it refers to the angle on the plane containing the maximum radiation where the radiation intensity becomes one half of the total beam. The region where the field strength of the signal from the antenna is minimum, or the direction in a radiation pattern of an antenna where there are almost no radiations, is called *Null*. The angle of separation between the first two nulls is called *Full Null Beamwidth (FNBW)*, see Figure 7. Beamwidth and side lobes have an inverse relation where, when the beamwidth decreases, the side lobes increases. One of the supreme parameters of an antenna is its *Directivity*, which is defined by the ratio of the radiation field intensity in a particular direction to the average radiation intensity in the overall direction. The directivity *D* can be calculated using the expression

$$D = \frac{U}{U_0} = \frac{4\pi U}{P_{rad}} \tag{3}$$

where *U* is the radiation intensity and U_0 is the radiation intensity of an isotropic source. The directivity of an isotropic source can be defined as 'the ratio of the radiation intensity in one direction to that of the isotropic source', see eq (3). For an isotropic antenna, directivity is unified because the maximum radiation intensity and overall radiation are the same. For the orthogonal component of the radiation pattern, partial directivity of an antenna for specific polarization is the ratio of radiation intensity related to a given polarization to the total radiations in all directions. In the spherical coordinate system, the total partial directivity for the two orthogonal components θ and φ is the sum of the individual directivities of the components and can be defined as

$$D_0 = D_\theta + D_\varphi \tag{4}$$

where D_0 is the maximum directivity, D_θ and D_φ are the partial directivities in the direction of the orthogonal components θ and φ.

$$D_\theta = \frac{4\pi U_\theta}{(Prad)_\theta + (Prad)_\varphi} \tag{5}$$

$$D_\varphi = \frac{4\pi U_{\theta\varphi}}{(Prad)_\theta + (Prad)_\varphi} \tag{6}$$

Another useful parameter which describes the antenna performance is *gain* which, although not dissimilar to directivity, collectively defines the efficiency and the directional properties of an antenna. For an antenna radiating in a given direction, a gain can be quantified as 'the ratio of the radiation intensity in a given direction to the radiation intensity of the same antenna power radiated isotopically'. The set of frequencies in which the performance of an antenna is to be taken into account is called the *bandwidth* of an antenna and these frequencies are usually scattered around the central or resonance frequency of the antenna.

When an EM wave is transmitted or received by an antenna, the polarization of the EM wave is termed *polarization of antenna* while the characteristic of the EM wave by which the direction of the time-varying electric field with relative magnitude can be described is known as the

polarization of the radiated wave. In far-field, the polarization is the direction of a vector normal to the plane wave whose electric strength is the same as that of the wave itself. Wave polarization can be categorized as linear, circular and elliptical polarization, where linear and circular polarizations are the special cases of elliptical polarization. A time-varying EM wave is said to be *linearly polarized* in space when the electric and magnetic field vector at that point remains on the same straight point at every instant of time. The time-varying EM wave is said to be *circularly polarized* in space when the electric and magnetic field vector at that point in space defines a circle as a function of time. In *elliptical polarization,* the electric and magnetic field vector in space forms an ellipse at that point as a function of time. Generally, the polarization of a receiving antenna is not the same as the alignment of the incident wave which is known as *polarization mismatch*. Therefore, the extracted power is decreased if polarization loss occurs. The ratio of the power received by an antenna from a plane wave having an arbitrary polarization to the power of the wave that would be received with maximum power is called a *Polarization Loss Factor (PLF)*.

The impedance presented by an antenna at its terminal or the ratio of voltage to the current at a pair of terminals is referred to as the *input impedance* of the antenna is calculated by

$$Z_A = R_A + jX_A \tag{7}$$

where Z_A is the input impedance at input terminals, R_A and X_A are the input resistance and reactance respectively, and X_A represents the imaginary part. The *Return Loss R* is the proportion of the signal that is reflected as a result of the impedance mismatch and refers to the loss of power and is measured in dB's as is presented by

$$R = -10\log\frac{\mathrm{Pi}}{\mathrm{Pr}} \tag{8}$$

where P_i is the incident power to the antenna and P_r is the reflected power from the antenna. As the *Reflection Coefficient* Γ is the ratio of forward and reflected voltages and voltages are proportional to the power, the Return Loss can also be represented as

$$R = -20\log(\Gamma) \tag{9}$$

A measure of impedance mismatch between the load and the transmission line, the *Voltage Standing Wave Ratio* (VSWR), can be equated by the ratio of maximum voltage to the minimum voltage. VSWR can be calculated by

$$VSWR = \frac{V_{max}}{V_{min}} \tag{10}$$

The VSWR of an antenna, in terms of reflection coefficient, can be calculated as

$$VSWR = \frac{1+\Gamma}{1-\Gamma} \tag{11}$$

The relation of the radiation energy P_R and the ohmic losses of power P_L to the received energy P_s is described by the Quality Factor Q, which is inversely related to the bandwidth of an antenna. How much power is consumed or lost by the antenna is defined by *radiation efficiency* and takes into account conduction, dielectric and reflection efficiency. While evaluating conduction and dielectric efficiency separately is problematic, it is usually described as e_{cd} and is defined as 'the

ratio of power delivered to the radiation resistance to the power delivered to radiation and loss resistance'. If R_r represents radiation resistance and R_L is the load resistance, then radiation efficiency can be defined by

$$e_{cd} = \frac{R_r}{R_{rL} + R_r} \tag{12}$$

The length of an antenna which indicates the open-circuit induced voltage by receiving an EM wave is known as the *effective length* of the antenna. The effective length l_e is a vector and far-field quantity which is represented by

$$l_e(\theta, \varphi) = \hat{a}_\theta \, l_\theta(\theta, \varphi) + \hat{a}_\varphi l_\varphi(\theta, \varphi) \tag{13}$$

where $l_e(\theta, \varphi)$ is the effective length of the antenna and $l_\theta(\theta, \varphi)$ and $l_\varphi(\theta, \varphi)$ are the effective lengths in the corresponding θ and φ directions. The power capturing characteristics of an antenna is described by *Effective Aperture*, which is defined as 'the ratio of the power available at the terminals of the antenna in receiving mode to the power flux density of an EM wave falling on the antenna in the same direction.' Given that the Effective Aperture is represented by A_e, it can be calculated by

$$A_e = \frac{P_T}{W_i} \tag{14}$$

where P_T is the total power delivered to the load and W_i is the power density of the wave falling on it. Other power capturing characteristics of an antenna related to area include *Scattering Area* A_S, *Loss Area* A_L, *Capture Area* A_C and Aperture Efficiency ϵ_{ap}. The following equations (15)), (16)), and (17)) can be used to calculate A_S, A_L, and A_C, respectively.

$$A_S = \frac{{V_T}^2}{8W_i}\left[\frac{R_r}{(R_L + R_r)^2}\right] \tag{15}$$

$$A_L = \frac{{V_T}^2}{8W_i}\left[\frac{R_L}{(R_L + R_r)^2}\right. \tag{16}$$

$$A_C = \frac{{V_T}^2}{8W_i}\left[\frac{R_T + R_r + R_{Lr}}{(R_L + R_r)^2}\right] \tag{17}$$

In general, the total capture area A_C is calculated by the sum of the A_S, A_L and A_e

$$A_C = A_e + A_L + A_S \tag{18}$$

The ratio of the Maximum Effective Area A_{em} and the Physical Area A_P is called *Aperture Efficiency* ϵ_{ap}, where the Physical Area is the actual area of the antenna and Effective Area of an antenna is not necessarily equal to the Physical Area.

$$\epsilon_{ap} = \frac{A_{em}}{A_p} \tag{19}$$

For aperture type antennas like horn reflectors and waveguides, the Maximum Effective Area cannot exceed the Physical Area but it can be equal as described by $A_{em} \leq A_p \; or \; 0 \leq \epsilon_{ap} \leq 1$. The Effective Area of a receiving antenna can also be described in terms of polarization of the

wave captured by it and is known as a *Partial Effective Area*, which is the division of power at the terminals to the power flux density of the plane wave falling on that terminals in the direction of a specified polarization conflicting with the receiving polarization of the antenna. In the case of wire antennas, the Maximum Effective Area is greater than the Physical Area if the area is split lengthwise along its diameter. Resultantly, electrically wire antenna appears larger than its physical length. The *Maximum Effective Aperture* A_{em} is directly related to maximum directivity of the antenna and calculated by

$$A_{em} = \frac{\lambda^2}{4\pi} D_0 \tag{20}$$

The relation between transmitted power and the received power of two antennas separated by a distance $R > 2D^2/\lambda$, where *D* is the largest dimension of either antenna, and is described by the following Friis Transmission Equation

$$\frac{P_r}{P_t} = [\frac{\lambda}{4\pi R}]^2 G_{ot} G_{or} \tag{21}$$

The *Echo Area σ* is located at the physical structure of the target object which intercepts the amount of power from an antenna scattered isotopically, and produces the same density and same power scattered by the actual antenna. The following radar equation describes the relationship between the rate of power received and transmitted by an antenna with the distance of the target from the transmitting and receiving antenna.

$$\frac{P_r}{P_t} = \sigma \frac{G_{ot} G_{or}}{4\pi} [\frac{\lambda}{4\pi R_1 R_2}]^2 \tag{22}$$

The rate of power receiving and transmitting also directly relates to the Echo Area.

1.4.4 Radar Cross Section (RCS)

When EM waves incident on a target, a specified polarization is commonly reflected or scattered in all directions. The reflected polarization is classified into two parts: the first part maintains the same polarization as that of the incident wave from the receiving antenna because the pointing vectors of scattered waves are in the same direction of the incident wave. The first part is referred to as Principal Polarization (PP). While the second part demonstrates a different polarization and referred to as Orthogonal Polarization (OP). Both polarizations are orthogonal to each other. When an object is targeted by an incident EM wave, it performs like an antenna which incorporates both near and far-fields of the scattered field. The RCS of the target object is measured by the intensity of the reflected energy from this antenna which has the same polarization as the receiving antenna. If the power density of the incident EM wave on a target is presented by P_{Di} and the target cross-section is denoted by σ, the amount of the power reflected is [120].

$$P_r = \sigma P_{Di} \tag{23}$$

The power density P_{Dr} of the scattered wave at receiving antennas is given by

$$P_{Dr} = \frac{P_r}{4\pi R^2} \tag{24}$$

Both (23)

$$\sigma = 4\pi R^2 \frac{P_{Dr}}{P_{Di}} \tag{25}$$

Assuming that the receiving antenna is in the far-field, the waves received from it would be classified as planar waves and (25) can be written as

$$\sigma = 4\pi R^2 \lim_{R\to\infty}\left(\frac{P_{Dr}}{P_{Di}}\right) \tag{26}$$

The RCS defined by the above equation is referred to as the target RCS. Understanding that the RCS is a measure of all the scattered waves from a target in the direction of the radar which possessed the same polarization. If σ_t is the total RCS of the wave scattered from the target, then $\sigma_t > \sigma$. By taking the spherical coordinate system (ρ, θ, φ), then at range ρ, the RCS is a function of (θ, φ). Assuming the direction of the propagation of the incident wave is defined by (θ_i, φ_i) and the direction of the propagation of the scattered wave is given by (θ_s, φ_s), then the condition when $\theta_i = \theta_s$ and $\varphi_i = \varphi_s$ is known as a monostatic RCS and the RCS measured by the radar at angles $\theta_i \neq \theta_s$ and $\varphi_i \neq \varphi_s$ is referred to as a bistatic RCS. The total RCS can be evaluated as

$$\sigma_t = \frac{1}{4\pi}\int_{\varphi_s=0}^{2\pi}\int_{\theta_s=0}^{\pi}\sigma(\theta_s,\varphi_s)\sin\theta_s d_{\theta_s} d_{\varphi_s} \tag{27}$$

The wavelength λ of the incident EM wave is proportional to the size of the target, known as the extent of the target. If the target extent is too small compared to the wavelength, then a radar will not be able to detect the target RCS, which is measured in dB or dBsm. The frequency region in which the extent of the target is comparable to the wavelength of the incident wave is referred to as a Rayleigh region whereas the optical region, where the target extent is much larger than the wavelength, is a frequency region. While many factors can affect the RCS measurements, the frequency of the incident wave, the radar aspect angle, the polarization, and the electrical spacing between the objects are worth mentioning [120].

1.4.5 RFID Technologies

Nowadays, all commercial industries and companies require a tracking system which identify their customers and products, and create the possibility of checking inventories for individual product consumption and compiling the history of a previous record. While this can be done manually, the chance for error becomes quite significant. Indeed, the error rate due to the manual entry is calculated at a high up to 2-3% [121] compared to the automatic data entry which is a reliable error-free method in which various techniques are included, such as barcode and RFID

technologies. Barcodes are a small in size, low-cost identification technique which requires line-of-sight to read the codes, which is the major difference between the barcode technique and the RFID technique, which does not require line-of-sight to access the coded information. The RFID system is usually comprised of a reader, which is connected to a database via a radio frequency link, and a tag with a frequency chip built into it; see Figure 8.

Figure 8. General Representation of RFID System [121]

In a conventional RFID system, a tag is comprised of an integrated circuit with an antenna and can be implemented on a paper or plastic surface, depending on the target application. The read range of these tags depends upon the frequency and type of the tag, and the antenna dimensions. There are various advantages for utilising the RFID tags over a barcoding system: firstly, no line of sight with the reader is required by the system to read it accurately; secondly, data can be both written and read; and thirdly, their capacity for simultaneous reading of data on a large number of tags by using different anti-collision techniques.

1.4.5.1 History

RFID technologies history has been dated back to eight decades ago when RFID was used in World War II. In 1940, Watson Watt, a Scottish physicist, was commanded to develop an aircraft system for the British [122]. He built an RFID system in which a transmitter was placed in a British plane to receive signals from ground stations and broadcast back to be classified as a friendly identity. The modulation methods are studied comprehensively in a paper published in 1940 [123]. The first extensive commercial RFID tag appeared in the 1960s carrying only 1-bit information and was primarily used for anti-theft activities in shops. Throughout the 1960s and ‘70s, RFID technologies were used mainly by the military to access sensitive sites, particularly nuclear sites. In 1980, based on the knowledge introduced in [124] and studied [125] since 1948, and with the enhancement of electronic components such as transistors, the idea of passive tags, generally known as chipless tags, was implemented. This technology served to provide great simplicity to the design of the conventional tag by removing the energy source and additional circuitry from the tag itself and consequently reducing both its complexity and cost. Nonetheless, as frequency and information control protocols were not defined at that time, RFID technology remained confined

to internet companies. During the 1980s, as industries and businesses extended, interest in the use of RFID technology increased simultaneously with the invention of personal computers, which created a simplification of data collection and management through the RFID tags.

In 1990, the International Standard Organization (ISO) proposed a set of regulations and developed a standard identification protocol that was coordinated with different countries with which different protocol standards had previously been associated. This was a vital step towards a worldwide deployment of RFID technology. Initially, the conventional RFID tags were made operational by the integration of a microwave diode into the Integrated Circuits (IC) with an antenna. The Auto-ID centre, a research institute founded with the research collaboration of the well-reputed Massachusetts Institute of Technology (MIT) in 1999, extended to Electronic Protocol Code (EPC) global in 2004, and became the organization responsible for converting barcodes to RFID, with the collaboration of ISO. In 2009, the Centre National de Reference RFID (CNRFID) was established to facilitate regulation and standard management.

During the last few decades, RFID technologies have become very widespread, being extensively used in various applications in almost all industries [126, 127], and there are now numerous RFID techniques in current commercial use, such as Near-Field Magnetic Coupled tags, UHF RFID tags and chipless RFID tags [128]. Most of the conventional RFID tagging techniques employ some kind of time-variant loading or scatterer modulation to transmit information into what is called a backscattered field [129-132]. This process of backscattering requires the physical movement of the object to be coded or electronically changed through impedance modulation or inductive coupling. Furthermore, the majority of traditional RFID tags are made from a near-field circuit with a low-cost chip at the centre. While the characteristics of this low-cost chip could be as simple as holding a single code or more complex to execute different algorithms, in the contrastive passive or chipless RFID tagging, the ID code is not saved in memory, using instead the actual physical features of the tag itself to send data [126].

1.4.6 Overview of Chipless RFID tags

Chipless RFID tags have gained considerable attention as a result of the non-existent battery and additional circuitry, with a significant advantage over conventional tags for their limited size, increased lifetime and low manufacturing cost [133]. The main advantage of these chipless RFID tags, however, is their promise of being extremely cheap and their adaptive versatility for being printed onto packages as simply as affixing paper barcodes. The second advantage of such tags is the absence of electrical circuits, consequently opening them for functional incorporation into applications where the tag could be exposed to the elements. These types of tags also lend themselves well to wearable applications where washing and heating may otherwise have affected an energy source [134].

The typical RFID system comprises a transmitter and a receiver, which is an adapted version of an Ultra-Wide Band (UWB) frequency radar [135]. An EM wave compromising a wide range of

frequencies is subjected to the RFID tag with the effect that the tag backscatters the received wave where this energy is picked up by the receiver, as shown in Figure 9. When an incident EM wave strikes the tag it induces a current in the conductive elementary cell at the resonant frequency. Furthermore, the chipless RFID tags are primarily worked by the resonance obtained from the metallic surfaces and do not carry electronic circuitry to handle communication protocols. Although many designs have been proposed for chipless RFID tags, they can be characterized into two general groups: the first group refer to time-domain-reflectometry-based designs for which the Surface Acoustic Wave (SAW) is an example, while the second group are classified as spectral-based tags and include the FSS technique. The phenomenon behind SAW-based RFID tags is the piezoelectricity in which EM waves entering into the tags are converted into acoustic waves by an Interdigital Transducer (IDT) positioned on the surface of the piezoelectric substrate. These acoustic waves, while propagating through the surface of the substrate, corresponding to conductive reflectors which are separated by a certain distance to enable the reading of ID codes stored on tags [136, 137]. While actual SAW RFID's are presently in commercial use, there are still some important issues that need to be addressed, including characteristics such as a size reduction and an increase in data capacity and reading range [128].

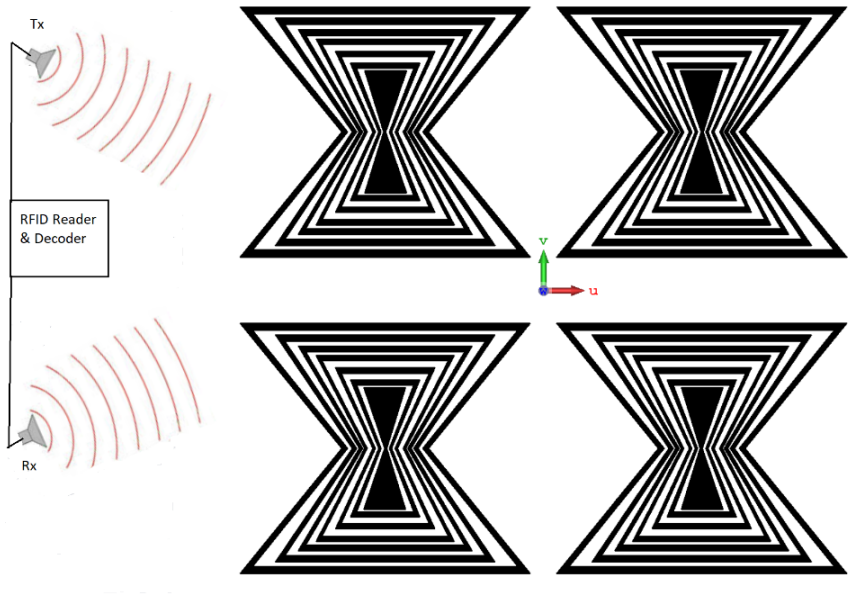

Figure 9. Chipless RFID System

FSS is a promising surface responsive technique in which, when the frequency of the EM wave matches with the resonant frequency of the FSS shape [138], an incoming EM wave either transmits or reflects completely or partially, depending on the nature of the two-dimensional array of conductive elements arranged on the particular dielectric substrate. While flexible substrates in the flexible electronic systems are mostly characterized by energy efficiency, lightweightedness, low manufacturing costs, reduced fabrication complexities and mechanical robustness [101], it is important to address a high flexibility level along with a high radiation performance, as well as the mechanical, electrical and thermal properties of substrate materials for this technique.

Understandably, chasing radiation perfection can, at times, cause increases in antenna costs and it is the substrate flexibility which dictates the bendability of the antenna. Critically, antenna deformation affects not only the radiation patterns and resonant frequency, but also the level of impedance matching, bandwidth, directivity, radiation energy and efficiency [74, 109]. Moreover, the compactness and desirable radiation characteristics of a flexible substrate, which are beneficial for wearable applications [134], are also required for high radiation efficiency [73, 115, 116].

1.4.6.1 **Encoding Techniques**

Although the reality that there is such a wide range in the variety of chipless RFID tags has created classification challenges, one form of classification that is determinable is in accordance with the encoding techniques in terms of time-domain encoding and frequency domain coding.

1.4.6.1.1 **Time-Domain Based Encoding Technique**

This type of encoding technique has been investigated extensively and is most commonly utilized in chipless RFID tags for which the antenna and chip have a common built-in structure [139, 140]. Time-domain based chipless RFID tags are generally comprised of certain passive components and a Transmission Line (TL) as the technique is based on the principle of reflectometry in which parasitic elements in this TL connected to the antennas, are positioned in such a way that they produce reflections at precise intervals of time. The radio frequency EM wave is propagated through the TL and passive elements, such as circulators [139, 140] and capacitors [141], to produce these reflections. The presence and the absence of reflections at given time intervals determine the identification pattern in terms of code words. With Time-domain based tags, the length of the TL is not related to the operating frequency, so this type of encoding technique encourages compatibility with various RFID frequency regulation and standards. Another advantage attributed to this coding is its comparatively large read range, in the order of a few meters, with the benefit of low bit capacity where the information, in terms of the number of bits stored, is less than 10 bits [126].

The major hurdle of this technique emerges in the design characteristics of the time-domain based RFID tag in the creation and positioning of the TL, which may attribute such length as to conversely generate measurable delays and increased tag size. Even the amplitude of the reflections in the time-domain encodings can be negatively impacted by the losses associated with TL length factors.

Time-domain based encoding was used to design the very first tag without a chip that appeared in the literature [142]. The SAW technique uses such temporal domain encoding techniques and is perhaps the pioneer of the development of chipless RFID tags, being credited as the first commercially implemented technique. The SAW RFID tags generally operate at an Industrial, Scientific and Medical (ISM) frequency band of 2.45 GHz [142, 143]. The operating principle of the SAW-based tags is illustrated in Figure 10. An incident EM wave falls onto a Transducer Connector Interface (TCI) and converts into a surface acoustic wave, which propagates through the piezoelectric reflectors to create a series of pulses at different time intervals. The SAW pulses

convert back to the EM wave by the TCI and are retransmitted to the reader. The identifier of the pulse is decoded at the receiving end. A Pulse Position Modulation (PPM) is achieved by modifying the position of the reflectors on the substrate [143].

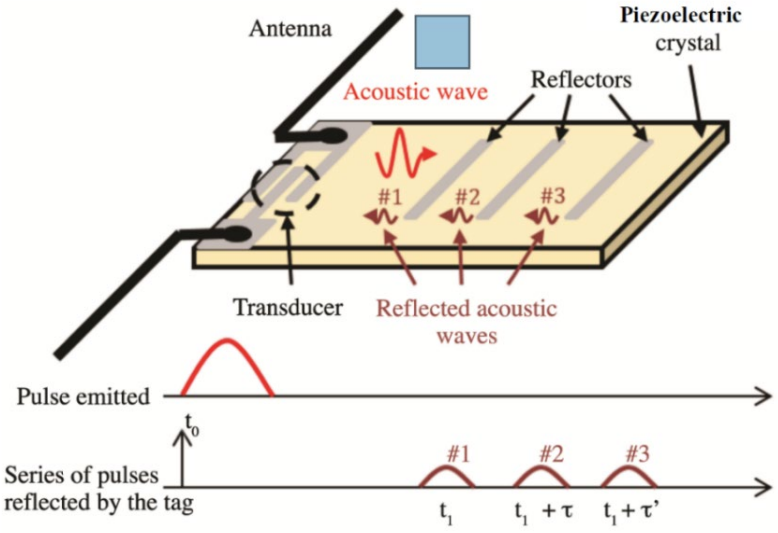

Figure 10. SAW-Based Chipless RFID Tags: Operating Principle [143]

The tag [143] has a capacity of 256 bits which is compatible with the EPC standard for conventional RFID tags, which usually have additional circuitry with it to generate more power. As an expensive piezoelectric substrate is used as the transducer for the SAW technique to generate the pulse at different time intervals, they are expensive compared to the chipless RFID tags that use frequency domain encoding. For the use of a non-piezoelectric substrate in SAW, the technique requires a long TL to produce the appropriate delays, which corresponds to increased losses and challenges in attaining specific coding densities. Consequently, the piezoelectric materials are preferred. To address the limitations of the SAW technique, such as its expense factors and confinement to the ISM band, several other designs have been made with temporal based encoding techniques, such as TL tags [144] and variable terminal impedance tags [145].

1.4.6.1.2 **Frequency-Domain Based Encoding Technique**

In the frequency-domain based technique, code words can be encoded into frequency signatures by the positioning of inductors near a microstrip line [105, 126]. The encoding process can also result from assembling an array of conductive resonators with an assortment of resonant frequencies, such as dipoles [22, 146], square type [147], ring-type [148, 149], Bow-Tie shaped [1, 2], octagonal-shaped [56], and other different, irregular and alphabetic shaped resonators [40, 150-153]. Coding is implemented by the presence and the absence of the conductive elements at certain positions, depending on the wavelength of the incident wave striking it or on the geometrical shape of the element. This coding technique is predominantly used to deploy passive or chipless RFID tags in which the code words are encoded through backscattered signals in terms of RCS and, requiring a considerably large spectrum, primarily uses the UWB band 3-10 GHz [38,

128].

The performance of the resonators in this category of encoding is influenced by the presence and the absence of a ground plane in the tag. The RFID tag design with the ground plane is similar to the microstrip structure, enabling them to exhibit high RCS and indicating encoding is easy, while the absence of this ground plane creates weaker RCS which conversely complicates the encoding process [121]. Nevertheless, due to its greater coding capacity, frequency-domain encoding is now extensively used and, based on the evolution of the frequency domain based RFID tags since 2008, there are three types of tags currently utilizing this coding technique [121]. The first type uses two separate antennas of the same radiation characteristics and polarization as a transmitter and a receiver with a planar filter which, as presented in [154-156], is usually comprised of a set of resonators as a filter referred to as planar filter tags, see Figure 11(a). As this first type is usually quite bulky, the second type has been introduced to reduce the weight of the tag by way of a bidirectional antenna being connected, as in [157, 158], with a resonant load to ensure the filter's operation, see Figure 11(b).

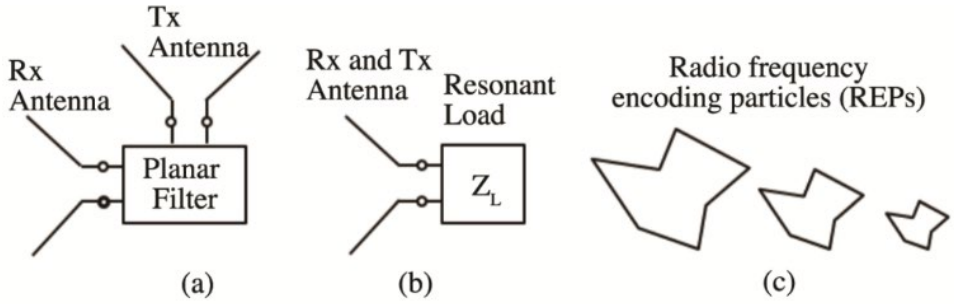

Figure 11. Evolution of Frequency Tags: a) Planar Filter Tags, b) Single Antenna Loaded with Resonant Element, and c) Radiofrequency Encoded Particle (REPs) [121]

The third and most recent approach provides the best coding densities and incorporates chipless RFID tags comprised of resonant scatterers. As described in the examples in [1, 16, 40, 56, 150, 153, 159-162], in this type, no antennas or additional circuitry are attached to the tag, which makes them very lightweight and low cost. These scatterers or resonators are referred to as Radiofrequency Encoded Particles (REP). In this study, this type of designed chipless RFID tags on polymer substrates applicable for general wearable IoT has been discussed in Chapters 4 and 5.

1.5 Substrate Materials for Flexible Wearable Devices

Substrate materials in the basic microstrip antennas and RFID tags are usually employed to support the conductive elements and to introduce flexibility in the device. The properties and the requirements for the substrate dielectric are elaborated in 1.2.2.2. The selection and implication of an insulating dielectric with the conductive plane is dependent on the specific application, operating frequency and the properties of the conductive elements. Several extensively used substrate materials are discussed in this section.

1.5.1 Polymers

Polymers are widely used as dielectric substrate for flexible devices. The highly resistant nonconductive materials are composed of repeated subunits of hydrocarbons known as monomers and are divided into two categories: Natural polymers, such as silk, rubber, starch and wool, and Synthetic polymers which are chemically prepared in laboratories, such as PVC, polystyrene and nylon. Synthetically prepared polymers, such as PI, PET, PTFE, PDMS LCP, have the merits of high flexibility, low cost, good soldering tolerance for fabrication, withstand high temperatures and maintain very low thickness. A detailed comparison of the properties and the selection of the appropriate polymers as a substrate for different applications is given in Chapter 2.

1.5.2 Textile

Textiles in clothing can be applied to antenna and RFID tags as a substrate, especially when combined with conductive threads to create a platform for the wearable device. There are numerous textiles and threads currently being employed, including cotton, wool, silk, viscose, and felt [101]. Electrical properties, such as relative permittivity and the loss tangent of textile substrates, are highly dependent on the pattern of sew-in materials, knit or woven, and the number of layers which define the thickness of substrate [114]. Parametric characterization of these dielectrics is very important as some textiles, such as Cordura and Ballistic, possess anisotropic qualities, which refers to their behaviour at different positions of the fabric [101]. Conductive polymers can also be used as a conductive element for wearable devices, where the coating of metallic conductors on a thread can achieve high conductivity and flexibility.

1.5.3 Paper

Paper, a substrate material which is low-cost and environmentally friendly, is in wide use. Indeed, it is the most significant substrate in terms of simplicity in the printing process in conjunction with the application of conductive inks as conductive elements, although characteristic features, such as low resistivity against moisture, lossy behaviour and frequency dependency, have made it less competitive against the other more resilient dielectric substrates [101].

1.6 Material Characterization Methods

For the design and fabrication of flexible antennas and RFID tags as wearable devices, comprehension of certain mechanical, electrical and thermal properties at the required frequency, such as the conductivity and the surface resistance of these conductive materials, is necessary, and their permittivity, loss tangent and temperature coefficient of resistance need to be characterized [101]. In the case of textiles, most of the parameters, such as the thickness of the thread, complex permittivity and conductive capacity need to be need to be determined or tested [101, 163].

The electrical properties of the conductive material such as its conductivity, conductive loss,

quality factor Q and transmission coefficient S_{21} can be analysed using the waveguide cavity method [114]. This method is also used to characterize the conductivity and surface resistance of conductive threads [101]. The microstrip resonator method is another popular method used to measure the electrical properties of the conductors. Similar to the waveguide method, it can be used to measure the dielectric loss and the permittivity of the dielectric substrate [114]. The Transmission Line (TL) method is a popular method that serves the same purpose [164]. In [165], a T-resonator microstrip line method is proposed to measure the loss tangent and the permittivity of dielectric for specific frequencies and, in [40, 153], another very effective method called the matrix-pencil two-line method is proposed for the same purpose.

1.7 Fabrication Methods

While there are various fabrication processes for fabricating the FES and wearable devices, such as the flexible antennas and RFID tags, this section analyses some of the more widely used fabrication techniques adopted commercially or used by the research sector.

1.7.1 Photolithography

In this manufacturing technique, the unwanted section of the desired conductive pattern on a dielectric substrate is removed by using a chemical agent or photoresists. This technology has grown very popular in 1960, dominating the PCB manufacturing industry for many decades as it produces very accurate and fine patterns. Presently, the wearable devices and electronic circuits which are manufactured by photolithography are utilizing positive photoresists, as negative photoresists result in inconsistency of the metallic pattern on the flexible substrate, sometimes known as edge-swelling. Photolithography is a very feasible technique for producing single, double and even triple layer PCB designs by etching the regions on either side of the substrate. Presently, this technique is not commercially widespread because of the involvement of dangerous chemicals, by-product production and low throughput [101].

1.7.2 Thermal Evaporation

This technique is conducted by photolithography as it involves a physical vapour deposition procedure in which a coated material is applied to a substrate film surface [166]. In this process, a solid material is heated and vaporised inside a vacuum chamber then deposited onto the surface of the substrate. The method is useful for the manufacturing of flexible antennas and RFID tags in which a pure atomic metal is used as the conductive material [101].

1.7.3 Screen Printing

In this technique, a mask of the desired design is first developed and applied directly to the flexible substrate or film. This is executed by using conductive inks, which are thermally deployed to evaporate unwanted solvents. Screen printing has been successfully implemented for many years

in the manufacturing of flexible antennas and RFID tags because of its simple and environmentally friendly process. Drawbacks associated with this technique include a limited control over the thickness of the pattern and characteristics of resolution, consistency and the number of layers needed for the patterns [35, 36].

1.7.4 Flexography

Flexography, a technique quite similar to screen printing, has gained much popularity by RFID tag manufacturing companies because of its high resolution, reel to reel processing on flexible substrates and its low-cost. In this process, the image of real tags or antennas is printed as an ink impression on the substrate film while the rest of the area is left free of ink [33]. The efficiency of the fabricated tags or antennas depends mainly on the conductivity of the radiating material and the sheet resistance, such that the consistency and the thickness of the pattern is crucial for its impact on sheet resistance [34]. Compared to the ink used in the screen printing process, the ink used in this technique requires a lower viscosity which results in the formation of a dry pattern with a thickness of $< 2.5\mu m$ on the surface of the substrate [101].

1.7.5 Inkjet Printing

One of the immensely popular techniques used to fabricate RF circuits and flexible RFID tags, inkjet printing is quite similar to conventional computer printing in which the image of a design is deposited onto a piece of the substrate by propelling droplets of the conductive ink. These droplets are usually of a pico-litre size which provides fine, high-resolution patterns.

1.7.6 Line Pattern

The line pattern technique is one of the most cost-efficient methods for the fabrication of FES in general and RFID tags and antennas in particular. This technique, initially proposed in 2001 [167], develops a negative of the image, using graphic software, which is then deposited onto a flexible dielectric substrate, such as a polymer. The substrate is then sonicated by applying high energy ultrasonic waves in toluene solution for ten seconds. This technique is commercially used to fabricate flexible field-effect transistors and RFID tags.

1.7.7 Embroidering

Wearable embroidered flexible devices have many advantages since the device can be embedded into any cloth materials rather than being attached or applied to them; making embroidery the preferred fabrication process for wearable antennas and textile-based RFID tags. This technique is useful for the direct implementation of conductive threads over the fabrics. Since no adhesive material is required in this technique, there are less adverse effects on the electrical properties of both the conductive and substrate materials [168]. For this method, material wrinkling and crumpling must be minimized to obtain the required radiation efficiency.

1.8 Bending and Crumpling Impacts on Wearable Devices

Wearable devices, such as flexible antennas, RFID sensors and tags, are critically affected by bending, twisting and crumpling. These deformative actions are sometimes inevitable, resulting in detrimental changes to the radiation performance of the wearable-device. To ensure the robustness and durability of the wearable device under flex conditions, a few important parameters for flexible devices are required to be tested for performance, such as shifts in resonant frequency, return loss, signal degradation and RCS [45]. While radiation patterns, directivity and gain are all factors which can be affected by bending [101], one of the major impacts of the bending is on the resonant frequency and return losses because the curvature on the device is prone to shift the resonant frequency either towards higher components or lower components of the resonant frequency and cause a change in its signal strength. The process of applied bending is predisposed to creating a mismatch of the impedance of TL and the feedline, as well as changing the capacitance between the resonators and causing a modification in the effective length of the radiation element [101]. More specifically, in the case of RFID tags, bending causes an alteration in the coupling coefficients due to a modification in the relative distance between the resonators [2]. Therefore, the most reliable wearable devices are considered those which tolerate the application of a certain level of bending to limit the adverse impacts on their radiation efficiency. For this reason, bending impacts on the resonant frequency, which include deviations from the central frequency, reductions in signal strength and the impact on the coupling coefficients of the resonators for the RFID tags, are the main focus for analysis and assessment in this present study.

1.9 Contribution and Organization

Targeting the above challenges, this dissertation poses my endeavours in the realization of flexible polymer-based wearable antennas and chipless RFID tags for general IoT applications; see Figure 12, the navigation diagram for the contribution in this thesis.

Firstly, a novel Bow Tie Chipless RFID tag is designed on PET substrate [1] and analysed for levels of bending at 27 mm and 14 mm. The same design is fabricated on PVC and PTFE Teflon and analysed for its bending capabilities [2]. The electromagnetic behaviour of the Bow Tie Chipless RFID tag and coupling coefficients are described and the maximum read range is measured [3]. Secondly, the flexibility of the polymer-based microstrip antennas, in [7], is analysed for the different range of frequencies and radiation characteristics, such as reflection coefficients and shift in resonant frequency, are measured and compared. Finally, two Octagonal-shaped Chipless RFID tags are designed by using conductive threads, HC12 and LIBERATOR 40 [6], on a cotton substrate and the electromagnetic behaviour of the tag, coupling coefficients, on-body testing, the maximum read range estimation and the bending analysis for 27 mm, 14 mm, and 7 mm are performed in Frankonia anechoic chamber [5, 6].

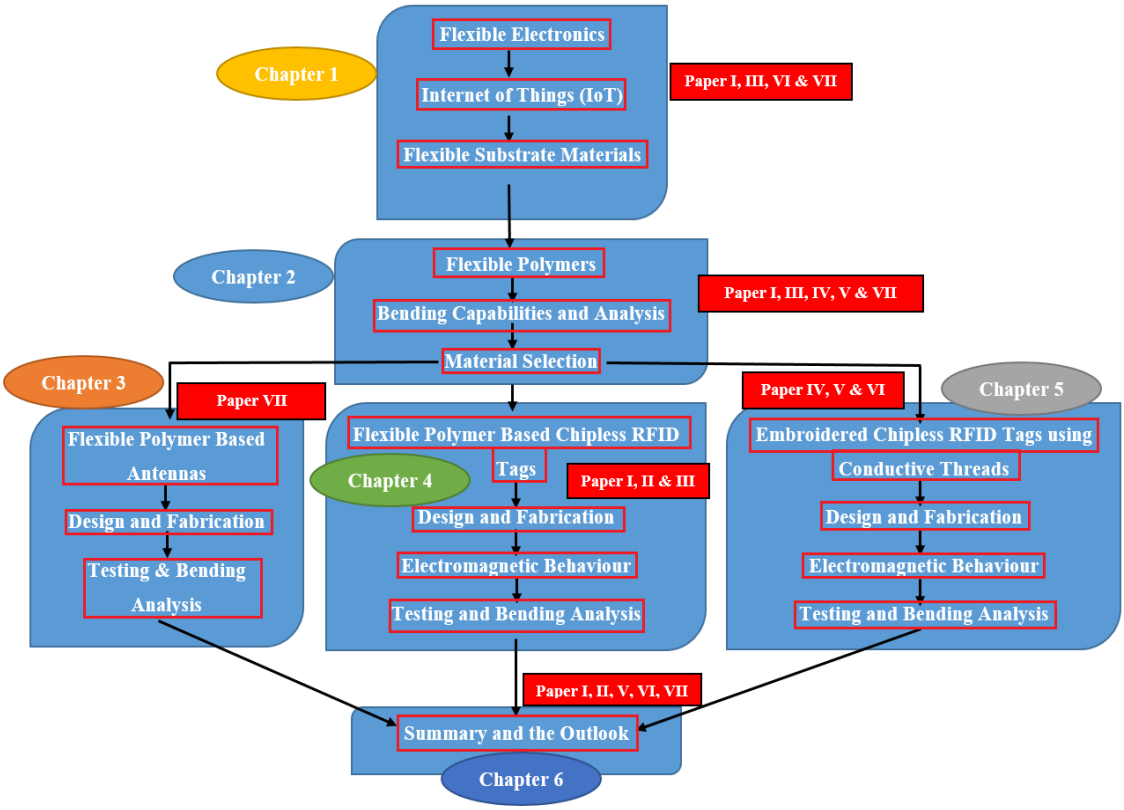

Figure 12. Navigation Diagram for Dissertation Contributions

1.10 Beyond the Scope of the Dissertation

The study and investigation covered in this thesis aim to provide a comprehensive overview of flexible wearable devices, such as flexible antennas and the chipless RFID tags, on flexible polymer substrates. However, owing to limited time affected by the COVID-19 outbreak and limited access to the working laboratories, the author is obliged to disregard some relevant experimental aspects and concentrate more on the significant topics that are presented in this study. Some relevant investigation areas which could have been include in this study but fell beyond coverage include:

- Conducting a more complete printing process of the flexible antennas and the chipless RFID tags on the polymer substrates.
- Tests and investigation of the properties for selected polymers to use as substrate materials.
- Feeding methods and impedance matching techniques for the flexible antennas with the feedline, especially for the higher frequencies above 5 GHz.
- Whether or not the bending of flexible devices has an impact on other radiation characteristics such as gain, directivity and efficiency, remains allocated to future work.
- Investigating bending capabilities for flexible antennas for different ranges of frequencies, where the range could be narrowed and divided into more bandwidths to analyse the impact more accurately.

Chapter 2: **Flexible Polymer-Based Antennas**

2.1 Introduction

Traditional antennas are customarily made of conductive wires or by etching metal patterns on rigid substrates. When subjected to stretching or are folded or twisted, these types of antennas become permanently deformed, if not broken, which renders them incompatible for applications that require high flexibility/bendability and are subject to this continuous deformation. Flexible antennas have gained much attention in recent years with their advantage of directly addressing this problem with their high flexibility, but also for their convenient integration with other microwave components [47], lightweightedness, energy efficiency, reduced fabrication complexity, easy mount-ability on conformal surfaces, their low cost, and for their abundant availability in the form of substrate films [116]. The concept of flexible wearable antennas has emerged from the progressive evolution of the FES.

Flexible electronics have become essential for applications requiring flexible displays and biomedical applications with complex curvilinear structures [169, 170]. Correspondingly, researchers have experimented on many materials in order to provide increased flexibility in electronic systems, including polymers, plastics, paper, textiles and fabrics as substrates of these systems. Each of these materials has its own individual characteristics in terms of how efficiently they can be bent, twisted and/or crumpled [16]. The bendability and flexibility characteristics of these materials make them advantageous for incorporation in designs for future smart electronics systems including application in the IoT.

For certain electronic and communication applications, the flexible characteristic of different materials is of great importance, with extensive use spreading into flexible displays, smart tags and wearable products as well as the flexible antenna developments [14, 15]. Indeed, the flexible displays and antenna systems are now considered an essential part of personal communication, industry, military, and telemedicine. These flexible devices have many utilizations in health monitoring systems, aeronautics and RFID tagging applications [45, 72, 78, 103, 115, 171-174]. Flexible circuits, such as carbon-nanotube thin films on plastic substrates, provide a conformal and lightweight construction. These flexible integrated circuits have many potential areas of application in embedded systems and other areas of electronics [175], with various types of flexible RFID tags already in widespread use [176]. Recent examples of flexible electronics include stretchable organic solar cells which can be used as biological sensors, active-matrix displays and stretchable power sources [177]. Some other novel applications more recently on the market include flexible displays and touch screens [178], electronic paper [179] and skin-like sensing robotic systems [15, 180, 181], just to name a few.

Flexible electronic devices able to be constructed with a wide variety of flexible materials, such as polymers, plastics, laminates, conductive foils and fabrics with their systems, the FES, categorically structured into four main constructive parts: substrate, backplane, front panel and

encapsulation. Figure 13 illustrates these four major parts of the FES. The appropriate selection of the base material upon which the whole circuit is produced, the substrate, is critical. The second part is the backplane, which is a PCB with slots for connecting electronic components. The next construction consideration is the front panel, customarily a metal sheet that supports the components and allows certain alteration to system components. An encapsulation layer, which encloses circuitry with a protective covering, is the final component. All of the FES parts must have some degree of bending capability without which it would conflict with the normal function of the FES.

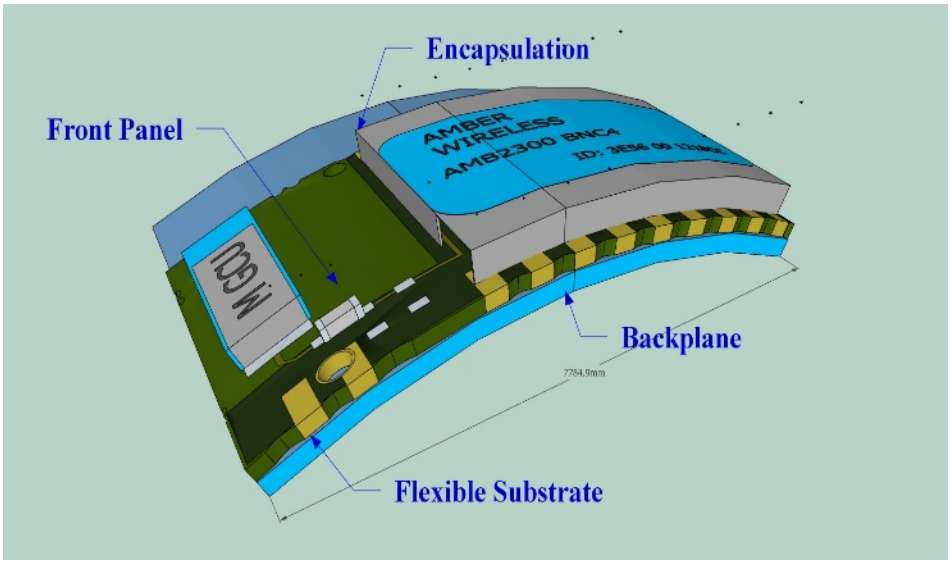

Figure 13. Major Parts of a Flexible Electronic System (FES)

The main objectives and contributions of this chapter relate to recent literature in the field and are subsequently summarised as follows:

- An overview of the history and chronological advancement in flexible electronics during the last six decades is presented. This illuminates the general structure of the FES, general properties, and selection of flexible material, to identify the desirable flexibility of dielectric substrates for specific applications.
- Elucidation of a general Transmission-Line model of a flexible polymer-based antenna, the impact on radiation characteristics by bending, general properties and the selection of flexible material to provide the desired flexibility of dielectric substrates for specific applications.
- The most efficient and relevant polymer substrates in terms of bending and flexibility, which is a key challenge for flexible IoT and wearable applications, are elaborated with certain profundity in an overview of related research work in the most recent literature.
- A detailed comparative analysis of physical, electrical, thermal and chemical properties of flexible polymer materials which have been used as a substrate to provide flexibility during the last few decades, is presented.
- The bending effects of flexible polymer substrate antennas on their radiation

characteristics for different frequency requirements are analysed and discussed with reference to the previously published articles.

The rest of the chapter is organized as follows: Section 2.2 illustrates the chronological advancement in the field of flexible electronics and the history of flexible substrate materials development. General flexible antennas for IoTs or wearable applications are presented in Section 2.3. This incorporates a presentation of the basic structure of smart flexible antennas, wearable electronic devices and bending capabilities in terms of the flexibility of substrate materials. Section 2.4 and 2.5 describe the different flexible materials useful for antenna construction and the features notable in characterizing their selection, with polymer characteristics discussed in detail. Section 2.6 and 2.7 demonstrate the analysis and resultant conclusions of the bending capabilities of different polymer-based flexible antennas on the radiation characteristics. Section 2.8 discusses the effects of bending on the resonant frequency, the reflection coefficient and the impact of loss tangent on the resonant frequency. The findings of the chapter are summarised in Section 2.9.

2.2 History of Flexible Electronics

The history of materials used to provide flexibility in devices dates back more than half a century. Table 3 shows the outlines of the developments. Six decades ago, flexible single-crystalline silicon solar cells were implemented on satellites. These materials were bendable, non-breakable and shaped conformably [36, 37]. A Thin Film Transistor (TFT) made of Tellurium was developed in 1968 on a piece of paper. In the same year, T.P Brody presented Mylar, Polyethylene and anodized Aluminium wrapping foil substrates [38]. In the mid-1980s, researchers achieved the highest ever curvature of any flexible electronic circuits.

During the 1980s, it was observed that the resulting circuit performance was not affected with as much as 1.6 mm in the curvature of the flexible substrate [182, 183]. Polymers were only deemed materials for insulating before the discovery of conductive polymers. After the discovery of Poly-acetylene in 1977, interest in conductive polymer materials in industries increased dramatically [184]. The development of Hydrogenated Amorphous Silicon Indium Tin Oxide (a-Si:H/ITO) cells on an organic polymer was another milestone in the advancement of flexible materials [185, 186]. Japan developed the Plasma Enhanced Chemical Vapor Deposition (PECVD) machines in the mid-1980s that provided a base for Si-H solar cell fabrication and led to the Active-Matrix Liquid Crystal Display (AMLCD) industry in Japan. Moreover, in the 1990s, flexible polyimide was of interest because of its flexibility, low cost and thermal endurance. Constant et al. [46] fabricated a Si-H TFT circuit on a flexible polyimide substrate in 1995, which was significant because this was the first time photolithography was used to affix Si-H TFT on rigid silicon to form a polyimide film [104, 187].

In 1996, a hydrogenated silicon Si: H/TFT was made on a flexible stainless-steel foil [187]. In 1997, a Polycrystalline Silicon (Poly-Si) TFT was successfully applied to a plastic substrate using laser annealing technology. In 2005, a rollable electrophoretic display was presented by Philips

and, in 2006, Samsung announced a 7-inch flexible liquid crystal panel [188, 189]. Furthermore, in 2006, Universal Display Corporation and the Palo Alto Research Centre presented a prototype flexible Organic Light-Emitting Diode (OLED) display which exhibited full colour and high resolution. It was constructed using a Poly-Si TFT backplane made on steel foil [190]. In 2008, Franky et al. [22] developed a White OLED (WOLED) on a 55-inch flat panel display using a vacuum deposition process. Then, in 2012, Indium Gallium Zinc Oxide (IGZO) was used as a backplane material which, advantageously, was compatible with flexible LCDs. Poor et al. [191] presented flexible displays on a plastic substrate, in 2012, for smart Televisions.

Table 3. Chronological Advancement of Flexible Electronics

Advancement in Flexible Materials	Year/Era	References
Early use of flexible material like straw with slurry for strengthening houses	BC	[192]
Discovery of electric conduction in organic materials	1862	[193]
Polymers conceptualized – rapid development followed	1920	[194]
The invention of flexible solar panels	1967	[195]
Implementation of flexible single silicon solar cells on satellites	1968	[195, 196]
Development of Thin Film Transistor (TFT) by Radio Corporation America (RCA)	1968	[182, 183]
Development of the first Liquid Crystal Display (LCD)	1973	[197, 198]
Implementation of Hydrogenated Amorphous Silicon (a-Si:H) cells on flexible polymers	1976	[199]
Development of the conjugated polymer ‘Polyacetylene’	1977	[184]
Development of a-Si:H/ITO cells on organic polymer	Early 1980’s	[185, 186]
Invention of Active Matrix Liquid Crystal Displays (AMLCD) in Japan	Mid 1980’s	[185]
Organic Light-Emitting Diodes (OLED) display on the flexible substrate	1992	[200]
Development of a-Si:H/TFT circuit on flexible polyimide	1994	[46]
Integration of OLED with a-Si TFT on a metal foil	1996	[187]
Development of a-Si:H/TFT on the flexible stainless steel foil	1996	[187]
Development of Polycrystalline Silicon (Poly-Si) TFT on a plastic substrate	1997	[201, 202]
Implementation of multilayer inorganic and polymer substrates	2003	[203, 204]
Phillips produce rollable electrophoretic displays	2005	[188]

Samsung develop a 7” flexible LCD	2006	[189]
Universal Display Centre and Palo Alto Research Centre present OLED displays with full colour	2006	[190]
Development of polymer hybrid material for permeation barriers	2008	[205]
Development of White Organic Light Emitting Diode (WOLED) displays	2008	[206]
Development of the first flexible smart phone called a ‘Paper Phone’	2011	[207]
Development of flexible displays on plastic for smartphones	2012	[191]
Curved OLED Display for 55-inch television and smartphones	2013	[208]
Flexible paper display for eBooks	2013	[209]
Flexible erasable writeable paperless tablet using LCPs	2013	[209]
AMOLED flexible display technology	2013	[210]
Flexible smart watches, flexible heartbeat and blood pressure measuring sensors, RFID tags, flexible reconfigurable antennas, flexible energy harvesting circuits	2013-2020	[211]

During the last seven years, there was a boom in the world of flexible electronic and wearable devices. From 2013-2020, flexible electronic devices such as flexible smart sensors, RFID tags, flexible reconfigurable antennas, flexible energy harvesting circuits and wearable technology brought a remarkable change in the healthcare, medical, industrial and entertainment sectors. According to a report published by IDTech, forecasts from 2020-2030, indicated that the decade would be a great challenge for all companies producing wearable electronic devices including smartwatches, hearables, smart clothing, skin patches, and Virtual Reality (VR) devices for general IoT applications [212]. Indeed, although IoT aims to connect everything to everything, the interface to this communication (the antenna) demands to be as flexible and as easy to use as possible. A class of materials that allow flexibility, and hence enable cheap and flexible deployment of antenna designs for faster and more practical IoT applications, are further investigated here.

2.3 Antennas for Flexible Wearable IoT

The IoT are a growing number of physical objects that are connected wirelessly via antennas [213] which have implications for the industrial automation, health and agriculture sectors, transportation and most importantly emergency responses to natural disasters. The IoT enables objects to share information and, when connected to decision-making algorithms, to make decisions accordingly. Nowadays, IoT devices are contributing to improving human lives and taking part in an expanding array of business applications. For instance, smart homes, in which

residents can control the climate of rooms or turn on/off appliances, such as TVs, alarm systems, monitoring systems and heating systems, through remote access to their homes, automatically and wirelessly [93].

Virtually all current mobile electronic devices communicate via the incorporation of passive antennas, which are constructed with a variety of materials. There are many advantages of flexible antennas over traditional rigid antennas, and the flexible antennas are gaining wider acceptance over the conventionally rigid materials because they can integrate lightweight, small thickness and low profile designs [103]. Compared to traditional antennas, there is a significant reduction in size and weight of flexible antennas by 50-70%, and this size can be further reduced up to about 90% of its original size for a specific frequency when a flexible substrate, such as a polymer, replaces the hard printed boards [104]. Additionally, the flexible antennas are very robust yet lightweight and can withstand high mechanical strains [105-107].

The following sections provide a tutorial on the flexible antenna structure, bending capabilities and common flexible materials used for flexible electronics.

2.3.1 Transmission Line Equivalent Circuit Model of Flexible antenna

Flexible antennas consist of a conductive layer and dielectric material backing. The basic flexible microstrip patch antenna is a layer of thin conductive strip placed on the top of a flexible substrate, as discussed in Chapter 1. A simple Transmission-Line (TL) model for a microstrip patch antenna is described in [214]. In this section, a co-planar microstrip with aspect ratio W_m/h with an open-end termination where W, L, Y_c and W_m, L_m, Y_{cm} are width, length and characteristic admittances for the microstrip patch and TL, respectively, h is the height of the substrate and Ys is the self-admittance or radiation admittance and represent the open-ended TL of the microstrip antenna. As seen in [214]**Error! Reference source not found.**, the general Transmission-Line model for a microstrip patch antenna consists of a three-port circuit. In the case of the microstrip feed line, the equivalent is represented by an open-ended admittance Y_S.

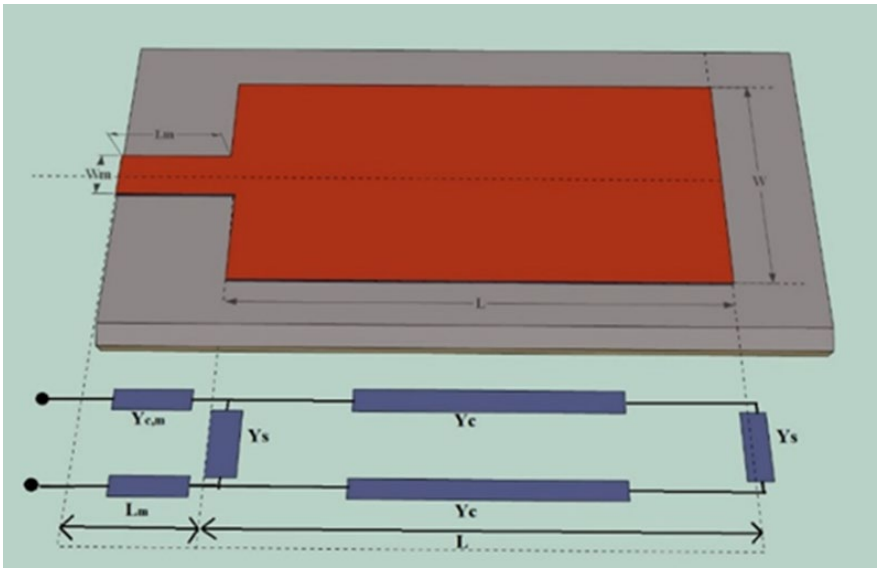

Figure 14. Transmission-Line Model of Flexible Microstrip Antenna

Figure 15 illustrates the bending characteristic of the substrate at various bending levels. The bending of the antenna will change the antenna geometry and shape. Generally, bending causes a change in the effective length, which resultantly introduces a change in the impedance characteristics of the antenna (i.e. mainly capacitance), causing a shift in the resonance frequency as well as a potential shift in the radiation pattern. Discontinuity in the shape or geometry of the antenna mainly leads to a distortion of the electric field between patch and ground plane [215, 216]. The model in Figure 16 describes the bending levels with additional capacitance, where the length L of the patch is broken up into n equal segments. This capacitance C_{bend} is an additional capacitance from the bend of the antenna and varies with the bending curvature, while γ is the propagation constant.

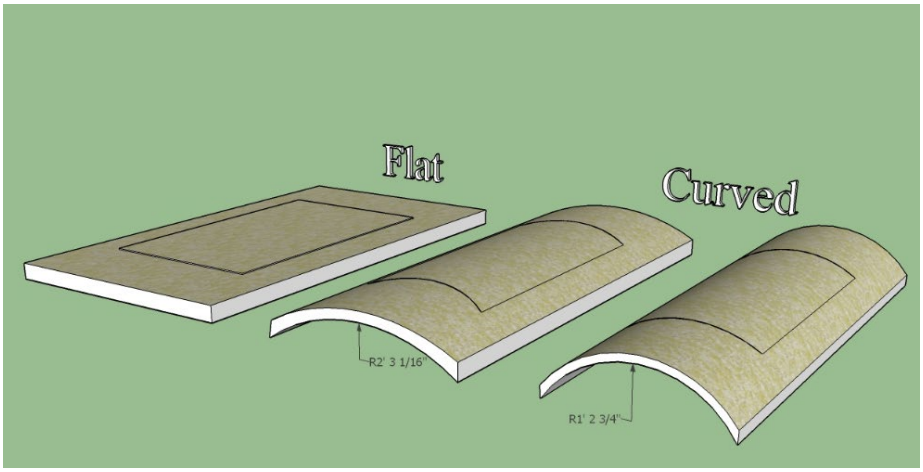

Figure 15. Flexible Substrate of Antenna with Bending

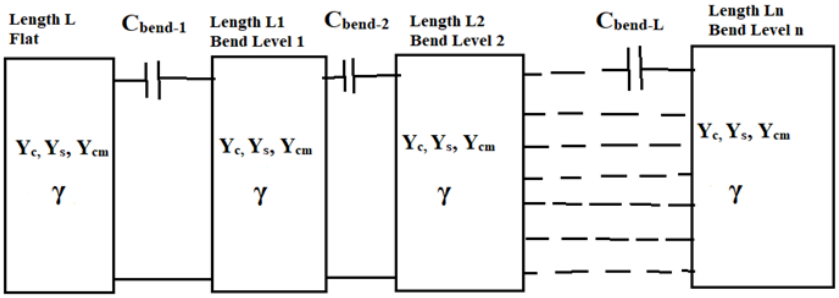

Figure 16. Antenna Equivalent Model for Bent Conditions

2.3.2 Flexibility and Bending Capability of Different Flexible Substrate Antennas

The effects of bending on electromagnetic radiation performance have been addressed in the literature [21, 47, 51, 108]. At its desired frequency, an antenna should, ideally, absorb all available energy when receiving and purge all its energy when transmitting. Under bent and flat conditions, according to [51], very small differences between input return losses are observed. The radiation pattern, the distribution of the electrical field that propagates from the radiating element of the antenna, is an important characteristic which is mostly dependent on its geography. The crumpling of the antenna may adversely affect the radiation pattern. In [21], the authors present a dual-band coplanar waveguide antenna fabricated on the 48 mm x 33 mm polyimide substrate that operates at the frequencies of 2.45 GHz and 5.75 GHz and found that crumpling demonstrated negligible impact on the antenna's performance, particularly regarding resonant frequency and gain, illustrating that up to 5.3 mm crumpling curvature causes only minor changes to the resonant frequency while yielding a high gain. Moreover, this antenna can be integrated into flexible electronic devices that operate in multiple frequency bands.

Different flexible materials that improve a bent antenna's efficiency and radiation characteristics have been considered in various studies and approaches [14]. Essentially, a bent antenna's performance is dependent on the electrical, physical, mechanical and chemical properties of the flexible substrate material. These properties can be adjusted by the combination of different flexible materials [108], [217]. In [47], the proposal of a UWB flexible antenna for flexible applications observed that a flexible substrate should consequently have high flexibility, robustness and exhibit high tolerance against twisting and bending [47]. In the following section, the effects of some flexible materials that have been used extensively for flexible antenna designs are described.

2.3.3 Fabrication Techniques for Flexible Antennas

The fabrication process of a flexible antenna primarily depends on the conductive and substrate material. The properties of conductive and dielectric material are discussed in Chapter 1, section 1-5. While various fabrication techniques, such as line patterning, flexography, screen printing,

photolithography, thermal evaporation, sewing and embroidering, and inkjet printing, are currently available for flexible antennas [101], there are effectively two approaches used to manufacture these flexible antennas. These methods are: i) bonding and merging of components to form a flexible substrate and ii) direct fabrication of the circuit onto the flexible substrate [104]. In the first approach, the entire circuit is fabricated on a carrier substrate like a silicon wafer or glass-plane before being transferred to the substrate in fluidic form [218]. While providing high circuit performance, this technique, also known as a transfer-and-bond approach [104, 219, 220], has a high production cost as its main limitation. Another limitation is evidenced by its small surface area coverage, measured in mol/cm^2. In the second approach, the antenna is directly fabricated onto the substrate by using techniques such as inkjet or screen printing [101]. The direct fabrication approach has two main advantages in that it is easy to implement and is cost-effective [195, 196]. More recent direct fabrication techniques, such as Flexography and Line pattern, are being used to attain high flexibility and robustness for the fabrication of RFID antennas [85, 101]. New process techniques, including the printing of etch mask [221, 222] and the additive printing of active device materials such as the fabrication of transistors using inkjet printing on polymers [223, 224], continue stimulating design ideas for new applications.

There are many applications in which substrate materials are coated or covered by conductive layers such as copper, silicon, silver or aluminium [11, 31, 225, 226]. To ensure a high level of flexibility, these conductive layers or coated fibres should be compatible with the flexible substrate [31]. For instance, in the direct fabrication technique, flexible materials might have a polycrystalline or amorphous nature that must be compatible with the conductive materials [104] as, contrarily, incompatibility may result in damage or failure of the circuit after fabrication. Therefore, the compatibility and nature of its crystalline structure become key factors in governing efficiency.

2.3.4 Materials for Flexible Antennas

Two major structural characteristics form an antenna: a conductor and a dielectric. The essence of this is maintained for both the flexible and conventional antenna. The antenna operates by way of a conductive material used as a radiating element or a ground plane with a dielectric material to act as a substrate that supports the radiating element [101]. The basic parts of a flexible or wearable antenna, discussed in Chapter 1, section 1.4.2, are illustrated in Figure 5Figure 6. The materials that are commonly utilized for the conductive layer of the antennas include pure metals, like copper, aluminium and silver as examples of these intrinsic metals, metals mixed with fabrics like conductive polyester, and conductive inks where silver nanoparticles are an example that allows an antenna to be printed on a substrate. Popular dielectric materials include polymers, paper, foam, plastic, textile fabrics and soft PCB.

Substrate materials are mainly used to support the conductive element of the antenna. Depending on the type of application, it is vital to choose a suitable flexible material as a substrate. In last few decades, various types of flexible materials have been adopted as substrates for antennas to provide

flexibility including textile or fabrics [36, 168, 227-230], paper [231-236] and polymers [14, 16, 20, 21, 31, 47, 49, 51-53, 55-57, 66, 70-74, 78, 79, 98, 108, 109, 115, 171, 201, 237-260]. Non-conductive textiles such as cotton, wool and silk, are combined with metallic conductive fibres to manufacture textile antennas [261, 262]. The relative permittivity of these materials depends on the thickness and the nature of the fabric, whether knitted or woven [114]. Alternatively, the paper is a low cost and environmentally friendly material which can be modified to be fire retardant to make it suitable as a substrate for flexible antennas [236], while polymers are highly resistant nonconductive materials composed of repeated subunits of hydrocarbons known as highly flexible monomers, low cost, with low thickness and a low loss tangent [263]. Flexible polymer materials are used abundantly as substrates for flexible wearable devices.

Several papers providing extensive reviews on wearable antennas have been published [163, 228, 229, 264-268]. In [264-266], antenna design, different materials, limitations concerning antennas and operation near the human body are reviewed. In [267], recent advancements in fabrication techniques for flexible antennas with a section on polymer-based substrate antennas are reviewed. In [163, 228, 229, 268], the review is focused more specifically on textile and fabric-based antennas for wearable application.

The highly resistant nonconductive polymer materials, monomers, are made up of repeated subunits of hydrocarbons and are divided into two categories: Natural and Synthetic. Natural polymers include materials such as Silk, Rubber, Starch and Wool while Synthetic polymers, which are prepared chemically in labs, include materials such as PVC, polystyrene and nylon. This section presents the different types of flexible polymers that have been investigated in the literature with a comparison of the factors that have an impact on the radiation parameters of microstrip patch antennas.

In this study, a complete survey on polymer-based flexible antenna applications for wearable and general IoT applications is presented. To the best of our knowledge, such a comprehensive review does not exist in the published literature to date. Focused on flexible polymer-based antennas and the bending and moulding effects on the radiation characteristics of antennas, five different types of polymer materials, PI, PET, PDMS, PTFE, Rogers RT/ Duroid and LCP, have been chosen that facilitate bending and flexibility as a substrate in an antenna of interest. The reason for choosing these particular materials is the fact that these five polymers, and with some inclusion of other polymers, cover more than 80% of polymer-based FES manufacturing and the design of flexible antenna and RFID tags.

2.3.5 Polyimide (PI)

PI is a thin, flexible and lightweight polymer that is extensively used as the core flexible material for supporting overlays for soft PCB processes, such as PI Films [47, 269]. PIs are widely used in Flexible Printed Circuits (FPC) exhibiting their flexible endurance, excellent tear resistance, low dielectric constant, dissipation factor, moisture absorption and Coefficient of Linear Thermal

Expansion (CLTE). PIs provide numerous advantages over other flexible substrates where, for example, their thinness and flexibility make them useful for small area instalments and creating 3-D static shapes. The PIs are also utilised for making flat panel displays, chip packaging, antenna substrates, mobile phones, Smartwatches, video cameras, and notebook computers [270]. PI is the most prescriptive material for IEEE 802.11 standards because of its high compatibility with signal processing circuits [240].

The Kapton Polyimide is a type of PI which is known for its flexibility and a good balance of physical, chemical and electrical properties. A reliable flexible substrate, Kapton is a low cost, has thermal endurance with mechanical robustness and a low loss factor over a wide range of frequencies [115]. Numerous compact Kapton based flexible antennas are represented with different dimensions, conductive materials and range of frequencies [45-50] as listed in Table 5. In general, Kapton shows good soldering tolerance for flexible antenna fabrication as it withstands high temperature, which is also a good feature for the thermal annealing of inkjet antenna printing [101]. The robustness and bending efficiency of Kapton PIs have been subjected to a curvature test under the flexibility and bendability tests have been performed, and the effects of deformation (radii or curvature) on an antenna and its radiation characteristics evaluated [16, 21, 47, 51, 52, 115].

Table 4. Comparison of General Requirements of Different Flexible Antennas Substrates [271-282]

Substrate	Model / Version	Physical/Mechanical Properties			Electrical Properties			Thermal/Chemical Properties			Comparative Analysis				
		Density (g/cc)	Tensile Strength X-Direction at 23C (Kpsi)	Tensile Modulus X-direction at 23C (Kpsi)	Dielectric Constants 100Hz-1MHz	Dielectric Strength (V/mil)	Dissipation Factor Tanσ at 100Hz-1MHz	Coefficient of Linear Thermal Expansion CLTE -15C to 300C (ppm/C)	Moist Absorption (%) at 23 C	Shrinkage (%) 30 min, 150C	Deformability	Thermal Stability	Moist sustainability	Electrical Stability	Fabrication Complexity
PI	Kapton HN, FN, HPP-ST	1.42 to 1.53 High	22 to 33 High	330 to 400 High	3.4 to 3.9 High	3500 to 7000 High	0.0013 to 0.0040 Low	20 Low	1.3 to 2.5 High	0.03 to 1.25 Low	Low	High	Low	High	Simple
PET	Melinex 401 Polyester	1.3 to 1.4 High	25 to 40 High	280 to 580 High	3.0 High	4000 to 4500 High	0.002 Low	19 to 20 Low	0.1 to 0.7 Low	0.5 to 1.1 Low	Low	High	High	High	Moderate

PDMS	Sylgard 184	0.97 Low	0.25 to 1.3 Low	0.522 to 0.126 Low	2.3 to 2.8 Low	342 to 551 Low	0.0015 to 0.0035 Low	340 High	0.1 Low	0.03 to 2.7 High	High	Low	High	Low	Moderate
PTFE	Teflon	2.1 to 2.25 High	3.9 to 4.1 Low	50 to 90 Low	2.1 to 2.72 Low	285 Low	0.0002 to 0.0025 Low	250 to 275 High	0 to 0.05 Low	1.5 to 3.0 High	Low	Low	High	Low	Complex
	Rogers Laminate RO3000, RO4000 RT/Duroid	2.0 to 3.0 High	20.3 to 29.5 High	65 to 300 High	3.0 to 10.2 High	780 Low	0.0004 to 0.0035 Low	10 To 17 Low	0.02 to 0.05 Low	0.05 to 0.1 Low	Low	High	High	Low	Simple/Printable
LCP	Rogers ULTRALAM L3000 LCP	1.4 High	29.0 High	327 High	2.9 to 3.14 High	3500 High	0.0025 Low	17 Low	0.04 Low	0.03 Low	Low	High	High	High	Complex/Non printable

Designs with Kapton based flexible antennas have been substantially generated. A compact UWB polyimide based flexible antenna is presented in [47] which, advantageously, shows very small susceptibility to deformation in terms of impedance matching and return loss. In [16], a polyimide substrate antenna under convex and concave bending presented no significant changes in the radiation pattern and frequency shift. Coating with different materials has also been used to alter its physical or electrical characteristics where, for example, in [51], Kapton is coated with parylene-C, and no significant change in return loss and radiation energy when the antenna is subjected to bending is observed and similar results were observed in [21] where the Kapton substrate is doped with conductive polymer Polyaniline (PANI) and undergoes vigorous crumpling. Two robust and flexible compact Kapton PI based antennas are designed in [45]: the first antenna has a dual-band while the second is designed for a single band. Both antennas have good radiation characteristics and can be used for flexible displays with WLAN and Bluetooth connectivity. In [98], a flexible UWB Kapton-based 16 antenna array is pioneeringly proposed to detect breast cancer. The antenna was fabricated in a flexible bra and operated in the frequency range of 2-4GHz which is within the bandwidth requirements used by Microwave Radar Imaging (MWI) for breast cancer. A wearable compact Kapton based antenna is designed in [52]. The authors reported that after the antenna is deformed, it exhibits only minor changes in resonance frequency and return loss.

2.3.6 Polyethylene Terephthalate (PET)

Polyethylene Terephthalate (PET) film is a flexible, strong and somewhat rigid dimensionally stable thermoplastic polymer resin, PET film is commonly known as Polyester. PET exists in both transparent (amorphous) and semi-crystalline form in accordance with its processing and thermal history [283]. An interesting material due to its thermal, electrical and moist stability and flexibility, PET has tremendous chemical resistive and physical properties [54, 282].

PET film has been used extensively in applications, such as medical packaging, tape backing, printing films and FPC, where substrate flexibility and transparency are required, and is well known as the substrate for microstrip antennas, flexible chipped and chipless RFID tags, fabrics, and a wide range of textiles and optoelectronics [22, 55-57, 239, 252, 253, 284].

In [56], a chipless RFID tag is designed with the FSS method and fabricated on PET and paper substrate. Dupont manufactured “Melinex 401” PET film was used in this design where an octagonal structure of silver paste was fabricated on it. The RCS shows different combinations of bit’s 0’s and 1’s transmitted and received successfully from the assembly of two horn antennas. The tag is bent for different radii with results showing that there is only a minor change in the RCS pattern, hence, it successfully achieved encoded information. In [1], our new Bow-Tie design was designed, printed and compared to an octagonal-shaped tag that was published in the [56]. Both tags were designed using CST studio and fabricated on low-cost flexible PET substrate.

In [58], a Substrate Integrated Waveguide (SIW) flexible antenna is designed and fabricated on a PET substrate. The radiation characteristics of the antenna, measured for different bending levels, demonstrated, for the first time, PET substrate compatibility with SIW technology. The results show the applicability of SIW technology for low-cost wearable IoT.

A Millimeter-Wave (MMW) flexible antenna on the PET substrate for 5G applications is reported in [106]. The Coplanar Waveguide (CPW) feed antenna, which is also applicable to non-polar surfaces and casual clothing, operates at Ka-band and promises a high gain with, for example, 8.2 dBi. In [59], a dual-band flexible reconfigurable antenna is fabricated on the PET polymer substrate where the proposed antenna can operate either on single band at 2.36 GHz or dual-band with 3.64 GHz of the resonant frequency. The antenna demonstrates good radiation characteristics on being curved for both On/Off states of PIN-diode.

2.3.7 Polydimethylsiloxane (PDMS)

Commonly known as Silicon, PDMS is an interesting polymer because of its softness and flexibility. PDMS has excellent rheological properties and is a flow-able, water-resistant, transparent and low-cost polymer with many attractive physical and chemical properties. Providing high deformability, flexible surface chemistry and low electrical conductivity [217, 278, 285], it is chemically inert due to its homogeneous and isotropic properties [286]. Indeed, PDMS has good chemical stability and a low dielectric constant between 2.3 to 2.8, see Table 4. The

aforementioned advantages and excellent qualities have made PDMS a good substrate choice for stretchable and flexible antennas [61-63] for which it has, consequently, been used extensively as a substrate in electronic devices and microsystem fabrication [14].

PDMS properties can be changed by doping them with other materials. More specifically, the mechanical, electrical properties and flexibility of a PDMS substrate can be changed by adding materials of different dielectric constants [108]. Additionally, PDMS, being stable at high temperatures, which are required for the processing of biological materials (40-95^{o} C), is attractive for applications requiring gradients [287-289]. Nevertheless, drawbacks associated with PDMS include fabrication complexity and a comparatively high cost against other flexible materials [14, 31, 64, 65].

A commonly used PDMS is the Sylgard 184 Silicone Elastomer, a transparent polymer with good flame resistance, low CLTE and dissipation factor, high deformability and moisture stability but low electrical and thermal stability. PDMS are extensively used in microfluidic systems, solar cells, industrial control systems, sensors, amplifiers, high voltage resistor packs and as a substrate in flexible electronics [278]. The general properties of Sylgard 184 are listed in Table 4.

PDMS-based flexible antenna designs have been published in numerous studies. The example flexible conformal antenna presented in [31] reports an embroidered conductive fibre material that is embedded over a ceramic PDMS substrate to get a high level of flexibility and stretchability. In [108], a WBAN PDMS-based flexible antenna is shown to experience a very small frequency shift of resonant frequency after bending with a high level of robustness and, in [66], a flexible folded dipole slot antenna is presented over a PDMS substrate. The proposed dipole slot antenna design exhibits good flexibility over bending and minor effects on return losses.

2.3.8 Polytetrafluoroethylene (PTFE)

PTFE is a common polymer that has very interesting properties. PTFE is chemically stable, water-resistant and can withstand an astonishing degree of contrast in temperature with a low of -200º C and a high of up to 250º C [277]. Resultantly difficult to melt even at high temperature, it is very dense and, while it is thermally stable compared to other types of plastics, PTFE has low mechanical characteristics [276]. The main advantage of PTFE rests on its versatility, consequently being suitable for many applications where it is widely used in engineering and manufacturing and its moisture and oil repulsive nature, which mean that PTFE is intensively utilised for storing corrosive materials [277, 290]. The mechanical properties of PTFE can be modified by adding glass, graphite and carbon and the doped PTFE might, for example, be able to maintain its high temperature and chemical characteristics [276].

Teflon is a commercially available PTFE polymer that has a combination of good mechanical, electrical, thermal and anti-friction properties. Teflon is a well-known flexible material because of its thermal stability and resistance to change in temperature, with a very high melting point where its functionalities continue over 260º C [275], as well as its resistance to corrosion and stable

dielectric constant over a wide range of frequencies [247]. Its properties serve to provide flexibility in antenna designs with PTFE Teflon aptly utilised in the RFID tag antenna designs. A brief comparison of PTFE properties with other materials is shown in Table 4.

Numerous research articles for antenna designs with a PTFE-based substrate have been published during the last few decades. In [70], a PTFE-based slot antenna made of conductive textile is presented were performing a bending analysis on the antenna over a spherical cylinder demonstrated that the antenna design exhibited high flexibility with a very small shift in the central frequency. Later, in [121], reflection characteristics are observed and measured in flat and spherically bent conditions by a flexible slot antenna over both PTFE and Polyester substrates [71] with a good agreement of flat and flex design of the proposed antenna being reported with evidence that, compared to antennas with a polyester-based substrate, the PTFE-based antennas have improved radiation characteristics.

Rogers laminate, a type of PTFE commercially available in the form of sheets, is widely used these days and, although having similar mechanical properties, differs from typical PTFE material with its dielectric constants. Its thermally stable dielectric constants with an expansion coefficient that is quite similar to copper, some prominent qualities include easy fabrication on PCBs, robustness, and excellent dimensional stability with typical etch shrinking [271-273]. Rogers Duroid substrates are another type of PTFE substrate that exhibits excellent matching and controlled impedance transmission over microwave circuits. Compared to natural PTFE, this material is more rigid but very stable at high temperatures [271]. PTFE materials such as Rogers Laminates and Duroids are commercially available and have the lowest electrical loss for processed PTFE, uniform electrical properties over frequency, excellent chemical resistance and low moisture absorption [274].

In [73], the proposal of a flexible Bow-Tie antenna designed with the Roger RO3003 substrate determined that the radiation patterns and return losses of the designed antenna were independent of the radius of curvature when the bending is larger than the antenna's dimensions. The effects of bending the CPW-fed flexible Bow-Tie slot antenna are demonstrated in [72] to observe that, after attempting different bending levels of the antenna, there were only minor changes in resonant frequency and radiation patterns of the proposed antenna. This means that the bending has almost no effect on the proposed CPW-fed flexible Bow-Tie slot antenna design.

2.3.9 Liquid Crystal Polymers (LCP)

LCP, a special class of crystalline Aromatic Polyester based on monomers [291], consists of a series of thermoplastics that have a unique set of properties, such as high heat resistance and tolerance, inherent flame redundancy and good weather sustainability. These LCPs have excellent chemical properties like their high anisotropy, which means flexibility, and their thermal expansion and stiffness are high in one direction. With good cycle repeatability due to their high melt flow [291, 292], they also exhibit tremendous mechanical properties, such as high strength,

modulus of elasticity and toughness [292]. The mechanical strength and elastic modulus of LCP substrates are equal to or above that of other common plastics. They have a dense crystalline structure, an excellent electrical insulator and are resistant to arc at the flame of high temperature [293]. Table 4 shows a comparison of LCP general properties with other compatible flexible substrates used for antenna designs. Unfortunately, LCPs are expensive and their high anisotropy causes weakness at weld lines where the material meets different molecules [292]. Another disadvantage of the LCPs is that they are difficult to fabricate because their density denotes that they have small spaces, as in little gaps in their crystal composition, such that processes like traditional etching which fabricate over crystal become difficult [74].

Despite the aforementioned LCP limitations, they are widely used as flexible substrates and have become one of the most desirable organic materials for high-frequency applications as they can withstand rises in operational frequencies and are very suitable for RFID antennas [75-77]. A design of series-fed two dipole antennas on the LCP substrate is presented in [74] where the bending effects on the proposed antennas are tested. The results demonstrated that bending has a minor effect on VSWR but evidenced decreased gain and directivity of the proposed antenna. In [8], a flexible dual-band LCP antenna is presented in [78] where radiation characteristics of the proposed antenna are measured at different bending angles and revealed that reflections are almost the same at a bending angle of 60 degrees as compared to the flat condition of the antenna. A Circularly Polarized (CP) flexible CPW fed antenna is presented on the LCP substrate [79]. The antenna is tested at various bending angles: 30^{o}, 60 ^{o}, 90^{o}, and 120^{o}, at 3.5 GHz and 5.8 GHz frequencies with reflection coefficients, at the different angles, showing a good correlation between simulated and measured values with just a slight shift in resonant frequency towards the lower component for bending angles at 60 ^{o} and 90^{o}. In [80], a CPW fed antenna is fabricated on an LCP substrate for WiMAX (3.5 GHz) and WLAN (5.8 GHz) applications and indicated good agreement of results for various degrees of curvature up to 120 degrees.

2.4 Comparative Analysis of Suitable Polymer Substrates for Flexible Antennas and RFID Tags

Table 2-5 depicts a comprehensive comparison between the antennas which are constructed from dielectric polymers: PI, PET, PDMS, PTFE and LCPs. This section provides an overview of these polymers and the variants which are widely used as flexible substrates for antennas. All these materials have proven bending capabilities and the table serves to present a range of experimental verification with measured and simulated results that have been reported in different articles. Kapton, a variant of PI which has high thermal and electrical stability, is a very common and widely used polyimide substrate for antennas. Sylgard 184, which has high moisture stability and bending capabilities, is commercially used as a flexible substrate. Teflon, Rogers Laminates and RT/Duroid are common commercially available PTFE's that possess good thermal and electrical stability. Compared to all of the other materials reported, Rogers UTRALAM is classified as the most electrically and thermally stable LCP and has the additional features of being oil and water

repellent.

Melinex 401 CW is a slippery surfaced, transparent and highly dense film that has many outstanding features over the other available substrate films: it has a high dielectric constant and tensile strength and a low dissipation factor and its temperature Co-efficient of Resistance (CTE), and, therefore, exhibits high thermal and electrical stability and low shrinking capabilities, as shown in Table 4. It does, however, have low deformability and moisture absorption capability compared to other substrates, making it less efficient for highly flexible applications.

As Sylgard 184 is an antenna substrate with low density ($\leq$ 1 g/cc) and possesses high deformability at standard temperatures, whereas the tensile strength of Kapton, Rogers Laminates and LCP are high ($\geq$ 5 Kpsi), comparatively, Sylgard 184 is more thermally and electrically stable. Indeed, both Teflon and Sylgard 184 are classified with a low dielectric constant ($\leq$ 3 at 100 Hz – 1 MHz) and low dielectric strength ($\leq$ 1000 v/mil) while possessing high radiation characteristics and, as conveyed in Table 4, high deformability can indeed be achieved for low density and tensile strength. The low CLTE ($\leq$ 30 ppm/C) of substrate materials such as PI, PTFE and LCP serve to make them more thermally stable and, furthermore, it is observed from Table 4 that all the substrates which have very low dissipation factors or loss tangents ($\tan\sigma \leq 0.01$ at 100 Hz – 1 MHz) lead towards electrical stability. The low values of moisture absorption, usually $\leq$ 0.1%, define the moisture stability of materials whereby, while PTFE and LCPs are highly moisture resistant, they are, contrastingly, difficult to fabricate as compared to other materials.

Table 5. Comparison of Curvature Effects on Radiation of Different Flexible Antenna Substrates

		Substrate	Conductive material	Ground Plane	Substrate ϵ_r	Substrate tanσ	Substrate Dimension (mm)	Substrate Thickness (μm)	Bending Level Curvature (mm)	Band/ Frequency F_o (GHz)	Return Loss $S_{1,1}$ Radar Cross Section RCS (dB)	Gain (dBi)	Applications
Polymer Substrate Materials	Polyimides (PI) [16, 21, 47, 51, 52, 115]	Kapton 200HN (2 mil 50 μm)	Silver Nano Particles	AMC	3.5	0.002	45x30	50.8	Flat	2.45	-29	NA	ISM
									r_1 = 27 mm	2.35	-30		
									r_2 = 13 mm	2.30	-28		
		Kapton 500HN (5 mil 125μm)	Silver Nano Particles	CPW Curved shape	3.5	0.0026	70x70	110	Convex / Concave	Multiband	Gain dBi Convex	Gain dBi Concave	WLAN ISM Bluetooth LTE WiMAX
									r_1 = 78 mm / r_1 = 78 mm	Bands	r_1 / r_2	r_1 / r_2	
									r_2 = 59 mm / r_2 = 59 mm	1) 0.87- 1.0	-1.2 / -1.2	-1.1 / -1.1	
									Unbent	2) 1.4- 2.2	0.9 / 1.0	0.9 / 0.9	
										3) 2.5- 2.7	2.3 / 2.5	2.1 / 2.2	
		Kapton 200HN (2 mil 50 μm)	Silver Nano Particles	NA	3.4	0.002	47x33	50.8	Flat	ISM/UWB 2.2–14.3	S_{11} (dB)		ISM UWB
											Flat	r_1 / r_2	
									r_1 = 10 mm	2.5-5.5	-23	-24 / -22	
										4.9-8.6	-37	-29 / -27	
									r_2 = 8 mm	10-14.3	-23	-24 / -27	
		Kapton 500HN + Parylene-C	Copper	Copper	3.5	0.0008	32x18	127	Flat	9 GHz	-35 dB	NA	WLAN UWB
					2.95			10	r = 40 mm		-32.5 dB		
		Kapton 500HN	PANI + MWCNT	NA	3.48	0.0026	48x33	130	Unrumpled	4.2	-17	NA	PCS
							35x33 (crump)		Crumpled at r = 5.5 mm	1.9, 5.7	-18, -26		WLAN
				NA	3.4	0.0020	30x33	50.8	Flat	8.8	-23	NA	UWB

		Kapton 200HN (2 mil 50µm)	Silver Nano Particles						r_1 = 9 mm	7.7	-26			
									r_2 = 7 mm	8.2	-24			
	Polyethylene Terephthalate (PET) [56, 59]	PET Polymer	Copper	Copper	3.0	0.008	59x4.75	100	Flat (Switch: OFF)	2.35, 3.61	-15, -12.5	NA		Dual Band
									r = 25 mm (Switch: OFF)	2.34, 3.64	-18, -15			
									Flat (Switch: ON)	2.41	-16			Single Band
									r = 25 mm (Switch: ON)	2.44	-21			
		Melinex CW 401	Micro-silver particles	NA	3.0	0.002	52x82	50	Flat	4.2, 5.3, 6.4, 7.5, 8.8	-28	NA		RFID RCS UWB
									r = 100 mm	4.4, 5.4, 6.5, 7.6, 8.9	-47			
									r = 60 mm	4.4, 5.3, 6.5, 7.4, 8.8	-49			
									r = 30 mm	4.5, 5.6, 6.7, 7.4, 9.6	-50			
									r = 16 mm	3.6, 4.3, 6.5, 7.6, 9.0	-50			
	Polydimethylsiloxane (PDMS) [14, 66, 108, 241]	PDMS Sylgard184	Copper	Copper	2.65	0.02	46.4x20	2000	Flat	6.35	-36 dB	NA		Wire-Less
		SU-8			2.9	0.04			Curvature K = 66.91	6.0	-17 dB			
		PDMS Sylgard184	Fibre Tissue	Fibre Tissue	2.85	0.02	50x40	2000	Flat	7.0	1.36	-26	-30	4.3	4.5	UWB
									r_1 =50 mm	8.0	21.0	-19	-17	3.9	3.7	
									r_2 = 25 mm	7.8	18.2	-28	-23	3.2	3.3	
		PDMS Sylgard184	Copper	NA	2.65	0.02	130x80	2000	Flat	381		-15		NA		TETRAPOL (385MHz)
									r = 230 mm	383		-18				
		PDMS	Nickel Gold Copper	NA	2.2	0.013	----------	5000	Flat	2.22		-28		NA		ISM Band
									r_1 = 80 mm	2.24		-43				
									r_2 = 40 mm	2.39		-34				
	Polytetrafloureothene (PTFE) [70, 71, 247]	PTFE	Copper	Copper	2.2	0.0009	25x50	127	Flat	3.5	13.3	-21	-19.5	NA		WiMAX X-Band
									r_1 = 50 mm	3.7	13.4	-16	-17.5			
									r_2 = 40 mm	3.9	13.4	-15	-18			
		PTFE	Conductive Textile	Conductive Textile	2.1	0.002	95x90	500	Flat	2.25		-26		NA		ISM Wearable ES
									r_1 = 200 mm	2.16		-38				
									r_2 = 150 mm	2.75		-13				

		PTFE	Conductive Textile	Conductive Textile	2.1	0.0002	95x90 offset of slot 28.6 and stub 25.0	500	Flat	2.5	BW 0.23	-15		NA	ISM Band
									r_1 = 225 mm	2.25	No BW	Below -10			
									r_2 = 150 mm	2.25	BW 0.05	-11			
	Rogers PTFE Laminates [294]	RO4003C	Copper	Copper	3.38	0.0027	80x60	200	Flat	3.0	3.8	-17	-20	NA	WLAN WiMAX
									r_1 = 100 mm	2.90	3.7	-18	-19		
									r_2 = 70 mm	2.95	7.7	-17	-16		
		RT/duroid 5880	Copper	Copper	2.20	0.0009	39x39	50.8	Flat	2.40-2.48 BW		-18		NA	ISM BandA
									r_1 = 60 mm	2.361-2.534		-17.9			
									r_2 = 40 mm	2.382-2.552		-17.7			
									r_3 = 20 mm	2.367-2.543		17.3			
		RO3003	Aluminium Silicon Nitride	NA	3.0	0.0010	-------	128	Flat	7.24		-23.5		NA	UWB
									r_1 = 40 mm	7.23		-18			
									r_2 = 20 mm	7.25		-18.5			
	Liquid Crystal Polymers (LCP) [74, 78, 109]	Rogers ULTRAL AM 3850	Silver Nano Particles	Copper	2.9	0.0025	13.2x4.2	100	Flat	29		NA		6.4	Wireless Devices
									r_1 = 6 mm	28				5	
									r_2 = 4 mm	28				4.8	
		LCP	Copper	Copper	2.9	0.002	26x16	50	Flat	6.4	7.4	-22	-20	NA	UWB Wearable applications
									15 degree (min. bent)	6.35	7.6	-20	-23		
									60 degree (max. bent)	6.4	7.8	-21	-20		
		LCP	Copper	Copper	2.9	0.002	19x50	100	Flat	5.20		-24		NA	ISM RFID UWB
									30 degree (min. bent)	5.20		-24			
									60 degree (max. bent)	5.25		-25			

2.5 Deformational or Bending Effects of Flexible Polymer Substrates on Antenna Radiation Characteristics

Table 5 is a major collection of the most significant and recent experiments on bending characteristics of these five polymer materials and antennas. In total, 50 experimental works have been analysed on flexible antennas with 20 experimental works selected for qualitative analysis to give the reader a comprehensive overview of the entire area for the range of different frequencies and applications. These experiments are carried out in different environment and with different fabrication and experimental procedures. However, comprehensive of the limitations, our experiments are grouped in the same frequency ranges with almost the same physical properties, see section 2.7. In addition, Table 5 describes the reflection coefficients, gain and the shifts in the resonant frequencies at various bending states for flexible polymer-based substrate antennas from the literature. In this table, polymers such as PI, PET, PTFE, PDMS and LCP with some variants are analysed from the previous articles and a comparative analysis of the radiation characteristics for specific applications and impacts of bending on return loss, resonant frequency and the gain of the antenna are also provided.

As a substrate of flexible antennas, the most extensively utilised polymer amongst these five polymers is PI. Kapton is a commercially available variant of PI. The choice of the polyimide Kapton as a substrate of the antenna is owed to its good physical balance, chemical, electrical properties and high thermal stability. Having the dimensions of 45 mm x 30 mm, 47 mm x 33 mm and 30 mm x 33 mm, Kapton 200HN, with a 50.8-µm thickness, is used as a substrate with silver nanoparticles as the conductive material in [115], [47] and [52]. Through bending analysis at the curvature of 13mm, [115] observes that the shift in resonant frequency is 80MHz, which is 0.36% of the resonant frequency of 2.45GHz, with a return loss of ±1dB. In [47], the highest 0.4% shift in the resonant frequency compared to the flat case is observed towards the first resonance frequency which is less than 50 MHz. In [52], Kapton 200HN is used as a substrate with silver nanoparticles as a conductor, where the highest frequency shift of 1.1 GHz is obtained when the antenna is curved to 9 mm with a smaller dimension and return loss increase by -3 dB due to an increase in directivity at 8.8 GHz. Similarly, Kapton 500HN, with an increased thickness of about 130 µm, is used in various flexible antennas as it has a higher dissipation factor and less resistivity compared to Kapton 200HN [280]. A compact Kapton based inkjet-Printed Multiband flexible antenna is reported in [16] on which convex and concave bending performed at a maximum level of 59 mm. The antenna covers four-wide frequency bands centred at 1.2, 2.0, 2.6 and 3.4 GHz. In convex bending, no significant shift of frequency is observed but in concave bending, a 3% frequency shift is detected towards the lower end with all frequency bands. At higher central frequencies, the gain is increased with convex bending of up to 59 mm due to the increase in directivity when the antenna undergoes this higher curvature. A compact flexible antenna for WLAN and upper UWB applications is presented in [51] in which Kapton 500HN is coated with Parylene-C to increase flexibility without much effect on return losses and gain. Wearable flexible antennas may undergo crumpling, which can affect their

radiation performance. In this study, Kapton 500HN is shown to be an efficient polymer which withstands a high crumpling level of up to 5.5mm. A Dual-Band Elliptical Polymer antenna that uses a flexible Kapton substrate doped with conductive PDMS is presented by Hamouda et al [21] who reported that the crumpling has an effect on the proposed antenna's performance at a high operating frequency of 5.8GHz with a maximum gain of 2.48dBi.

PET film has extensively been used in applications where flexibility and transparency of the substrate are required. In [59], a reconfigurable folded slot antennas antenna is fabricated on the PET substrate and its radiation characteristics are observed at ON and OFF states. At the ON state, with the antenna as a single band at 2.42 GHz with a curvature of 25 mm, its resonant frequency only shifts by 0.1 %. Similarly, in [56], the RCS of an RFID tag fabricated on the PET substrate over various bending states successfully achieves a read range of 3.5 m for a working bent tag up to 16mm. These results are graphically analysed in the discussion part of this paper.

PDMS is a well-known polymer because of its tremendous rheological properties as a flow-able, water-resistant, transparent and low-cost polymer with many attractive physical and chemical properties. The PDMS polymer Sylgard 184, because of its excellent bending features, is used as a flexible substrate in various proposed designs. It is used as a substrate with 2-mm thickness and dimensions of 50 mm x 40 mm (fibre tissue) in [241] and 130 mm x 80 mm (patch) in [108]. As a fibre tissue, the proposed Transparent Flexible Polymer Fabric Tissue Antenna in [241], undergoes bending level maximum at 25 mm with measured results showing that the resonant frequencies are shifted towards higher components about 0.085% of operating frequency at 7 GHz and 0.25% of operating frequency at 17.5 GHz. While the return losses fluctuate because of the change in directivity when the antenna is in bending state, for flexible W-BAN antennas, the frequency shift is negligible for all curvatures up to 230 mm [108], likely due to the small bending curvature.

PTFE polymers, like Teflon and Rogers laminates, are mostly used in flexible electronics with limited use in flexible antenna designs due to the PTFE having relatively low deformability and even less electrical stability to bend, as shown in Table 4. In [71], a comparative analysis of PTFE substrate antennas with polyester fabric substrate antennas is subjected to curvature. A significant effect on the antenna performance is observed at the bending level of 225 mm on the PTFE substrate antenna and causes a minor shift in resonant frequency. However, for the same PTFE substrate with the same dimension of 95 mm x 90 mm but with a thickness of 500 µm instead of 127 µm, evidences the central frequency being shifted by 84 MHz towards a lower frequency at 200 mm radial curvature and leads to a reduction in the bandwidth from 239 MHz to 162 MHz and an increase of the reflection coefficient S_{11} to -10 dB [70].

LCP is a highly anisotropic special class of crystalline polymer that is based on monomers. It has good chemical properties which are suitable for various flexible antenna applications and, in [78], a dual-band antenna is fabricated on LCP substrate. The fully flexible antennas are developed to operate at 2.45GHz and 5.8 GHz frequencies, showing identical reflections for the bend up to 60 degrees or 3.5 cm of a radius of curvature.

2.6 Discussion

To investigate the bending behaviour of flexible antennas, some challenges and limitations need to be considered, such as substrate thickness, antenna dimensions, feeding techniques, physical properties of materials and most importantly the frequency range for which the antenna is designed. However, our categorisation of the flexible antennas, based on the five main polymer materials PI, PET, PDMS, PTFE and LCP in recent notable literature, groups the polymers for their similarities in physical properties and comparable dimensions. Furthermore, the decision to divide them into three specific ranges of frequencies 2.2 to 2.5 GHz, 2.5 to 5.0 GHz, and greater than 5.0 GHz permit the antennas to be investigated while avoiding abrupt changes on radiation characteristics of the antennas which could make our analysis unrealistic. Although, there is a recognisable impact from the changes in frequency for different antennas with the same substrate material, not being adequate for a specific frequency range provides us with further scope for investigating these for such results and is recommended for a future endeavour.

Table 5 shows the effect on performance that the bending of antennas has when using different substrate materials. The comparison of the bending effects on resonant Frequency Shifts (FS) is registered as a percentage (%) and signal strength in terms of reflection coefficient (S_{11}) have been analysed and discussed in this section. In order to understand the behaviours of flexible polymers in terms of FS, the operating frequency bands are divided into three ranges for different applications, e.g., 2.2-2.5 GHz, 2.5-5.0 GHz and 5.0-30 GHz with bending ranging from 200 to 6 mm; see Figure 2-7. (a), (b) and (c).

2.6.1 Effect of Bending on Resonant Frequency

Comparing the entries in Table 5, it can be deduced that the effects of bending or curvature of different polymer substrates have a different impact on FS at different levels of bending. The resonant frequency and the return loss are analysed for polymer-based antennas for a curvature up to 6 mm. Figure 17 (a), (b) and (c) present the average shifts from the central Frequency (F) ranging from 2.2 GHz up to 11 GHz.

Figure 17 (a) shows the average shifts from the central frequencies for the band 2.2-2.5 GHz, which is the commonly used frequency band for ISM applications, such as Wi-Fi and Bluetooth. In this context, PI is less affected, with an average of only 2.93% of this central frequency with the Highest Shift (HS) of 6.52% and Lowest Shift (LS) of 0.45%, by bending from 200 mm to 6 mm curvature Radius (R). In contrast, the PTFE based antennas are highly impacted by bending with an average frequency shift of about 11.7% (HS: 18.88%, LS: 14.14%).

Alternatively, as illustrated in Figure 17(b), for the operating frequency range of 2.5-5.0 GHz, which lies in X-Band and is suitable for WiMAX applications, PTFE based flexible antennas have proven to be more efficient by providing an average frequency shift of approximately 4% (HS: 10.25%, LS: 0.56%); whereas, as depicted in Figure 17(c), the PTFE and LCPs are very efficient in this higher

range of frequencies, from 5.0-30 GHz, where smaller shift in frequency are observed with about 0.138% and 1.57% on average respectively.

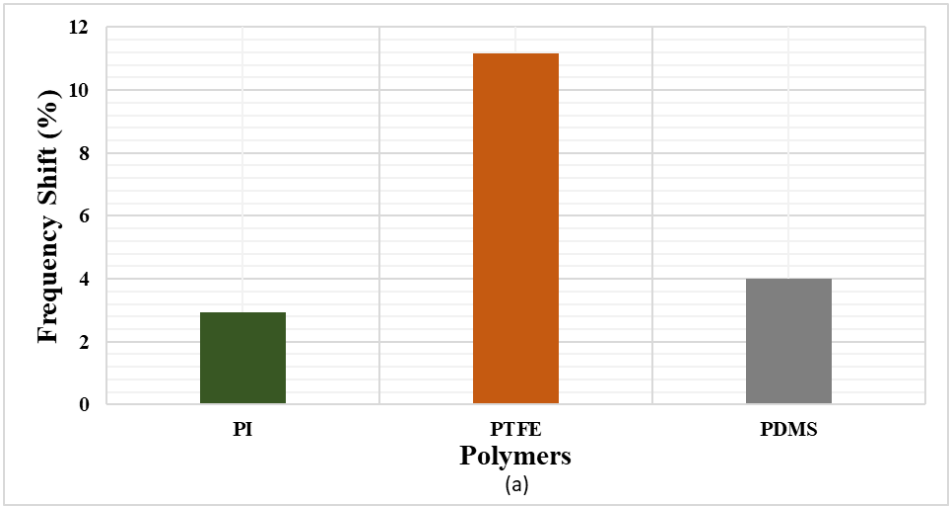

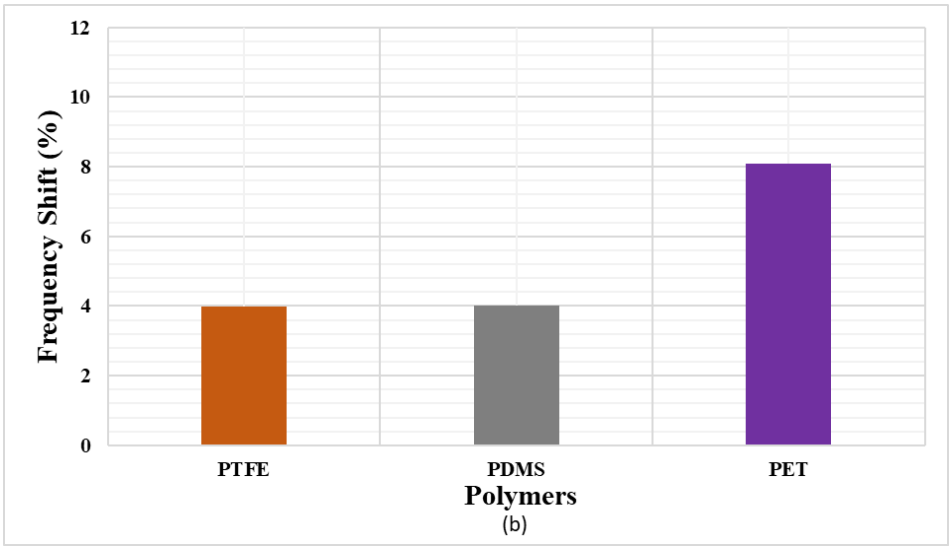

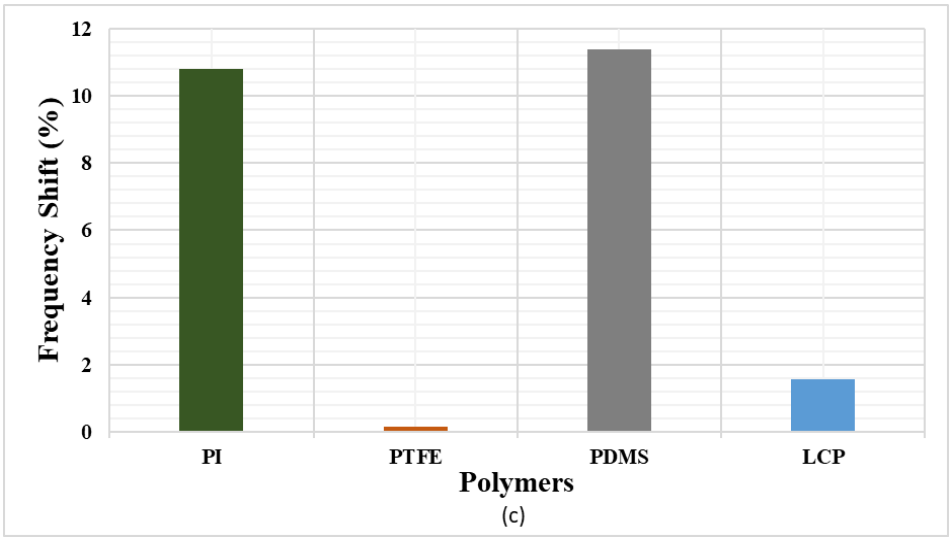

Figure 17. Average Frequency Shift in Central Frequency for (a) PI, PDMS and PTFE at 2.2-2.5 GHz, (b) PTFE, PDMS and PET at 2.5-5.0 GHz, (c) PI, PTFE, PDMS and LCP at greater than 5 GHz

2.6.2 Effect of Bending on Reflection Co-efficient (S_{11})

One of the impacts of bending on an antenna's performance is the reflection, or scattering, of waves and resultant impedance mismatch. While an impedance miss-match should occur when a flexible antenna is bent and crumpled, this simultaneously leads to a change in signal strength, which often decreases [295], although sometimes increases, after bending the antenna. Figure2-8 (a), (b) and (c) represents the twisting effects of an antenna on S_{11}.

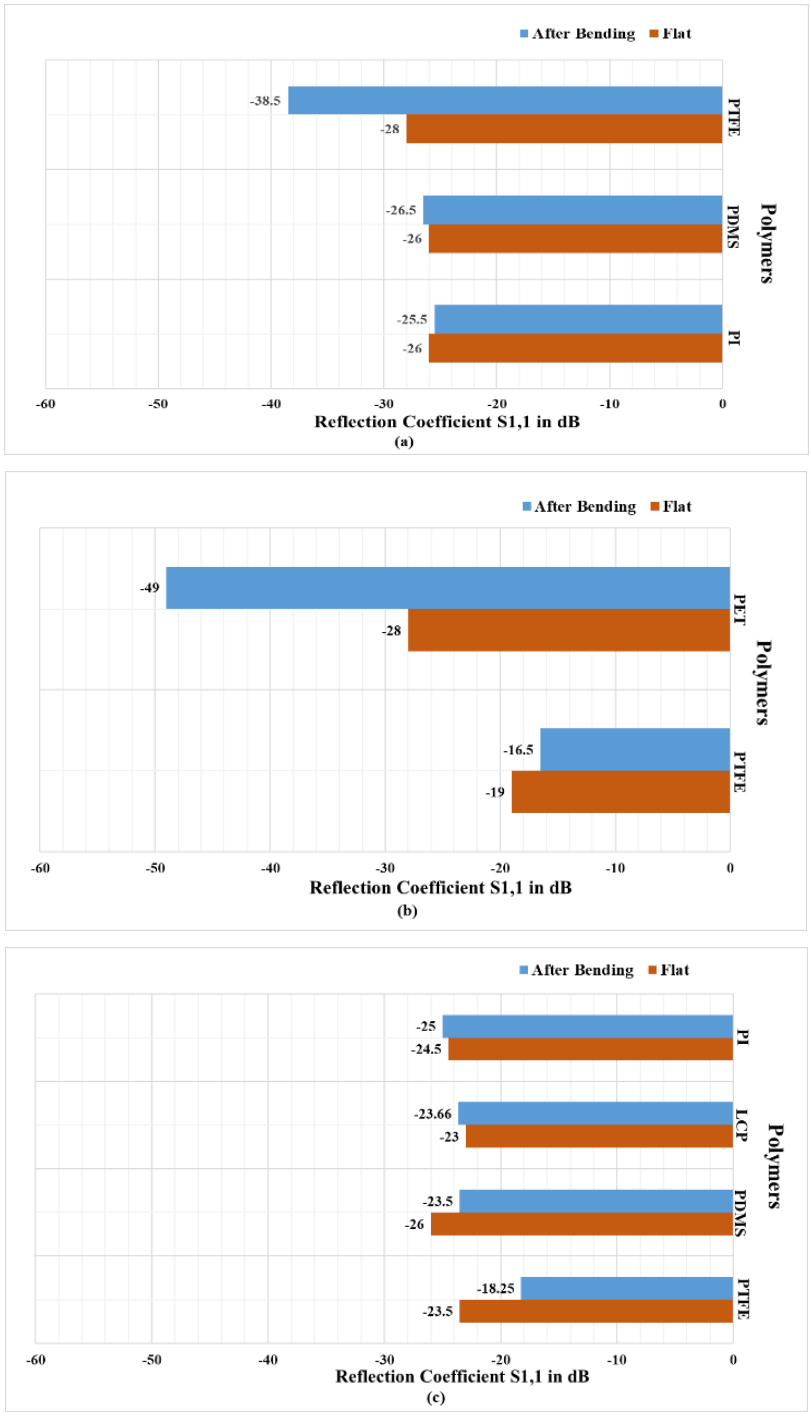

Figure 18. Average Change in S_{11} in dB of Polymer-Based Substrate Antennas for (a) PI, PDMS and PTFE at 2.2-2.5 GHz, (b) PTFE, PDMS and PET at 2.5-5.0 GHz, (c) PI, PTFE, PDMS and LCP at greater than 5 GHz

For analysis of the effects of bending on impedance mismatch, or the reflection co-efficient S_{11}, the average of S_{11} is evaluated from a flat case to a bending level up to 6 mm for different frequencies ranges. Figure 18(a), (b), and (c) represents the percentage deviation of S_{11} for flexible antennas with polymer substrates. Demonstrating PI and PTFE as the least affected flexible antenna polymer substrates, with an average of less than 2% change in S_{11} for the 2.2 to 2.5 GHz frequency range, see Figure 18(a), in variance, for the 2.5 to 5.0 GHz frequency range, while PTFE-based antennas have better signal strength after bending, the PET-based antennas have a high average signal degradation and mismatch of about 13.15%. Meanwhile, for the higher than 5 GHz frequency range, both the PI-based and LCP-based antennas experience lesser impact on S_{11}, about 2% and 2.8% respectively, and an increased average signal strength, see Figure 18(c). In this context, PTFE is badly impacted by approximately 23.3% change in its S_{11}, which indicates a lot of signal degradation when it is bent up to 6 mm on average for frequencies higher than 5 GHz, see Figure 18(c).

2.6.3 Impact of Loss Tangent (σ) variations on Resonant Frequency

The constitutive parameter of dielectric (polymer), called permittivity, is a complex value which is expressed as $\varepsilon = \varepsilon_0\varepsilon_r = \varepsilon_0 (\varepsilon' - j\varepsilon'')$. Where ε_0 is the permittivity of a vacuum which is 8.854×10^{-12} F/m [295]. The value of ε normally depends on the frequency, the roughness of the polymer surface, and its temperature [295], as well as the moisture absorption and purity of the material [296].

In this present literature review, the behaviour of polymer substrates in terms of their dielectric constants have been analysed and presented in graphs to demonstrate how the operating frequency is affected by the change of ε, see Figure 19. The effect of the increase in ε of the material on the percentage central frequency shift is also analysed. Figure 19 also illustrates that polymers with ε ranging from 2.3 to 2.8 are less influenced by bending, whereas, from 2.8 to 3.0 suffers consistently large shifts in frequency.

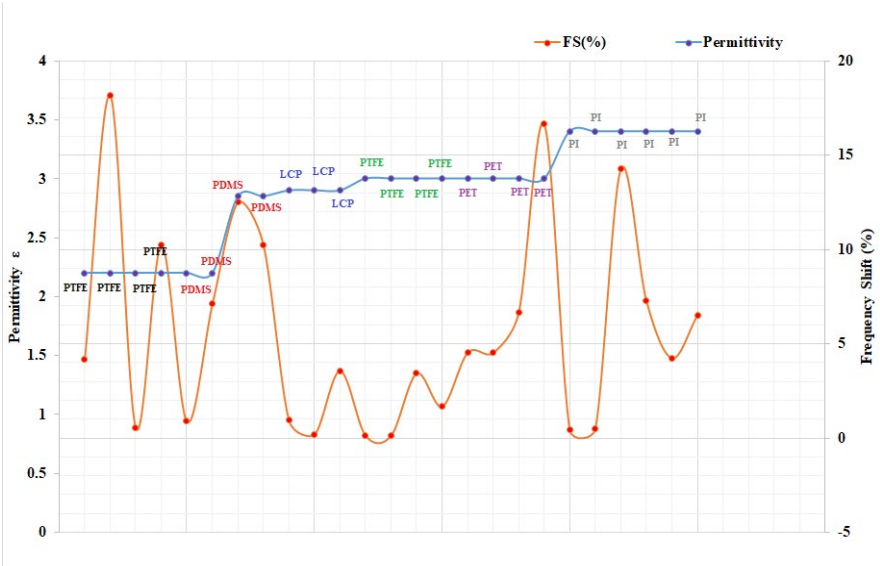

Figure 19. Average Shift in Central Frequency for PTFE, PDMS, LCP and PET-Based Antennas with Permittivity Variations for < 6-mm bending with 2.2 to 7.5 GHz Frequencies

While the dielectric constant of flexible substrates lies in the range of 2.2 to 12 [119], lower values of the dielectric constant reduce the surface waves and increase the impedance bandwidth and antenna gain [297]. Concludingly, polymer materials, with their dielectric constants that range from 2.2 to 3.4, are preferable for use in flexible antenna designs and RFID tags, see Table 6.

Table 6. Polymer Substrate with Respective Range of Permittivity

Polymers	Permittivity (ε)
PTFE laminates	2.2-3
PDMS laminates	2.2-2.85
LCP	2.9
PET	3
PI Kapton	3.4

2.7 Summary

A comprehensive discussion on flexible antennas with polymer substrates for the general flexible IoT is presented in this chapter. While IoT applications are rapidly growing and connecting various smart devices together, the flexibility of these IoT is an important characteristic, which subsequently requires flexible antennas for aspects of communication. Polymers such as PI, PDMS, PTFE and LCP are widely used in flexible electronics and flexible antenna designs. In this literature review, a comparative analysis of the properties of various polymer materials is presented with an overview of polymer-based flexible antennas which can be used for flexible IoT. Radiation characteristics of flexible antennas, such as return losses, gains and directivity are drastically affected when the proposed antenna undergoes degradation or curvature. It is concluded that bending has a huge impact on the radiation characteristics of an antenna when subjected to bending, where, beyond a certain level of curvature, radiations are too distorted to obtain good results.

Chapter 3: **Design Fabrication and Bending Analysis of Flexible Polymer Substrate Antennas**

3.1 Introduction

Flexible wearable wireless devices are gaining exceptional fame because of their profound characteristics of being lightweight and low cost, having low power consumption and high flexibility with robustness and a compact size. Traditional wireless devices such as antennas on the conventional rigid substrates were difficult to integrate into wearable systems such as the Body Area Network (BAN) as compared to the flexible antennas [18, 298]. BAN is a communication standard for low power consumption devices working around a human body for a variety of applications such as medical, consumer electronics and personal entertainment. Wireless devices act as a node for BAN applications and are responsible for communicating with each other by transferring data to a remote server [18, 298]. These wireless devices could be a sensor, or an actuator, which incorporates a memory unit and an antenna that needs to both receive and transmit data. The development of flexible antennas as wearable devices is an important research area that needs to address the development process for the necessarily flexible antennas, which is quite different to that of the conventional antennas based on rigid substrates.

The design procedure for the development of the flexible substrate antennas, illustrated in Figure 20, is comprised of five major steps. Firstly, the preferred conductive and the preferred substrate material are selected according to the required application, in this case for a wearable flexible antenna. The selection of the substrate material for the wearable application is generally quite challenging because of its necessity for compatibility with the human body and ability to withstand moulding and bending without distorting its radiation characteristics. The second step is to investigate the electrical, mechanical and thermal properties of the proposed dielectric flexible substrate in terms of its conductivity, resistivity for conductive material and loss tangent, permittivity, dielectric strength, tensile modulus, CLTE, density and moisture absorption, as a suitable flexible substrate needs to possess a high level of deformability, thermal and electrical stability with low fabrication complexity. Once the conductive and the substrate material are selected for the antenna, the next step is to design the antenna. This includes the designation of a geometrical shape appropriate for the required application for its frequency requirement, its mathematical modelling, which includes a dimensional and parametric analysis, as well as the simulation and optimization of the design. In the fourth step, an appropriate fabrication technique, based on the materials, is selected for the reproduction of the design onto the flexible substrates. Finally, the fabricated flexible antenna is tested for various radiation characteristics such as reflection coefficients, radiation patterns, gain and directivities of antenna. Further qualitative tests for wearable applications, irrelevant to conventional antennas on rigid substrates, such as bending impact on *S*-parameters, durability, robustness, moisture and thermal tests, are also necessary.

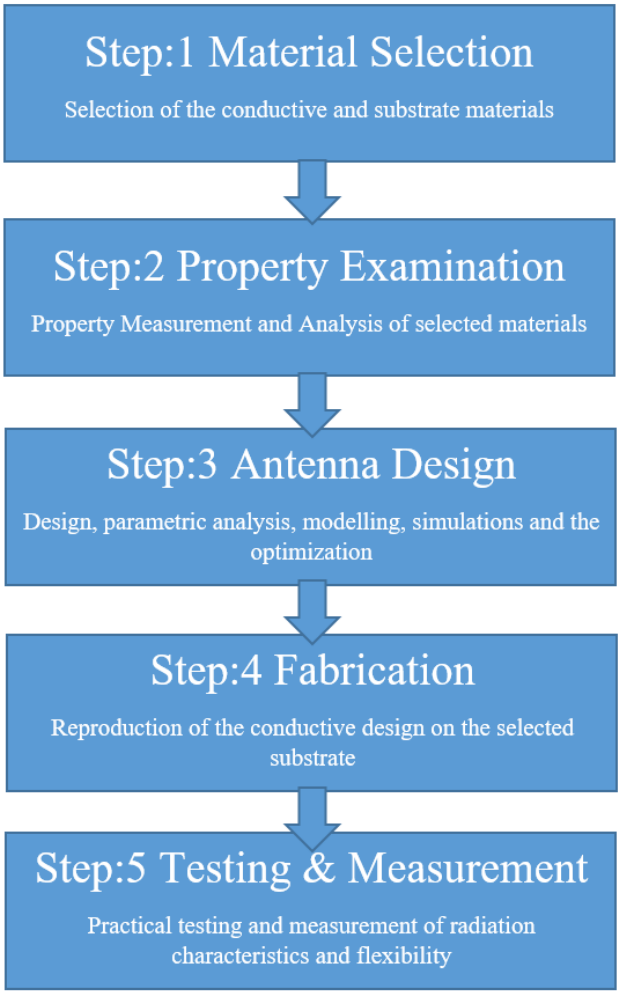

Figure 20. Design Procedure for Flexible Substrate Antenna

In this chapter, three different flexible polymer substrate antennas are designed and fabricated for different groups of frequencies, based on the discussion and analysis in Chapter 2.

3.2 Polymer Substrate Flexible Antenna Design

Significant research has been thrust onto Polymers over the last few decades for their application in flexible antennas with their advantages of high flexibility, convenient integration with other microwave components [47], being lightweight, energy efficient, having reduced fabrication complexity with easy mount-ability on conformal surfaces, low cost and in abundant availability in the form of substrate films, gaining substantial attention [116]. In this study, attention is dedicated to the design and investigation of flexible polymer-based wearable antennas. The different steps for the flexible polymer-based antennas design procedure are described below.

3.2.1 Material Selection

To comply with the flexibility requirements of the antennas, the materials selected for the conductor in general and the substrate more specifically, need to be highly flexible and mechanically robust.

Detailed analysis on the conductive and substrate materials have been demonstrated in Chapter 2 where Table 2. General Requirements of Substrate Materials for Flexible Devices, describes the range of properties for suitable polymer substrate materials. In the case of the conductive material, which is the ground plane and radiating element, copper is selected for its qualities of being highly conductive and possessing very low resistivity. Moreover, copper is highly flexible, withstands a high level of bending and crumpling and also has high tensile strength with an ability to withstand repeated pressure and deformations, and is resistant to corrosion and oxidization. See Table 7 for the properties of pure copper.

Table 7. Properties of Pure Copper

Properties of Pure Copper [299]							
Physical		**Electrical**		**Mechanical**		**Thermal**	
Melting Point	Density	Conductivity	Temperature Coefficient	Tensile Strength	Modulus	Thermal Conductivity	CTE
1083º C	8.96 g/cm^3 at 20º C	58 MS/m at 20º C	0.0043/K at 0-100º C	224-314 MPa	137.8	401 W/m-K at 0-100º C	17.0×10^{-6} m/m-K at 0-100º C

The selection of an appropriate polymer substrate is very important for flexible antennas. It should be highly flexible, easy to integrate with a conductive material and have a high tolerance level of bending or crumpling as well as repeatability endurance. The requirements of polymer substrates for flexible antennas are given in Table 2. To corroborate with the impact of curvature on different polymer substrates, PET (Melinex 401), PTFE Teflon and flexible PVC have been chosen. The selection of these three dielectric polymers is based on the analysis of their physical, electrical and thermal properties being suitable for bending applications.

3.2.2 Property Examination

After the selection of the conductive and substrate materials, the next step is to analyse the properties of the selected materials. The propagation and loss properties of the dielectric substrate need to be known for the prospective material before being implemented as the substrate of the antenna. For this purpose, the properties of the conductive material and the polymers: PET, PTFE Teflon and PVC sheets, are tested via the Intelligent Polymer Research Institute (IPRI) of the University of Wollongong (UOW) and listed in Table 8. IPRI is a key research strength at the UOW with state-of-the-art laboratories for the investigation and examination of synthetic polymers. Results indicate that the PTFE Teflon 100-µm thickness sheet has the highest density, temperature CTE and shrinking capability, at 150º C, and the lowest dielectric strength, dissipation factor and moisture absorption capability. This establishes Teflon as a good choice for a moisture and thermal resistant polymer material. The next substrate, PET with 70-µm thickness, possesses very good physical and electrical properties, such as high tensile and dielectric strength and low dissipation factor, making it very suitable for highly deformational applications. The Flexible PVC is a low-cost material with high strength, which is formed by the addition of compatible plasticizers to the PVC to lower the

crystallinity of the material. It has very good resistance to Ultraviolet (UV) radiations and is non-reactant to various organic materials, such as crude oil at high temperature. Comparatively, it has the worst physical properties such as the lesser ability to withstand high pressure and deformability. Hence, these three polymer substrates, in terms of their ability to withstand high bending can be placed in the order of PET, then PTFE and then PVC with the lowest position. Classification in terms of thermal properties would restructure this ordering to PVC, then PET and then PTFE, with the Teflon at the lowest position. The implications of certain curvatures on these materials could ascertain further impact on the use of one of these polymers as the selected substrate for the antennas. As already discussed in Chapter 2, it is the bending of the antenna with a flexible polymer substrate which most impacts its resonant frequency, *S*-parameters and radiation efficiency. Figure 21 shows the actual PET, Teflon and PVC polymer sheets used as the substrates in fabricating our proposed flexible antenna design. After the properties of the polymer substrates and the conductive and substrate material have been tested, the next step is to develop the antenna's shape and design.

Table 8. Properties of Flexible Polymers: PET, PTFE, PVC

Substrate	Model / Thickness	Physical/Mechanical Properties			Electrical Properties			Thermal/Chemical Properties		
		Density (g/cc)	Tensile Strength X-Direction at 23° C (Kpsi)	Tensile Modulus X-direction at 23° C (Kpsi)	Dielectric Constants 100 Hz to 1 GHz	Dielectric Strength (V/mil)	Dissipation Factor Tan σ at 100 Hz to 1 GHz	CTE -15° C to 300° C (ppm/C)	Moisture Absorption (%) at 23° C	Shrinkage (%) 30 min, 150° C
PET	Melinex 401 Polyester 70 µm	1.3	25	420	2.07	4000	0.002	19 to 20	0.1 to 0.7	0.5 to 1.1
PTFE	Teflon 100 µm	2.1	3.9	65	2.70	285	0.0002	250 to 275	0 to 0.05	1.5 to 3.0
PVC	Flexible PVC-O 110 µm	1.4	2.2	217	3.70	635	0.04	6 to 7	0.2 to 1	0.2 to 2

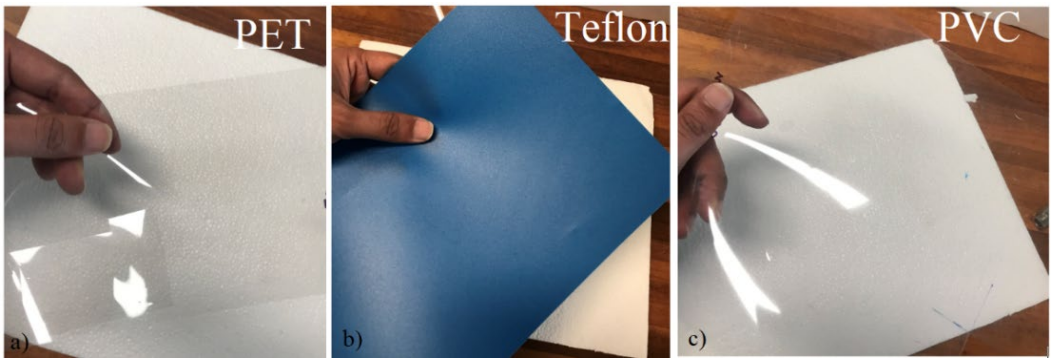

Figure 21. Polymer Film sheets a) Transparent PET b) PTFE Teflon c) Transparent PVC

3.2.3 Antenna Design

Once the comprehensive examination and verification of the properties of the selected materials is completed, the design and the shape selection for the antenna remain crucial. According to different specific applications and frequency requirements, various designs have already been published for flexible microstrip antennas, their specific applications and frequency requirements including: aperture coupled antennas [34, 257, 300], Planar inverted-F antenna [301, 302], monopole and dipole antennas [53, 66, 253], various alphabetic shaped, E-shaped, F-shaped and H-shaped antennas [8, 110, 248, 303], and antennas based on the CPW feed [72, 237, 247]. These are all microstrip antennas and fabricated on flexible substrates.

The basic microstrip patch antennas are mostly used in wireless applications due to their simple shapes, lightweightedness, small size, and because they support linear and circular polarization, are capable of dual and triple frequency band operations, have low fabrication and manufacturing costs and are easy to fabricate and integrate with IoT [24, 57, 68, 112, 168, 215, 242, 245]. Being extremely compatible with flexible polymer-based antennas, a microstrip patch antenna design is selected for flexibility testings.

While there are some limitations, such as a narrow bandwidth as a function of the thickness of the substrate material at higher frequencies above 5 GHz, these do not impact our target purposes, including the testing of the bending capabilities of polymers on the radiation characteristics of the antenna. There are, however, also some disadvantages, such as low gain and efficiency, and surface wave excitation [118], where, unfortunately, this surface wave excitation results in power loss as the power is scattered when the antenna bends and resultantly causes degradation of signal strength. The low efficiency of the microstrip patch antennas is due to the high Q factor resultant of these losses in relation to the antenna.

Amongst the various shapes possible for microstrip patch antennas, the simpler to design and optimise E-shape is selected with the gap between the feedline and the patch G_{pf}, see Figure 22, providing wider bandwidth compared to a simple patch antenna. Therefore, to determine the flexible polymer-based antenna behaviours for different applications, nine E-shaped microstrip antennas are designed to operate in three frequency ranges: 2.2-2.5 GHz, 2.5-5.0 GHz and 5.0-30 GHz.

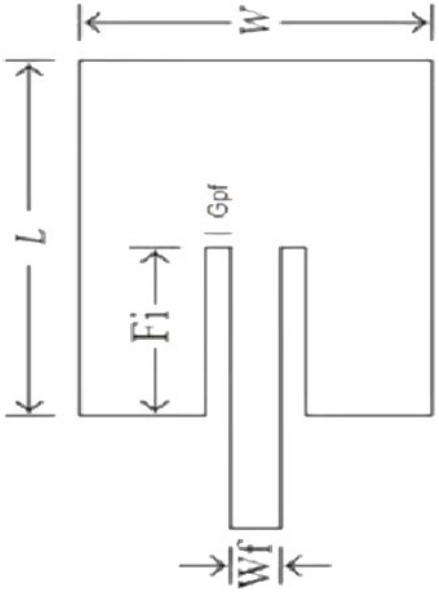

Figure 22. Structural Diagram of E-shaped Microstrip Antenna

3.2.3.1 E-shaped Microstrip Patch Antenna on PET Substrate

To corroborate the impacts of bending, an E-shaped microstrip patch antenna is initially designed on the PET substrate for the operating frequency of 2.45 GHz. Two more antennas with the same shape and characteristics are then made on the Teflon and PVC substrates. The steps involved in the design of the flexible antenna are described in this section.

3.2.3.2 Antenna Structure and Parametric Formulations

The geometrical structure with the parameters of the E-shaped microstrip flexible antenna is shown in Figure 22. Where, W is the width, L denotes the length, W_f represents the width of the feedline, G_{pf} is the gap between the patch and the feedline and F_i defines the length of the feedline. In this study, rather than detailing the antenna basis such as the TL model or a step by step evaluation of the parameters, attention is given to the basic concepts and the equations used to drive the parameters.

The width W of the antenna is provided in [118], calculated by using

$$W = \frac{c}{2 f_0 \sqrt{\frac{(\varepsilon_r + 1)}{2}}} \tag{28}$$

where c = the velocity of the light at 3×10^8 m/sec, ε_r = the dielectric constant of the substrate and f_0 = the resonant frequency at 2.45 GHz. The fringing effect, due to the field along the edges of the patch, is a function of the dimensions of the patch and the height h of the substrate. Therefore, the length of the antenna L appears greater than its main body length by ΔL [118]. The physical E-plane is demonstrated in Figure 23.

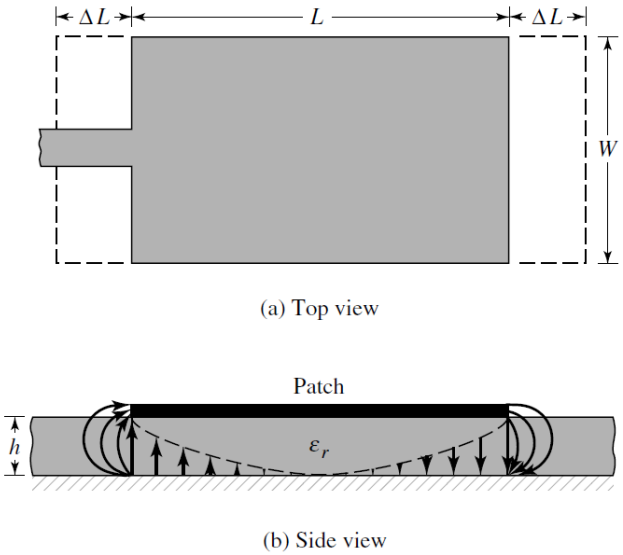

Figure 23. Physical and Effective Length of Microstrip patch Antenna [118]

Figure 23 shows that the actual length *L* has extended on each end of the patch by the distance ΔL which is a function of the effective dielectric constant ε_{reff} and the ratio of the width of the patch to the height *h* of the substrate *W/h*. The normalized extension in the length, in [304], is given by

$$\Delta L = 0.412h\frac{\left(\varepsilon_{reff}+0.3\right)\left(\frac{W}{h}+0.264\right)}{\left(\varepsilon_{reff}-0.258\right)\left(\frac{W}{h}+0.8\right)} \tag{29}$$

At lower frequencies, the initial value of ε_{reff} is referred to as static value, in [118], and are given by

$$\varepsilon_{reff} = \frac{\varepsilon_r+1}{2}+\frac{\varepsilon_r-1}{2}\left(1+12\frac{h}{W}\right)^{-1/2} \tag{30}$$

such that the effective length of the patch antenna now becomes

$$L = L_{eff}+2\Delta L \tag{31}$$

with the effective length calculated by (32.

$$L_{eff} = \frac{c}{2f_0\sqrt{\varepsilon_{reff}}} \tag{32}$$

The length and the width of the ground plane and substrate in the microstrip patch antenna is the same and can be calculated by

$$L_g = 2\times L \text{ and } W_g = 2\times W\,. \tag{33}$$

For the next equation, F_i is considered the length of the feed line and *A* is the multiplication factor which depends on the height of the substrate which varies from 6 to 15, see (34) to calculate F_i.

$$F_i = \frac{A \times h}{2} \tag{34}$$

In (28), the resonant frequency for a microstrip patch antenna for any TM_{mn} mode can be calculated by

$$f_0 = \frac{c}{2\sqrt{\varepsilon_{reff}}}\left(\left(\frac{m}{L}\right)^2 + \left(\frac{n}{W}\right)^2\right)^{1/2} \tag{35}$$

where m and n are the modes along the length and width of the patch.

In many applications where the compactness of the antennas is very important, the flexible substrate material is required to possess high permittivity to achieve great miniaturization factors. As a consequence of this, the Q factor of the antenna becomes higher, which in turn causes increased bandwidth degradation [101] and, correspondingly, means that impedance matching is very important in these types of antennas. Various techniques have been used in previous research to match the impedance with the feed line, including, for example, using lumped components [101, 119] and Planar Inverted-F Antenna matching [305] and, while our resolution for this circuit between the feed line and the antenna incorporates a co-axial feed with a lumped component, rather than detailing the design of this impedance matching technique, this chapter retains its focus on the antenna design and fabrication and the bending capabilities of different polymer-based substrate antennas.

3.2.3.3 **Optimization of** Parameters **and Software Simulations.**

While the antenna parameters are evaluated according to the previous equations, and the properties described in Table 9, the antenna performance is evaluated by simulating the design using CST microwave studio suite 2019, a specialist tool for evaluation 3D electromagnetic simulations. With the CST design simulation obtaining the S-parameters (S_{11}) of the antenna, the resultant reflection co efficient of the design is given in Figure 24.

Table 9. E-Shaped Flexible Patch Antenna Parameters

Parameters	Value (mm)	Description
L	35.33	The length of the patch
W	43.29	The width of the patch
W_g	86.58	The width of the ground plane and PET substrate
W_f	1.5	The width of the feed line
L_g	70.66	The length of the ground plane and substrate
h_t	0.035	The height of the copper conductor
h_s	0.07	The height of the PET substrate
G_{pf}	1.5	The gap between the patch and the feed
F_i	5.0	The length of the feed line

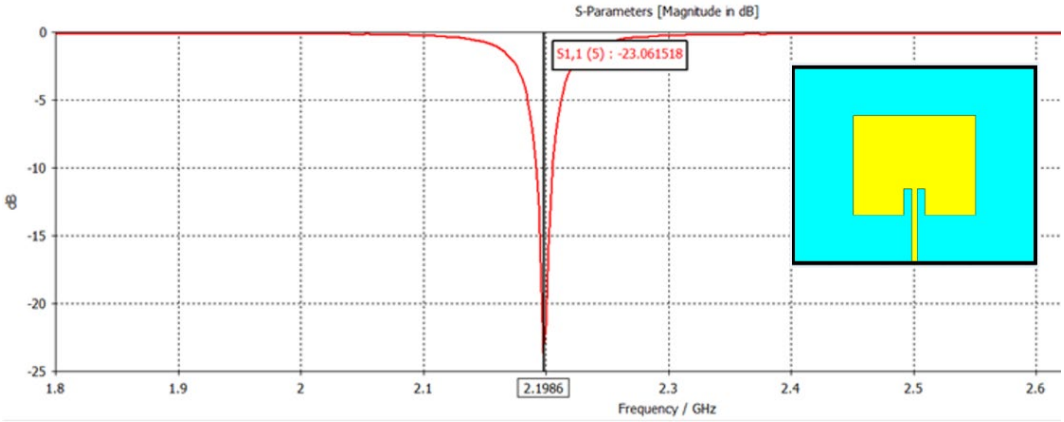

Figure 24. *S*-Parameters of E-shaped Flexible Antenna on PET Substrate

The E-shaped microstrip patch antenna on the PET substrate is analysed by varying one of the physical parameters while keeping the others constant. First, the length of the feed line F_i is varied from 1 mm to 10 mm to observe the impact on the reflection coefficient. Figure 25 illustrates how the *S*-parameters are maximised when F_i = 9.5 mm.

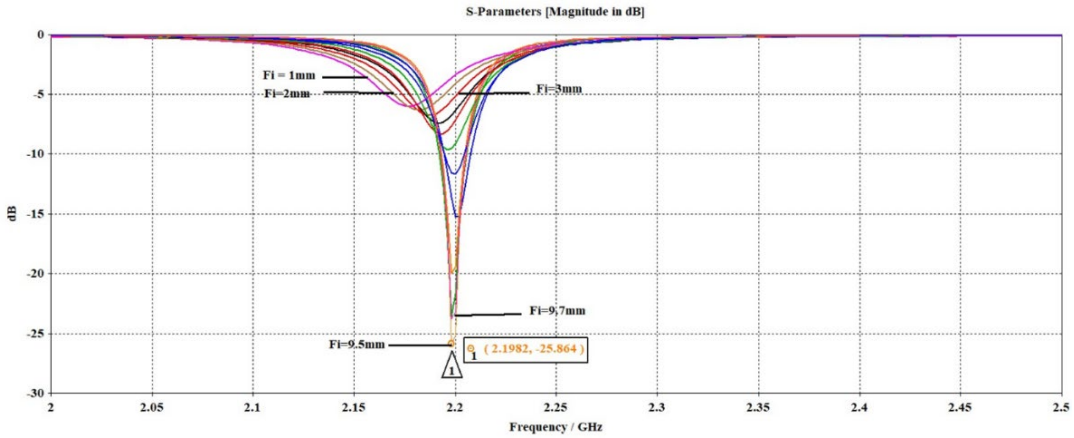

Figure 25. Impact of F_i Variation on *S*-parameters

Then, by keeping the F_i constant at 9.5 mm, the impact of the variation of W_f from 0.5 mm to 1.9 mm and on the *S*-parameters where W_f equals 1.7 mm, -32 dB S_{11} is obtained which in terms gives good impedance matching as illustrated in Figure 26.

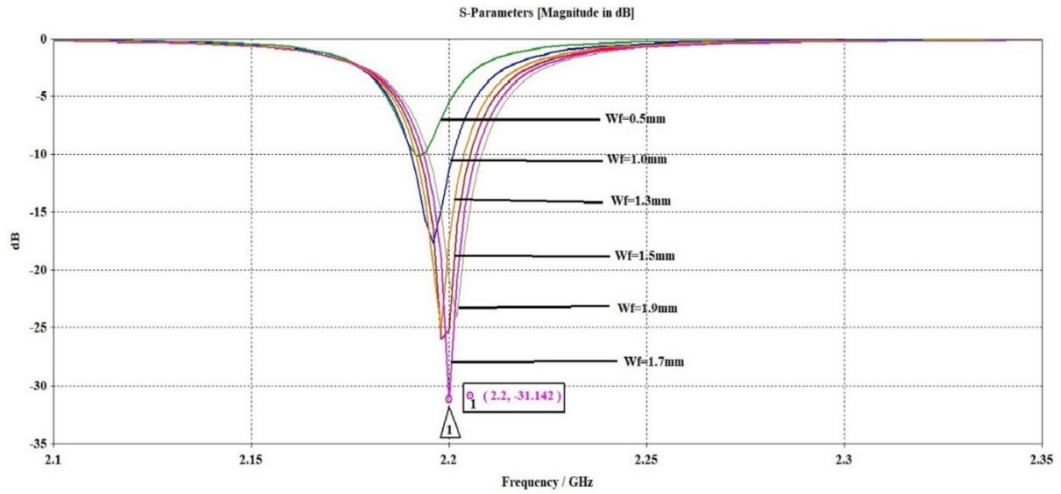

Figure 26. Impact of W_f Variation on *S*-parameters

By maintaining the resultant maximum values constant for the optimised feed line length and width, F_i 9.5 mm and W_f 1.7mm, the next step is to vary the size of the gap between the feed line and the patch G_{pf} the impact on G_{pf} can be determined. Results from the variations from 0.2 mm to 2.4 mm, illustrated in Figure 27, indicate that the reflection coefficient is best suited at the value of 2.2 mm.

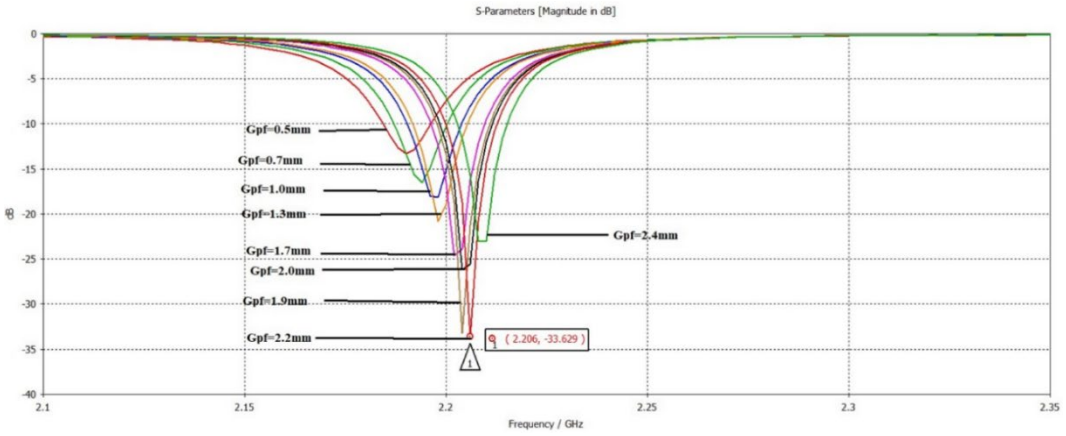

Figure 27. Impact of G_{pf} Variation on *S*-parameters

The optimization of these three parameters F_i, W_f and G_{pf}, provides an improved version of the *S*-parameters, as illustrated in Figure 28. Corresponding variations to the length and the width of the microstrip patch are analysed in the next step where the patch length L is varied from 35.33 mm to 32.1 mm and its width W is varied from 43.29 mm to 33.5 mm to determine the impact on the reflection coefficient with these variations, see Figure 29. The variation in the L and W of the patch antenna generated a great impact on the resonant frequency where shifting it from 2.22 to 2.47 GHz resulted in a decrease in both L and W. The resonant frequency 2.448 GHz is obtained at L = 32.1 mm and W = 33.5 mm. Finally, the F_i, Wf and G_{pf} are further simulated with the collected results for a final optimization with Figure 30 illustrating the resultant optimized design of the E-shaped microstrip patch antenna. The optimized results are then listed in Table 10.

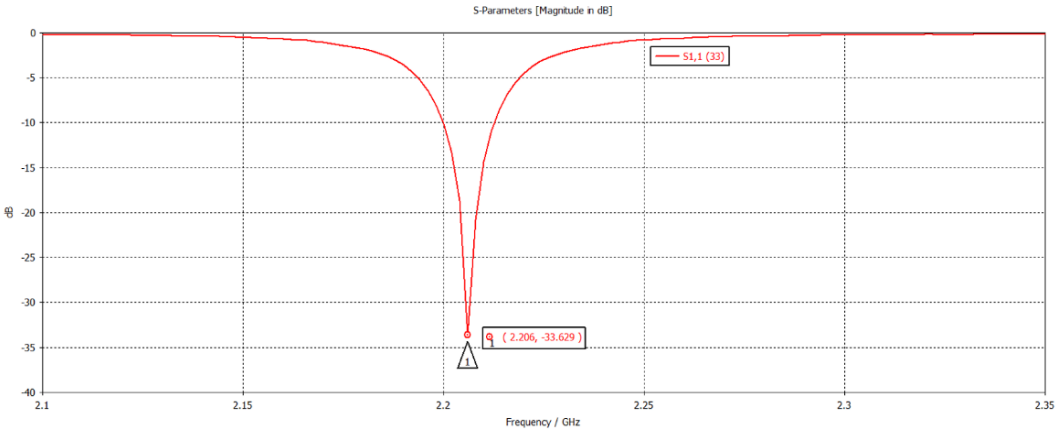

Figure 28. Improved *S*-Parameters by Optimizing at F_i = 9.5 mm, Wf = 1.7 mm and G_{pf} = 2.2 mm

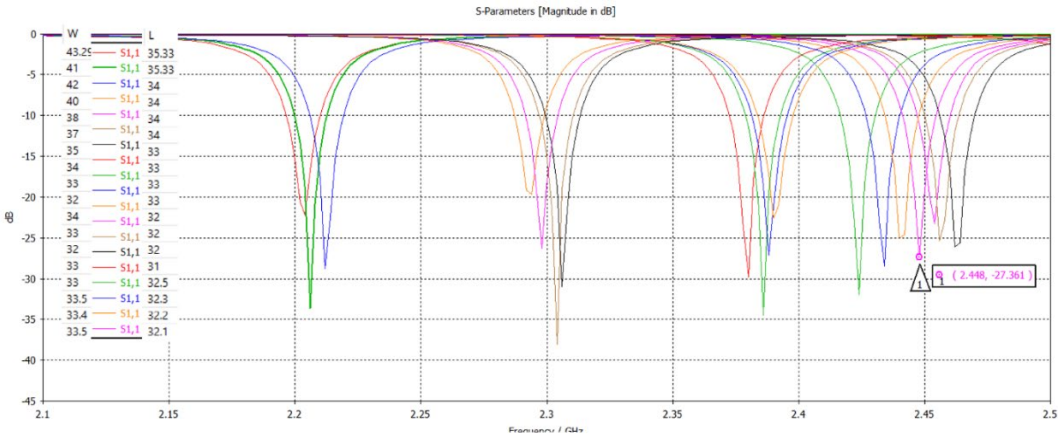

Figure 29. Impact of *L* and *W* Variations of the patch on *S*-parameters (at *Fi* = 9.5 mm, *Wf* = 1.7 mm and Gpf = 2.2 mm)

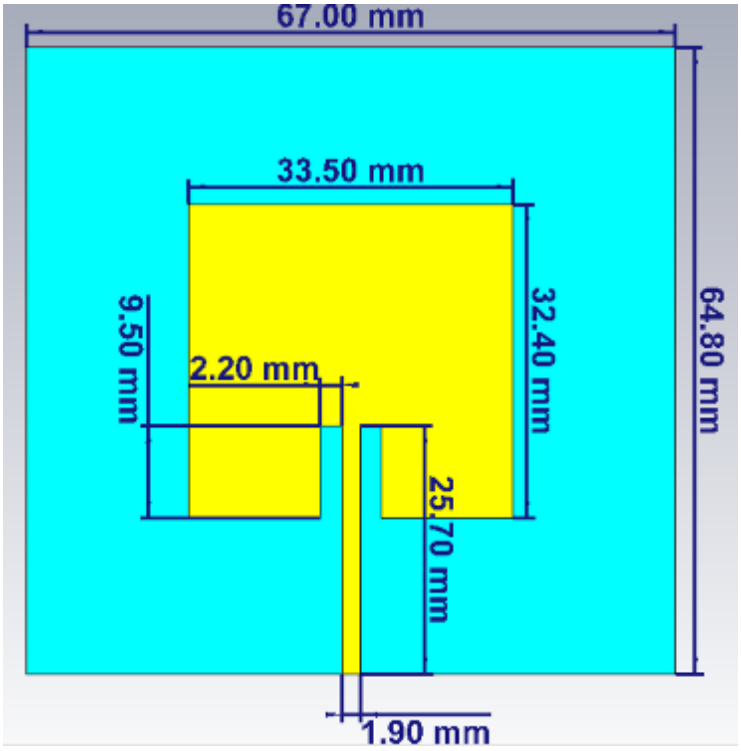

Figure 30. Optimised Design of E-Shaped Microstrip Flexible Patch Antenna at 2.45 GHz

Table 10. Optimised Parameters of E-Shaped Flexible Patch Antenna on PET Substrate

Parameters	Value (mm)	Description
L	32.4	The length of the patch
W	33.5	The width of the patch
W_g	67.0	The width of the ground plane and PET substrate
W_f	1.9	The width of the feed line
L_g	64.2	The length of the ground plane and substrate
h_t	0.035	The height of the copper conductor
h_s	0.07	The height of the PET substrate
G_{pf}	2.2	The gap between the patch and the feed
F_i	9.5	The length of the feed line

The *S*-parameters for the optimised design are shown in Figure 31 while the other radiation characteristics of the design, such as radiation patterns, VSWR, E-field and the surface current on the surface of the antenna are given in Figure 32.

In the simulation results for the near-field 2D analysis, in Figure 32, the VSWR, which is the ratio of the output power to input power, becomes zero at 2.44 GHz indicating that no reflection occurs when all the power is transmitted at this frequency, as seen in Figure 32(a). The distribution of the E-field and the H-field over the surface of the design are illustrated in Figure 32(b) and Figure 32(c), respectively. The far-field radiation results of the antennas is given in Figure 33, where good radiation patterns are observed in the E-plane and a 6.96 dBi gain is achieved, which is excellent for transmitting energy.

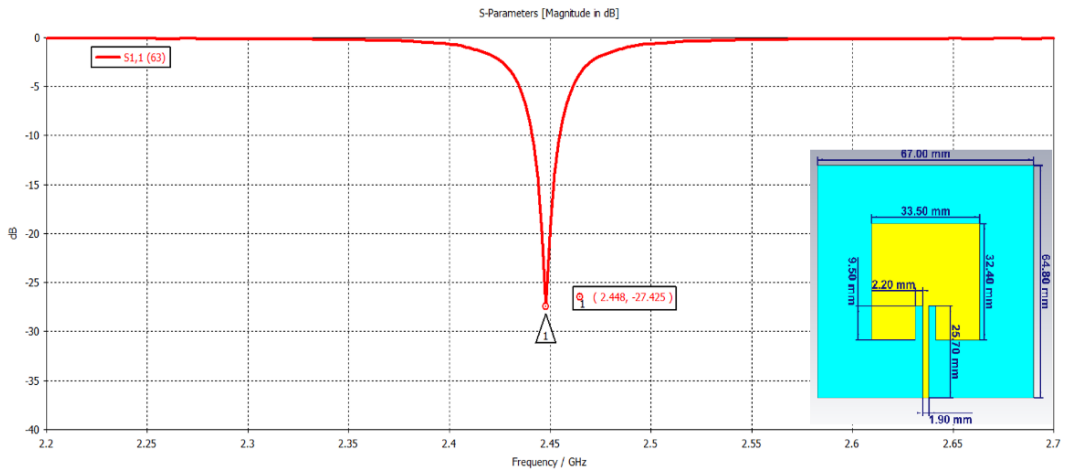

Figure 31. Parameters of Optimised E-Shaped Microstrip Flexible Patch Antenna at 2.45 GHz

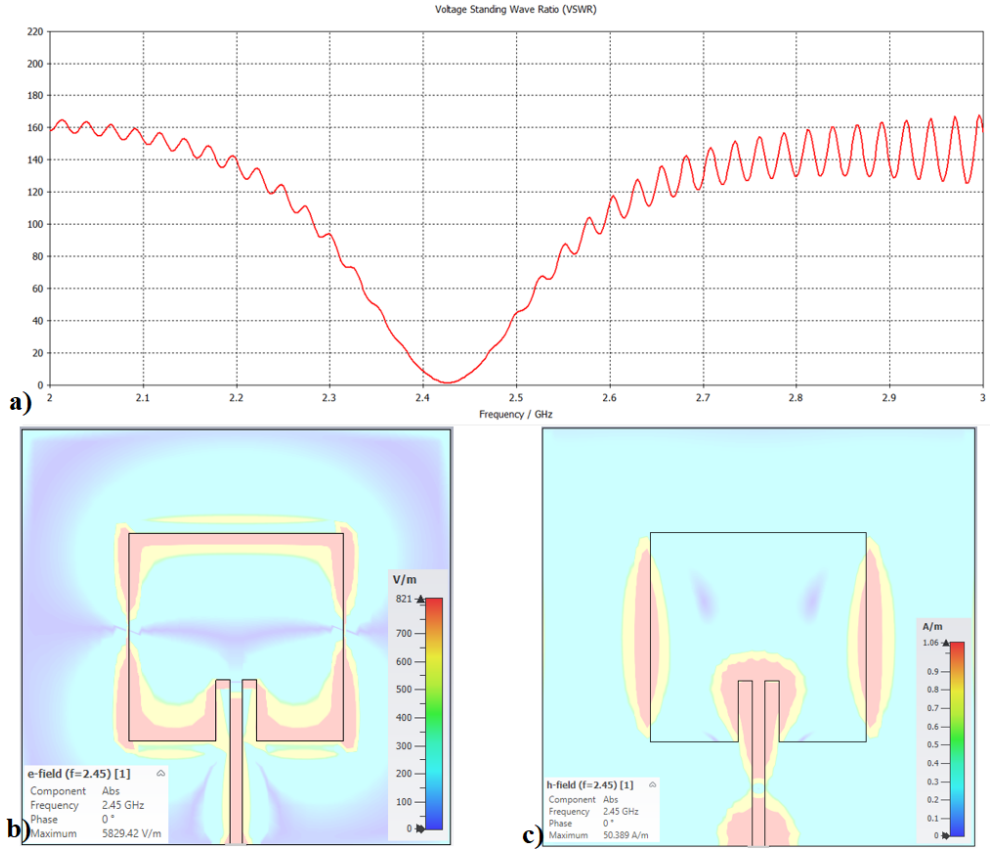

Figure 32. Near-Field Analysis of E-shaped Microstrip Flexible Patch Antenna a) VSWR b) E-Field c) H-Field

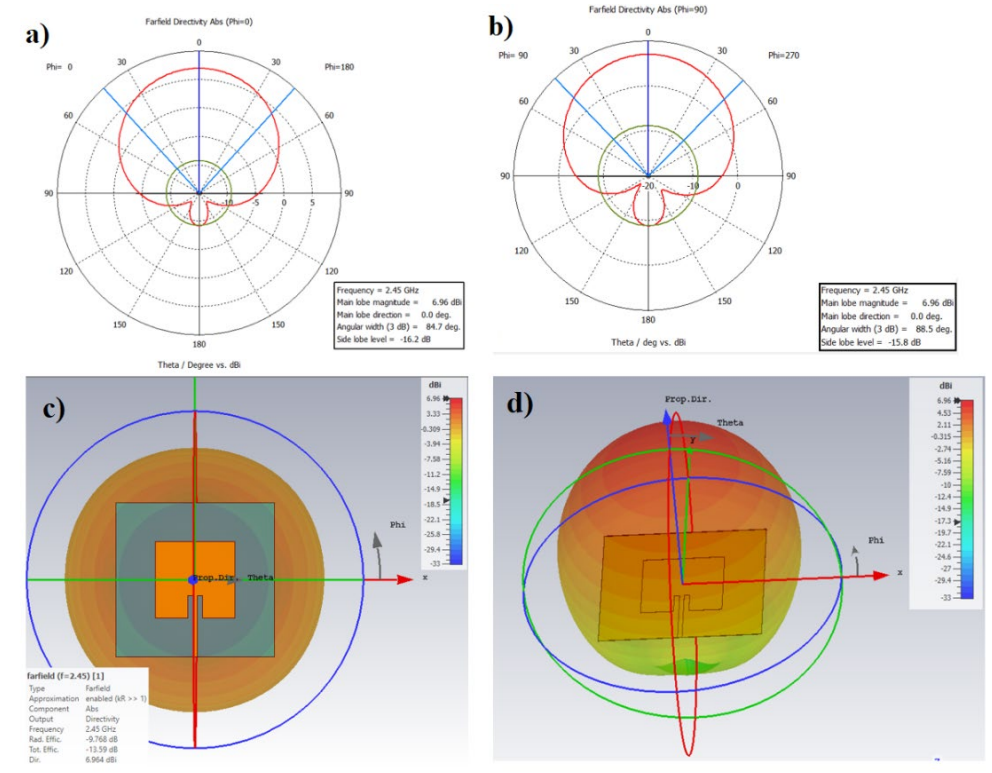

Figure 33. Far-Field Analysis of E-shaped Microstrip Flexible Patch Antenna on PET Substrate: Radiation Patterns a) at Phi = 0 b) at Phi = 90, c) Radiation Efficiency d) Directivity

3.2.4 Antenna Fabrication

With the excellent results obtained in the simulation process, the antenna design is ready for fabrication. For this next step, to fabricate the antenna on the PET substrate, copper is used as the conducting material and the ground plane and the tag printing is executed on a Universal Laser Systems (ULS) PLS6MW with Lens: 2.0 MW and Laser: 10.6-micron wavelength – CO2 Laser. An RP-SMA female miniature connector with the dimensions 1.7 mm x 4.1 mm, 8 mm is used for the microstrip feed line. The thickness of the ground plane and substrate is 0.105 mm and the total thickness with the copper patch is 0.14 mm with the Keysight Vector Network Analyzer (VNA) series E5063A being used to perform the measurements, see Figure 34.

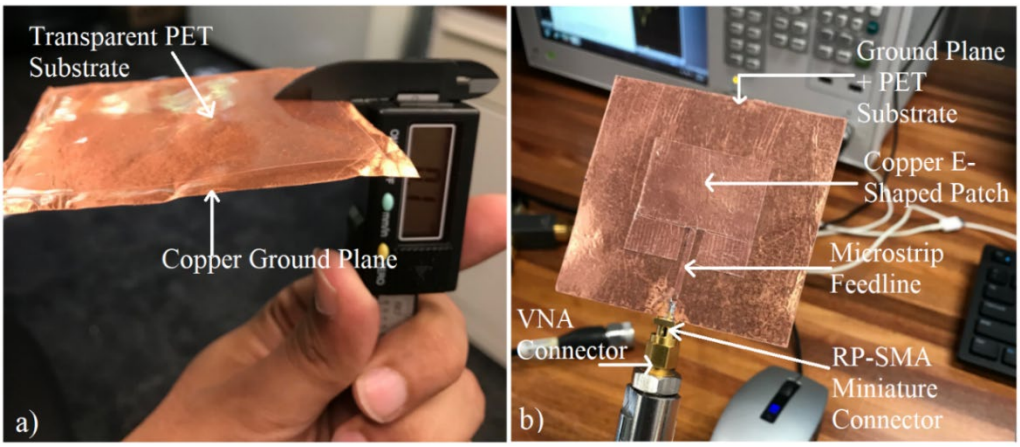

Figure 34. E-Shaped Flexible Microstrip Patch Antenna on PET Substrate
a) Thickness Measurement b) Fabricated Antenna Connected to VNA

Operating at the 2.45 GHz frequency, and following the same procedures and fabrication steps to corroborate the bending effects of radiation on other polymer substrates, the antenna design is then reproduced on both the Teflon and PVC substrates with 100 µm and 110 µm thickness respectively, as shown in the Figure 35.

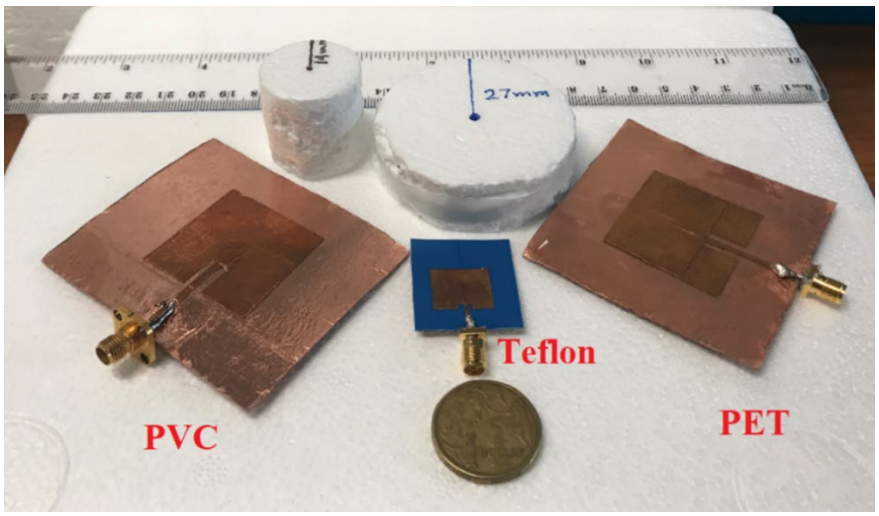

Figure 35. Actual Aspects of Fabricated E-Shaped Microstrip Antennas operating at 2.45 GHz on Substrates PVC (left), Teflon (Centre), and PET (right)

3.2.5 Measurements

So far this investigation has studied the antenna operating at 2.45 GHz. The frequency range analysis is now amplified to the three target frequency ranges 2.2 to 2.5 GHz, 2.5 to 5.0 GHz and greater than 5.0 GHz to analyse the effects of bending levels of 14 mm and 27 mm on the three selected antenna substrates, PET, Teflon and PVC. Understanding that these three substrates were chosen for their excellent physical, electrical and thermal properties, as described in Table 8, where Teflon has relatively low deformability but is very efficient in moist conditions and has high thermal efficiency, and PVC has very high flexibility but moderate electrical properties. Moreover, PET and PTFE Teflon are commercially available in the very cost-effective form of film sheets. Subsequently, nine flexible patch antennas are fabricated on PET, Teflon and PVC substrates, three for each range of frequencies to corroborate the bending impact on the resonant frequency and reflection coefficient, and the resultant impact on the loss tangent variation on the resonant frequency. Correspondingly, three antennas are designed to operate at 2.45 GHz, three at 4.25 GHz and three for 7.45 GHz.

3.2.5.1 Introduction to the Frankonia Chamber for Measurements

To conduct the measurements, testing is performed in the Frankonia anechoic chamber with a frequency range of 30 MHz to 40 GHz at a measuring distance of 3.0 m. The external dimensions of the chamber are 7355 mm × 3755 mm × 3300 mm and the size of the uniform area is 1.5 m × 1.5 m. The chamber provides excellent RF-Shielding which is less than 90 dB for the frequency range of 1-40 GHz, typical for the pan-type module made of 2.0 mm galvanised steel, see Figure 36. VNA is used inside the Frankonia anechoic chamber.

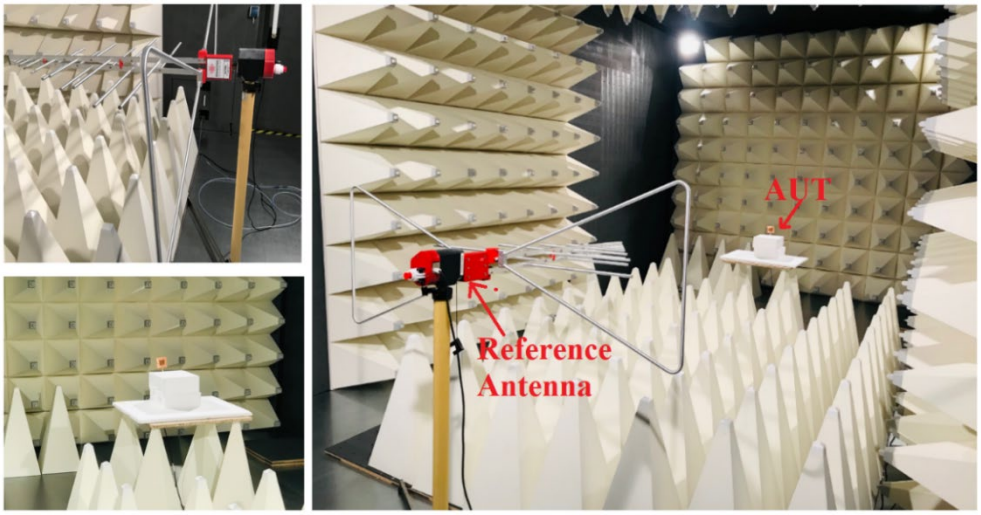

Figure 36. Frankonia Anechoic Chamber

3.2.5.2 Measurements of the *S*-Parameters

As discussed earlier, the effects of bending flexible polymer-based antennas have an impact on radiation characteristics such as resonant frequency, reflection coefficients and the gain. The impact on the *S*-parameters, in which the percentage shift, or the deviation, of the resonant frequency and the loss of signal strength, is discussed in detail in Chapter 2. The reflection coefficient S_{11} of the three polymer substrate antennas operating at 2.45 GHz is presented in Figure 37.

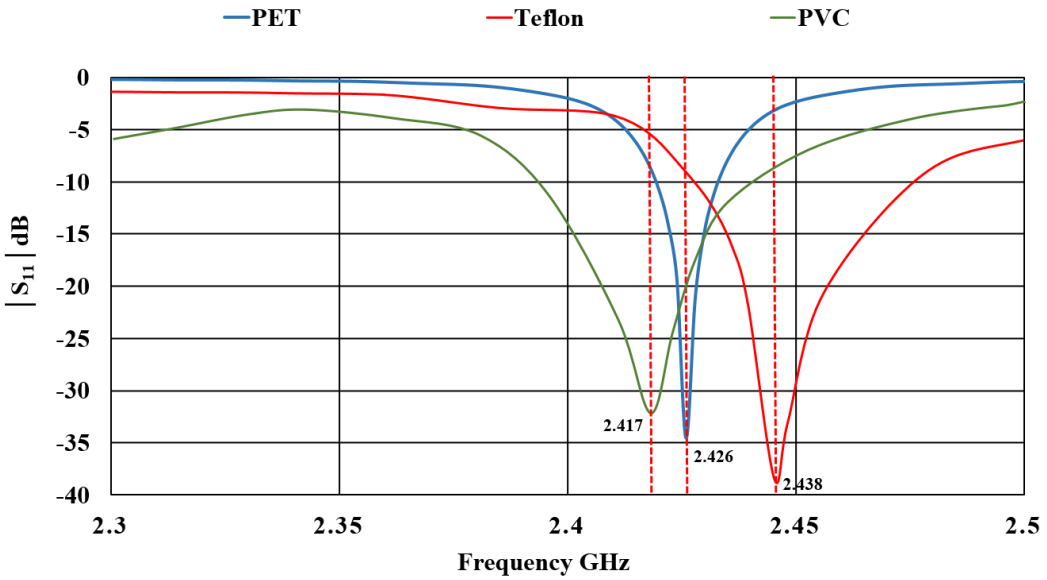

Figure 37. Reflection Coefficients of E-Shaped Flexible Polymer Substrate Antennas on PET, Teflon and PVC Substrates operating at 2.45 GHz

The measured results of the reflection coefficients S_{11} of the PET, Teflon and PVC substrate antennas operating at 2.45 GHz in the chamber show the resonant frequencies of 2.426 GHz, 2.438 GHz and 2.417 GHz, respectively. The reflection obtained for the PET-based antenna is -35 dB, the Teflon-based antenna is -39 dB and the PVC-based antenna is -32.5 dB. Similarly, the S_{11} parameters of the antennas designed for the operating frequency of 4.25 GHz and 7.45 GHz are presented in Figure 38 and Figure 39, respectively.

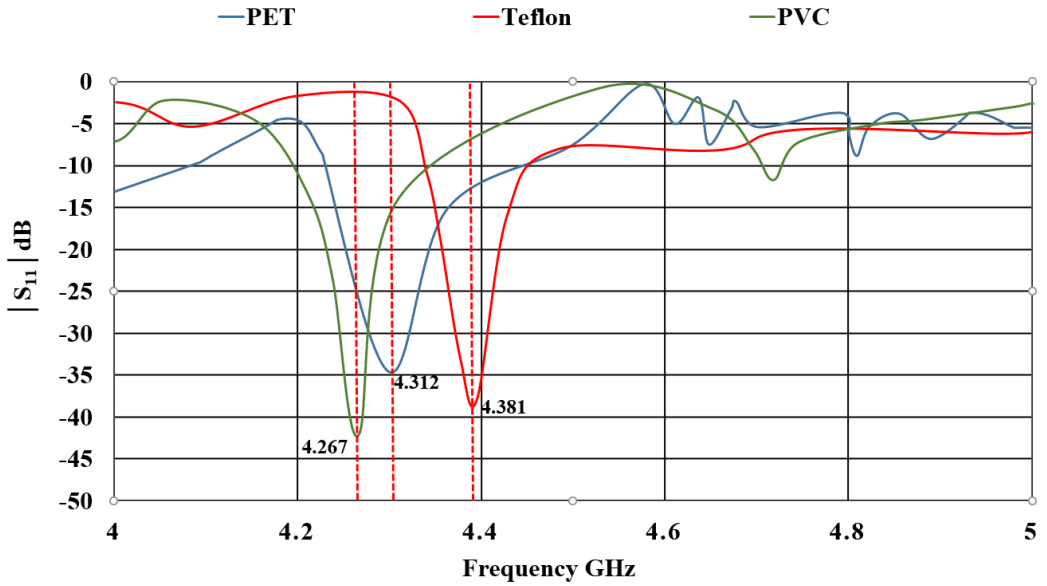

Figure 38. Reflection Coefficients of E-Shaped Flexible Polymer Substrate Antennas on PET, Teflon and PVC Substrates operating at 4.25 GHz

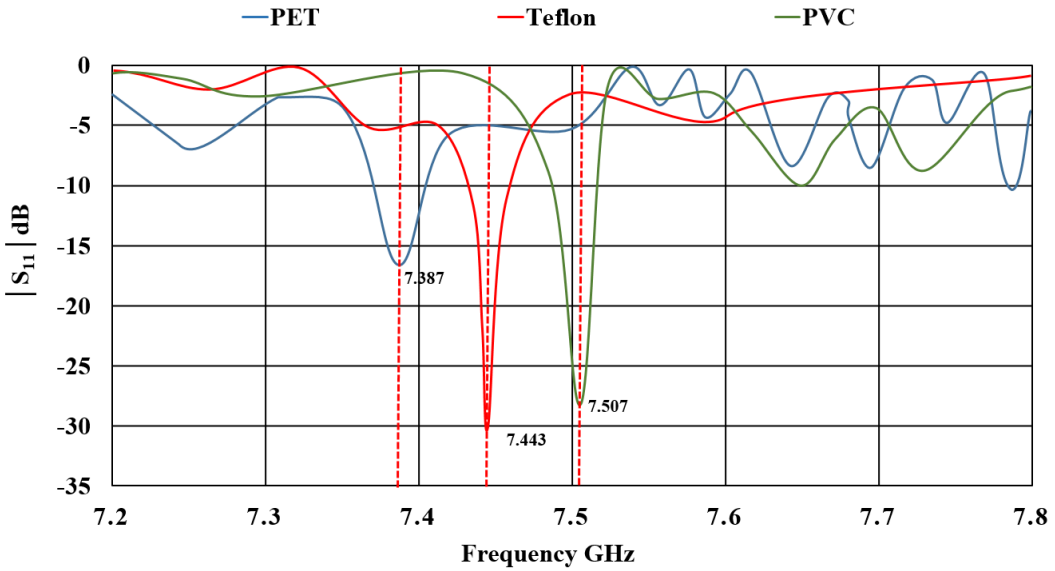

Figure 39. Reflection Coefficients of E-Shaped Flexible Polymer Substrate Antennas on PET, Teflon and PVC Substrates operating at 7.45 GHz

3.3 Bending Analysis

The bending of flexible antennas is different for the different range of frequencies which becomes very crucial at higher frequencies because of the small size of the antenna, impedance mismatching and the narrow bandwidth. The tested frequency ranges are divided into three groups to analyse the stable response in each range of frequency, as described earlier in this chapter. For this purpose, the effects of bending levels on the PET, Teflon and PVC substrate antennas for the bending levels of 14 mm and 27 mm are analysed for the flexible polymer antennas with an operating frequency of 2.45 GHz, 4.25 GHz and 7.45 GHz which lie within the three frequency ranges of i) 2.2-2.5 GHz, ii) 2.5 to 5.0 GHz and iii) greater than 5 GHz. To establish a consistent bend to the flexible antenna, polystyrene foams cylinders are used with the radial curvatures of 27 mm and then 14 mm, as demonstrated in Figure 40. In this figure, the bending of the flexible antenna on the foam at 27 mm, then 14 mm, and the connection with the VNA are exhibited.

The S_{11} parameters are obtained for these bending stages and compared with the parameters in a flat condition. Figure 41, depicts the reflection coefficients of the flexible PET, Teflon and PVC substrate antennas operating in the first range at 2.45GHz with a bending level of 27 mm and then 14 mm. Similarly, the reflection coefficients of each of the flexible antennas operating in the second two ranges, at 4.25GHz and 7.45GHz, with bending levels of 27 mm and then 14 mm are presented in Figures 42 and 43, respectively.

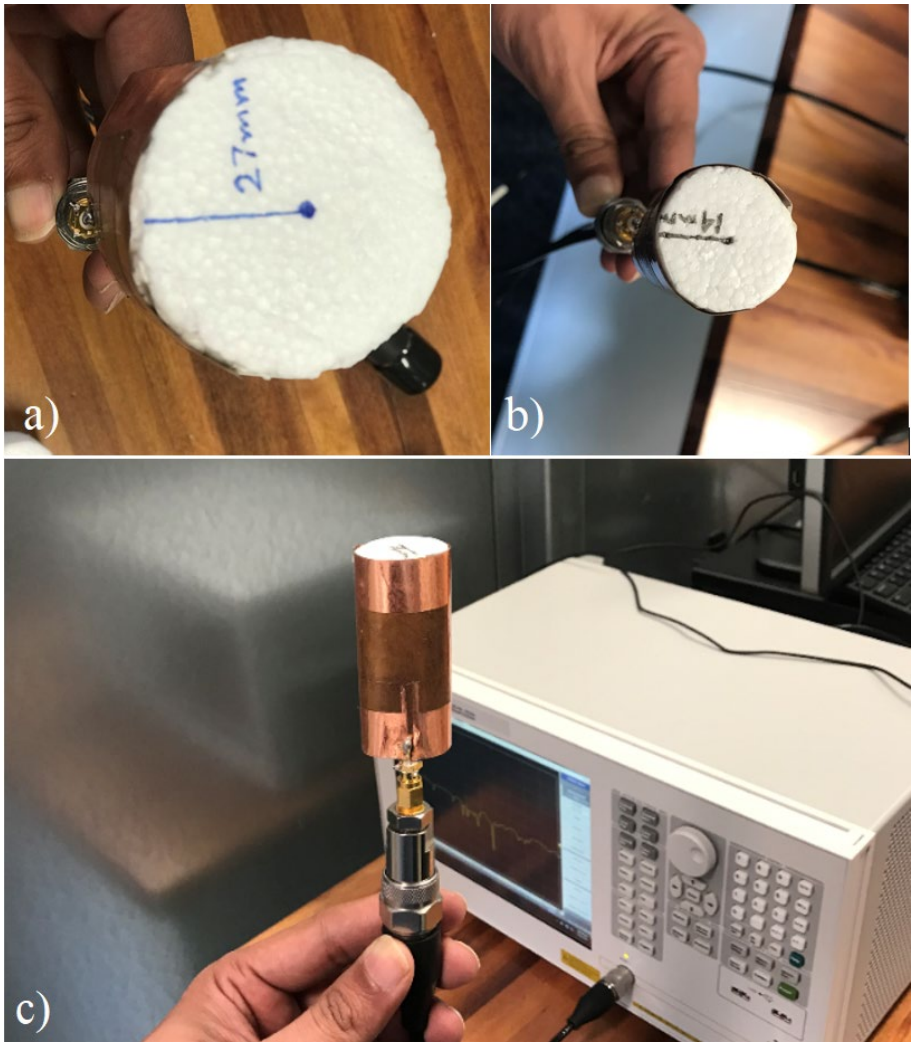

Figure 40. Cylindrical Polystyrene Foam to produce Flexible Antenna Bend a) at 27 mm b) at 14 mm c) Connected to VNA at 14 mm

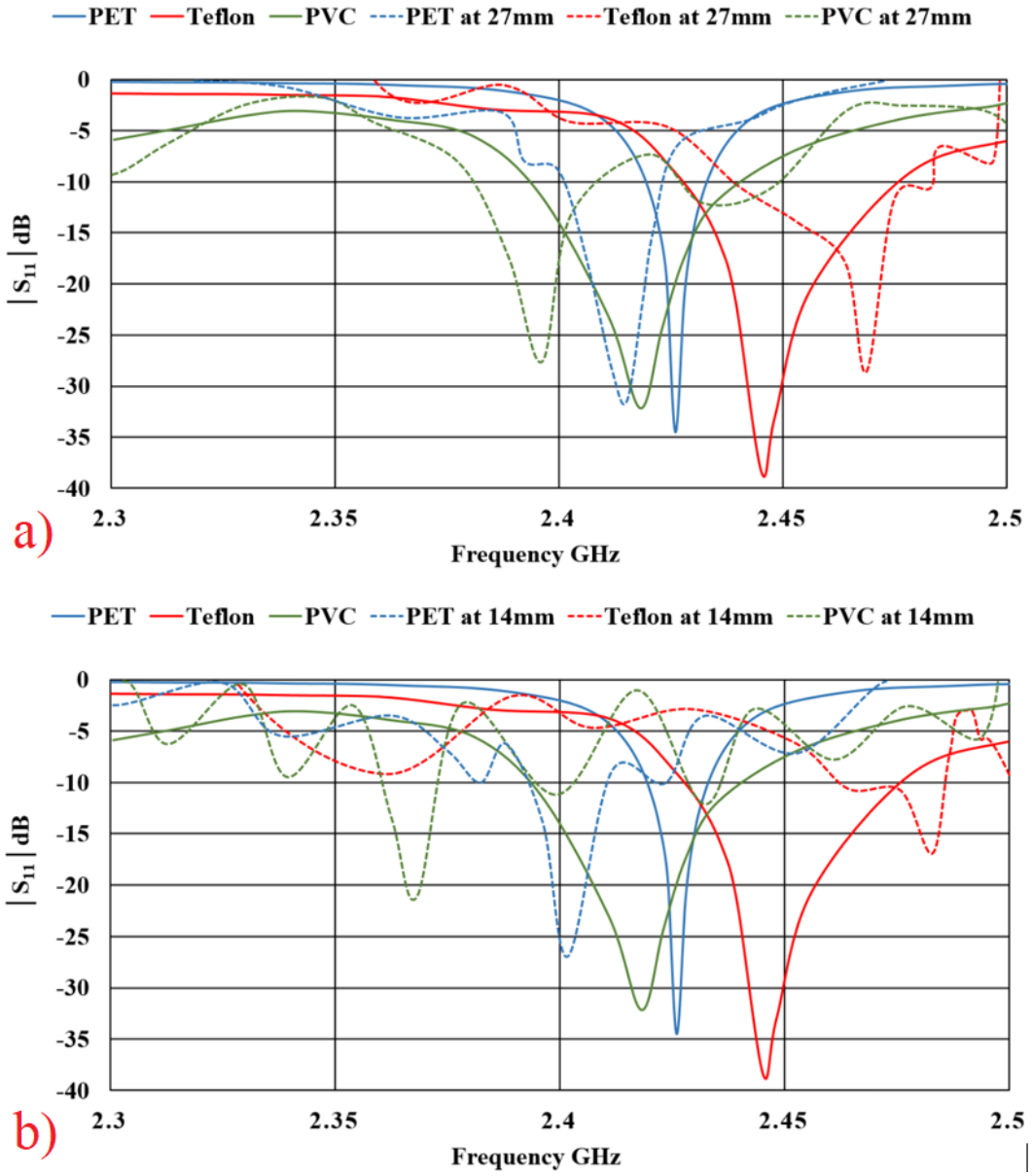

Figure 41. Operating at 2.45 GHz, Reflection Coefficients of E-Shaped Flexible Polymer Substrate Antennas on PET, Teflon and PVC Substrates Non-Bent and with Bending a) 27 mm b) 14 mm

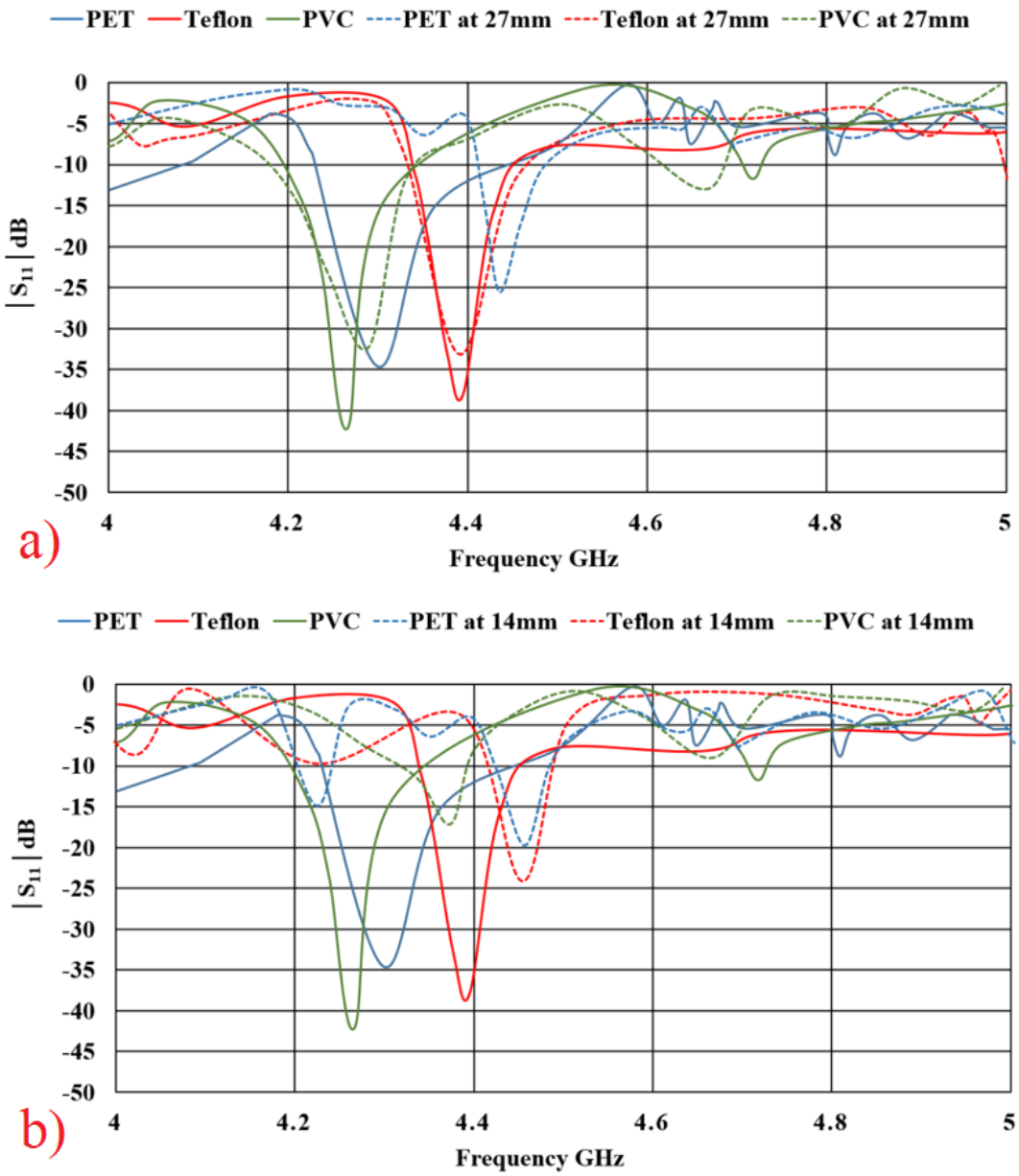

Figure 42. Operating at 4.25 GHz, Reflection Coefficients of E-Shaped Flexible Polymer Substrate Antennas on PET, Teflon and PVC Substrates Non-Bent and with Bending a) 27 mm b) 14 mm

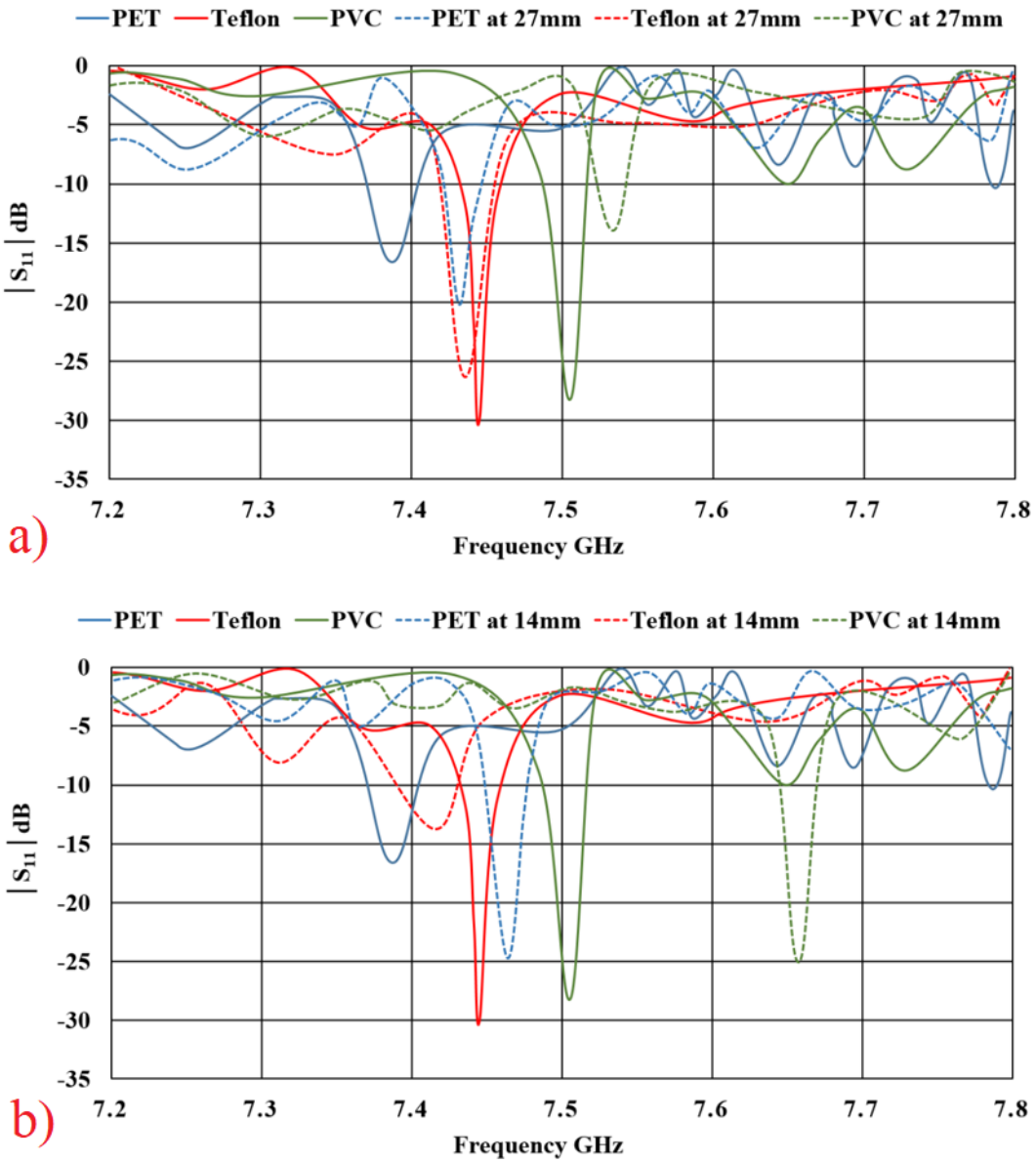

Figure 43. Operating at 7.45 GHz, Reflection Coefficients of E-Shaped Flexible Polymer Substrate Antennas on PET, Teflon and PVC Substrates Non-Bent and with Bending a) 27 mm b) 14 mm

3.3.1 Effect of Bending on Resonant Frequencies

The results obtained from the experimental verifications of the *S*-parameters inside the chamber, have been analysed with the shift in the resonant frequency for the various bending levels provided in Table 11, where it is deduced that the bending or curvature with bend states of 27 mm and 14 mm on polymer-based antennas generate different impacts on their FS.

As observed on the flexible antennas operating at 2.45 GHz, which is a frequency in the ISM-band used for domestic purposes that lies in the first group ranging from 2.2-2.5 GHz, the Teflon-based antennas undergo the highest percentage shift of frequency, of approx. 1.25%, towards the highest components of the resonant frequency for a bending state of 27 mm. This result is matched with the analysis provided in section 2.7.1. Contrastingly, the PET and PVC based flexible antennas

possessed less than 1% of frequency shift towards the lowest components of the operating frequency, indicated by the negative sign with the percentage shift and at the high-level of the radial curvature up to 14 mm, the PET substrate antenna gives very little deviation from the resonant frequency compared to the flat state, which is about 0.99% towards the lowest component, see Figure 41.

For the second operating frequency of 4.25 GHz which lies in the C-band suitable for the WiMAX frequency, the *S*-parameters of the flexible microstrip patch antennas reveals that Teflon is much less affected by bending up to 14 mm, providing a 0.25% and 1.61% frequency shift toward the highest components for the bending states of 27 mm and 14 mm, respectively, see Table 11 and Figure 42. In Chapter 2, in the analysis for operating frequency range 2.5-5.0 GHz, PTFE based flexible antennas were also ascertained to be more efficient by providing 4% of the shift on average. Hence, for this operating range, Teflon is a good candidate as a flexible substrate in terms of the deviation from the resonant frequency of the antenna. Conversely, the PET-based flexible antenna which was very efficient within the 2.2-2.5 GHz range, is highly impacted by bending in terms of frequency shift while operating at the 4.25 GHz frequency, see Table 11.

Table 11. Percentage (%) FS in Resonant Frequencies for Flexible Antennas on PET, PTFE and PVC Substrates at 3 Operating Frequencies with Bend Conditions of 27 mm and 14 mm

	Substrates		PET	PTFE	PVC
Resonant Frequency (GHz)	**Operating at 2.45 GHz**	Flat	2.426	2.438	2.417
		27 mm	2.412	2.469	2.394
		Shift (%)	-0.58	1.25	-0.96
		14 mm	2.402	2.484	2.366
		Shift (%)	-0.99	1.85	-3.42
	Operating at 4.25 GHz	Flat	4.312	4.381	4.267
		27 mm	4.442	4.392	4.294
		Shift (%)	2.92	0.25	0.62
		14 mm	4.468	4.453	4.366
		Shift (%)	3.49	1.61	2.26
	Operating at 7.45 GHz	Flat	7.387	7.443	7.507
		27 mm	7.425	7.429	7.541
		Shift (%)	0.51	-0.01	0.45
		14 mm	7.464	7.421	7.658
		Shift (%)	1.03	-0.29	1.97
	*The negative sign with the frequency shift (%) indicates that the shift occurs towards the lowest components of the frequency				

Understanding that the size of the antenna decreases with the increase in operating frequency and the impedance mismatching could be a problem, as with higher level bending and with higher frequency levels, the dissipation factor and dielectric constant of the polymer substrates could also vary. Keeping all these conditions in mind and by performing extensive electrical properties tests,

three antennas are designed and tested in the chamber for the higher operating frequency of 7.45 GHz. At the higher frequencies, above 5 GHz, impedance matching and feed line connection is a critical phenomenon that affects performance, however, although examined and successfully attained, these are not included in the investigative focus on bending capabilities for this dissertation. The PVC based flexible antenna is impacted most by the highest bending level of 14 mm, which gives a 1.97% shift towards the highest component of frequency, whereas the PET-based substrate antenna gives very little deviation from resonant frequency compared to the flat case and, once again, the Teflon-based flexible antenna has almost no impact of bending at 27 mm and at 14 mm only a 0.29% shift towards the lowest components of the operating frequency, see Table 11. This tested condition confirms that depicted in section 2.7.1, analyses of previously published research.

3.3.2 Effect of Bending on Reflection Coefficient S_{11}

The *S*-parameters of the designed antennas have been critically analysed to examine the effects of bending on impedance mismatch or the reflection coefficient S_{11} and the signal strength after bending. The impact of bending on the reflection coefficient of the flexible antennas operating at a different range of frequencies is examined by testing the three categories of i) 2.2-2.5 GHz, ii) 2.5-5.0 GHz and iii) greater than 5.0 GHz, where the antennas, designed on PET, PTFE and PVC, are analysed in the chamber for bending levels of 27 mm and 14 mm. The *S*-parameters depict the impact of the different levels of bending on the reflection coefficient in terms of signal strength and the impedance mismatch with the TL. A significant change in signal strength is caused by the bending or twisting of a flexible antenna because of the impedance mismatch with the TL or the creation of the surface waves. While signal strength may improve after bending because of its impact on the directivity of the antenna, most of the time it actually decreases, see Figure 41, 42 and 43.

In Figure 41, when a radial curvature of 27 mm is applied over the flexible antennas operating at 2.45 GHz, compared with the flat status of the antennas, the Teflon-based antenna is highly impacted with approx. 28% signal degradation whereas the PET-based antenna is less impacted with approx. 7.7% reduction in its signal strength. This degradation, although more extreme, is similarly observed with the 14 mm bending process where the Teflon-based antenna suffered a high 55% reduction in signal strength and the PET-based antenna demonstrated the least degradation with 23%.

For the experimental analysis of the flexible antennas operating at 4.25 GHz, in Figure 42 however, the Teflon-based antenna suffered the least degradation. Compared with the flat status of the antennas, for the bending level of 27 mm, the Teflon substrate bore the least impact of only 14% of signal strength reduction, which simultaneously defines its impedance mismatch at 27 mm and confirms the analysis in Chapter 2 in section 2.7.2. The signal strength reduction for both the PET and PVC substrate antennas is almost similar at approx. 22%. Indeed, with the 14 mm bending, the PVC-based flexible antenna suffered an immense signal reduction of approx. 60% whereas the Teflon substrate antenna possesses the least signal strength degradation of 25% lower than its flat status strength.

In Figure 43 with the comparison of the signal strengths in a flat condition for the flexible antennas operating at the higher 7.45 GHz frequency, the *S*-parameters illustrate that for the bending of the antennas to 27 mm, Teflon, as the substrate of the antenna, shows the least degradation with a low 12%. This contrasts with the PVC-based antenna which is heavily impacted with approx. 50% signal reduction. However, when the bending curvature increases to 14 mm, the impact measurements are reversed with the Teflon substrate antenna being impacted with a high 55% reduction in its signal strength The experimental results demonstrate that, with around 9% reduction, the PVC-based antenna has the highest tolerance for the increased bending with its comparatively low signal strength degradation and impedance mismatch being the least affected in this category. In this analysis, a PVC-based antenna is ascertained to be the most efficient for the frequency range greater than 5 GHz.

3.3.3 Dielectric Constant (ε) and the Resonant Frequency Shifts (%)

The permittivity ε of the polymer substrate, its Dielectric Constant, is a complex value which depends on the frequency, the roughness of the surface of the material and the temperature. As mentioned in section 2.7.3, flexible substrates for wearable applications normally have dielectric constants from 2 to 12 where lower values of its dielectric constant, from 2.2 to 3.5, serve to reduce the surface waves and increase the bandwidth and gain of the antenna in frequencies ranging from 2.2 to 7.5 GHz. Consequently, the three substrates used for the flexible antennas in this study, PET, Teflon and PVC, have the dielectric constants of 2.07, 2.70 and 3.70 respectively.

For the flexible antennas operating at 2.45 GHz, the PET-based flexible antenna which possesses a dielectric constant of 2.07, just under the ideal range of 2.2 to 3.5, is the least impacted by bending at 14 mm with a shift of only 0.99%. On the other hand, with the flexible antennas operating at the 4.25 GHz and 7.45 GHz, Teflon, with its dielectric constant inside the ideal range of 2.7, proves to have a low affectation in terms of the resonant frequency deviation from its flat status for the highest level of bending up to 14 mm. It is observed that the Teflon-based antennas, for the operating frequencies of 4.25 GHz and 7.45 GHz, possess shifts from the resonant frequency of only 1.61% and only 0.29%, respectively. While the PVC-based flexible antennas, with their 3.7 dielectric constants above the ideal range, possess a high shift of frequency while undergoing bending at 14 mm where they provide the highest level of deviation of 3.42% and 1.97% for the operating frequencies of 2.45 GHz and 7.45 GHz, respectively. Hence, from these experimental verifications, in addition to the comprehensive literature review in Chapter 2, a modified range of dielectric constant of 2-3.5 is recommended for polymer substrate antennas operating in a 2.2-7.5 GHz range for flexible wearable applications.

3.4 Summary

This chapter is comprised of the design, fabrication and testing of flexible antennas on PET, PTFE Teflon, and PVC polymer substrates operating at different ranges of frequencies. For this purpose,

three antennas are designed on each of these polymers operating at 2.25 GHz, at 4.25 GHz and at 7.45 GHz. Opting for the E-shaped design and using copper as the conductive material, the design of each antenna is performed in six steps: material selection; property examination; antenna design and simulations; fabrication; and testing in the chamber. The CST microwave studio computer simulator is used to both design and optimise the antenna designs and all tests are performed in the Frankonia anechoic chamber.

The bending of the flexible antennas is analysed in each of the different range of frequencies whereby the effects of bending levels of 27 mm and 14 mm on the PET, PTFE Teflon and PVC substrate antennas are analysed in comparison with the non-curved states of these flexible polymer antennas with operating frequencies of 2.45GHz, 4.25 and 7.45 GHz and are linked to the analysis presented in Chapter 2. These operating frequencies are positioned within the following three ranges of frequencies: i) 2.2-2.5 GHz; ii) 2.5 to 5.0 GHz; and iii) greater than 5 GHz. For the antennas operating in the first range at 2.45 GHz, the PET-based and PVC-based flexible antennas were observed to possess a less than 1% frequency shift towards the lowest components with the Teflon PTFE-based antennas showing the highest impact with a percentage shift of frequency of 1.25% for the 27 mm bend state. With the 14 mm radial curvature, the PET substrate antenna gave the best performance with 0.99% of frequency deviation from its flat status. For the second range, at an operating frequency of 4.25 GHz, the Teflon-based antenna contrastingly possessed the lowest frequency deviation which was 0.25% and 1.61% for bending levels of 27mm and 14mm respectively and for the operating frequency of 7.45 GHz, in the third range, the Teflon-based flexible antenna presented almost no impact of bending at 27 mm and for 14 mm only a 0.29% shift towards the lowest components of the operating frequency. The PVC-based flexible antenna was impacted the most for the highest bend level where, in terms of the impedance mismatch at 14 mm bending, with a 1.97% shift, the PVC substrate antenna is ascertained to be the most efficient for this frequency range.

As the bending of flexible antennas highly impacts S-parameters and the central frequency shifts, suitable physical, electrical, mechanical, and thermal properties can be used to amplify the performance of the flexible antennas for the bending capabilities.

Chapter 4: **Polymer-Based Chipless RFID Tags**

4.1 Introduction

The RFID tags based on polymer substrates can possess very enticing characteristics including high flexibility, crumpling and stretchability, being lightweight, possessing corrosion and humidity resistance, an ease of processability, and most importantly being low cost and easy to fabricate. A significant aspect that does need to be addressed, however, are the radiation and scattering characteristics caused by bending to certain curvatures.

This chapter provides an overview literature review of RFID and briefly elaborates the basic conceptions regarding RFID tags before giving emphasis to the encoding techniques for the tags on polymer substrates. With the introduction of a novel Flexible Bow Tie Chipless RFID tag using the FSS approach with a frequency ranging from 4 to 18 GHz, its design, fabrication, testing and comparative analyses are presented and compared to an Octagonal-shaped tag already published in the literature. The two chipless RFID tags being compared are both designed and fabricated on a PET substrate.

The proposed novel flexible Bow Tie Chipless RFID tag, published in [1], has a design based on a traditional bow tie structure. The bow tie-shaped antenna configuration was selected because it provides the most intense surface current flows across the edges with a resonating elementary cell [73] which allows more powerful reflection characteristics. Unlike the octagonal [56], square [306], circular [160] and triangular [307] designs, the bow tie design is also recognised as providing increased flexibility in designing for a specific range of frequencies. Furthermore, compared to closely placed symmetrical surfaces, asymmetrical surfaces, such as the bow tie, are known to diminish mutual coupling [159].

The proposed design represents a 4-bit chipless RFID tag with a periodic pattern of cells applicable for various wearable and IoT applications. In this design, the polarization feature of non-periodic bow tie-shaped cells is taken into account to obtain destructive and constructive interferences. The projection of the incident waves and reflected fields are decoded in terms of bits assigned to RCS [56]. This RCS parameter characterizes the level of scattering of a target object, with a tag being the target object in this case, and can be extracted as a function of the incident angle of the transmitted signal which depends on the frequency. The RCS results of the second tag, the periodic Octagonal-shaped Chipless RFID Tag design, are compared with the proposed Bow Tie Chipless RFID Tag design and the transient behaviour by the application of EM wave on the 4-bit Bow Tie-shaped Chipless RFID Tag is explained.

In this chapter a simple equivalent model of the tag, by using Singularity Expansion Method (SEM)-based circuit modelling, is presented. Furthermore, the coupling coefficients and the induced currents over the bow tie-shaped resonators (rings) are evaluated and transient response of the Bow Tie RFID tag is analysed. Besides, an FSS-based Bow Tie RFID tag on different polymer substrates

to analyse the bending capabilities and effects on RCS are tested in the chamber. The polymers are highly resistant nonconductive materials made up of repeated subunits of hydrocarbons known as monomers [290]. They are divided into two types: Natural polymers, such as silk, rubber, starch and wool and Synthetic polymers which are chemically prepared in laboratories, like PVC, polystyrene and nylon etc. To facilitate bending and flexibility in different antennas and RFID's, polymers such as Polyimides (PI), Polydimethylsiloxane (PDMS), Polytetrafluoroethylene (PTFE), Rogers RT/Duroid and Liquid Crystal Polymer (LCP) are widely used as the most appropriate substrates [101]. Finally, the maximum read range of the flexible Bow Tie tag is measured.

4.2 Background: RFID Technology

During the last few decades, microsystem technology has not only focused on the size of components but also the flexibility of the electronic structures. Resultantly, flexible electronics have become essential for applications that require flexible displays and biomedical applications with complex curvilinear structures [169, 170]. Similarly, the flexibility of different materials is of great importance in electronics and communications as they are used extensively for flexible displays, smart tags, wearable products and flexible antennas [308]. Moreover, these flexed systems are widely used in healthcare monitoring systems, aeronautics and for the Radio Frequency Identification (RFID) tagging applications [128].

RFID is a well-known technology extensively used in diverse applications [126, 127] where, current RFID techniques in commercial use include, but are not limited to, Near-Field Magnetic Coupled tags, UHF RFID tags and chipless RFID tags [128]. Most of the conventional RFID tagging techniques use some kind of time-variant loading or scatterer modulation to transmit information into the backscattered field [129-132]. This type of backscattering requires the physical movement of the object to be coded or electronically changed through impedance modulation or inductive coupling. The majority of these traditional RFID tags are made from a near-field circuit and incorporate a low-cost chip at the centre. While the characteristics of this low-cost chip could be as simple as holding a single code or be sufficiently complex to execute different algorithms, in the contrastive passive or chipless RFID tagging, the ID code is not saved in memory, instead, using actual physical features of the tag itself to send data [126].

These passive RFID tags have gained considerable attention with design and application prospects for the non-existent battery and additional circuitry. With further significant advantage over conventional tags in characteristic features like their reduced size, increased lifetime and low manufacturing cost [133], the foremost advantage of these chipless RFID tags, most certainly, is their promise of being extremely cheap while sustaining an adaptive versatility, allowing them to be printed onto packages or other materials as simply as affixing paper barcodes. This, combined with the unequivocal advantage of the similar absence of electrical circuits in these tags, consequently further opens the tags to design implications for functional incorporation into applications where tags could be exposed to the elements with no detrimental effects. Correspondingly, these types of

tags very naturally lend themselves to wearable applications where washing and heating may otherwise affect an energy source [134].

The conventional chipless RFID system comprises a transmitter and a receiver which branches out as an adapted version of a UWB frequency radar [135]. An EM wave, which compromises a wide range of frequencies, is subjected to the RFID tag with the effect that the tag backscatters the received wave. The resounding energy is picked up by the receiver, as shown in Figure 44. When this reverberating incident EM wave strikes the tag, the vibrated connection induces a current in the elementary cell at the resonant frequency. This resonance then periodically effects all of the other resonators and hence results in spikes or dips when it reaches the receiving antenna. The information is then decoded in terms of RCS, where the presence of spike corresponds to high '1' and the absence of resonance corresponds to '0'.

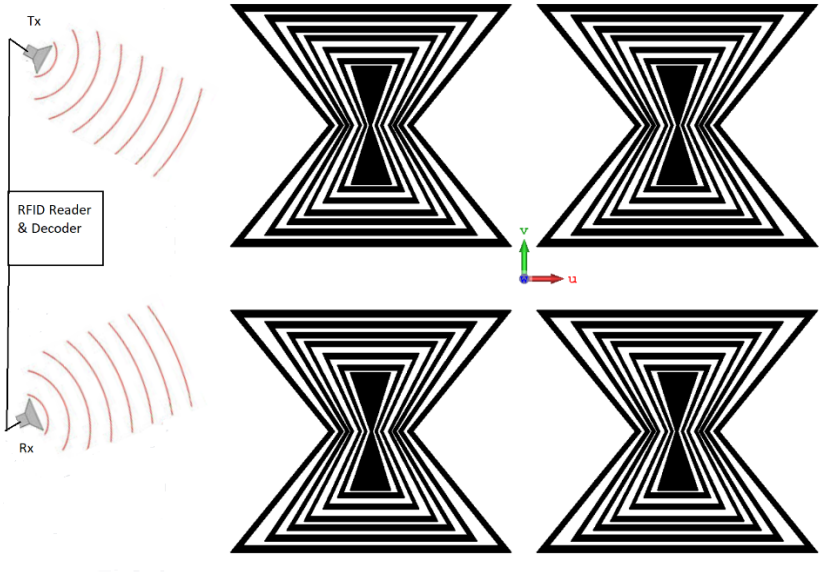

Figure 44. 2×2 Array Chipless RFID System

Beyond the confinement of the chipless RFID tags being primarily operated by the resonance obtained from metallic surfaces, and not carrying electronic circuitry to handle any communication protocols, many designs have innovatively been proposed for chipless RFID tags. These designs are characterized by two general approaches: The first group refers to time-domain-reflectometry-based designs for which SAW is an example whereas the second group, classified as spectral-based tags, incorporate the FSS technique.

The phenomenon behind SAW-based RFID tags is the piezoelectricity in which EM waves entering into the tags are converted into acoustic waves by an IDT positioned on the surface of the piezoelectric substrate. These acoustic waves, while propagating through the surface of the substrate, corresponding to conductive reflectors which are separated by a certain distance to enable the reading of the ID codes stored on the tags [136, 137]. While actual SAW RFID's are presently in commercial use, there are still some important issues that need to be addressed, including characteristics for size reduction and an increase in data capacity and reading range [128].

To this aim, the FSS is a promising technique in which, when the frequency of an EM wave matches with the resonant frequency of the FSS shape, the incoming EM wave either transmits or reflects completely or partially, depending on the nature of the two-dimensional array of conductive elements arranged on the particular dielectric substrate [138]. While flexible substrates in the FESs are mostly characterized by energy efficiency, lightweightedness, low manufacturing costs, reduced fabrication complexities and mechanical robustness [101], it is important to address a high flexibility level without losing sight of a high radiation performance as well as the mechanical, electrical and thermal properties of the substrate materials appropriate for this technique. Understandably, chasing radiation perfection can, at times, cause increases in antenna costs and, indisputably, it is the substrate flexibility that dictates the bendability of the antenna. Antenna deformation critically affects not only the radiation patterns and resonant frequency, but also the level of impedance matching, bandwidth, directivity, radiation energy and efficiency [74, 109]. Moreover, the compactness and desirable radiation characteristics of a flexible substrate, which are useful for wearable applications [134], are also required for high radiation efficiency [73, 115, 116]. The flexible polymer-based chipless RFID tag, with its application as a polymer-based chipless RFID tag embedded on cloth, maybe a good candidate to finally address these challenges, see Figure 45.

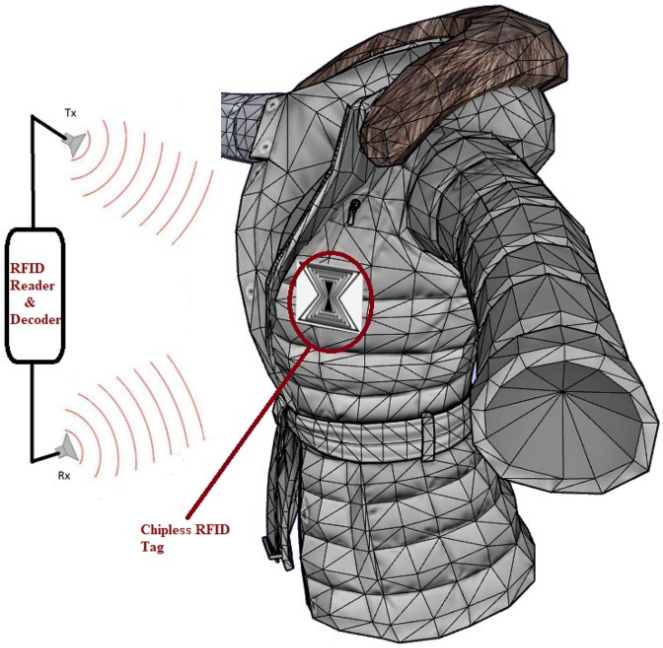

Figure 45. Chipless RFID Tag Embedded on Cloths

Research on wearable wireless communication and flexible devices has increased rapidly in recent years, due to its suitability for applications targeting personal communication systems [309] and flexible antennas and RFID tags are now used to keep track of several daily-routine activities, such as heartbeat and blood pressure measurement, the distance walked, the steps are taken and the calories burnt [126]. RFID tags such as these are extensively used as wearable sensors as well as for other general IoT applications. The IoT relies on smart environments comprised of wireless sensor networks [91] and personal area networks [310, 311] in which interaction with the IoT infrastructure

must be uniquely identified. One immense challenge for this is the need to commence a seamless integration of IoT solutions both with the surroundings and with people [312]. The growth in wearable technology and the success of wearable devices has only really been hampered by specific limits like the lack of materials and manufacturing techniques to embark on this seamless integration with electronic parts [40] with sufficient robustness in washing, drying and moulding [30, 313].

4.3 Fabrication and Testing in Chamber

To verify the simulated results achieved in CST studio, both the Bow Tie and Octagonal antennas are fabricated on PET substrates of 70-micron thickness. The printing is accomplished using the Universal Laser Systems (ULS) PLS6MW with Lens: 2.0 MW and Laser: 10.6-micron wavelength – CO2 Laser with the obtained RCS results from the tags being analysed by the VNA in an anechoic chamber as shown in Figure 46(a).

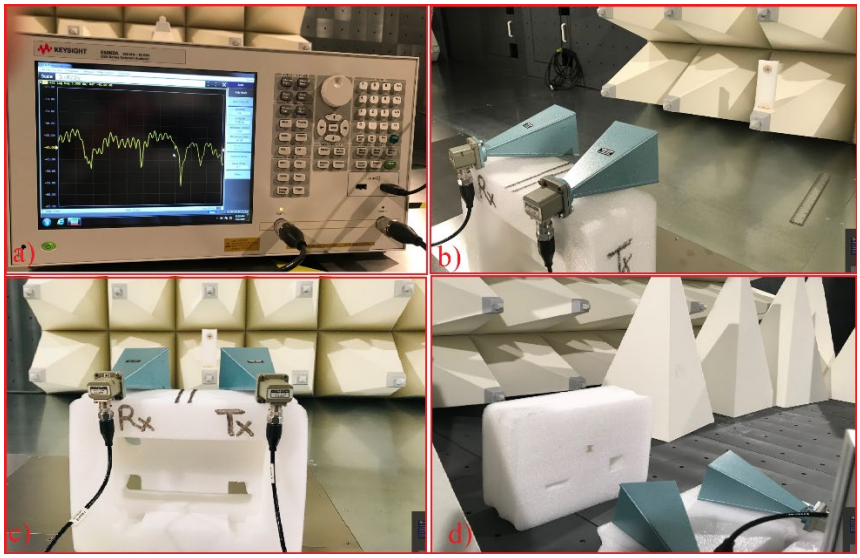

Figure 46. Experimental Setup and Apparatus in Chamber a) VNA b) Octagonal Tag Analysis c) Two Identical Horn Antennas using as Tx and Rx Antennas d) Testing and RCS Measurements of Bow Tie Chipless RFID Tag

For this purpose, VNA is used with two identical horn antennas operating at 4 GHz to 18 GHz frequencies. Test results of both RFID designs in the Frankonia chamber, which has a pre-compliance testing frequency range up to 40 GHz, are shown in Figure 46(b-d). The actual aspects of the fabricated tags are shown in Figure 47.

4.3.1 Simulated and Measured RCS Results

The RCS obtained from the simulation and experiments for both designs are shown in Figure 48. The measured and simulated results indicate that both tags are in good stead for obtaining 4-bit coding patterns. The printing of the tags, however, was not a straight forward exercise as the line tracks, being extremely thin, proceeds with the consequence that the current distribution in the measured results is not as clear as the simulated results with this factor most evident in the higher frequency part of the imaging where there is a discrepancy in determining the ultimate bit encoded.

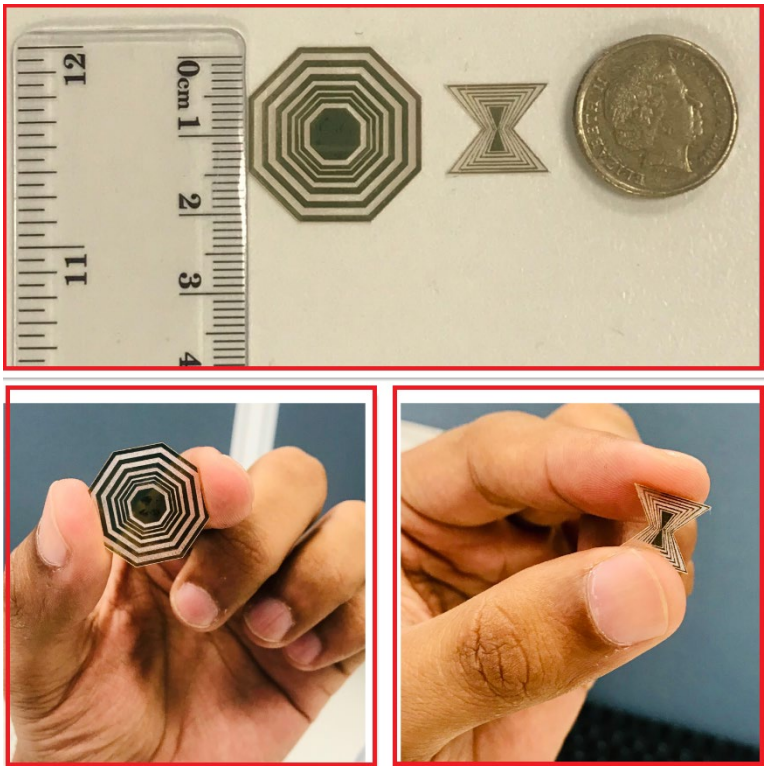

Figure 47. Actual Aspects with Dimensional Comparison of the Octagonal and Bow Tie Chipless RFID Tags

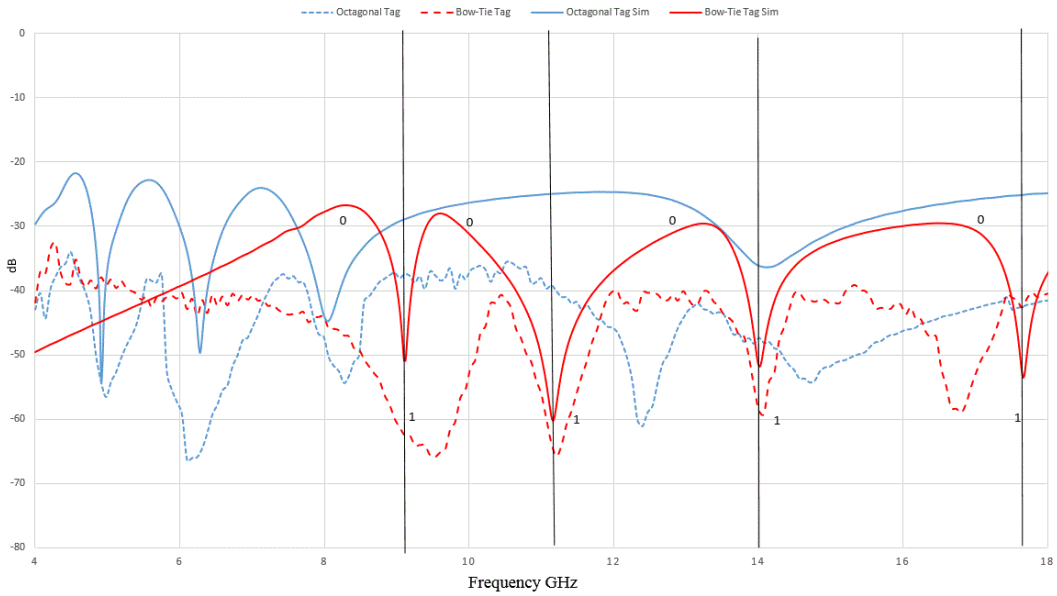

Figure 48. Measured and Simulated RCS Results for Bow Tie and Octagonal Chipless RFID Tags on PET Substrate

4.3.2 Comparative Analysis of the Octagonal and Bow Tie Chipless RFID Designs

A comparison of the essential characteristics of the two RFID tags is illustrated in Table 12. Most notable are the distinctions in dimensions and operating frequency ranges where the Bow Tie Chipless RFID tag is much smaller, at approximately half the size, and operates at the higher 8 GHz -18 GHz. Moreover, the transition of RCS in dBs from minimum (0) to maximum (1) states of the

Bow Tie Chipless RFID tag is 28% more than the Octagonal Chipless RFID tag, which makes it easier to detect bits after being scattered through the tag.

Table 12. Comparison of Octagonal and Bow Tie Chipless RFID tags

Chipless RFID Tags	Octagonal	Bow Tie
Structure	Periodic	Non-Periodic
Size of Tag (mm)	25x25	13.44x10.44
Unit Cell Dimension (mm)	6.6 x 6.6	1.86 x 5.41
Operating Frequency (GHz)	4 to 12	8 to 18
No of Outer Rings	6	6
No. of Bits Stream	8	8
Bits Transitions from min (0) to max (1) (dB)	25	32

4.4 Design and Operation of Chipless RFID Tags

In [56], the presented Octagonal Chipless RFID tag designed on a flexible PET substrate, encodes a bit sequence through different combinations of ring structures that resonate with constructive and destructive interferences. When the tag is subjected to a wideband incident EM wave, a surface current *J* is induced on the elementary cell of the tag [149, 314, 315]. This current, in turn, generates its own backscattered wave *Es*, which is then transmitted to the receiver antenna. When two rings are placed around the elementary element at the centre and the additional rings surround it, further currents J_{out} are induced on the outer rings which, in turn, induce surface currents J_{in} on the inner ring. This destructive interference results in backscatter waves *Es*. To control whether the wave is destructive or constructive, one of the rings needs to short circuit, otherwise, both rings need to remain open-circuited as, if both rings are short-circuited, the induction of in-phase (no phase difference) surface currents J_{in} and J_{out} [56]. Hence, in this octagonal design, periodic cells are both opened and short-circuited to obtain the necessary destructive and constructive interferences for the incident waves to be reflected. Consequently, an RCS is able to encode a string of bits. In this study, two RFID tags for UWB frequencies are designed, operating in the 4 -18 GHz band and based on FSS technique: the new Bow Tie design and the Octagonal tag, which is reproduced in accordance with the already published design [56]. In terms of operation, once the incident wave strikes onto a unit of the conductive surface and matches the resonant frequency, it is either transmitted or reflected depending on the position of the array of elements. The resonant frequency depends on the inductance *"L"* and capacitance *"C"* of the metallic rings which surround the cell unit [138]. The resonant frequency can be calculated by

$$Fr = \frac{1}{2\pi\sqrt{LC}} \tag{36}$$

Error! Bookmark not defined.

Figure 49 shows the simulated surface current distribution over the cell unit and all of the periodic bow tie cells after being subjected to an incident EM wave *(Ei, Hi)*. The surface current density *J* tends to be highest and almost constant in all vicinities of the Bow Tie tag except for the vertical portions at the base and ceiling. The area where a high surface current is registered corresponds to the inductive area of the tag while the surface area with low or minimum surface current relates to the capacitive behaviour of the tag.

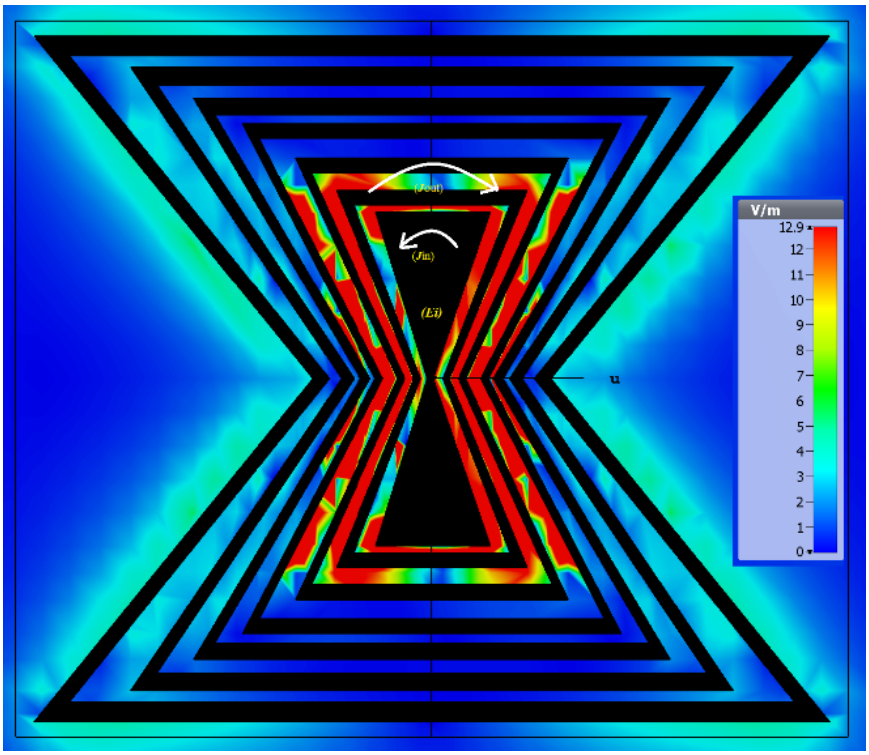

Figure 49. Simulated E-Field Showing Induced Surface Current Distributions

When two Bow Tie rings are placed in a manner that the elementary element is in the centre and the rest of the rings surround it, as shown in Figure 49 surface current J_{in} on the inner ring (the innermost ring), and a surface current J_{out} on the outer ring (the first consecutive to innermost ring), are induced. In this case, all the surrounding Bow Tie rings, constituting the whole structure, interact with each other and with the other rings to create a specific frequency response. The standing waves produced by these surface currents are approximately equal but opposite in phase which creates polarization with an odd multiple of the difference of π phase. It is, therefore, the result of this destructive interference that creates the backscattered wave which, in turn, produces the frequency response.

4.4.1 Octagonal Chipless RFID Tag

After first designing an Octagonal Chipless RFID Tag using gold as the conductive material on a flexible 25 mm × 25 mm PET substrate with 70-µm thickness and permittivity of 2.077 ε, in order to attain more precise results, the dimensions of the tag were further optimized, as illustrated in Figure 50. The unitary element of this design is composed of concentric octagonal rings.

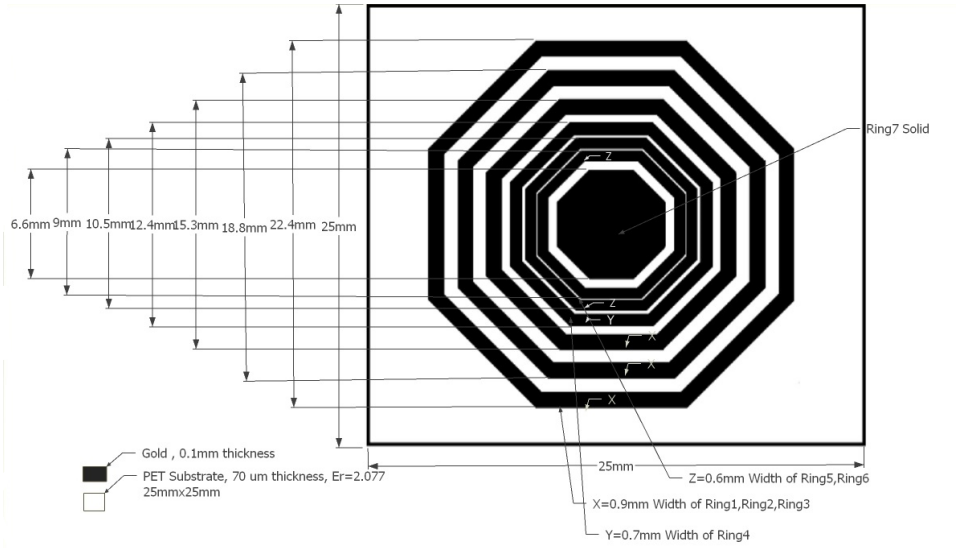

Figure 50. Octagonal Chipless RFID Design and Dimensions

4.4.2 Novel Chipless Bow Tie RFID Tag

Our evolutionary design proposal of a bow tie for a Bow Tie Chipless RFID Tag is based on the FSS technique. This design base was selected on the knowledge that with the traditional bow-tie structure, the most intense surface current flows across the edges with the resonating elementary cell [73]. The Bow Tie tag is designed on a 13.44×11.56 mm^2 PET substrate of 70-µm thickness with conductive gold rings varied in thickness. CST MICROWAVE STUDIO was used to optimize the design and obtain appropriate dimensions. Figure 51 shows the design aspect of this novel Bow Tie RFID tag which delivers notably improved results as compared to the previous Octagonal RFID design [73].

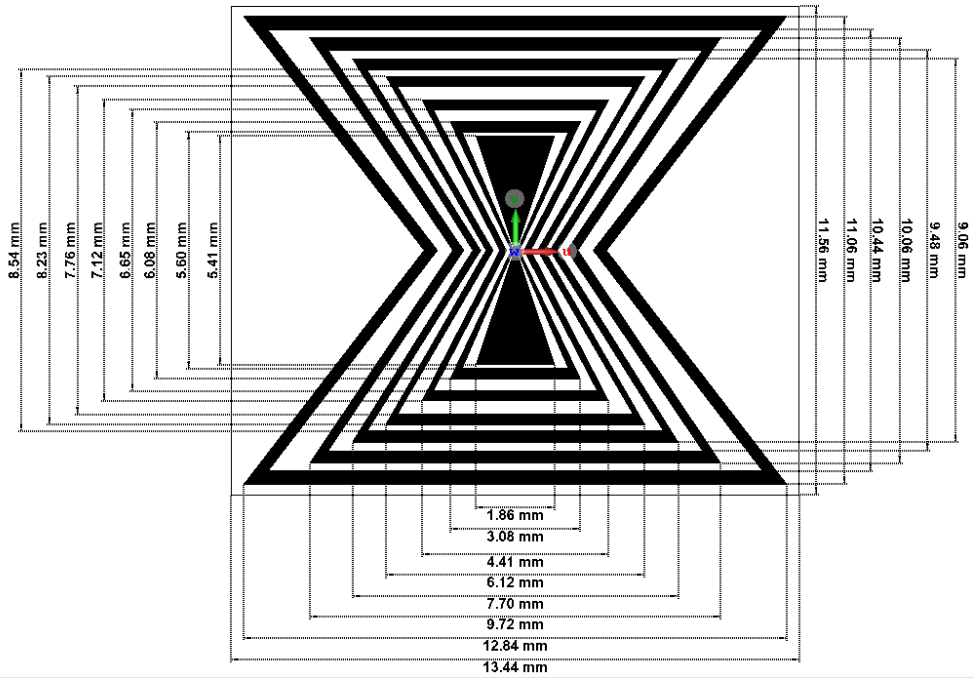

Figure 51. Bow Tie Chipless RFID Design and Dimensions

4.5 Electromagnetic Behaviour of the Bow Tie RFID Tag

The circuit model of the Bow Tie Chipless RFID tag provides insight into the electromagnetic response of the circuit when an incident EM wave strikes at the tag and the induced current re-radiates into the scattered fields. The current induced on the tag can be evaluated in different ways. One method is based on SEM in which the current induced on the tag is expanded in terms of the singularity poles of the tag. Since the concept of SEM was introduced, it has been widely used in circuit theory, and, for a long time, this technique has been more specifically used in evaluating electromagnetic response and for designing chipless RFID tags [157, 158, 316].

4.5.1 SEM-Based Equivalent Circuit of Chipless RFID Tags

This section presents a solution for the SEM-based equivalent circuit of the Octagonal Chipless RFID tag which is evaluated as a collection of poles *Sn*, coupling coefficient *Rn* and the entire function F_e in the complex frequency domain. The scattering analysis is performed by representing the chipless RFID tag with an equivalent circuit representation, see Figure 52. For the electromagnetic response, the RFID scatterer is assumed to be a Perfectly Electric Conductor (PEC) in free space. Let N be the total number of scatterers where an incident electric field E^i strikes at the surface of the tag and E^s represents the scattered electric field with polarization vectors $\hat{a}_i$ and $\hat{a}_s$, respectively. The E^i causes an induced current J_n and the global resonances are modelled in the time-domain as damped sinusoidal corresponding to the Complex Natural Response (CNR) of the scatterer with the weighting residue represented by coupling coefficients R_N. The distance between the two scatterers is optimised in such a way that the coupling between one and the alternative scatterer is very small to be negligible. Hence, the coupling is considered between only two scatterers at a time, and ignore the effects of the others on them. The SEM-based circuit equivalent model of the Octagonal Chipless RFID tag, presented in Figure 52, demonstrated that $R_1, R_2, \ldots R_N$, $L_1, L_2, \ldots L_N$ define the resistances and the inductances, respectively, and $C_1, C_2 \ldots C_N$ is the inductance between two consecutive scatterers for N number of resonators.

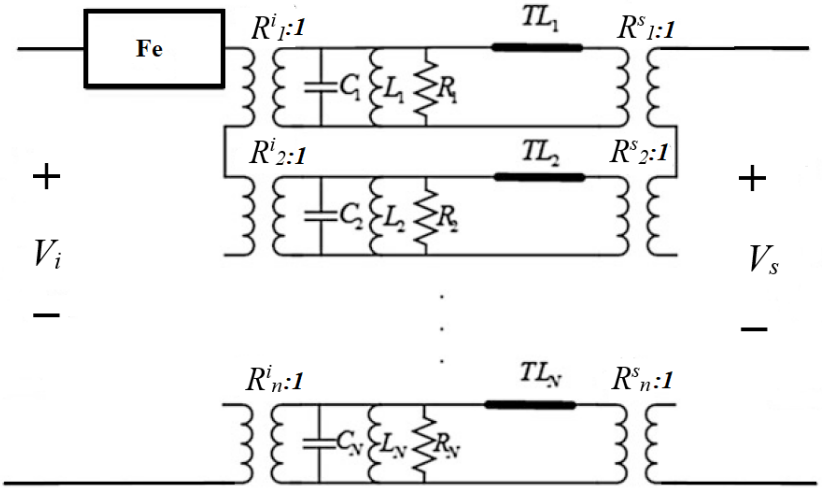

Figure 52. SEM-Based Equivalent Circuit of a Bow Tie RFID Tag with *N* number of Resonators

E^i is coupled to the CNR by coupling coefficients $R_1, R_2 \ldots R_n$, which depend on the direction and the polarization of the incident electric field, and these values $R_1, R_2 \ldots R_n$ of the coupling coefficients have no impact of E^s. Each CNR is represented by a parallel RLC circuit in series with a delay line, or the Transmission-Line, which describe the CNR turn-on time, and F_e shows the early-time response of the tag. The input V_i and output V_s voltages are defined at the transmitting and receiving antennas ports, respectively. Figure 53 shows the geometry of a Bow Tie tag when E^i strikes at the surface of the tag and the E^s electric field is scattered with polarization vectors $\hat{a}_i$ and $\hat{a}_s$.

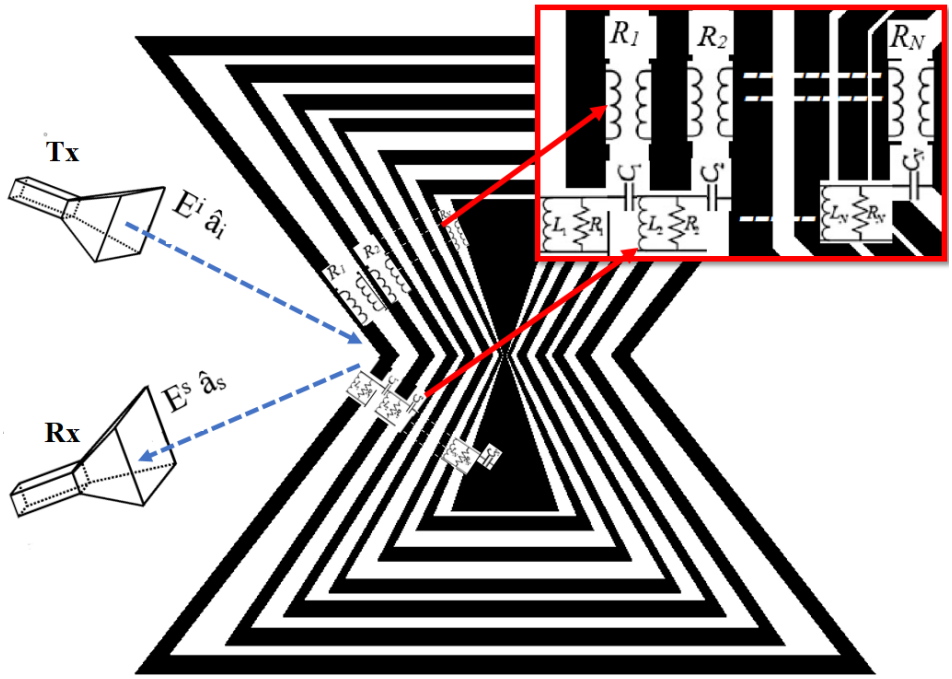

Figure 53. Geometry and Internal Circuit Modelling of Bow Tie RFID Tag Influenced by Incident Electric Field E^i

Assuming the incident electric field as a Dirac-delta function, then the transfer function of the tag in the complex s-plane is defined as in [128], can be written as (37).

$$H_t(\hat{a}_i, \hat{a}_s; s) = \frac{E^s(r;s)}{E^i(r;s)} \tag{37}$$

After some mathematical alterations, the transfer function, in terms of an early time response $H_e(s)$ and a late time response $H_1(s)$ with CNRs, can be written as

$$\begin{aligned} H(s) &= H_e(s) + H_1(s) \\ &= H_e(s) + \sum_{n=1}^{N} \left[\frac{A_n}{s - s_n} + \frac{A_n^*}{s - s_n^*} \right] \end{aligned} \tag{38}$$

where

$A_n = \frac{C}{2}\left(1 + j\frac{1+\alpha_n}{\omega_n}\right)$ and the CNRs of the circuit are described by

$$s_n = \alpha_n + j\omega_n \tag{39}$$

$$\alpha_n = -\frac{\omega_0}{2Q}$$

and

$$\omega_n = \frac{\omega_0}{2}\sqrt{4-\frac{1}{Q^2}} \tag{40}$$

Where Q is kept below 0.5 for low power losses, as described in [128], and the RFID first resonator resonates at $f_1=\omega/2\pi$.

4.5.2 Evaluation of Surface Current Distribution (Jn) and the Coupling Coefficients (Rn)

For the current distribution over the first resonator, the outermost Bow Tie ring I_1 and the induced voltage V_1 due to incident fields correspond to the impedance Z_1 of the resonator for the current distribution over the Bow Tie scatterers to be evaluated by discretising the length of the ring into N number of segments [128] as shown in Figure 54.

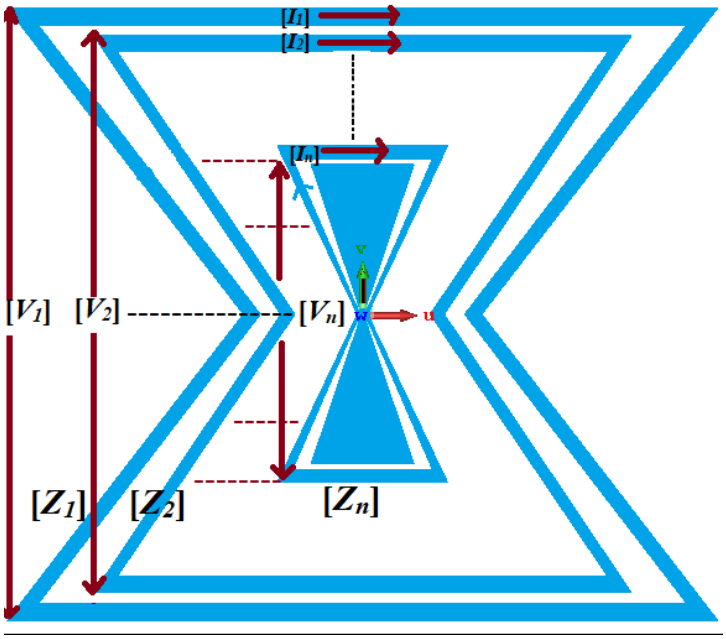

Figure 54. Induced Voltages and Currents Distributions over Tag Surface

Equation (41) represents the magnitude of the current flowing through the resonators where $[Z_1]$ corresponds to $N\times N$ matrix referred to as system impedance matrix, $[I_1]$ and $[V_1]$ are the response vector of N×1 corresponding to the incident field, see Figure 54.

$$[I_1]=[Z_1]^{-1}[V_1] \tag{41}$$

The CNR's for the first scatterer is calculated from

$$[Z_1(s_n)][I_1(s_n)]=0$$
$$\square_1(s_n)=\det(Z_1(s_n))=0 \tag{42}$$

The CNR's for the first resonator is obtained by expending $\square_1(s_n)$ in complex Taylor series as given in

$$\square_1(s_n) = \square_1(s_0) + \square_1'(s_0)(s - s_0) + \ldots = 0 \tag{43}$$

By keeping the first two terms of the equation and ignoring the rest of the values the CNR, S_n, is obtained from

$$s_n = s_0 - \frac{\square_1(s_0)}{\square_1'(s_0)} \tag{44}$$

where S_0 is the initial resonant frequency estimation, by repeating this procedure, more accurate values can be evaluated for the first scatterer. The first more accurate value of resonance for the Bow Tie design was calculated at approximately 9.2 GHz. By modifying (40), the current distribution for the first resonator of the Bow Tie Chipless RFID tag is evaluated as

$$[I] = \sum_n \frac{R_n}{s - s_n}[J_n] \tag{45}$$

where R_n is the residue of the n^{th} pole and J_n is the surface current distribution over the surface of the scatterer, which is evaluated in the next section. The time-domain response can then also be obtained by applying an inverse Laplace transformation to (44).

To study the mechanism of scattering by a 4-bit Bow Tie Chipless RFID tag, the surrounding medium is assumed to be a free space with permittivity ε_0 and permittivity μ_0, the scatterer is PEC and the thickness of the tag, which is very small, is considered to be zero. When an incident an incident field E^i strikes, the induced current J_n over the surface creates the scattered field E^s from the tag which can either be obtained from Electric Field Integral Equation (EFIE) or Magnetic Field Integral Equation (MFIE) [317]. The EFIE is used, represented in Laplace form [318], and is used in terms of Green's function and evaluated by

$$E^s(r;s) = \mu s \iint_A \left[\left(\vec{\bar{I}} - \frac{1}{k^2}\nabla\nabla \right) G_0(r, r'; s) \right] . J(r, r'; s) dS' \tag{46}$$

where A represents the surface area of the Bow Tie Chipless RFID tag, $\vec{\bar{I}} = \hat{x}\hat{x} + \hat{y}\hat{y} + \hat{z}\hat{z}$, k represents the propagation constant $k = s/c$ in the complex frequency domain and G_0 defines the scalar Green's function in the free space. Green's function is an impulse response of an inhomogeneous linear differential operator with specified boundary conditions. Here, $G_0\,(r, r')$ is a Green's function of a linear differential operator *'s'* and is evaluated by

$$G_0(r, r'; s) = \frac{e^{-jk|r - r'|}}{4\pi\,|\,r - r'\,|} \tag{47}$$

The coupling coefficients are then evaluated by using

$$R_n(s_n) = -\frac{\left\langle J_n(r), E^i{}_t(r;s_n)\right\rangle_r}{\left\langle\left\langle J_n(r), \left\langle \frac{\partial \vec{G}(r,r';s)}{\partial s}\Big|_{s=s_n}, J_n(r')\right\rangle_{r'}\right\rangle_r} \tag{48}$$

Equation (48) shows that the coupling coefficient depends on E^i and the natural modes $J_n(r)$ at the resonant frequency.

$$\left\langle J_n(r), E^i{}_t(r;s_n)\right\rangle_r = 0 \tag{49}$$

The evaluation of coupling coefficients R_1 to R_4 proved to be somewhat complicated in the case of the Bow Tie Chipless RFID where the distance between two consecutive Bow Tie-shaped rings is inconsistent and the mutual coupling is a variable which changes with the distance between rings, see Figure 55.

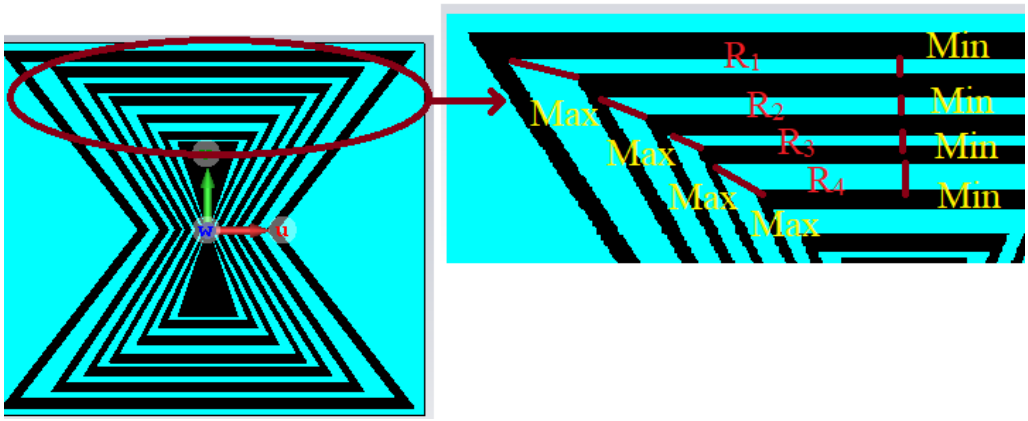

Figure 55. Variation of Distances between Consecutive Bow Tie-shaped Rings

Consequently, coupling coefficients need to be evaluated by the minimum and maximum distance values between two consecutive rings at corresponding resonances. Table 13 illustrates, for example, that. at a frequency of 9.2 GHz, the values of coupling coefficients between the first two consecutive rings are calculated at a -0.010 minimum and a -0.021 maximum with a minimum spacing of 1.2 mm and a maximum 0.23 mm spacing, respectively, for frequency.

Table 13. Coupling Coefficients for Corresponding Resonances

n	**Resonant Frequency**	**Spacing Between Resonators Min to Max (mm)**		**Coupling Coefficients**	
	F_{0n} (GHz)	D_{min}	D_{max}	**Minimum *Rn***	**Maximum *Rn***
1	9.2	0.23	1.2	-0.01	-0.021
2	11.3	0.35	0.9	-0.012	-0.017
3	14	0.17	0.6	-0.009	-0.014
4	16.9	0.52	1.1	-0.014	-0.02

Similarly, the progressive values are calculated in Table 13 for the corresponding resonant frequencies of 11.3, 14 and 16.9 GHz. The maximum value of R_n from the table is -0.021 which is a sufficiently low value that assures a reliable reading of the coded information. To reduce the mutual coupling, the average spacing between the resonators can be increased, although, as a consequence, the size of the tag would be significantly increased.

4.6 Radiation Characteristics of Bow Tie Chipless RFID Tag

The Bow Tie Chipless RFID is geometrically periodic but its unique shape makes it very effective for achieving different bit code variations when illuminating it with incident EM waves. Figure 56 illustrates the E-Field, the H-Field and the surface current induced on the surface of the tag analysed in this section.

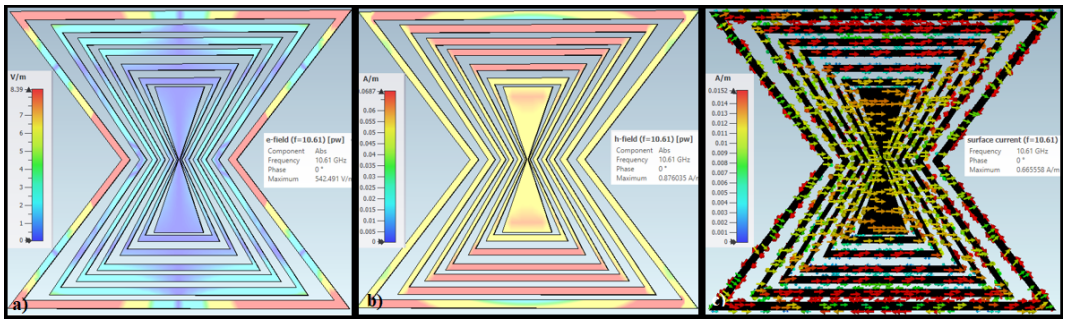

Figure 56. Radiation Characteristics at Resonant Frequency a) E-Field b) H-Field c) Surface Current *J*

4.6.1 Impact of Incident Wave angles (θ, φ) on RCS

While the unique shape of the Bow Tie Chipless RFID increases the effectivity of achieving a variety of bit codes when it is illuminated with an incident wave, the bow tie shape is geometrically periodic and dependent upon the polarization of the wave fall on it from a 20 cm distance. This section analyses the behaviour of the tag with Vertical *V* and Horizontal *H* position of the tag, and the polarization of the incident wave on the surface. Furthermore, the RCS values of the tag are obtained from the scatterer for different angles of the incident wave θ and φ.

The RCS fluctuates as a function of the object, in this case, the RFID tag, the aspect angle and the frequency [120]. By taking a spherical coordinate system (ρ, θ, φ), at range ρ, the RCS is a function of (θ, φ). The direction of the propagation of the incident wave is defined by (θ_i, φ_i), the direction of the propagation of the scattered wave is given by (θ_s, φ_s), and the condition when $\theta_i = \theta_s$ and $\varphi_i = \varphi_s$ is known as monostatic RCS [120]. This section analyses the variation of the incident wave $E(\theta, \varphi)$ concerning various angles (0°, 15°, 30°, 45°, 60°, 75°, 90°) on the surface of the Bow Tie RFID tag. Figure 57 and Figure 58 represent the RCS variation with the change of angle θ of the incident wave at *V* and *H* positions of the tag respectively. The tilt angle α of the RFID tag is kept 0° for this analysis.

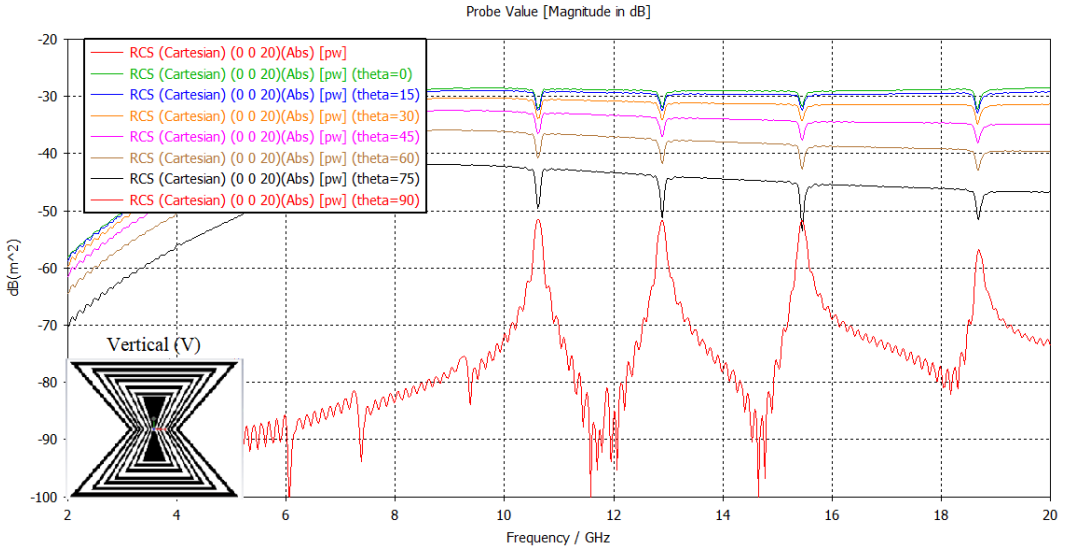

Figure 57. RCS of Scattered Field E^s with different Rotational Angles θ of Incident Field E^i at Vertical *V* Tag Position

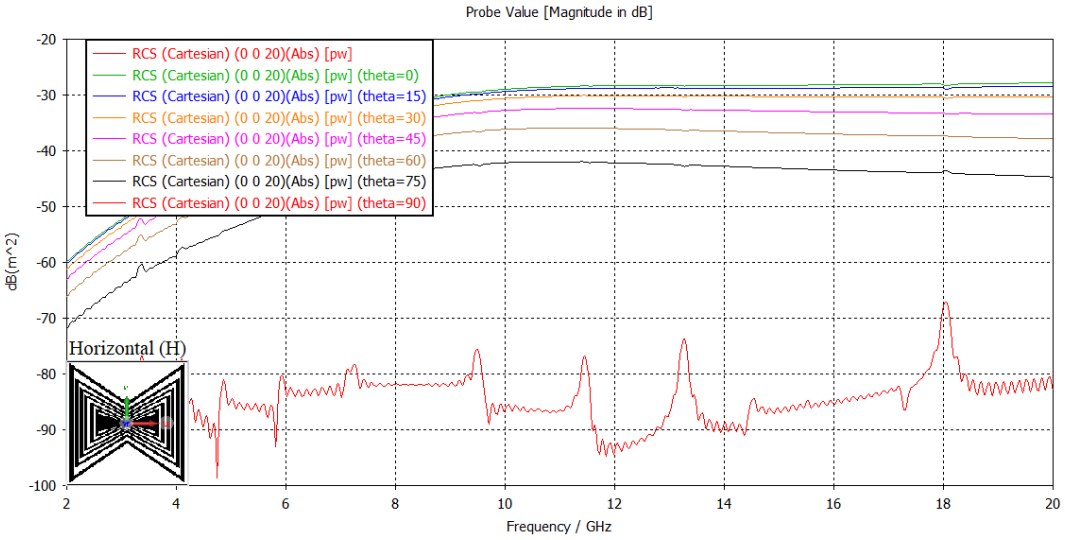

Figure 58. RCS of Scattered Field E^s with different Rotational Angles θ of Incident Field E^i at Horizontal *H* Tag Position

The impact of the variation of θ of the incident wave on the *V* position of the tag indicates that the monostatic RCS response of the RFID tag continues improving with an increase of the θ until 75°. For the angle of $\theta = 90°$, in Figure 57, since both incident and scattered waves are aligned, a distorted version of RCS is obtained. Contrastingly, due to the non-symmetrical shape of the RFID tag, Figure 58 shows that the RCS for the θ variation on a *H* position of the tag is not impacted, as the Bow Tie RFID tag design is polarized in only one dimension. Similarly, the monostatic RCS is analysed by variations of the φ angle of the wave for both *V* and *H* positions of the tag as depicted in Figure 59 and Figure 60.

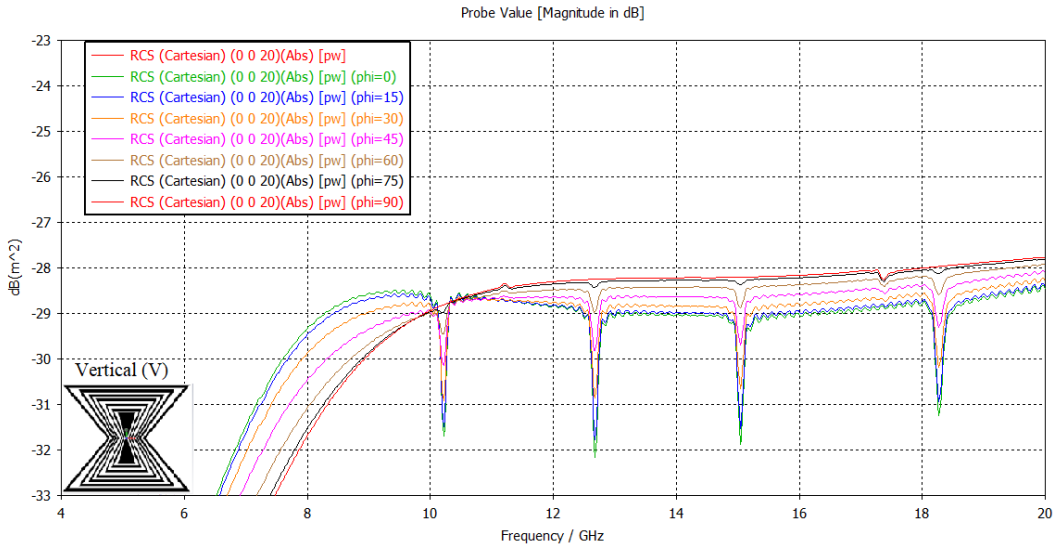

Figure 59. RCS of Scattered Field E^s with different Rotational Angles φ of Incident Field E^i at Vertical *V* Tag Position

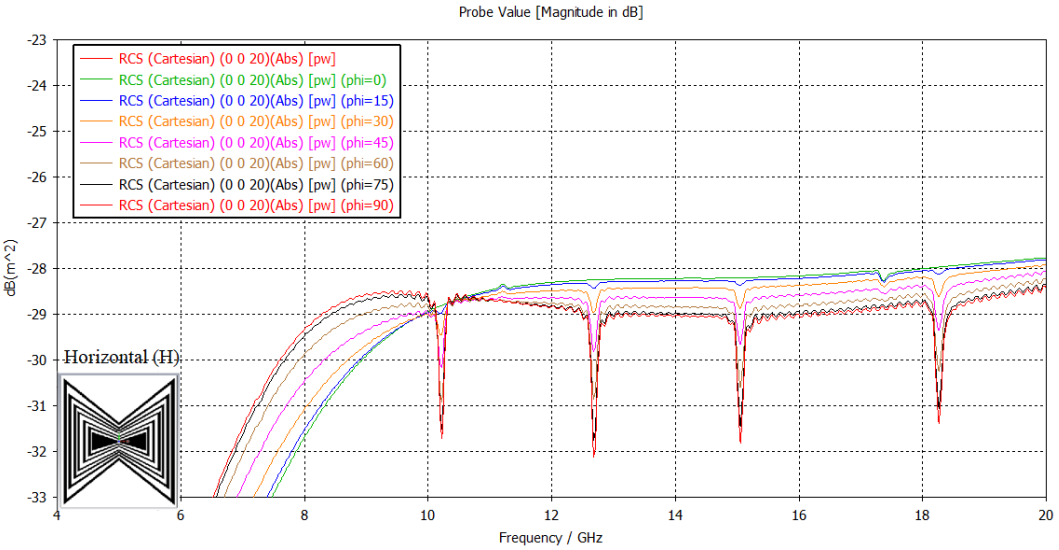

Figure 60. RCS of Scattered Field E^s with different Rotational Angles φ of Incident Field E^i at Horizontal *H* Tag Position

Observation of the backscattered RCS, according to the variation of the incident angle φ of the wave, clearly shows that the RCS obtained is a flat line for the angles $\varphi = 90°$, $\varphi = 0°$ for *V* and *H* position of the tag, respectively. Analysis indicates that the non-resonance result of the horizontal line occurs because, for these angles, the angle of the incident φ becomes perpendicular to the surface at *V* position and parallel to the surface of the tag at *H* position where the flat RCS is another characteristic resultant of the non-symmetrical FSS shape of the tag. In contrast, when $\varphi = 0°$, $\varphi = 90°$ for *V* and *H* position of the tag, respectively, a well detectable RCS is observed.

4.7 Impact of the tilt angle (α) on RCS

The tilt angle defines the position of the tag in relation to the corresponding axis and the direction of the incident wave. In the Bow Tie design, a variation of the tilt angle α of the tag from the positive

x-axis is obtained and the impact on RCS is described in Figure 61and Figure 62 for *V* and *H* position of the tag, respectively.

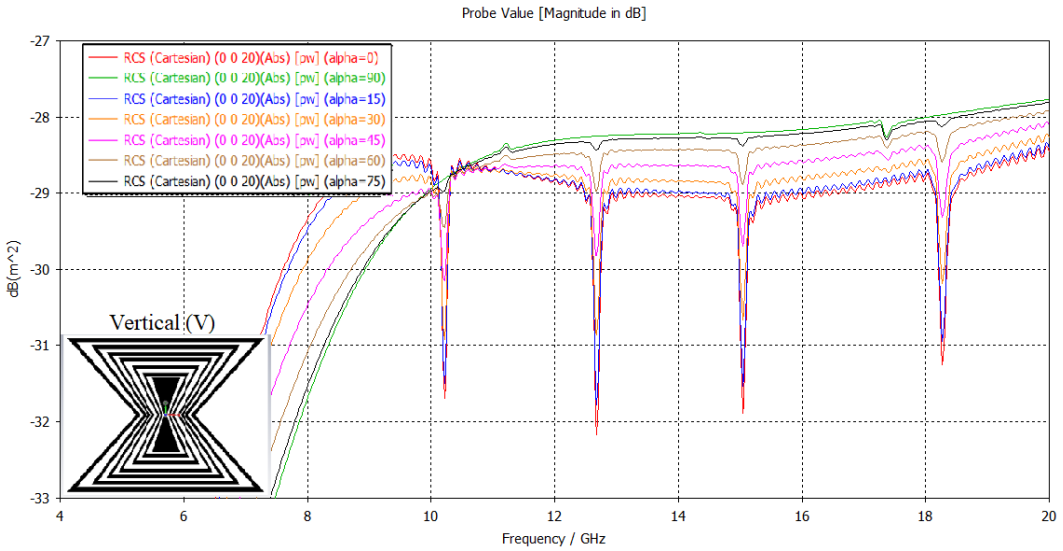

Figure 61. RCS of Scattered Field E^s with different tilt Angles α of the Bow Tie Chipless RFID tag at Vertical V Tag Position

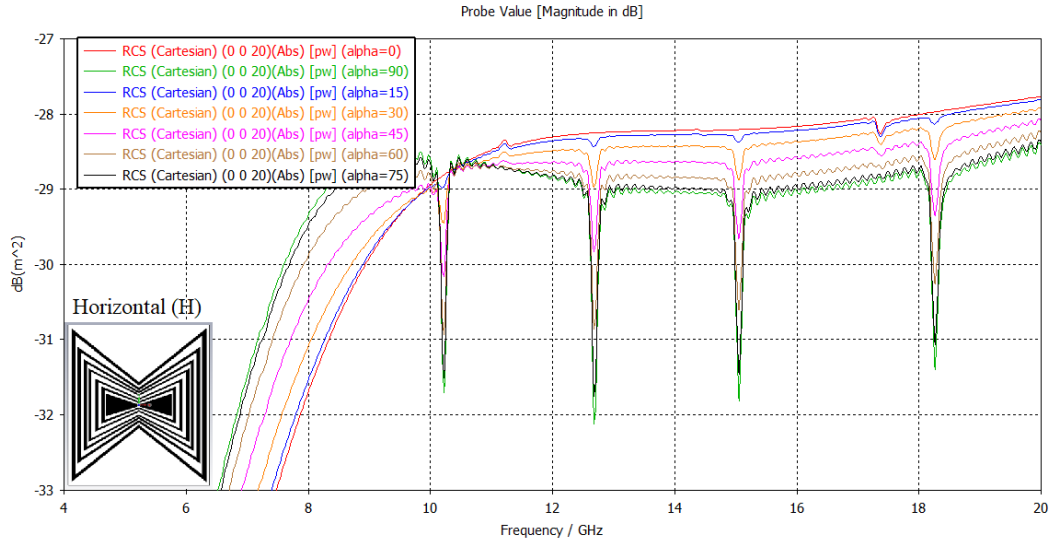

Figure 62. RCS of Scattered Field E^s with different tilt Angles α of the Bow Tie Chipless RFID tag at Horizontal *H* Tag Position

The direction of the incident wave and the position of the target for the corresponding axis matters equally in terms of RCS detection. Here, α indicates the position of the tag and the θ and φ angles are at 0°. When the value of angle α = 0°, where the tag is at the *xy* plane and the incident wave is striking from the direction of the *z*-axis, maximum bit codes are detectable in terms of RCS at *V* position, see Figure 62. Contrastingly, the maximum detectable RCS for *H* position of the tag is achieved when the value of α = 90°.

4.8 Constructive and Destructive Interferences and Bit Code Formation

As mentioned in section 4.3, the tag encodes a bit sequence through different combinations of ring structures that resonate with constructive and destructive interferences. In this section, for these interferences of the induced field on the surface of the tag, the resonators, or the scatterers, of the Bow Tie RFID tag are analysed individually to obtain codeword formulations. Understanding the importance of studying the directional behaviour of the induced current produced by the incident wave on the surface of the tag for the detectable RCS and codeword formulation, as illustrated in Figure 63, the first four resonators of the tag are considered in this investigation of the directional behaviour of the current.

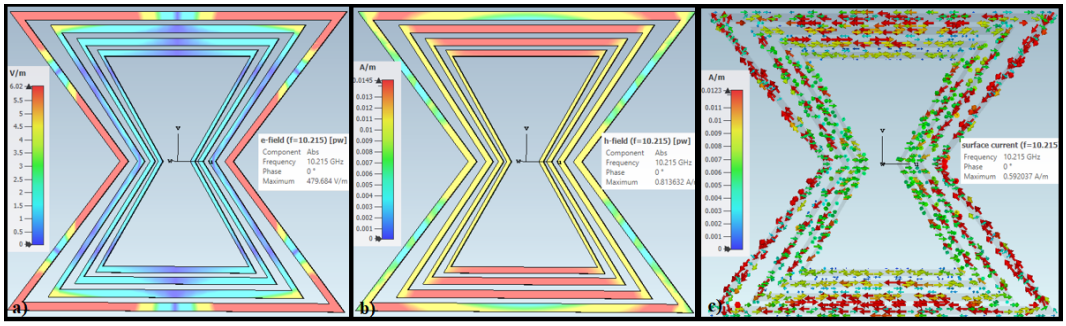

Figure 63. Four Resonators of Bow Tie Chipless RFID tag at First Resonant Frequency a) E-Field b) H-Field c) Surface Current *J*

Analysis of the first four rings determined that the direction of the current may be changed by implanting a short circuit, via a stub, between two consecutive resonators. To demonstrate this, two stubs, introduced at two specific places between the first two scatterers, resulted in negating the direction of current and consequently produced a destructive interference of the incident wave, as seen in Figure 64.

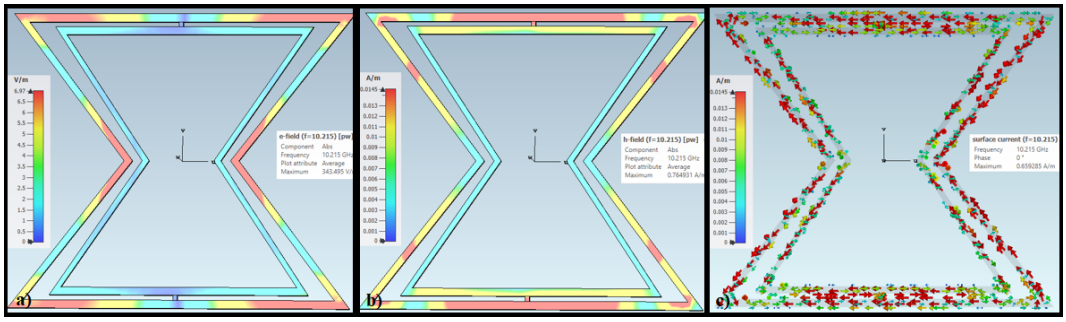

Figure 64. Two Resonators Shorted by Stub Positioning in Bow Tie Chipless RFID tag to Introduce Destructive Interference at First Resonant Frequency a) E-Field b) H-Field c) Surface Current J_{in} and J_{out}

When these two resonators are joined with this short circuit stub and are impinged with E_i, a surface current is induced as J_{in} at the inner ring and as J_{out} on the outer ring. The current distribution of the two scatterers are equal in magnitude but opposite in phase at the resonant frequency of 10.125 GHz, see Figure 64(c). The distance between these two resonators is so small that in the far-field they can be considered a single source, where the scattered field E_s, created by these two resonators, is

considered to be oppositely polarized by an odd multiple of π phase. As such, the two resonators destructively interfere in the free space [314].

The positioning of the stub which creates this conductive link between the two resonators is very important in order to obtain the inverse direction of the current which, in turn, cancels the impact of the other resonator to acquire this destructive interference. For this reason, a series of samples have been designed to optimize the exact placement of the stub. Figure 64(a) and (b) depict the electric and magnetic fields on the tag at the first resonant frequency of 10.215 GHz. As with the first two resonators, stubs are placed to introduce the same short circuits between three and four resonators for resultant scatterer configurations. Figure 65 and Figure 66 illustrate the short circuit stub the position for three and then four resonator configurations, respectively, with the corresponding E and H-Fields, and the induced currents.

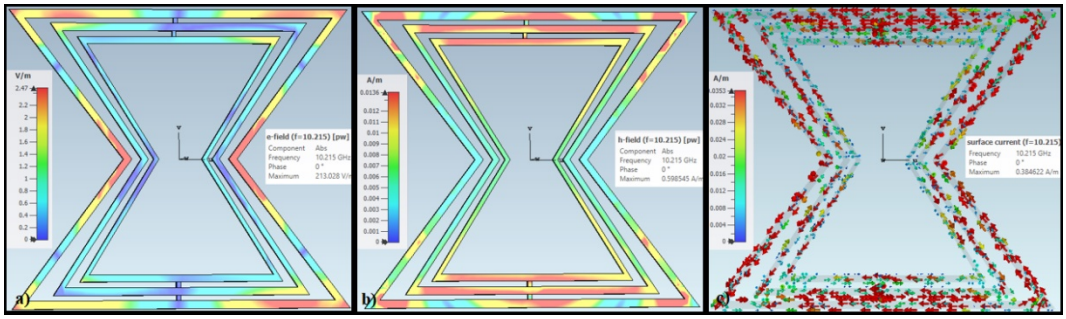

Figure 65. Three Resonators with Positioned Stub on Bow Tie Chipless RFID tag for Destructive Interference at First Resonant Frequency a) E-Field b) H-Field c) Surface Current J_{in} and J_{out}

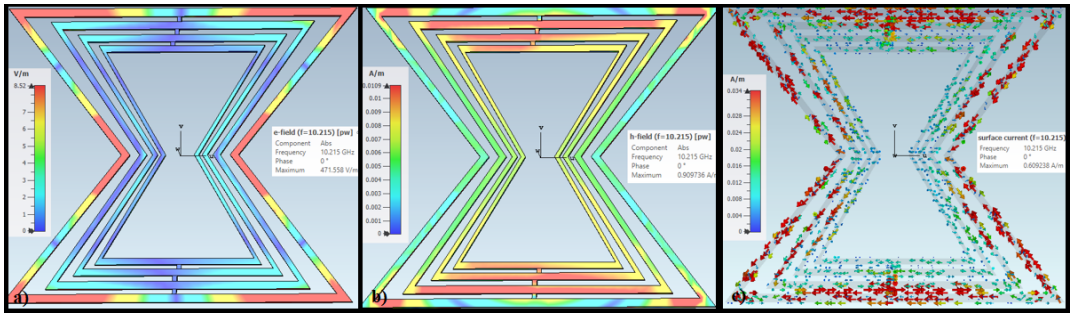

Figure 66. Four Resonators with Positioning Stub on Bow Tie Chipless RFID tag for Destructive Interference at First Resonant Frequency a) E-Field b) H-Field c) Surface Current J_{in} and J_{out}

Since a tag without any stubs has all RCS the spikes in its frequency signature, it is suitable for implementation as a reference tag to be able to produce an ID code on the tag. A reference tag, a tag without any short circuit embedded in it, is shown in Figure 51. When no short circuit is present, logic-1 is assigned to the RCS spike between two resonators. The absence of a spike, also called a notch, is assigned logic-0. In Figure 67, different code IDs are generated by using the short stub position at an appropriate position on the resonators. The outer resonators define the most significant bits.

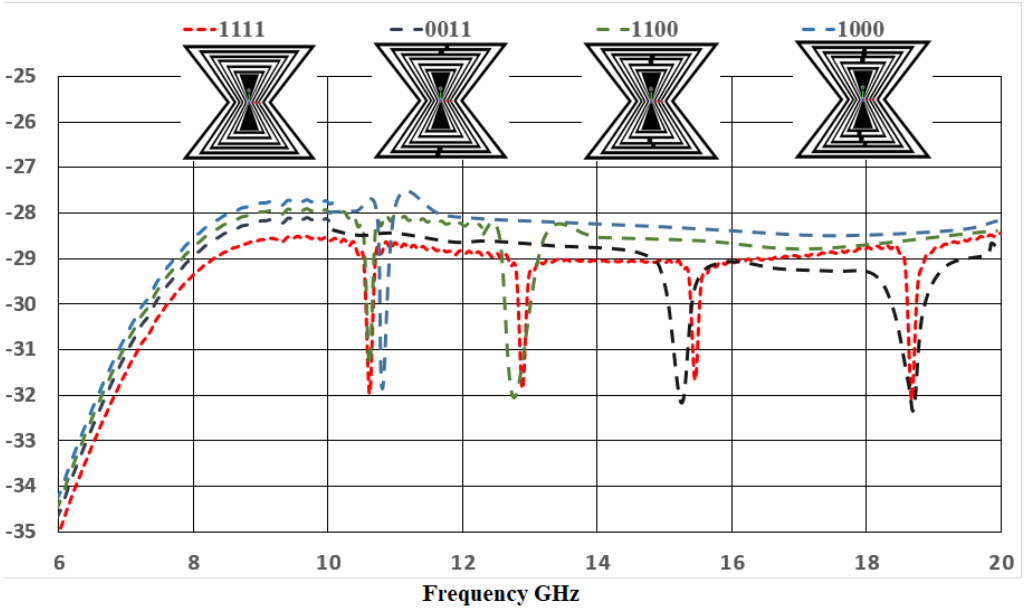

Figure 67. RCS Measurements in Chamber for the Bow Tie Chipless RFID Tag with Four different ID's

4.9 Bending and Folding Effects of RFID Tag on RCS

The Bow Tie Chipless RFID tag is designed and fabricated on PET, Teflon and PVC substrates of thicknesses 70 µm, 100 µm and 110 µm respectively, as shown in Figure 68(a), (b), and (c), to corroborate the bending effects of radiation from different polymer substrates. Using the FSS technique, the design base was selected on the knowledge that, for the traditional bow-tie structure [1], the most intense surface current flows across the edges with the resonating elementary cell [73]. For testing purposes, gold is used as the conducting material and the printing of the tag is executed using the ULS with 2.0-MW Lens and 10.6-micron wavelength CO2 Laser. Using VNA, operating in the frequency range of 4-18 GHz, to conduct the measurements inside the anechoic chamber with two identical horn antennas that are maintained a distance of 12 cm away from the bent tags, see Figure 69(a) and Figure 69(b). The effect of the radial curvature on the RCS of the tags has been published previously [2].

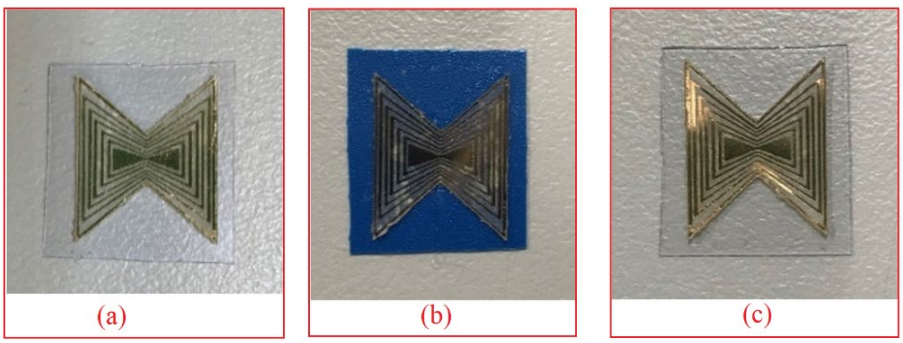

Figure 68. Bow Tie Chipless RFID tags with Polymer Substrates, a) PET b) Teflon and c) PVC

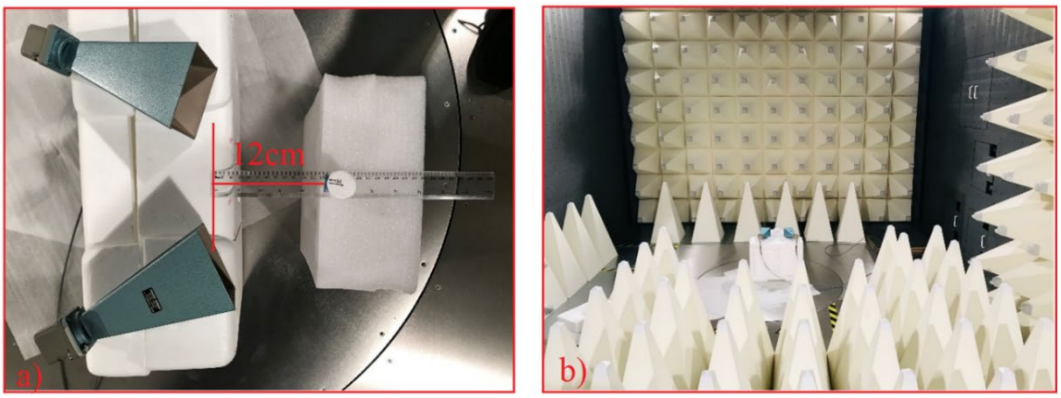

Figure 69. Experimental Set-up RFID a) Bent Tag 12cm from Horn Antennas b) Tag Inside Frankonia Chamber

The measurements are taken from the bending of Bow Tie RFID tags under the conditions of form and size: being flat or curved at 14 mm and 27 mm, for each of the three different substrates: PET, Teflon and PVC. Actual aspects and flexibility at different curvatures are illustrated in Figure 70.

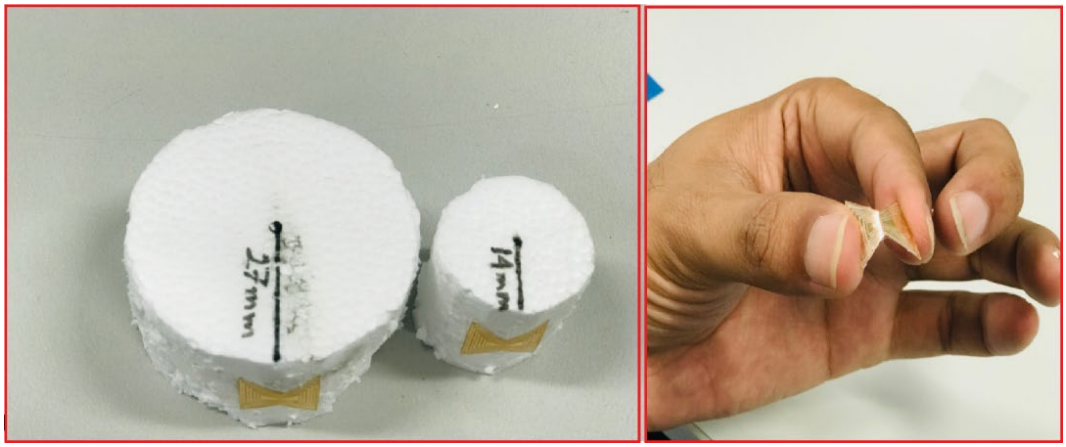

Figure 70. Actual view of Bow Tie RFID tags bent over 27 mm and 14 mm radii with the Level of Flexibility

The measurement results are reported for tags in Horizontal *H* position at the anechoic chamber. As elaborated in Section 4.1, the bending of tags and antennas causes a resonance frequency shift and signal degradation. Figure 71(a), (b) and (c) illustrate exactly how the performances of the bent tags are affected by modifying the curvature radii. While, normally, as the bent radius decreases, the obtained |RCS| is lower, in this case, with the distance of tag maintained at 12 cm, and 0 dBm signal power, very small reduction on the backscattered power and the shift in the resonant frequency is observed. It is therefore quantified that the information stored on the bent Bow Tie tag can successfully be recovered with a various bending radius of up to 14 mm.

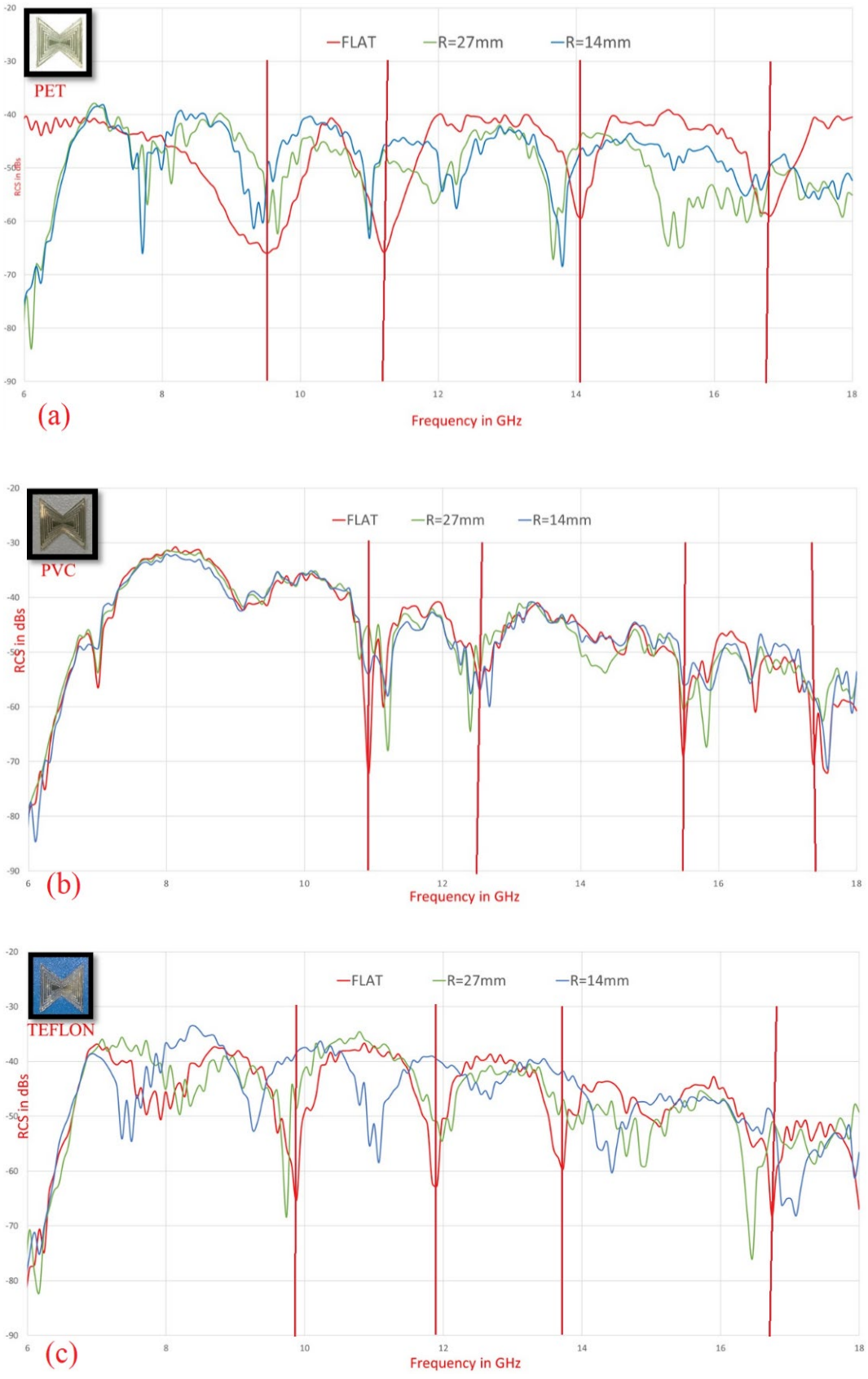

Figure 71.|RCS| Measurements and the Bending of Bow Tie Chipless RFID tags at R = 27 mm and R = 14 mm with a) PET Substrate b) PVC Substrate c) Teflon Substrate

Observation of how the performances of bent tags are affected by changing the bending radius of a tag are illustrated in Figure 71(a), (b) and (c), which depict the bending capabilities of the RFID tag with the selected three substrate materials: a) PET b) Teflon and c) PVC, respectively. Given that the obtained |RCS| is lower as the bent radius decreases, and that the distance of the measuring setup from the tag is preserved at 12 cm with the power of 0 dBm remaining almost constant, the RCS graphs show that when the RFID tags with the PET and Teflon substrates undergo a bending curvature of R = 27 mm, there is about a 4% to 6% shift in frequency from the resonant frequency for the lower frequency band of 8-14 GHz. For higher frequencies, up to 18 GHz, these frequency shifts increase to more than 10% and for all RCS results at 27 mm, there is little degradation of RCS in dB's, due to the small 12-cm distance between the reader and RFID tag. On the other hand, for the bending curvature of R = 14 mm, in Figure 71(a) and (b), the shifts in resonant frequencies and signal degradation are much higher for both the PET and Teflon substrate-based RFID tags. For the RFID tag with the PVC substrate, although there is an expected reduction on the backscattered power, the frequency shift, shown in Figure 71(c), is much smaller and with no noticeable degradation of the signal observable. Hence, the results demonstrate that the information stored on the bent chipless RFID tags made with all three substrates, can be recovered successfully.

4.10 Maximum Read Range Estimation

This section provides the maximum read range of a Bow Tie Chipless RFID tag on PET substrate. The complex RCS feature σ^{Tag} of the Octagonal Chipless RFID designs can be obtained by the following equations, which are described in [162].

$$\sigma^{Tag} = \left[\frac{S_{21}^{Tag} - S_{21}^{No-Tag}}{S_{21}^{Ref} - S_{21}^{No-Tag}}\right]^2 \sigma^{Ref} \tag{50}$$

where S_{21}^{No-Tag} is associated with the measurement taken in the empty chamber, S_{21}^{Ref} corresponds to the reference value taken from the defined setup, which, in this case, is a copper square of 50 mm x 50 mm, although any conductive surface could be selected. The σ^{Ref} is associated with the simulation results for the same reference. The results achieved for all the tags confirm conformity between the measured and simulated designs.

The radar equation [319] is used to evaluate the maximum read range of the RFID tag where RCS is calculated numerically by the equation

$$R = \sqrt[4]{\frac{G_T\, G_R \lambda^2 \sigma^{Tag} P_T}{(4\pi)^3 P_{min}}} \tag{51}$$

Where G_T and G_R are the gains from the transmitting and receiving horn antennas, P_T is the power transmitted by VNA to measure the RCS, λ is the wavelength. P_{min} is the minimum power received by the receiving antenna and σ^{Tag} is the experimental value of RCS obtained from (50). For maximum read range calculations, σ^{Tag} is taken for 1111-bit codes for flat case. The results obtained from a series of experiments, determined an average σ^{Tag} of around 0.02 m^2. The maximum read

range is evaluated for -10 dBm, -3 dBm and 0 dBm transmitted power from VNA and the maximum range observed is 1.80 m which is extendable to 2.15 m for 3 dBm power.

Table 14. Maximum Read Range Estimation

P_{min} (dB)	G_T (dBi) G_R (dBi)	λ^2 (m)	σ^{Tag} (m^2)	P_T (dB)	R (m)
-70	10	1.06×10^{-3}	0.02	-10	1.01
				-3	1.52
				0	1.80
				3	2.15

4.11 Summary

The chapter overviews a literature review of RFID, basic knowledge regarding the RFID tag and encoding techniques for the tag on polymer substrates. A novel Bow Tie tag was designed using CST studio and fabricated through a laser etching technique on low-cost flexible PET. The Bow Tie Chipless RFID tag relies on the FSS approach with a frequency ranging from 8 to 18 GHz and is compared with the common FSS Octagonal-shaped Chipless RFID tag. Both tags are fabricated using laser printing on PET substrates and subjected to a series of comparative experiments for RCS calculations, with the results, obtained in an anechoic chamber, determining that the average transition from minimum (0) to maximum (1) is 25 dB for the Octagonal design and 32 dB for the Bow Tie design.

The tag design is composed of six concentric Bow Tie-shaped loop resonators with one unitary element. The SEM-based circuit modelling is demonstrated, the transient behaviour of the Bow Tie Chipless RFID tag is performed and the coupling coefficients and induced currents over the surface of Bow Tie-shaped rings are evaluated. Designed and fabricated on three polymer substrates, PET, PTFE Teflon and PVC, the bending effects of the flexible Bow Tie Chipless RFID tag operating within the range of 4-18 GHz are studied and analysed with measured results conducted inside an anechoic chamber in a series of comparative experiments for RCS. The experimental results for bending capabilities of the tag are noted for radii curvature of 27 mm and 14 mm and demonstrate that the information stored on a tag can easily be recovered for a bending level up to 14mm. The bending capabilities of the Bow Tie Chipless RFID tag using PVC proved to be high and with little shift in frequency or signal degradation, categorically making the PVC material a very apt polymer substrate for the RFID tag. Hence, radiation characteristics for equivalent levels of bending can be maximized by selecting the more appropriate flexible polymer materials with appropriate physical electrical and thermal properties. On evaluating the maximum read range, the Bow Tie RFID tag proved to be more robust and accurate with the variation of distance up to 1.8 m at 0 dBm, which is extendable to 2.14 m for higher input power. The result undeniably provides a 4-bit Bow Tie Chipless RFID tag design which is compact and able to be deployed commercially for general IoT applications.

Chapter 5: **Wearable Conductive Fibre Chipless RFID Tags**

Wearable antennas and RFID tags are essential components of any wearable wireless communication system. Besides being wearable, the wearable sensors of the conventional devices are lightweight, low-cost, washable and durable, garment-integrable and flexible. Conductive textiles are more extensively in use these days as they possess outstanding properties like extraordinary mechanical conformability, wearability comfort and brilliant biocompatibility. This chapter focuses on the conductive textiles for chipless RFID sensors, with the design, fabrication and testing of two embroidered Octagonal-shaped Chipless RFID tags on the cotton fabric being presented for IoT applications.

5.1 Introduction

The IoT relies on smart environments; comprises of wireless sensor networks [91] and personal area networks [310, 311], in which each object that interacts with the IoT infrastructure must be uniquely identified. Consequently, one of the biggest challenges in this technology is to integrate seamless IoT solutions based on the surroundings and people [312]. Correspondingly, clothing, with its easy adaption and utilisation in everyday life, is considered a suitable prospect to facilitate this challenge and progressively become the next interface between the real and the digital world [40]. Research on wearable wireless communication and flexible devices has already been increasing quite rapidly in recent years as a result of its expanded usability, particularly in applications for Personal Communication Systems (PCS) [309]. For example, flexible antennas and RFID tags are now being used to keep track of several daily-routine activities such as heartbeat and blood pressure measurements as well as the distance walked, the steps taken and the calories burnt [126], and the wearable electronics have already been exploited to track the vital signs of infants and elderly people [320]. Similarly, the emphasis on ‘smart clothing’, a more specific growing research area, is enhancing traditional clothing with modern technology to add functionality beyond traditional use. Some of these clothing enhancements have begun to incorporate advanced textiles interwoven with circuitry which are at present quite extensively used for emergency medical situations, firefighting and military applications [321, 322].

At present, this wearable technology is increasingly being employed in the rapid development of intelligent materials applicable to the manufacturing of smart garments. The integration of smart devices into clothing has become essential for the monitoring of physical activities and wellness. These garments usually consist of conductive fibres, such as conductive polyester, and, as substrates, non-conductive fibres, such as cotton and wool. Although, there are several conductive fibres available on the market [40, 323], the growth of wearable technology and the success of wearable devices has been hampered by limits in the lack of materials and manufacturing techniques for seamless integration with electronic parts [40] to facilitate the necessary robustness for washing,

drying and ironing [30, 313]. Recently, the European Commission stated that a future wearable smart device should be shapeable, stretchable and washable on demand, and should be similar to natural clothing in terms of comfort, breathability and washability [324]. To concord with these delimitations, one very potential strategy is to implement chipless devices with lower energy consumption [153, 325] and for which an embroidered chipless RFID tag is a very prospective candidate which transcends the aforementioned constraints.

The rest of the chapter is organised as follows: Section 5.2 presents a literature review on wearable antennas and fabric-based chipless RFID tags; Section 5.3 demonstrates the design and fabrication of embroidered chipless RFID tags on cotton substrates; and Section 5.4 presents the simulation results.

5.2 Literature Review on Wearable Antennas & Chipless RFID Tags

The wearable embroidery RFID tag has many advantages since it can take the form of any shape, such as an alphabetic letter, a logo, or other special character, and can be embedded in any cloth, instead of merely being attached to one. Wireless applications with different fabrics and textiles are utilized for the wearable antennas [1, 2, 23, 126, 127, 134, 260, 303, 326-330] and RFID tags [331, 332] have been applied to many of the wearable sensors and smart clothes with the wearable antennas mostly designed for WLAN, GPS, military and police-related applications [23, 327-329]. While the effect of the body *near* conductive textile material as an antenna has been researched [23, 328], so too has the flexible and attachable antenna *on* a human body been studied [295, 327]. A dual-band textile antenna is designed in [303] and, in [330], the fabric construction of the electro-textiles and their effect on the efficiency of the e-textile patch antennas are discussed. The ultra-wideband wearable antenna designed in [327, 329] demonstrates that an embedded UHF RFID tag using electro-textile or thread can be applied to wearable and flexible tag antennas and attached to any flexible surface or wire. A single-feed rectangular-ring antenna designed for ISM band, proposed for wireless body networks, is introduced in [168] and, in [227], a fully textile frequency-signature chipless tag consisting of a microstrip line is proposed with multiple resonators.

Nevertheless, available literature on chipless RFID tags for wearable fabric applications is very limited [227, 331-333]. A sewn a RFID tag for wearable application is presented in [331] on the flexible polyester substrate and different patterns of codes of a cell using the FSS technique are successfully achieved by establishing different arrays of them. Unfortunately, the authors claim that while the device performs well in free space, when closer than 7.5 mm to the human body, its performance degrades. Then, in [332], while multiple resonators on an L-shaped RFID tag are investigated, which could depolarize the incident wave in orthogonal polarization, the reported results are obtained by fabricating the tag on a rigid substrate which is commonly used for PCBs. Although the same author later presented an entirely textile-based chipless RFID tag, the innovation is limited to just a few modifications being applied to the hairpin resonator [40, 334].

The most recent literature on a fully textile-based chipless RFID tag for tracking applications is reported in [40]. The proposed tag is based on a frequency signature by using a 50 Ω microstrip line comprising of an adjustable multi-stopband structure and two cross-polarized monopole antennas. Compared to the other textile-based RFID tags, this 3-bit chipless tag is embedded for both the transmitting and the receiving tag antennas with the binary identification code encapsulated in the frequency signature of the multi-stopband structure.

In this investigation, two embroidered chipless RFID tags are sewn into cotton fabric with conductive fibre. This design represents a 4-bit chipless RFID tag with a periodic pattern of cells applicable for various wearable applications. The octagonal design is proposed to assure the independence of the polarization feature, and for its symmetry feature as the symmetrical design allows the tag to be read independently for any rotational angle. Moreover, the octagonal periodic cells are opened and short-circuited to obtain destructive and constructive interferences for the incidents waves, which are reflected and decoded in terms of bits assigned to RCS [56], as the RCS is a parameter that characterizes the level of scattering of a target object, in this case, the tag. The RCS is frequency dependent and can be extracted as a function of the incident angle of the transmitted signal.

In recent years, the idea for developing smart garments or smart clothes has become a growing topic of interest for wearable wireless technologies that enable communication solutions concerning people and objects. Soon, the communication between humans beings, humans to devices and objects, navigation and GPS supported system, health monitoring and leisure activities will be executed through wearable objects [334]. Incidentally, a key role is played by wearable antennas and RFID tags which implement an easy and comfortable wireless linking capacity from our clothes to the surrounding environment.

Wearable RFID technology can be implemented through several techniques, with one of the simplest realizations being a conventional etching technique on commonly used substrates and then embedding them on wearable clothing [335]; see Figure 72. Unfortunately, this technique is not very effective in terms of washing, durability or mechanical stresses, making our proposition for embroidered RFID tags, made of conductive fibre, even more promising. For a seamless integration of antennas and RFID tags with cloths, embroidery is an emerging technology and for this, a few conductive yarns have already been reported in [31, 40, 41, 43, 134, 146, 227, 322, 331, 336, 337].

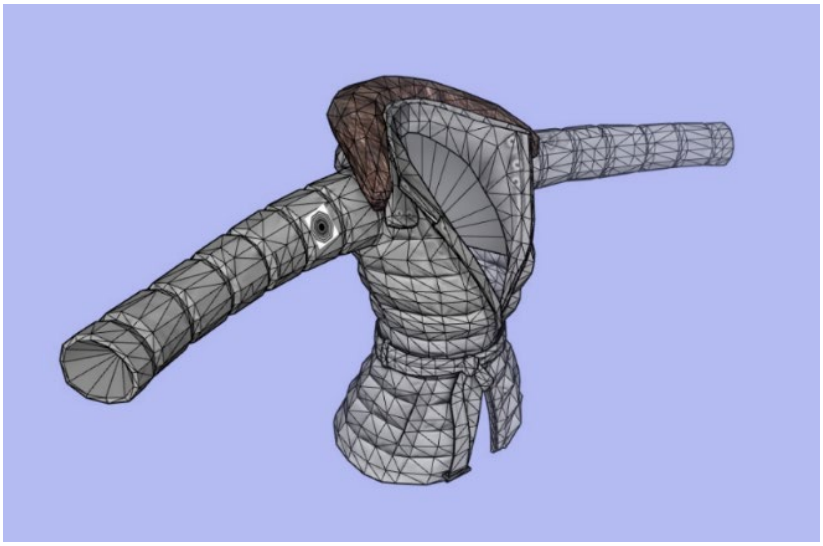

Figure 72. Etched RFID tag on Clothes

While the embroidered RFID tags are easy to implement on clothes, clothes, creating simplicity for an enduring connection between the chip and sewed tag remains an alluring challenge. Endeavours to embroider chipless RFID tags on clothes aim to address this, by serving to increase durability and washability while reducing the costs of manufacturing [331]. A chipless RFID system is a combination of antenna functions for data reading, with the scatterer(tag), receiving and transmitting characteristics, which are required to both code and decode the obtained information, see Figure 73.

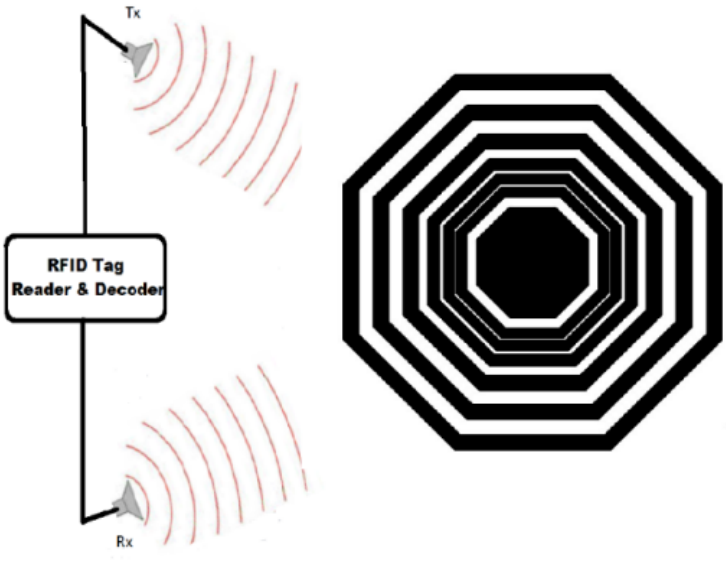

Figure 73. Structural Diagram of Chipless RFID System

Accordingly, our two Octagonal-shaped RFID tags, based on the FSS design technique, are designed to operate between 8 GHz to 18 GHz frequencies, using two different conducting fibres. The FSS, having been quite extensively investigated and studied over the last six decades for two-dimensional metallic structures on dielectric substrates [338, 339], is a technique for which the physical characteristics of the unit element are very important with the unit element being surrounded by

other periodic shapes. With the symmetrical shape of the tag, the design is independent of polarization and there have already been a few other designs, reported in other research literature in [147, 162, 340], comprising, for example, of circular and square shapes which are independent of the polarization due to their symmetry. Our use of the octagonal shape also provides code readability independent of any rotational angle.

5.3 Embroidered Chipless RFID Tags

5.3.1 Tag function & Material Characterisation

Extracting an identifier (ID) from the proposed embroidered RFID tag which works on the backscattering technique, is completely different to a conventional tag. The chipless RFID system comprises of a transmitter and a receiver with an adapted version of UWB frequency radar [135]. Despite receiving increased attention, Chipless RFID tags still require more experimental work to make them applicable commercially to be able to occupy a place in the market [56]. An Octagonal Chipless RFID tag is presented in [56] where different codes, based on the constructive and destructive interferences occurred, are generated for different combinations of ring structures. In this design, the octagonal periodic cells are opened and short circuit to obtain both destructive and constructive interferences for the incidents wave which are reflected and decoded in terms of bits assigned to RCS. As illustrated in Figure 73, when an incident wave *(Ei, Hi)* strikes the array of RFID tags, a current is induced in the elementary cell at the resonant frequency of 8.5 GHz. Furthermore, while most of the traditional RFID tags are made from a near-field circuit with a low-cost chip at the centre [126] to save the ID code in its memory, this chip can either hold a single code or be more complex to have the ability to execute different algorithms because, in chipless RFID tagging, the physical features of the tag are used to send data instead [6]. Moreover, the chipless RFID tags work off the resonance obtained from the metallic surfaces, which makes any electronic circuitry to handle communication protocols redundant with the RFID system requiring only one transmitter and reader to receive the bitstream reflected from RFID tags, as depicted in Figure 73.

As such, the chipless RFID tags are primarily designed to function off the resonance obtained from the metallic surfaces and have no need to carry any electronic circuitry to handle communication protocols. Although many designs have been proposed for chipless RFID tags, they are generally characterized by two main groups: the time-domain-reflectometry-based designs, for which SAW is an example, and spectral-based tags such as the FSS technique. FSS is an auspicious technique in which an incoming EM wave is either reflected completely or partially depending on the nature of the conductive element when the frequency of EM waves matches with the resonant frequency of the conductive object [128]. The FSS-based chipless RFID system shown in Figure 73 is an adapted version of the UWB frequency radar [135]. A chipless RFID system combines the antenna functions of the scatterer(tag), receiving and transmitting characteristics for reading information which, in terms of the RCS, requires data coding and decoding to be obtained.

The RCS is a parameter which characterizes the level of scattering of a target object, with the tag being the target object in this case. The RCS can be extracted as a function of the incident angle of the transmitted signal and depends on the frequency. Different coding techniques have been used to link a given electromagnetic signature and a distinctive ID, with common methods based on the time-domain analysis of the impulse response. Other techniques have used the UWB frequency analysis which has been discussed in Chapter 1 in detail. In our chipless RFID design, a simple and reliable coding technique related to the presence or the absence of peaks at several frequency points [161] is used, where one bit is equal to one resonant peak.

For this investigation, an Octagonal Chipless RFID Tag is first designed by embroidering polyamide fully silver-coated HC12 conductive thread as resonator rings on a plain cotton substrate with 25 mm x 25 mm dimension, 90-µm thickness and permittivity ε_r of 2.1 at 8 GHz and 2.0 at 18 GHz. The HC12 conductive thread is skin-friendly, comfortable, biocompatible and washable, and therefore ideal for smart textile applications [341]. This first design is named the HC12-Tag. The second embroidered octagonal RFID tag is designed using LIBERATOR 40 twisted highly conductive silver-coated threads on cotton fabric with the same dimensions, see Figures 74 and 75. This tag is named the LIB40-Tag. The Liberator thread, known as Vectran™ by Kuraway, is comprised of a polymer core making it a high-performance multifilament yarn spun from LCP [342]. The thread is twisted in such a way that the reflective properties of the foils are used completely, adding texture and depth to the design. The inner polymer yarn has an extremely high tensile strength, roughly five times stronger than steel, and remains as flexible as regular threads [342]. The complex permittivity is extracted by the Keysight N1501A Dielectric Probe Kit.

The two conductive threads used in this study, HC12 and LIBERATOR 40, with the linear mass density of 2 x 220 and 200 DEN respectively, are highly conducive for their very low DC linear resistivity < 100 Ω/m. Table 15 features the characteristics of these materials. Generally, the conductivity of a sewn conductive thread is relatively low, as compared to conventional conductive materials such as copper, aluminium and silver, so the quality factor of the conductive resonators could generate a frequency resonance with a larger bandwidth that could potentially limit the frequency resolution of the retrieving system [331].

Table 15. Properties of the Conductive Threads [341, 342]

RFID Tags	HC12-Tag		LIB40-Tag	
Shape	Octagonal		Octagonal	
Conductive Thread	HC12 100% Silver Coated Polyamide		LIBERATOR 40 LB40 AG-130	
Linear Mass Density (DEN)	2 x 220		200	
Resistivity	< 100 Ω/m		< 3.25 Ω/m	
Permittivity (ε_r)	1.5 @ 8 GHz	1.4 @ 18 GHz	1.75 @ 8 GHz	1.7 @18 GHz
Thickness of Thread	90 µm		120 µm	
Substrate	Cotton		Cotton	
Thickness of Substrate	0.25 mm		0.25 mm	

5.3.2 Optimised Tag Design

Optimization is necessary for a tag or surface which is based on the FSS technique, both to achieve the required reflection and to improve the perimeter quality [343]. Similarly, the tag dimensions of HC12-Tag and LIB40-Tag are both optimized for their parameters and conduction losses to obtain optimal results. The unitary element of their designs, illustrated in Figure 74 and Figure 75, is composed of the concentric octagonal ring. In such an FSS structure, the design endeavour mainly focuses on the geometrical definition. To understand the behaviour of the concentric octagonal tag design, a simplified version of the design is first analysed with a unitary element being examined for the impact on the first resonator ring before all of the rings are analysed together. When this simplified tag is illuminated by an incident EM wave, a current is induced on the elementary unit cell [56]. This phenomenon is similar to the Bow Tie-shaped rings discussed in Chapter 4. Likewise, in the Octagonal-shaped RFID tag, the energy is transferred in terms of constructive and destructive inferences to the adjacent rings, and different patterns of bits can be obtained by adding short circuits between the rings. The thickness of the resonator rings varies from maximum to minimum from the outer to the inner ring to achieve maximum polarization [138]. To attain this, multiple layers of threads are used to stitch six resonator rings around the unitary element of the Octagonal RFID tag. The RF conductivity of the conductive tag depends on the sewing pattern, which may vary with multiple threads at one position [344].

For the HC12-Tag, the width of the strip is very important for decreasing resistance and attaining radiation efficiency. To meet optimised FSS shape dimension requirements, the strip length is varied from the 1st to 6th resonator from 0.9 mm to 0.6 mm, and the gap between resonators is varied from 0.9 mm to 0.1 mm, also to avoid extensive mutual coupling between consecutive resonators, see Figure 74.

Although the LIB40-Tag is optimised in the same way as the HC-12-Tag, the octagonal shape dimensions are adapted slightly, see Figure 75, to compensate for the difference in thread characteristics where the LCP coated LIBERATOR 40 thread, Vectran™, is slightly thicker but its *'ε_r'* is more stable with the change in frequencies and is more conductive with a resistivity of less than 3.25 Ω/m, see Table 15.

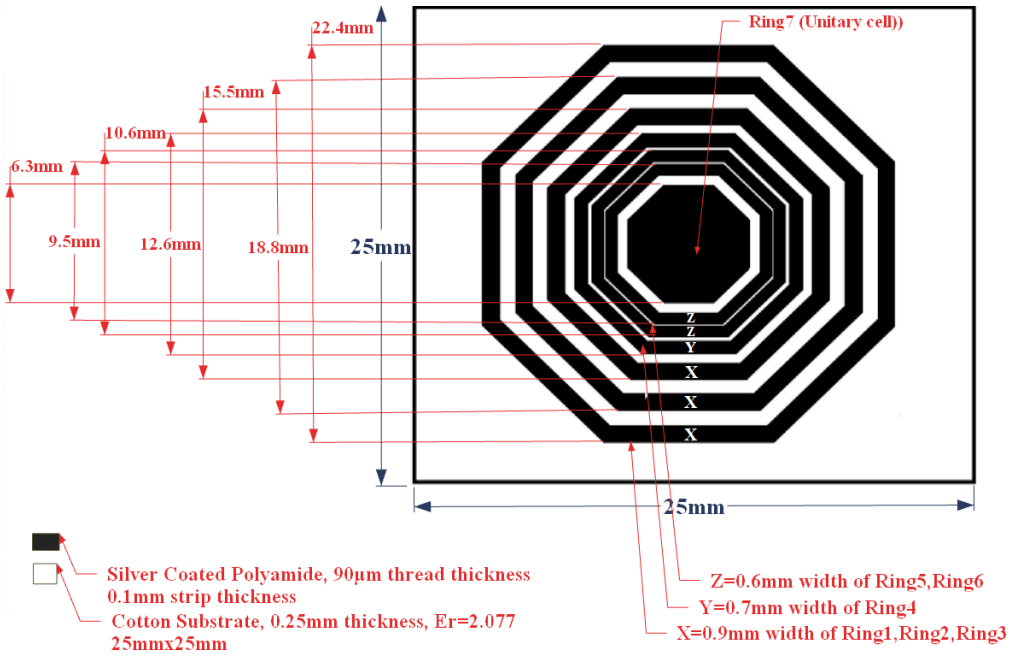

Figure 74. Optimised Octagonal Chipless RFID HC12-Tag Design

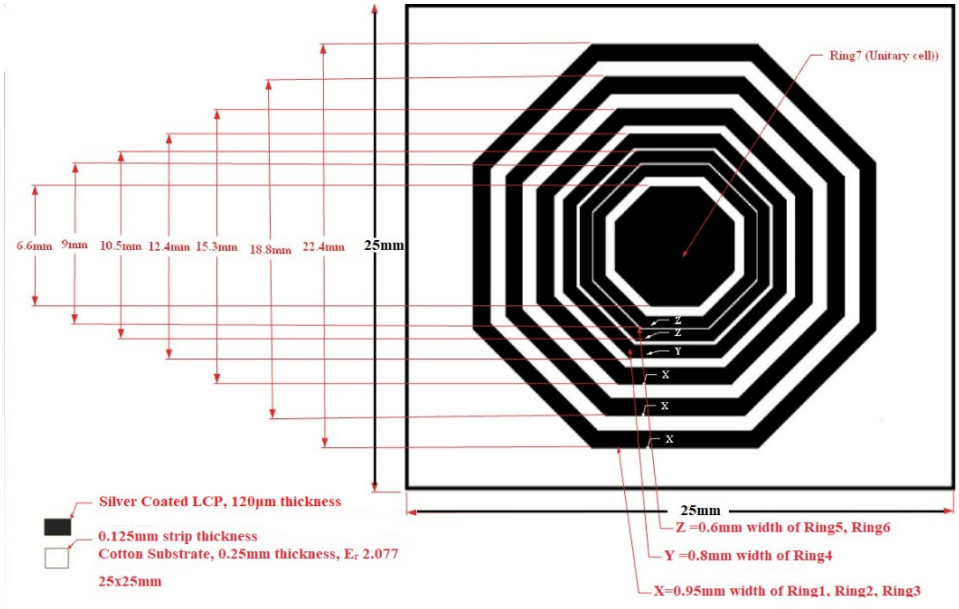

Figure 75. Optimised Octagonal Chipless RFID LIB40-Tag Design

The unitary element is filled with sewed conductive threads with 3.15 mm and 3.3 mm length on each of the eight sides of the octagonal shapes for HC12-Tag and LIB40-Tag, respectively. To maintain a seamless design on the cotton fabric, the conductivity of the inner unitary ring and for all resonators is kept between 10^3 to 10^4 S/m and the total thickness is maintained at 1 mm. This is achieved by using the commercial ZSK Technical Embroidery System JCZA 0109-550 with a resolution of 1 mm. This system can use F-Head and W-Head sewing technologies to embroidered designs on fabrics. For ease of fabrication, the F-Head technology, a common embroidery technique apt for generating satin stitch or running stitch with conductive threads for many wearable applications including E-Textiles and Smart Textiles, [345] is employed to fabricate the Octagonal-shaped RFID tag. See Figure 76Figure 1 for the embroidered octagonal tags on cotton fabrics.

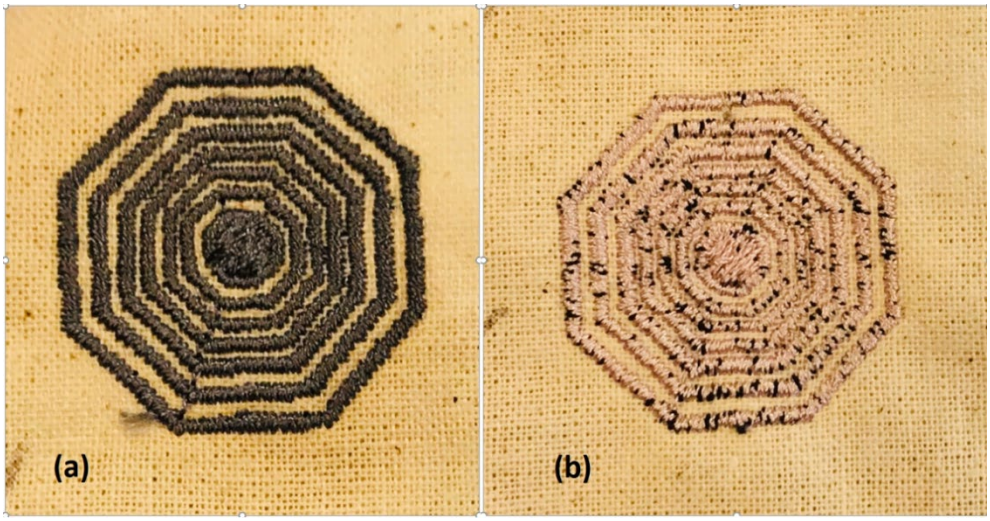

Figure 76. Embroidered Chipless RFID Tags a) HC12-Tag b) LIB40-Tag

The conductivity of the sewing pattern is essentially affected by the density of the threaded stitches per surface unit and the orientation of the fabric. Even with the octagonal geometrical shape selection, with all the resonators concentrically aligned to attain maximum conductivity [56], there are still noticeable losses due to the fabric properties but, with an electrically thin structure, the considerable losses are mostly due to conductive losses.

5.3.3 The Coding Principles of Embroidered RFID Tag

While there are actually a few designs reported in the investigative literature which comprise shapes which are independent of polarization due to their symmetry, such as the circular and square shapes in [147, 162, 340], the octagonal shaped tag design is also independent of polarization due to its symmetrical shape which provides code readability independent of any rotational angle. As described previously, this particular design is based on the FSS technique in which the physical characteristics of the base unit element, a unitary octagonal shape in this case, is very important because once this element is designed, other surrounded shapes are created around it, and periodically repeating the unitary element shape with some optimization is a common principle of the FSS technique [138, 338].

The production of different codes (1's or 0's), as discussed in Chapter 4 for the Bow Tie-shaped design, depends on the constructive and destructive interferences of the induced surface current J on the scatterer. An octagonal reference tag is designed and optimised on cotton to produce a maximum bitstream of 1111 before the short-circuited embroidered tags are designed. Before fabrication, the electromagnetic behaviour of the octagonal-shaped design is analysed.

5.4 Electromagnetic Behaviour of Octagonal Chipless RFID Tag

The mathematical model of an Octagonal Chipless RFID tag provides insight into the electromagnetic response of the circuit when an incident EM wave strikes at the tag and the induced current re-radiates into the scattered fields. While the current induced on the tag can be evaluated in

different ways, one method is based on the SEM in which the current induced on the tag is expanded in terms of the singularity poles of the tag. The concept of SEM has been widely used in circuit theory and will be used in Section 5.4.1 of this chapter to evaluate the electromagnetic response and transient analysis of the chipless RFID tags [157, 158, 316].

5.4.1 SEM-Based Equivalent Circuit of Chipless RFID Tag

In this chapter, the SEM-based equivalent circuit of the Octagonal Chipless RFID tag is presented where the solution is obtained by evaluating the collection of poles S_n, a coupling coefficient R_n and the entire function F_e in the complex frequency domain. The scattering analysis is performed by representing the chipless RFID tag with an equivalent circuit representation as illustrated in Figure 77. For the electromagnetic response, the RFID scatterer is assumed to be a PEC in free space. Let N be the total number of scatterers where an incident electric field E^i strikes at the surface of the tag and the scattered electric field E^s has polarization vectors $\hat{a}_i$ and $\hat{a}_s$, respectively. The E^i causes an induced current J_n and the global resonances are modelled in the time-domain as damped sinusoids corresponding to the CNR of the scatterer with some weighting residue named as coupling coefficients R_N. The distance between the two scatterers is optimised in such a way that the coupling between one scatterer and the other is so small as to be negligible.

The SEM-based circuit equivalent model of the Octagonal Chipless RFID tag is depicted in Figure 77 where $R_1, R_2, \ldots R_N$, and $L_1, L_2, \ldots L_N$ define the resistances and the inductances and $C_1, C_2, \ldots C_N$ represents the inductance between two consecutive scatterers for N number of resonators.

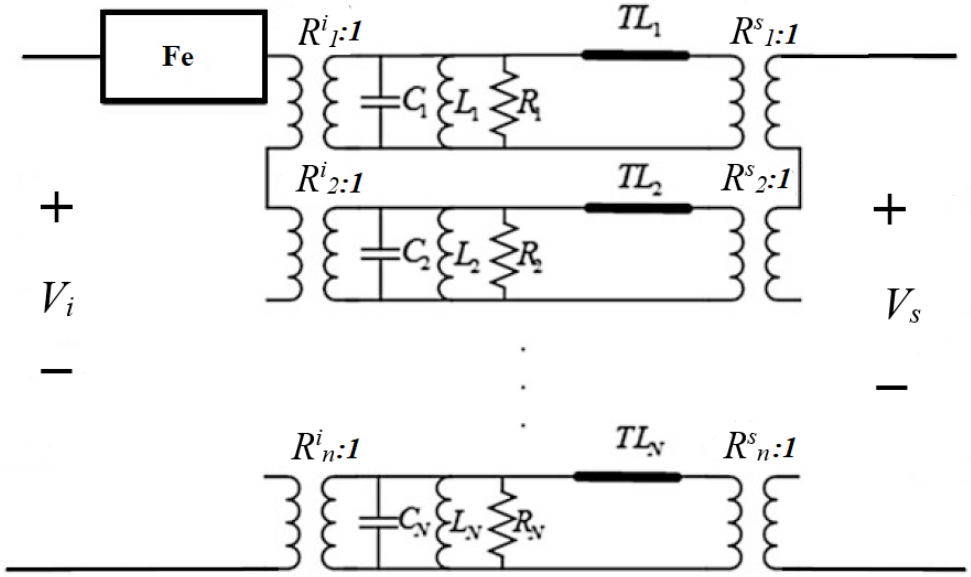

Figure 77. SEM-Based Equivalent Circuit of Octagonal RFID Tag with *N* number of Resonators

The E^i is coupled to the CNRs by coupling coefficients R_1, R_2, R_n which depend on the direction and the polarization of the incident electric field, and these values $R_1, R_2 \ldots R_n$ of the coupling coefficients have no impact of E^s.. Each CNR is represented by a parallel RLC circuit in series with delay in TL, which describe the turn-on time of the CNR, while F_e shows the early time response of the tag. The

input voltages V_i and output voltages V_s are defined at the transmitting and receiving antennas ports, respectively.

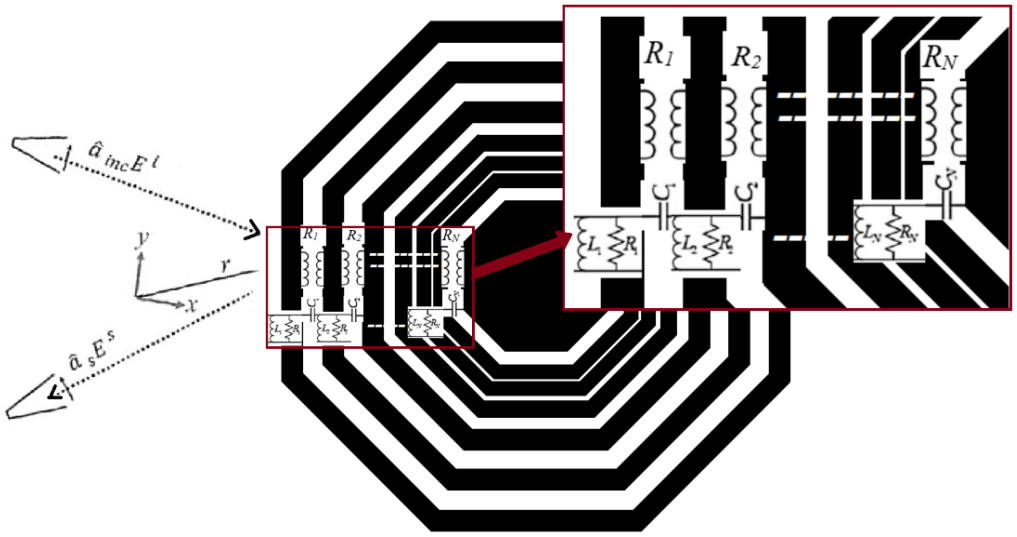

Figure 78. Geometry of Octagonal RFID Tag Illuminated by Incident Field E^i

Figure 78, shows the geometry of the Octagonal tag when E^i strikes at the surface of the tag and the E^s electric field is scattered with polarization vectors $\hat{a}_i$ and $\hat{a}_s$, assuming the incident electric field as a Dirac-delta function. The transfer function of the tag in the complex s-plane is defined as shown in Eq (52), based on [128].

$$H_t(\hat{a}_i, \hat{a}_s; s) = \frac{E^s(r;s)}{E^i(r;s)} \tag{52}$$

Equation (53) represents the transfer function $H(s)$ in terms of early-time response $H_e(s)$ and late time response $H_1(s)$ with CNRs, obtained after mathematical processing as discussed in [128].

$$H(s) = H_e(s) + H_1(s)$$
$$= H_e(s) + \sum_{n=1}^{N}\left[\frac{A_n}{s - s_n} + \frac{A_n^*}{s - s_n^*}\right] \tag{53}$$

where $A_n = \frac{C}{2}\left(1 + j\frac{1+\alpha_n}{\omega_n}\right)$ and CNRs of the circuit are described by (54) and (55):

$$s_n = \alpha_n + j\omega_n \tag{54}$$

$$\alpha_n = -\frac{\omega_0}{2Q} \quad \text{and} \quad \omega_n = \frac{\omega_0}{2}\sqrt{4 - \frac{1}{Q^2}} \tag{55}$$

where the RFID first resonator resonates at $f_1 = \omega/2\pi$.

The current distribution over the first resonator, the outermost octagonal ring, is I_1, and V_1 is the induced voltage due to incident fields corresponding to the impedance Z_1 of the resonator. The

current distribution over the octagonal scatterers can be evaluated by discretising the length of the ring into *N* number of segments [128] as shown in

$$[I_1]=[Z_1]^{-1}[V_1] \tag{56}$$

Here, $[Z_1]$ corresponds to the N×N matrix referred to as a system impedance matrix, $[I_1]$, and $[V_1]$ represents the response vector of N×1 corresponding to the incident field, see Figure 79.

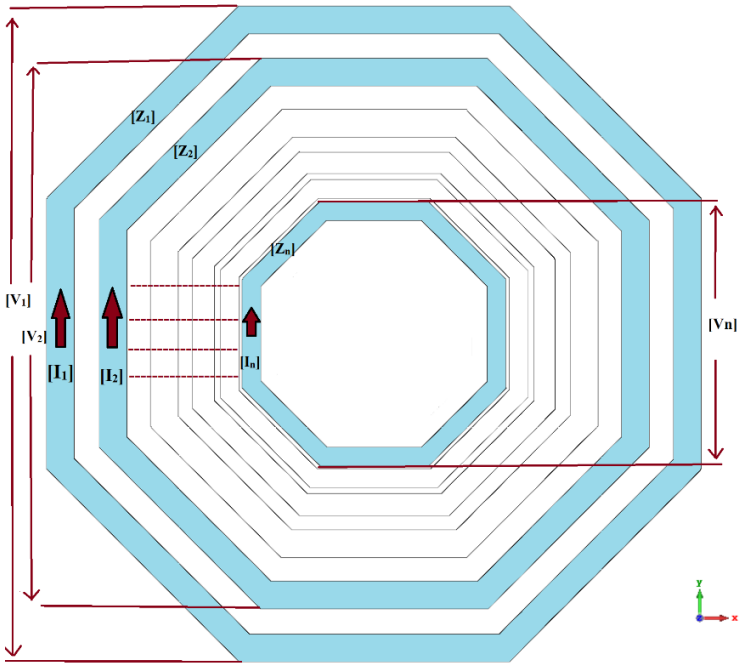

Figure 79. Induced Voltages and Currents Distribution

The CNRs for the first scatterer is calculated using (57).

$$\begin{gathered}[Z_1(s_n)][I_1(s_n)]=0 \\ \Delta_1(S_n)=\det[Z_1(S_n)]=0\end{gathered} \tag{57}$$

Similarly, the CNRs for the first resonator are obtained by expending $\square_1(s_n)$ using the complex Taylor series, as in (58).

$$\Delta_1(s_n)=\Delta_1(s_0)+\Delta_1'(s_0)(s-s_0)+\ldots\quad=0 \tag{58}$$

By retaining the first two terms of the equation, and by ignoring the rest of the values, the CNR S_n, is obtained using

$$S_n=S_0-\frac{\Delta 1(s0)}{\Delta 1'(s0)} \tag{59}$$

Where S_0 is the initial estimate of a resonant frequency, repetition of this procedure refines the assessment into more accurate values for the first scatterer, where the HC12-Tag provided a resonance calculation of approximately 7.95 GHz and the LIB 40-Tag obtained around 8.35 GHz.

Modification of equation 5 serves to obtain the current distribution for the first resonator of the Octagonal Chipless RFID tag, as shown in (60).

$$[I] = \sum_n \frac{R_n}{s - s_n}[J_n] \tag{60}$$

where R_n is the residue of the n^{th} pole, and J_n represents the surface current distribution over the surface of the scatterer, as evaluated in Section 5.4.2, a time-domain response can also be obtained by applying the inverse Laplace transformation on (60).

5.4.2 Transient Scattering of E-Field by SEM Method and Evaluation of Surface Current Distribution J_n and the Coupling Coefficients R_n.

In order to study the mechanism of scattering by a 4-bit Octagonal Chipless RFID tag, the surrounding medium is supposed as free space with permittivity ε_0 and permeability μ_0, the scatterer is PEC and the thickness of the tag, being very small, is considered to be zero. Hypothesizing that an incident field E^i strikes and the induced current over the surface of the tag is J_n, then the scattered field E^s from the tag is either obtained from the EFIE or MFIE [317]. The use of EFIE, illustrated in Figure 80, is represented in Laplace form in (61), based on [318].

$$E^s(r;s) = \mu s \iint_A \left[\left(\vec{\vec{I}} - \frac{1}{k^2}\nabla\nabla \right) G_0(r,r';s) \right] . J(r,r';s) dS' \tag{61}$$

where A represents the surface area of the Octagonal Chipless RFID tag, k represents the propagation constant $k = s/c$ in the complex frequency domain, $\vec{\vec{I}} = \hat{x}\hat{x} + \hat{y}\hat{y} + \hat{z}\hat{z}$ and G_0 defines the scalar Green's function in the free space, as shown in (62).

$$G_0(r,r';s) = \frac{e^{-jk|r-r'|}}{4\pi\,|r-r'|} \tag{62}$$

The Green's function G_0 satisfies the Sommerfeld radiation conditions as discussed in [128], and represented in (63).

$$\lim_{r\to\infty} r\left(\frac{\partial}{\partial r} + jk \right) G_0(r,r';s) = 0 \tag{63}$$

By using dyadic interpretation of Green's function, the scattered field from (63) can be written in the form of inner product, as in (64).

$$E^s(r;s) = \left\langle G_0(r,r';s), J(r';s) \right\rangle_{r'} \tag{64}$$

Where the Dyadic Green's function G is defined as in (65).

$$\vec{\vec{G}}(r,r';s) = -\mu s \left(\vec{\vec{I}} - \frac{1}{k^2}\nabla\nabla \right) G_0(r,r';s) \tag{65}$$

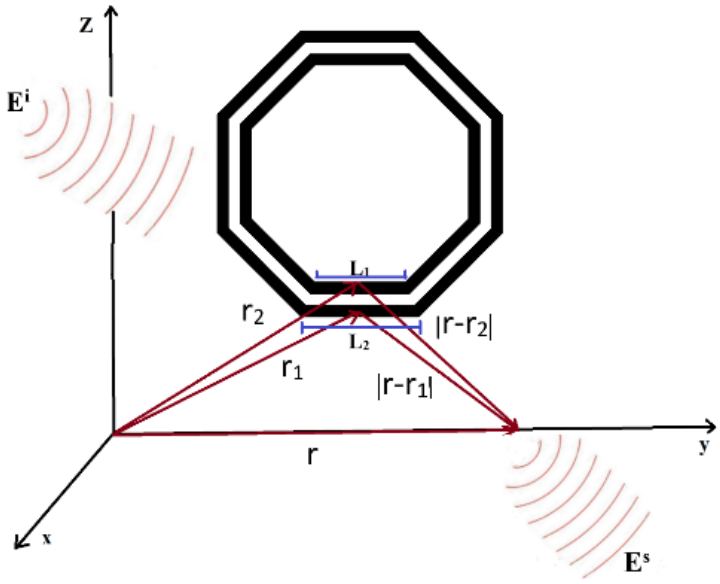

Figure 80. Scattered Wave Evaluation and Implication of Green's Function by L1 and L2 of Two Consecutive Resonators

The associated radiation condition's for $\vec{\vec{G}}$ is given as in (66).

$$\lim_{r\to\infty} r\left(\nabla \times jkr' \times\right)\vec{\vec{G}}(r,r';s) = 0 \tag{66}$$

The inner product represented in (64) is given as in (67) .

$$\left\langle A,B\right\rangle_a = \int A.Bda \tag{67}$$

Assuming the first resonator of the tag and PEC in free space, then the boundary conditions on the tag surface is given by

$$\hat{t}.\left(E^s(r;s)+E^i(r;s)\right)=0 \qquad \forall r\in A \tag{68}$$

where $\hat{t}$ is the vector tangential to the tag surface, now the EFIE for the first scatterer is given by

$$\left\langle \vec{\vec{G}}(r,r'),J(r')\right\rangle_{r'} = -E^i{}_t(r) \qquad \forall r\in A \tag{69}$$

The solution of the (69) is obtained by using Method of Moment (MoM), after discretising the surface on the tag into *N* number of isolated meshed and applying Galerkin's technique, the expression can be written as shown in (70).

$$\begin{aligned} \Gamma_{mn}.J_n &= I_n \\ J_n &= \Gamma_{mn}{}^{-1}.I_n \end{aligned} \tag{70}$$

Thus, (70) shows the current distribution on the surface of tag in which singularity poles of the RFID tag are the zeros of the determinant of the coefficient matrix Γ as represented in (71).

$$\det(\Gamma_{(S_k)})=0 \qquad k=1,2,3.... \tag{71}$$

These singularity poles are the CNRs of the tag. When an incident source field strikes the tag, the

current distribution on the surface of the tag shows damped oscillations. In the SEM, this current distribution is an analytical function in the complex *s*-plane, except for CNRs, as in (72).

$$J(r;s) = \sum_{n=-\infty}^{+\infty} \frac{a_n(r;s)}{s - s_1} + J_e(r;s) \tag{72}$$

Since the time-domain response is a real value signal, the value in (72) can be written as

$$s_n = s_{-n}^{\ *}$$

$$a_n(r;s^*) = \left[a_n(r;s)\right]^* \tag{73}$$

$$J_e(r;s^*) = \left[J_e(r;s)\right]^*$$

Where $s_n = \alpha_n + j\omega_n$ is the n^{th} CNR of the octagonal tag scatterer, which has been defined using (54). Similarly, J_e(r;s), known as the entire function, is required in s-plane for each pole in the infinite series to ensure the convergence of the series [317, 346] and $a_n(r;s)$ is a weighting function which is assumed to be a separate quantity in the spectral form, as represented in (74).

$$a_n(r;s) = R_n(s)J_n(r) \tag{74}$$

Here J_n(r) corresponds to the natural mode of the tag at the n^{th} resonant frequency and R_n(s) is the dependent residue of the poles which represents the coupling coefficients. The current distribution close to S_n given in (75) is obtained by inserting (74) into (72) and simplifying it.

$$J(r;s) = \frac{R_n(s)J_n(n)}{s - s_1} + J_e(r;s) \tag{75}$$

By using power series and expanding $\overleftrightarrow{G}$ and E_i around $S = S_n$ and presented in (76) and (77).

$$\overleftrightarrow{G}(r,r';s) = \sum_{m=0}^{\infty} \left| \frac{1}{m!} \frac{\partial^m \overleftrightarrow{G}(r,r';s)}{\partial s^m} \right|_{s=s_n} (s - s_n)^m \tag{76}$$

$$E^i_{\ t}(r;s) = \sum_{m=0}^{\infty} \left| \frac{1}{m!} \frac{\partial^m E^i_{\ t}(r;s)}{\partial s^m} \right|_{s=s_n} (s - s_n)^m \tag{77}$$

Finally, by inserting (75), (76) and (77) into (69), the new expression can be written as in (78).

$$\left\langle \sum_{m=0}^{\infty} \left| \frac{1}{m!} \frac{\partial^m \overleftrightarrow{G}(r,r';s)}{\partial s^m} \right|_{s=s_n} (s-s_n)^m, \frac{R_n(s)J_n(r)}{s-s_n} + J_e(r;s) \right\rangle_{r'}$$

$$= -\sum_{m=0}^{\infty} \left| \frac{1}{m!} \frac{\partial^m E^i{}_t(r;s)}{\partial s^m} \right|_{s=s_n} (s-s_n)^m$$

$$\left\langle \begin{matrix} \overleftrightarrow{G}(r,r';s_n) + (s-s_n) \dfrac{\partial \overleftrightarrow{G}(r,r';s)}{\partial s}\Big|_{s=s_n} \\ + \dfrac{(s-s_n)^2}{2} \dfrac{\partial^2 \overleftrightarrow{G}(r,r';s)}{\partial s^2}\Big|_{s=s_n} \ldots, \dfrac{R_n(s)J_n(r)}{s-s_n} + J_e(r;s) \end{matrix} \right\rangle_{r'} = \tag{78}$$

$$-E^i{}_t(r;s_n) - (s-s_n) \frac{\partial E^i{}_t(r;s)}{\partial s}\Big|_{s=s_n} - \frac{(s-s_n)^2}{2} \frac{\partial^2 E^i{}_t(r;s)}{\partial s^2}\Big|_{s=s_n} - \ldots$$

where, by balancing the coefficients of (78) according to the power of $(s-s_n)$ and the coefficients of $(s-s_n)^{-1}$ at $s = s_n$, the following equation is given

$$\left\langle \overleftrightarrow{G}(r,r';s_n), J_n(r') \right\rangle_{r'} = 0 \tag{79}$$

The matrix form of the above equation shows that the determinant of the coefficient matrix should be zero at CNR, that the poles are completely dependent on the Dyadic Green's equation $\overleftrightarrow{G}(r,r';s_n)$ and also that they are aspect and source free parameters of the RFID tag. Furthermore, for each CNR, S_n there will be a no-trivial natural mode J_n(r) which is the solution of (79). Similarly, the magnetic coupling factor can be described by using magnetic current distribution $M_n(r')$, as shown in (80) .

$$\left\langle M_n(r'), \overleftrightarrow{G}(r,r';s_n) \right\rangle_{r'} = 0 \tag{80}$$

By equating the coefficients of $(s-s_n)^0$ to (74) in the following:

$$\left\langle \overleftrightarrow{G}(r,r';s_n), J_e(r';s) \right\rangle_{r'} + R_n(s_n) \left\langle \frac{\partial \overleftrightarrow{G}(r,r';s)}{\partial s}, J_n(r') \right\rangle_{r'} = -E^i{}_t(r;s_n) \tag{81}$$

$$R_n(s_n) = -\frac{E^i{}_t(r;s_n) - \left\langle \overleftrightarrow{G}(r,r';s_n), J_e(r';s) \right\rangle_{r'}}{\left\langle \left\langle \dfrac{\partial \overleftrightarrow{G}(r,r';s)}{\partial s}\Big|_{s=s_n}, J_n(r') \right\rangle \right\rangle_{r'}} \tag{82}$$

Using (79) and the inner product of the sides of (82) by $M_n(r)$, the coupling coefficient can be found, as in (83).

$$R_n(s_n) = -\frac{\left\langle M_n(r), E^i{}_t(r;s_n)\right\rangle_r}{\left\langle\left\langle M_n(r), \left\langle \frac{\partial \vec{\vec{G}}(r,r';s)}{\partial s}\bigg|_{s=s_n}, J_n(r')\right\rangle_{r'}\right\rangle_r} \tag{83}$$

Note that the inner product of the LHS is performing on r', thus both sides of (83) are a function or *r*. For EFIE, where symmetric matrices are encountered, the coupling vectors and natural modes are similar, as discussed in [317]. Hence, the above equation can be written as in (84).

$$R_n(s_n) = -\frac{\left\langle J_n(r), E^i{}_t(r;s_n)\right\rangle_r}{\left\langle\left\langle J_n(r), \left\langle \frac{\partial \vec{\vec{G}}(r,r';s)}{\partial s}\bigg|_{s=s_n}, J_n(r')\right\rangle_{r'}\right\rangle_r} \tag{84}$$

Equation (84) shows that the coupling coefficient depends on E^i and natural modes J_n(r) at the resonant frequency.

$$\left\langle J_n(r), E^i{}_t(r;s_n)\right\rangle_r = 0 \tag{85}$$

In the case presented in (85) where the condition satisfies the related mode is not exited by E^i and the coupling coefficients in (80) are only obtained from the CNR's of RFID Tag. The entire function J_e(r;s), discussed in (72), enters into an early time response and becomes difficult to obtain via a simple way [317].

In this octagonal design, coupling coefficients are evaluated between two consecutive octagonal rings at corresponding resonances, depending on the gap between them, see Table 16.

Table 16. Coupling Coefficients for HC12-Tag and LIB40-Tag for Corresponding Resonances

n	Resonant Frequency F_{0n} (GHz)		Consecutive Rings	Gap Between Resonators (mm)		Coupling Coefficients R_n	
	HC12-Tag	LIB40-Tag	HC12-Tag LIB40-Tag	HC12-Tag	LIB40-Tag	HC12-Tag	LIB40-Tag
1	8	8.5	1-2	0.9	0.95	-0.011	-0.009
2	10.2	10.5	2-3	0.9	0.95	-0.012	-0.010
3	12.5	14	3-4	0.6	0.5	-0.022	-0.019
4	16.5	17.5	4-5	0.3	0.2	-0.029	-0.022

The values of the coupling coefficients between the first two consecutive rings for HC12-Tag and LIB40-Tag are -0.011 and -0.009 calculated for the spacing of 0.9 mm and 0.95 mm for 8.0 and 8.5 GHz frequency, respectively, see Table 16, where *n* presents the number of resonances or spikes of RCS. The coupling becomes very intensive between the higher orders of the rings such as between

rings 5 and 6. It becomes obvious that there is no conductive link between them, although this is more likely due to the reduced conductivity of the conductive thread as compared to a pure conductor, such as copper, at this high frequency. Therefore, as there is no resonance at this higher order, the rings behave like a single ring. With all R_n values evaluated for corresponding resonant frequencies for both designs, the maximum values of R_n, as shown in Table 16, are -0.029 and -0.022 for HC12-Tag and LIB40-Tag respectively. These are sufficiently low values to assure a reliable reading of the coded information. To reduce the mutual coupling, the average spacing between the resonators can be increased, although, as a consequence, the size of the tag would be significantly increased.

5.5 Experimental RCS Measurements and Code Verifications

This section conveys the experimental results of the embroidered Octagonal Chipless RFID tag designs through simulations and measurements received in the chamber. The performance of the 4-bit Octagonal RFID tag is verified by the RCS sequences obtained from the results categorized in the form of bitstreams of 1's and 0's, as depicted in Figure 81 and Figure 82. These results are obtained initially for the maximum reading range of 180 cm with a 0-dBm power set on VNA.

5.5.1 Simulated & Measured Results

Both Octagonal RFID tags were designed using CST MICROWAVE STUDIO to attain optimized results. First, the octagonal-shaped RFID tag with HC12 thread is fabricated on cotton fabric, see Table 5-10. The octagonal-shaped design is optimised for the resonant frequency of 8 GHz and, based on the dimensions and the gap between the first two consecutive resonators to avoid mutual coupling [121] and the smoothness of sewing surface to maintain proper surface current density. As a result, the first resonant peak with an RCS equal to -51.54dB with a 3 dB bandwidth of 320 MHz is obtained, see Figure 81. While the RCS results can also be described in terms of dBsm, to understand the bandwidth variation, these are described in dB's here. The structure is composed of 6 resonators around the unitary cell to generate four resonance peaks, or a 4-bitstream. Because of the minute distance between the first two resonators, these consecutive resonators next to the unitary element behave like a single resonator with very high mutual coupling. The tag is then optimised to achieve the next resonances at 10.2, 12.5 and 16.5 GHz frequencies, with 400, 450 and 490 MHz bandwidths respectively.

The bandwidths achieved for the composite resonators are quite satisfactory considering the lower conductivity of the thin strips of the tag. The strip length is varied to obtain accurate resonance as, if the width is larger, the conductivity and inductance are higher, where there is a higher chance of mutual coupling. Therefore, there is a trade-off between the width of the strips and the gap the in resonator rings to achieve the required scattering resonance. The RCS obtained by the measured values is in good agreement with the simulated values of the HC12-Tag, except that the 3rd resonance peak is 9% towards the higher values compared to the simulated peak value. Although this might be

the result of a mutual coupling effect between the 3rd and 4th resonator of the fabricated tag, see Figure 81. Furthermore, the measurements observed for the maximum transition from 0 to 1, in terms of RCS values, is around -25 dB, which is good for reader detection of the occurrence of the bit codes and indicate that the interaction between the resonator rings creates a repetitive RCS response. Each frequency resonance is dependent on the ring diameter, the width of the strip, and the gap separation between rings. Understanding that, due to strong mutual coupling, the unitary element and the first outer ring correspond to a singular resonance where, as expected from the simulated values, 4 bits are obtained.

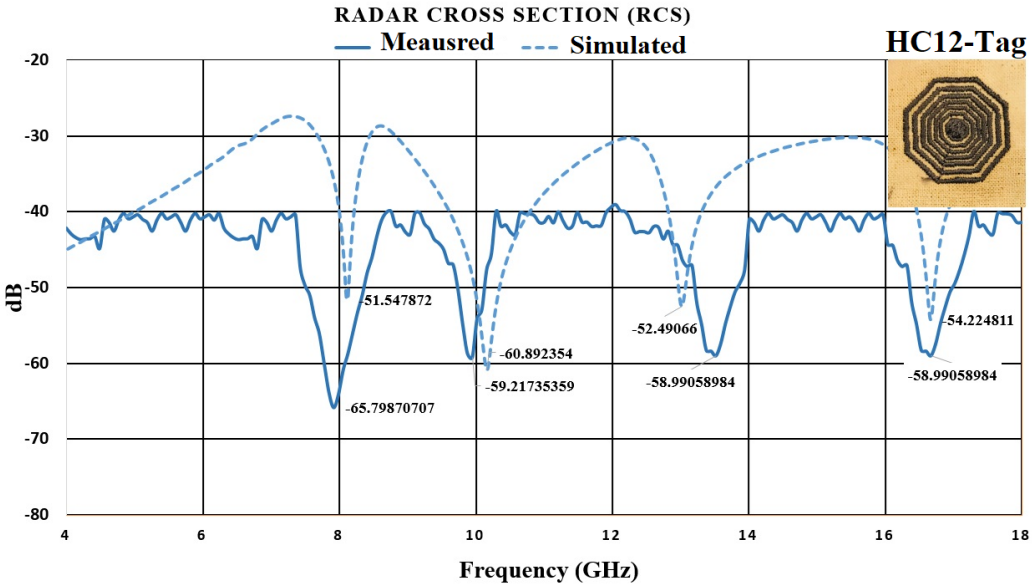

Figure 81. Simulated and Measured Results for HC12-Tag

For the LIB40-Tag, the same octagonal model is simulated with the different specifications of the conductive thread, LIBERATOR 40. As this thread is highly conductive and slightly thicker than the HC12, the LIB40-Tag design is optimized around the central operating frequency of 8.5 GHz. While following the same process as the HC12-Tag, the LIB-40, the strip gap is adjusted to vary from 0.9 to 0.2 mm to correlate the strip inductance to the resonant frequency. The simulated RCS received closer to -50 dB with a 3-dB bandwidth of 300 MHz. The next resonance peaks are obtained at 10.5 GHz, 14 GHz and 17.5 GHz with the corresponding 3-dB bandwidth of 450 MHz, 400 MHz and 380 MHz, respectively. The RCS measurements for LIB40-Tag are illustrated in Figure 82.

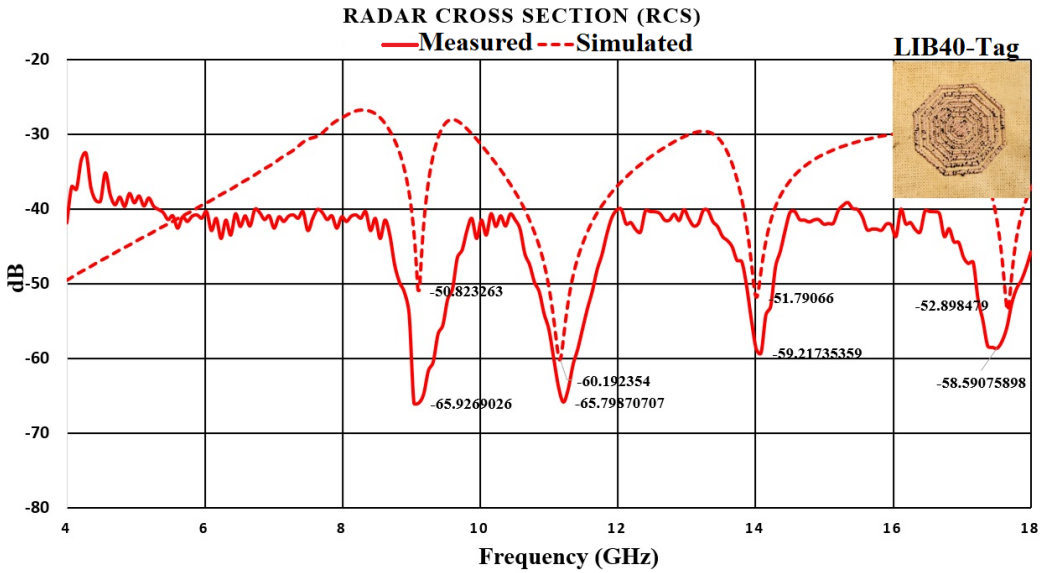

Figure 82. Simulated and Measured Results for LIB40-Tag

5.5.2 The Experimental Setup

To verify the achieved simulated results, both RFID tag designs are analysed by VNA in the chamber, with the experimental setup depicted in Figure 83. A series of experiments have been performed for both tag designs with the bit patterns retrieved precisely in terms of RCS.

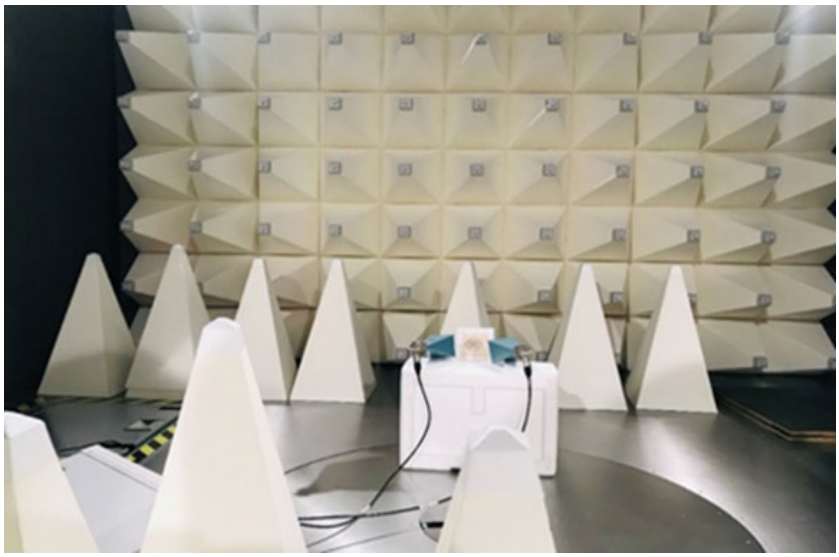

Figure 83. Experimental Setup in Anechoic Chamber

5.5.3 Code Verifications and Performance of the Tags

In most cases for FSS-based RFID designs, the production of different codes of different bitstreams (1's or 0's) principally depends on the constructive and destructive interferences of induced surface current *J* on the scatterer [1]. Hence, to obtain different RCS patterns in terms of 1's and 0's, resonators of the octagonal RFID tag can be shorted to each other. For a periodic octagonal structure,

short circuits can be inserted to connect two adjacent rings so that the distribution of the surface currents can be modified to change the far-field response [2, 56]. In this case, short circuits are applied symmetrically at four points of the two consecutive rings which force the standing waves to have a similar phase, see Figure 84.

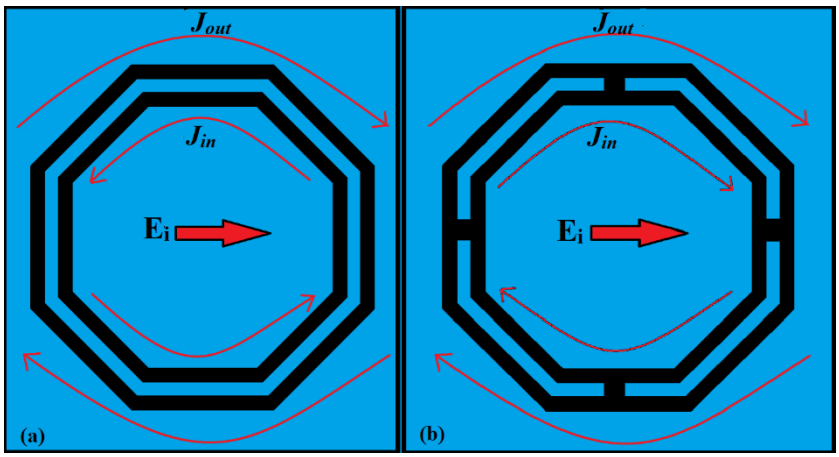

Figure 84. Direction of E-Field E^i and Surface Current J for two Consecutive Resonators (a) Open Circuited, J_{in} and J_{out} out of phase (b) Short circuited, J_{in} and J_{out} in-phase

Therefore, the radiated E-field produced from these equivalent current sources (J_{in} and J_{out}) constructively interferes in free space, and subsequently, suppresses the resonance whereby different codes are generated and successfully read for the various patterns.

Initially, the open-circuited octagonal reference tag is designed and embroidered on cotton to produce a maximum bitstream of 1111. The short-circuited embroidered tags are then designed and a series of bitstreams 1111, 1011, 0111, 0011, 1010 and 0000 are obtained for the HC12-Tag, see Figure 86. Similarly, a bitstream of 1111, 1011, 0111, 0011, 0010 and 0000 are successfully retrieved for the LIB40-Tag design, see Figure 85. The complex RCS feature (σ^{Tag}) of the Octagonal Chipless RFID design is obtained by the following (86), as elaborated in [162].

$$\sigma^{Tag} = \left[\frac{S_{21}^{Tag} - S_{21}^{No-Tag}}{S_{21}^{Ref} - S_{21}^{No-Tag}}\right]^2 \sigma^{Ref} \tag{86}$$

Where S_{21}^{No-Tag} is associated with the measurements recorded in the empty chamber, S_{21}^{Ref} corresponds to the reference value obtained from a defined setup, which could be on any conductive surface, here, a copper square of 50 mm x 50 mm is employed. σ^{Ref} is associated with the simulation results for the same copper reference surface. The results for both tags show a good agreement between the measured and simulated designs.

5.5.3.1 Verification for HC12-Tag

As stated earlier, when the plane wave from the transmitting horn antenna *Tx* falls onto the octagonal tag, a current is induced on the surface of the resonators on the respected frequencies. For the HC12-Tag, as depicted in Figure 5-14, these frequencies are 8, 10.2, 12.5 and 16.5 GHz, and realise the generation of code 1111, remembering that the unitary element (ring 7) and the very next outer ring

behave like a singular resonator due to the strong mutual coupling. The other bits, 1011, 0111, 0011, 0010 and 0000 are successfully generated and retrieved, see Figure 86.

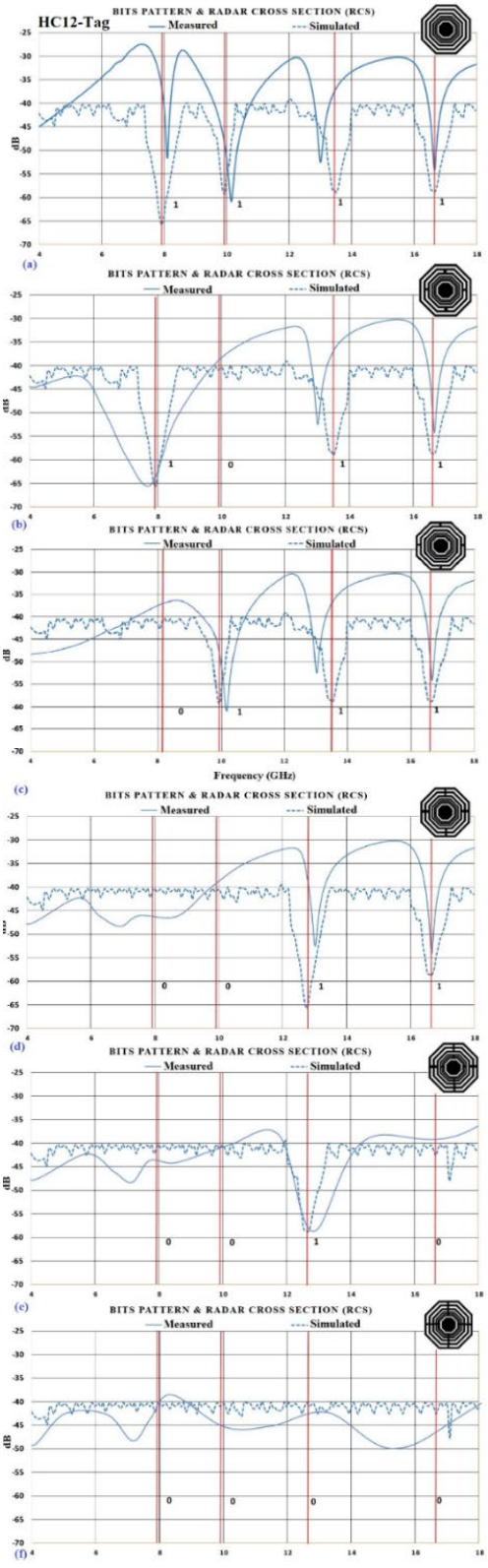

Figure 86. 4-Bit Code Generation in Terms of |RCS| Measurement For HC12-Tag a) 1111 b) 1011 c) 0111 d) 0011 e) 0010 f) 0000

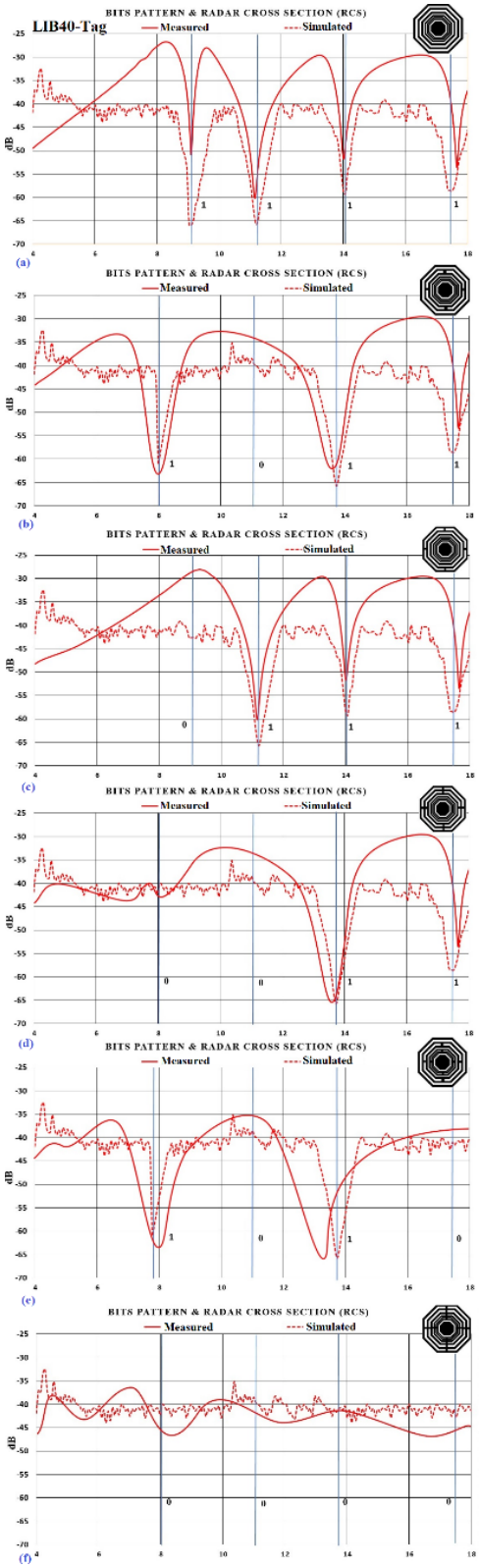

Figure 85. 4-Bit Code Generation in Terms of |RCS| Measurement For LIB40-Tag a) 1111 b) 1011 c) 0111 d) 0011 e) 1010 f) 0000

5.5.3.2 **Verification for LIB40-Tag**

The second Octagonal Chipless RFID tag, LIB40-Tag, is designed to work within the UWB frequencies from 8 to 18 GHz with resonance peaks at 8.5, 10.5, 14 and 17.5 GHz, as depicted in Figure 85, to realise the generation of bits 1111. Similarly, the other bits 1011, 0111, 0011, 1010 and 0000 are also successfully generated and retrieved.

5.5.4 On-body RCS detection

The detection of codes for clothing and wearable textile is difficult and challenging especially for chipless RFID tags because the RCS of the chipless tag is much lower than the RCS of the human body, so there is always a chance that the RCS of the tag may become suppressed by the stronger response of the human body [331]. Furthermore, the human body RCS response varies with each body movement; even human breathing further changes the RCS response of the tag. To overcome this, placement of the RFID tag is preferred at a safe distance of 0.5-1.0 cm between the body and the fabric to decrease losses due to the conductivity of the human body [331]. Therefore, it is more feasible to detect RCS responses for short-range operations from the tag and the human body which means that the detection setup is not farther than 18 cm, with 10 cm to the aperture and 8 cm from the feed line to the aperture. In this regard, an experimental set up is arranged as depicted in Figure 87.

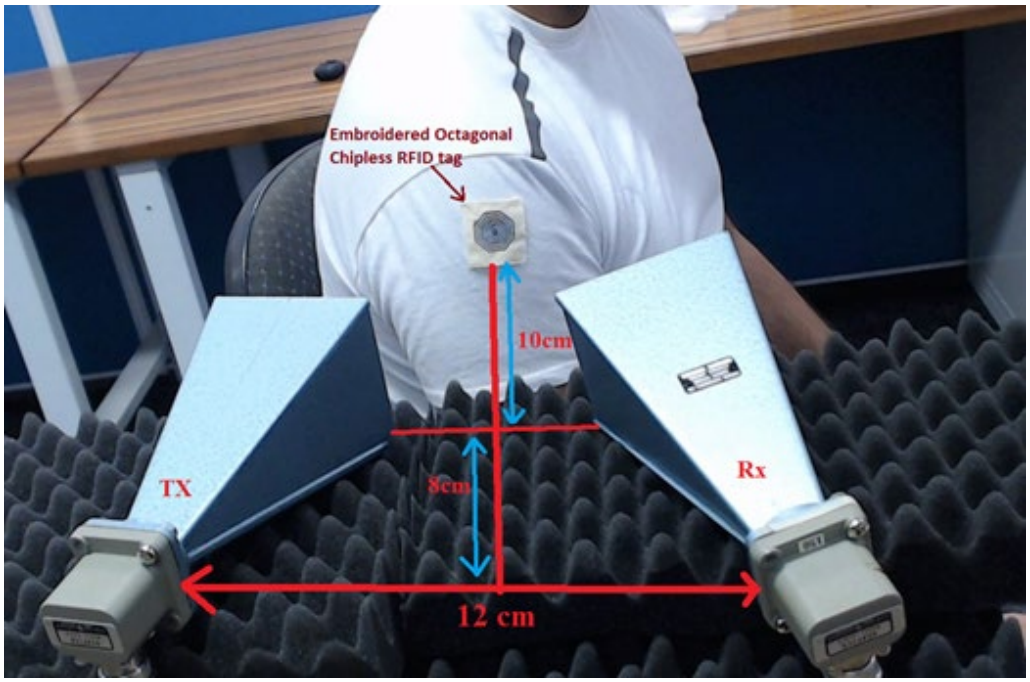

Figure 87. On-Body RCS Measurement Setup for Embroidered Chipless RFID tags

For the HC12-Tag, the first resonance is observed at 8.25 GHz, with other resonances generated at 10.18, 13.6 and 16.8 GHz, which are only 0.5 to 5% of the measured values of the same tag in free space in the chamber; see Figure 88. The maximum shift is observed at the first resonator peaks of both in the chamber and on-body testing results which are around 4.12% towards the higher frequencies. The best result is obtained at the fourth resonator peaks with a shift of about 0.59%, demonstrating a good correlation of the measured values in the chamber and on-body calculations.

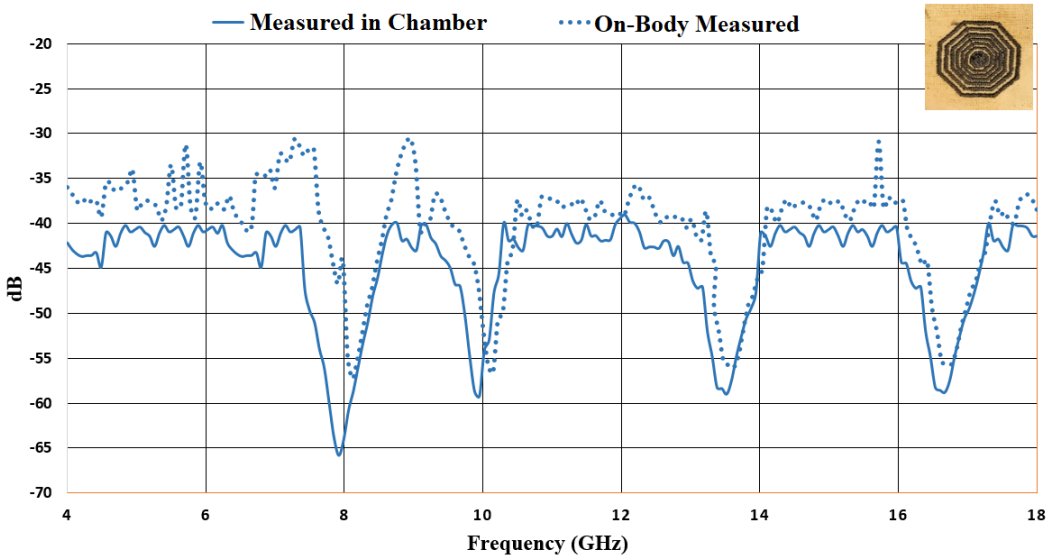

Figure 88. RCS Measurements for HC12-Tag Measured in Chamber and on-body on a Right Arm as depicted in Figure 87

Similarly, the single tag of LIB40-Tag is also tested on the upper right arm of the human body for the same environment and experimental setup as HC12-Tag. The first resonant peak is obtained at 9.65 GHz and following with 11.3, 14.2 and 17.8 GHz, as depicted in Figure 89. The maximum shift is observed at the first resonator peak while the lowest is observed at the second resonator peak which are shifts of around 5.6% and 0.44% respectively, towards the higher value of frequencies.

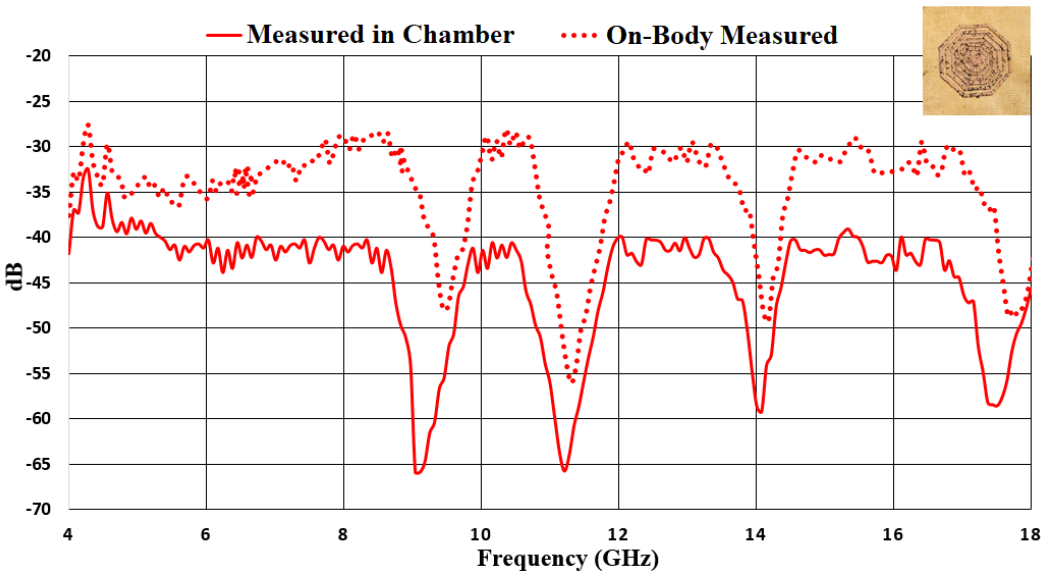

Figure 89. RCS Measurements for LIB40-Tag Measured in Chamber and on-body on a Right Arm as depicted in Figure 87

Conclusively, the results shown in Figure 88 and Figure 89 confirm that the on-body response is well correlated with the response of the free space measurement of the tags in the chamber. However, these results are only possible for close range operations, with 18 cm in this case. The on-body RCS measurements results demonstrate considerable distortion and even faded as the distance of tags from the source antennas increased from 18 cm. A shift of resonant frequencies is observed between the range of

5% to 30% for both of the designs when the distance increased from 18 cm to 60 cm. Another important factor is the distance between the tag and the skin of the body, where the closer the tag is to the skin, the higher the correlation between on-body RCS and the free space experimental values.

5.5.5 Bending Analysis of Embroidered Chipless RFID Tags

The bending and folding capabilities of chipless RFID tags for wearable applications are crucial. The radiation characteristics of the chipless RFID tags based on flexible substrates are dependent on this flexibility and crumpling ability [115, 116, 260], which is useful for wearable applications [134]. Both of the Octagonal Chipless RFID tags are designed on cotton fabric which has a good capability of bending, folding and stretching. In this section, a series of experiments have been performed on both of the RFID designs to validate their bending capability at a variety of radius of curvatures. For this purpose, polystyrene foam is used to mould samples of single tags for each design for the radius of 27 mm, 14 mm and 7 mm.

To corroborate the effects on the RCS measurements by bending, both embroidered tags are individually subjected to a certain curvature by attaching the tag samples to the moulds. For this, the single octagonal embroidered tag for each design with the maximum bitstream of 1111 is chosen, and all experiments are taken into the anechoic chamber to reduce the impact of external RF interferences. As an octagonal shape is independent of polarity, the tags are placed in the horizontal position for all experimental readings and VNA is used for transmitting electromagnetic plane waves at 0 dBm from 100 cm. Figure 90 illustrates how the implication of the three different curvatures of 27 mm, 14 mm and 7 mm modify the RCS measurements of the HC12-Tag. The RCS measurement recorded for the non-bent or flat state of the HC12-Tag is represented by a blue solid line.

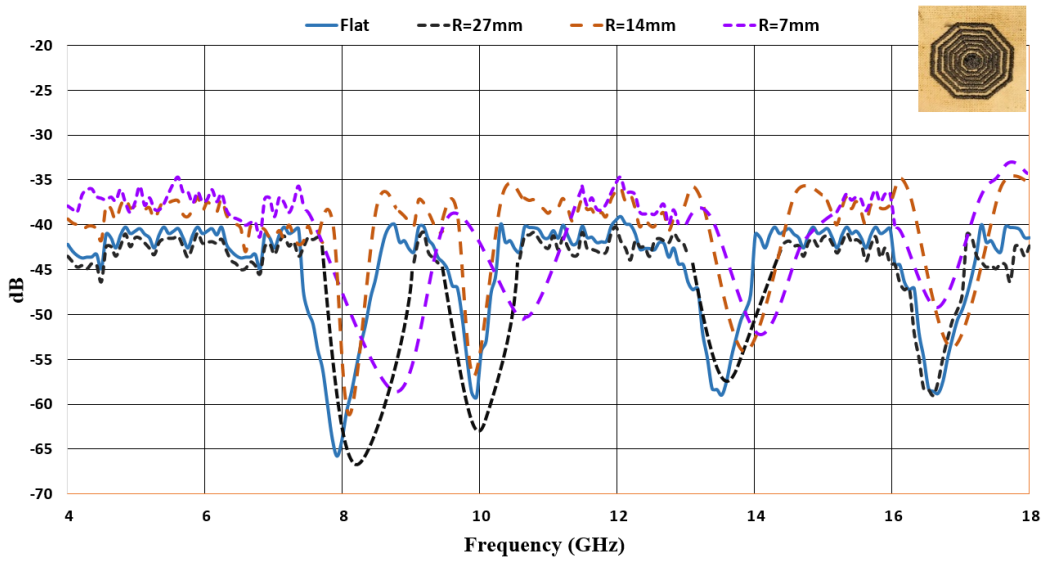

Figure 90. HC12-Tag: Chipless RFID Tag Bent with Radii of 27 mm, 14 mm and 7 mm.

A simple observation of Figure 90 brings the realisation that at a curvature of 27 mm the |RCS| obtained for HC12-Tag is lower than the flat state of the tag, converse to the scattering measurements of the tag for 14 mm and 7 mm radii which are higher. With the decrease of the curvature to 7 mm the resonant shift also

became prominent, although the |RCS| peaks remain retrievable for the implication of all the curvatures up to 7 mm for the HC12-Tag. Resultantly, it is concluded that the bits stored on the embroidered RFID tag for different patterns can successfully be recovered for various bending states at least down to that of the 7-mm radius.

With the highly conductive Liberator 40 thread used to embroider a tag on the cotton substrate, the RCS measurement recorded in Figure 91 for the non-bent or flat state of the LIB40-Tag is represented by a red solid line. The |RCS| results obtained for this LIB40-Tag at various bending states of 27 mm, 14 mm and 7 mm, all similarly obtained in the chamber, representing the impact of bending, most significantly at 7 mm on the average RCS.

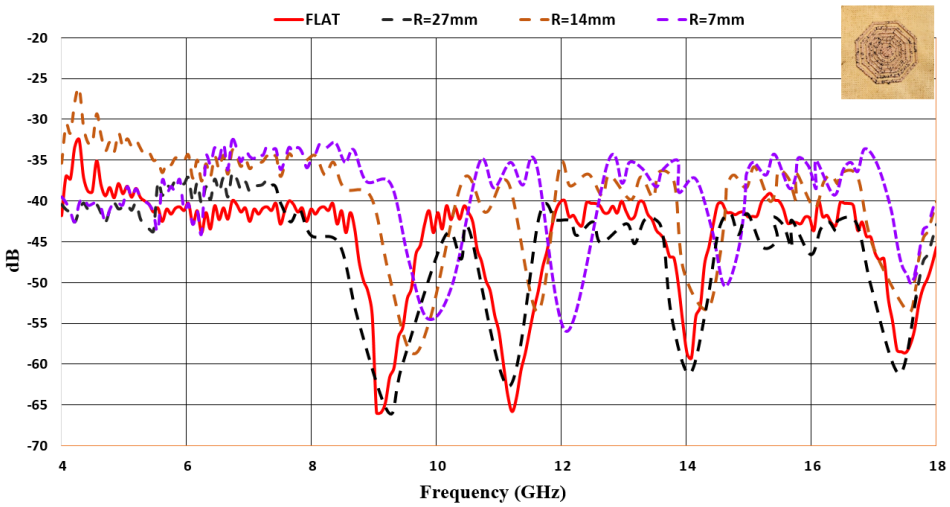

Figure 91. LIB40-Tag: Chipless RFID Tag Bent with Radii of 27 mm, 14 mm and 7 mm

Despite the noticeable shift in resonant frequency and the signal degradation compared to the non-bent reference tag readings, the |RCS| peaks are significantly retrievable and represent a successful bending analysis on both designs has proven their reliability in terms of bending for each of the various stages of curvature.

5.6 Maximum Read Range Estimation

This section provides the maximum read range of the Embroidered Chipless RFID tag using the radar equation [319] with the numerically calculated RCS based on (87) as follows:

$$R = \sqrt[4]{\frac{G_T\, G_R \lambda^2 \sigma^{Tag} P_T}{(4\pi)^3 P_{min}}} \tag{87}$$

Where G_T and G_R are the gains of the transmitting and receiving horn antennas, P_T is the power transmitted by the VNA to measure the RCS, λ is the wavelength, P_{min} is the minimum power received by the receiving antenna and σ^{Tag} is the experimental value of RCS as obtained from Eq. (35). For maximum read range calculations the σ^{Tag} is obtained for 1111 bit pattern with the average RCS established as 0.002 m^2 and 0.0019 m^2 for the HC12-Tag and the LIB40-Tag, respectively. The read range is evaluated for -10, -3 and

0 dBm transmitted power from VNA for both designs and the maximum range results for 0 dBm power observed 1.94 m for the HC12-Tag and 1.85 m for the LIB40-Tag; see Table 17.

Table 17. Maximum Read Range Estimation for HC12-Tag and LIB40-Tag

Octagonal Tags	P_{min} (dB)	G_T (dBi)	G_R (dBi)	λ^2 (m)	σ^{Tag} Avg m^2 / dBsm	P_T (dB)	R (m)
HC12-Tag	-80	10	10	1.40×10^{-3}	0.002 / -26	-10	1.09
						-3	1.63
						0	1.94
LIB40-Tag	-80	10	10	1.24×10^{-3}	0.0019 / -27	-10	1.04
						-3	1.56
						0	1.85

5.7 Comparative Analysis with Existing Literature

Table 18, shows the comparative analysis of the proposed tag with existing embroidered Chipless RFID tags designs. The proposed chipless RFID designs with conductive fibres are robust and have a larger read range and, to the best of our knowledge, the bit density of 1.56 bits/cm^2 of this fully textile Embroidered Chipless RFID tag design is the highest achievable for the high frequency of 8-18 GHz.

Table 18. Comparative Analysis with Existing Textile Chipless RFID Tags

	[331]	[333]	[43] Ext. [40, 153]	This Work
	Polyester / Fibre	Nickel & Copper Coated Polyester / Flexible Reece	Non-Woven NWCF / Pile	1-Silver Coated Polyamide / Cotton & 2-Conductive Yarn Spun from LCP / Cotton
Area (mm^2)	88 × 17	25 × 20	40 × 40	25 × 25
No of Bits	3	8	8	4
Bit Density (bits/cm^2)	4.98	0.625	2	1.56
Freq(GHz)	3-6	2.5-6.5	1.8-3.2	8-18
σ (S/m)	3000	---	2.27×10^5	5000
Ave RCS (dBsm)	-32	-28	---	-27
On-Body R.R (cm)	20	---	---	18
Bending 'r' (mm)	---	---	---	7
R_{Max} (cm)	168	---	---	180

5.8 Discussion and Conclusion

In this chapter, an entirely-textile seamless octagonal embroidered design is proposed by the fabrication of two highly conductive threads HC12 and LIBERATOR 40 on cotton fabric. These threads are commercially available and relatively inexpensive. An SEM-based circuit modelling of the octagonal-shaped tag is presented and coupling coefficients are obtained by transient analysis. The maximum coupling coefficients for both of the designs obtained are -0.029 and -0.022, which are sufficiently low

values that assure reliable reading of the coded information. The behaviour of both tags is thoroughly studied and verified experimentally for different patterns of bitstreams measured in terms of RCS. Furthermore, the periodic octagonal design is selected to increase the read range of the tag up to 180 cm although up to 2.4 m can be achieved for a peak based codification. On-body RCS measurements are recorded 18 cm from the body with codes from both designs achieved accurately, although the LIB40-Tag design demonstrated more precision due to the very low resistivity of its thread with less than 3.25 Ω/m. Finally, several bending conditions experimentally verified the behaviour of the designs for which both tags were subjected to a maximum bend of 7 mm curvature where detectable RCS was obtained to verify bitstreams. Despite the encouraging results, additional research is still needed to reduce the mutual coupling evidenced between resonators and to further increase the tag's capacity.

5.9 Summary

This section offers an overview of this chapter. After providing a brief survey on wearable RFID tags and the importance of wearable chipless RFID sensors in general IoT, a seamless octagonal embroidered design is proposed through the fabrication of two highly conductive threads HC12 and LIBERATOR 40 on cotton fabric. Designed for the frequency range of 8-18 GHz, the first tag is designed using silver-coated polyamide conductive fibre (HC12) and the second tag with the highly conductive Vectran (LIBERATOR 40), a multifilament yarn spun from LCP, then embroidered on cotton fabrics. The threads are commercially available and relatively inexpensive. In contrast to the traditional RFID tag, the ID code is not saved in the memory of the chipless RFID tagging which instead uses the physical features of the tag to send data. These tags are designed with optimisation using CST studio and precisely fabricated by using commercial ZSK Technical Embroidery System JCZA (0109-550). Composed of six concentric octagonal loop resonators with one unitary element, the SEM-based circuit modelling for the octagonal-shaped tag is performed, with the behaviours of EM scattering waves and the coupling coefficients evaluated. The desired data bits are obtained through a series of comparative RCS experiments in an anechoic chamber. The experimental results obtained demonstrate that the 4-bit data is accurately retrieved with the variation of distance by up to 1.8 m at 0 dBm with an average transition from minimum '0' to maximum '1' of -27dB for both designs. Furthermore, the experiments recorded on-body RCS measurements and observed the bending effects on both tags down to 7 mm. This octagonal embroidered Chipless RFID tag is a fully textile design that is compact and can be deployed commercially in various IoT applications.

Chapter 6: **Conclusion and Outlook**

6.1 Summary Preamble

This chapter will form a summary of the author's contributions in analysing, designing, and fabricating wearable antennas and RFID tags using flexible polymer substrates, which are essential components for any wearable wireless communication system and presents an overview of the wearable chipless RFID tags based on flexible polymers and conductive fibres for general IoT applications. The dissertation is comprised of primary and secondary research elements in which the 'primary' research undertaken for this dissertation has been separated into three major research categories of investigation: polymer properties; flexible antennas and RFID tag design and fabrication; and conductive textile-based flexible tags for wearable applications. The purpose of studying the properties of polymer substrates is to encounter new ways of introducing flexibility into wearable or IoT applications for specific ranges of frequencies. The first element of this primary investigation is focused on analysing the various polymers which are in extensive use as flexible substrates for the FES and wearable applications. In this part, the flexibility of various polymer substrates has been analysed in terms of their physical, mechanical, electrical and thermal properties. The second component of this investigation emphasizes the designing, fabricating and testing of polymer-based flexible chipless RFID tags for wearable applications. In this part, a novel Bow Tie Chipless RFID tag is presented on a flexible polymer substrate and its bending capabilities are analysed. The third area of the primary research thesis investigation presents the conductive textile-based chipless RFID tags which are gaining extensive use these days because of their outstanding properties of extraordinary mechanical conformability, brilliant biocompatibility and wearability comfort. In this part, two fully textile wearable chipless RFID tags using conductive polymer-based threads are presented, and the impact of bending them at different levels is analysed. The secondary research objective of the study is to investigate the FES and the basic structure of the flexible antennas and RFID tags by using the transient response of the circuit models to find the coupling coefficients of the tags. This final chapter provides a conclusion for these three primary research investigations of the thesis, provides an overview of the results and conclusions from each focus point of the primary research study and provides possible future research suggestions, fruitful for wearable and IoT applications. The three primary research areas covered in this dissertation are discussed in Section 6.1.

6.1.1 Part 1: Analysis and selection of a suitable flexible polymer substrate and bending capabilities at a different range of frequencies

The first area of investigation includes the primary and secondary research incorporated in Chapters 2 and 3 which have focused on the most efficient and relevant polymer substrates in terms of bending and flexibility, which is a key challenge for flexible IoT and wearable applications and includes polymers such as PI, PET, PDMS, PTFE and LCP which cover more than 90% of the polymer-based flexible wearable industry. This part emphasized a detailed comparative analysis of the physical, electrical, thermal and chemical properties of the flexible polymer materials which have been used as substrates during the last

few decades to provide flexibility, which, in the process of appropriate substrate selection for flexible antennas, simultaneously serves as a beneficial guide to better match their compatibility with specific wearable applications. It also provided an analysis of the bending effects on radiation characteristics of the flexible polymers PET, PTFE Teflon, and PVC as substrates for antennas operating in three different frequency ranges: i) of 2.2-2.5 GHz, ii) 2.5-5GHz and iii) greater than 5 GHz.

6.1.1.1 **Original Contribution**

In this first part on substrate properties, based on the detailed analysis of the flexible polymer substrates presented in Chapter 2, nine microstrip patch antennas are designed and fabricated on the flexible PET, Teflon and PVC polymers, three of each operating at 2.45 GHz, 4.25 GHz, and 7.45 GHz frequencies, with each laying in one of the three frequencies ranges, and then analysed for the flexibility of each of the polymers. All the results are obtained in the Frankonia anechoic chamber to analyse the flexibility and bendability of the antennas.

In the first phase of designing, three antennas were designed and fabricated on PET, Teflon and PVC substrates operating at 2.45 GHz which is the common ISM band. The selection of the substrate materials was based on the analysis in Chapter 2. Initially, an E-shaped flexible microstrip patch antenna was designed on the PET substrate by simulating it on CST microwave studio and finding the radiation characteristics. Following the same steps, two more antennas were then designed and fabricated on Teflon and PVC polymers. The S_{11} parameters were obtained in the chamber for the bending stages of 27 mm and 14 mm and compared with the parameters in a flat condition. It was observed that for a bending state of 27 mm, the PET and PVC based flexible antennas possessed a less than 1% frequency shift towards the lowest components, whereas, the Teflon-based antenna showed 1.25% which is the highest percentage shift of frequency for the 27 mm bend state. At a 14 mm radial curvature, the PET substrate antenna gave the best performance with a 0.99% frequency deviation from the flat state. In terms of the impedance mismatch and the signal degradation, the PET substrate possessed the least degradation, demonstrating that PET can be classified as a good and very prospective candidate for the flexible wearable applications operating in the ISM band.

In the second phase of designing, three antennas were designed and fabricated on PET, Teflon and PVC substrates operating at 4.25 GHz which lies in C-band (4-8 GHz) and is suitable for WiMAX applications. For the bending capability test, the Teflon-based antenna possessed the least frequency deviation which was 0.25% and 1.61% for bending levels of 27 mm and 14 mm, respectively, whereas, the PET version, which was good for the 2.45 GHz frequency, showed a maximum shift of 3.49% at the 14 mm bending level. In terms of signal strength, Teflon as a substrate is the least impacted with only 14% signal strength reduction at 27 mm whereas, with the 14 mm bending, both PET and Teflon based antennas suffered more than 40% reduction in their signal strength and impedance mismatch. Therefore, it can be concluded that for operating frequencies of 4.25 GHz, in C-band, Teflon based wearable antennas are a good prospect for flexible wearable applications.

In the third phase of the designing, three more antennas were designed and fabricated on PET, Teflon

and PVC substrates operating at 7.45 GHz which also lie in C-band and is suitable for satellite communication. This part was the most complicated to deal with due to the small-sized antennas causing difficult TL connection with the microstrip feed line. For bending analysis, the results obtained demonstrate that the Teflon-based flexible antenna has almost no impact of bending at 27 mm and only a 0.29% shift towards the lowest components of the operating frequency at 14 mm, whereas, the PVC-based flexible antenna generates the most impact for the highest level of bend at 14 mm by giving 1.97%. In terms of the impedance mismatch at 14 mm bending, the PVC substrate antenna is determined to be efficient for this frequency range. Resultantly, it is conflictive to declare which substrate is best for this range, although impedance mismatch is more critical at higher frequencies as compared to the resonant frequency shift, and as such, PVC can be implicated as an acceptable flexible substrate operating at 7.45 GHz frequency.

6.1.1.2 **Future Work and Recommendations**

In this part of the study, the bending capabilities of various polymers used as substrates for wearable antennas were compared for the different range of frequencies. In this study the flexibility analysis is categorised for three frequency groups, the first group of 2.2-2.5 GHz is important for ISM applications, the second group of 2.5-5 GHz is perfect for Radars, Mobile Phones, and Commercial Wireless LAN applications and the third group of frequencies greater than 5 GHz is essential for 5G mobile communication. Understanding the fact that just a small change in operating frequency might impact the radiation characteristics in general and *S*-parameters and impedance mismatch in particular, the three groups of frequencies were selected. The first group (2.2-2.5 GHz) was small enough to see the impact of bending, however, the size of the second (2.5-5.0 GHz) and the third group (greater than 5 GHz) of frequency ranges could be narrowed to target more specific analysis of bending capabilities. Hence in future, the smaller sized frequency ranges or an increased number of groups with small bandwidths is a recommendation to investigate polymer substrate flexibility more accurately.

Based on the analysis of the polymer substrate antennas presented in Chapter 2, PI, PET, PDMS, PTFE and LCP are the five most abundant flexible polymer substrates selected for bending analysis and the practical implementation of PET, PTFE Teflon and PVC substrate were selected for flexibility testing. In the future, based on the comprehensive comparative analysis of the properties of polymers substrates presented in Chapter 2, some other polymers or some specific variants of these five polymers with comparable or mostly suitable physical, electrical, mechanical and thermal properties could be used to amplify the testing of materials for the bending capabilities of wearable antennas and RFID tags.

As the bending of flexible antennas highly impacts its *S*-parameters and impedance matching, which are crucial for receiving and transmitting the information, this first part of the study emphasizes these considerations by more specifically regarding the bending impacts on *S*-parameter impedance mismatch, and the signal degradation. The bending of flexible antennas, however, also has an impact on other parameters such as directivity, gain, radiation pattern and polarization and in future, the span of this study could be broadened to further consider the effects on these other parameters.

6.1.2 Part 2: Design Fabrication and Testing of Flexible Chipless RFID tags on Polymer Substrates

The second area of investigation includes the primary research incorporated in Chapter 4 to create a functional and versatile low-cost flexible antenna. Antennas, in the form of low-cost RFID tags on flexible polymer substrates, are the key enabler for item-level tracking and the identification towards IoT. The RFID tags based on polymer substrates can possess very enticing characteristics such as high flexibility, crumpling and stretchability, an ease of processability, being lightweight and having corrosion and humidity resistance which make the tags so favourable that they are in extensive use these days as wearable sensors and for general IoT applications. In this second part of the study, Octagonal and Bow Tie-shaped Chipless RFID tags were designed and fabricated on a flexible PET substrate to analyse the bending capabilities for various levels of bending. The novel Bow Tie Chipless tag was then further examined with designs using the PET, PFTE Teflon and PVC substrates to compare the RCS results in the chamber for bending levels of 27 mm and 24 mm.

6.1.2.1 **Original Contribution**

In this design and fabrication part of the thesis, two chipless RFID tags were designed and fabricated on the PET substrate using gold as the conductive material on the flexible substrate. Firstly, the existing design of an Octagonal Chipless RFID Tag was produced, and then the proposed novel flexible Bow Tie Chipless RFID tag was introduced and had its RCS and efficiency compared with the octagonal tag. As the traditional bow-tie structure provides the most intense surface current flows across the edges with a resonating elementary cell, as elaborated in Chapter 4, this shape was selected for the proposed design with a prospective of receiving code words better in terms of RCS. Comparative analysis of both tags determined the most obvious difference, that the Bow Tie Chipless RFID tag is approx. 50% smaller than the Octagonal RFID tag while both maintain a 4-bit capacity. The Bow Tie also registers a higher operating frequency, ranging from 8-18 GHz, as well as a 30% more transition of RCS in dBs from minimum (0) to maximum (1) states, making it easier to detect bits after being scattered through the tag [1].

In this part of the study, a circuit modelling of the 4-bit Bow Tie Chipless RFID tag was demonstrated to provide insight into the electromagnetic response of the circuit when an incident EM wave strikes at the tag. For this purpose, SEM was used whereby the current induced on the tag is expanded in terms of the singularity poles of the tag and the coupling coefficients R_n for the bow tie-shaped resonators. This is the first time in the research literature that the SEM has been used to evaluate the coupling coefficients of bow tie-shaped resonators. Although the spacing between the resonators of the tag is not constant, such that the R_n value keeps changing with the variation of the spacing, the maximum value of R_n observed was -0.021, which is a sufficiently low value that assures reliable reading of the coded information. The formation of bits by stubbing or shorting the resonators, the impact of incident wave angles (θ, φ) and the impact of the tilt angles (α) on the RCS of the Bow Tie Chipless RFID tag are demonstrated and with the maximum read range evaluated, the Bow Tie RFID tag has proven itself to be more robust and accurate with the variation of distance up to 1.8 m at 0 dBm which is extendable to 2.14 m for higher input power [3].

To corroborate the bending effects of radiation from different polymer substrates, the Bow Tie Chipless RFID tag was designed and fabricated on PET, Teflon and PVC substrates of thicknesses 70 µm, 100 µm and 110 µm respectively, and operating at 8-18 GHz. The measurements of the RCS were obtained for tags in a Horizontal *H* position in the anechoic chamber for the bending states of 27 mm and 14 mm where the performances of the bent tags were affected by modifying the curvature radii. The distance of the tag from the two identical horn antennas was maintained at 12 cm with 0 dBm power, so that an expected signal degradation would be observed over the bend. At 27 mm bending, for the lower range of the frequency 8-14 GHz, the PET-based and Teflon-based substrate RFID tags provide a 4-6% frequency shift from the resonant frequency at flat conditions and more than 10% with a higher range up to 18 GHz. However, the PVC based RFID tag demonstrates the least frequency shift with less than 2% and even less signal degradation for all ranges of frequencies from 8-18 GHz at the highest bend level with 14 mm. This result matches the analysis of the PVC substrate with flexible antennas operating at 7.45 GHz signifying that at the high frequencies, PVC is a good candidate for wearable devices such as chipless RFID tags and flexible antennas [2].

6.1.2.2 **Future Work and Recommendations**

In this part of the thesis, a 4-bit Bow Tie-shaped Chipless RFID tag was designed and fabricated using the FSS technique to encode data in the frequency signature of the RCS. The asymmetric property of the tag to change its polarization could be used to increase the bit capacity of the tag in future. For example, an array of 2×2 Bow Tie-shaped Chipless RFID tags on flexible polymers positioned at specific distances would attain the higher 16-bit of data. For testing purposes, gold was used for being an excellent conductor, but, for more cost-effectiveness, copper would be a preferable option for use in the future. The resultant tag is robust and successfully encoded in terms of RCS at a distance of 1.8 m for 0 dBm power from the source. The read range could be increased to 3 m by increasing the input power up to the safe value of 10 dBm with a read range maximum up to a high range of frequency 8-18 GHz.

The coupling coefficient was measured for the flat status of the bow tie-shaped 4-bit tag understanding that the bending of the tag would change the distance between the resonators and hence the corresponding inductances and the capacitances would also change. This, in turn, would cause changes in the coupling coefficients of the tags to a higher value for which the information would not be accurately read. So, another way to describe the impact of bending on flexible RFID tags is to analyse the coupling coefficient in a bent state. Therefore, in future, a bent state circuit modelling of the tag could give a better understanding of the impact of bending on the coupling coefficients of the resonators of the chipless RFID tag.

This Bow Tie Chipless RFID tag, utilised PET, PTFE Teflon and PVC substrates for the purposes of obtaining desired flexibility. In future, some other polymers with comparable or suitable physical, electrical, mechanical and thermal properties could be tested to expound further bending capabilities and applications for these wearable chipless RFID tags.

6.1.3 Design Fabrication and Testing of Fully-Textile Chipless RFID tag using Conductive Polymer Threads on Fabrics

The third area of investigation includes the primary research incorporated in Chapter 6 to develop wearable flexible devices imbedded in textile materials. In this investigation of the changing properties of textiles was a promising approach to develop wearable flexible devices. With the dielectric polymers merged with conductive material to produce a composite compound known as conductive polymers, the investigated wearable embroidery RFID tag has many advantages since it can be embedded into a fabric rather than simply being attached to the piece of cloth. In this third part of the dissertation, two octagonal-shaped Chipless RFID tags were designed and embroidered by using conductive threads coated with a conductive polymer into the cotton fabric. The octagonal-shaped tags are composed of six concentric elements which are designed using CST studio and precisely fabricated using the commercial ZSK Technical Embroidery System JCZA (0109-550). The SEM-based circuit modelling and the transient behaviour of the octagonal-shaped tag enabled an evaluation of the coupling coefficients of the octagonal rings. Then, an on-body RCS analysis and the bending impacts on the RCS at bending levels of 27 mm, 14 mm and 7 mm was performed in the chamber before evaluating the maximum read range.

6.1.3.1 **Original Contribution**

This third part of the study was completed in three phases. In the first phase, the electromagnetic behaviour of the 4-bit octagonal-shaped RFID tag was visualized using the SEM-based analysis, when an incident EM wave strikes at the tag and the induced current re-radiates into the scattered fields. The evaluation of the results resolved as a collection of poles S_n, a coupling coefficient R_n and the entire function F_e in the complex frequency domain. To the best of the author's knowledge, this is the very first time that SEM-based circuit modelling has been performed on the octagonal concentric rings of RFID tags to evaluate the coupling coefficients for the optimised octagonal designs [6].

In the second phase of this part of the investigation, two octagonal-shaped flexible chipless RFID tags were designed and fabricated on a plain cotton substrate. The conductivity of the sewing pattern is mainly affected by the orientation of the tag and density of the stitches of thread per surface unit. To attain maximum conductivity, the octagonal geometrical shape was selected and all the resonators were concentrically aligned. Firstly, the Octagonal Chipless RFID Tag was designed by embroidering a polyamide fully silver-coated HC12 conductive thread on a plain cotton substrate operating at the 8-18 GHz frequency. Secondly, a similar-shaped Octagonal RFID tag was designed using Liberator 40, a highly conductive silver-coated polymer thread on cotton fabric operating at 8-18 GHz. The polymer in the core of this Liberator, or Vectran™ by Kuraway, is a high-performance multifilament yarn spun from LCP. With both of these threads being highly conductive, skin-friendly, comfortable, biocompatible and washable, they are deemed ideal for wearable applications and have been employed here, for the very first time, on the RFID tag application [5].

In the final phase of this part, the desired data bits are obtained for both RFID tags by a series of comparative experiments for RCS in an anechoic chamber. The maximum coupling coefficients obtained for both of the designs were -0.029 and -0.022, which are sufficiently low values that assure reliable reading

of the coded information. The behaviour of both tags was thoroughly investigated and experimentally verified for different patterns of bit words measured in terms of RCS with the obtained results demonstrating that the 4-bit data is accurately retrieved with the variation of distance by up to 1.8 m at 0 dBm. The on-body response of RCS is well correlated with the response of the free space measurement of the tags in the chamber. The on-body RCS measurements observed very distorted results, which even faded when the distance of the tags from the source antennas increased from 18 cm. A shift of resonant frequencies were observed between the ranges of 5% to 30% for both of the designs if the distance is increased from 18 cm to 60 cm. The read range was evaluated for -10 dBm, -3 dBm and 0 dBm transmitted power from VNA and the maximum range observed 1.94 m for the HC12-Tag and 1.85 m for the LIB40-Tag for 0 dBm power. Hence it is concluded that both of the designs are well suited for wearable applications [4].

To substantiate the behavioural effects on the RCS read by bending, a series of experiments were performed on both of the RFID designs to validate their capability after being bent with various radius of curvatures. For this, single octagonal embroidered tags for each design with a maximum bit codes of 1111 was chosen and all experiments were taken into the anechoic chamber to reduce the impact of external RF interferences. This bending analysis was performed for the radius of 27 mm, 14 mm and 7 mm and compared to the RCS results of the tags with flat conditions. The EM waves were transmitted at 0 dBm from a distance of 100 cm. Despite the noticeable shift in resonant frequency and the signal degradation as compared to the reading of the non-bent reference tag, the |RCS| peaks were significantly retrievable. Hence, a successful bending analysis on both designs has proven their reliability in terms of bending for the various stages of curvature [5].

A comparative analysis of the proposed tag was performed against existing embroidered chipless RFID tags designs. These embroidered chipless RFID tag designs are fully textile with a bit density of 1.56 bits/cm^2. To the best of our knowledge, it is the highest achievable bit density for such a high frequency of 8-18 GHz. The proposed chipless RFID designs with conductive fibres are robust, have a larger read range, and are compatible with any wearable or general IoT application.

6.1.3.2 Future Work and Recommendations

This section provides insight into the enhancement and future modification of the embroidered Octagonal Chipless RFID tags. In the last phase of this part of the study, the two 4-bit Octagonal-shaped Chipless RFID tags were embroidered onto cotton fabric using conductive fibre, operating at 8-18 GHz frequency range, and tested for bending capabilities. The bit storing capacity of the tag, while currently 4 bits, could be increased to 16 bits by implanting an array of these tags. For example, following the optimization techniques discussed in section 5.3.2, a grouping of four octagonal-shaped tags could be embroidered on a cotton cloth of 50 cm × 50 cm.

Figure 92 depicts the 2×2 array of Octagonal Chipless RFID tags which could be fabricated on a cotton substrate to get 16 bits of coded information. To attain a seamless integration of the tag with fabrics, the conductivity of the conductive polymer thread is very important for the embroidered chipless RFID tags. Therefore, to obtain even better results and to retrieve bits more accurately in terms of RCS, conductive

threads with higher conductivity are suggested for future wearable applications.

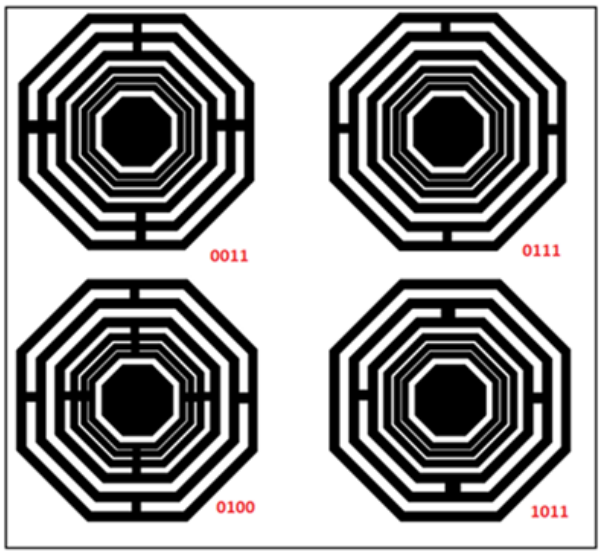

Figure 92. Array of 16-bit, 2×2 Octagonal Chipless RFID Tags

6.2 Concluding Statement

The research presented in this thesis gives emphasis to the investigation of flexible polymer substrates, the design and the fabrication of flexible polymer-substrate wearable devices such as flexible antennas and smart tags for wearable or general IoT applications. Flexible polymer substrates such as PI, PET, PDMS, PTFE, LCP and polymers coated in conductive fibres are investigated. One of the principle objectives of this study determined to investigate the capability of the wearable devices to flex and function properly under bending conditions. For this purpose, radiation characteristics such as return loss of polymer-based substrate antennas and the RCS of flexible polymer-based chipless RFID for various ranges of frequencies are analysed. A variety of flexible polymer substrate antennas and chipless RFID tags are designed and fabricated using PET, PTFE Teflon and PVC as substrates and comprehensive bending analysis has been performed and presented. These designs include a novel Bow Tie Chipless RFID on a PET substrate and two Embroidered Octagonal-shaped Chipless RFID tags by using different conductive threads, HC12 and LIBERATOR 40, on cotton fabrics. The promising results achieved in this comprehensive investigation which presents the implications of experiments on polymer-based substrate wearable devices, illustrates that these devices are robust, small in size, low-cost, washable and most importantly highly flexible. Hence, a comprehensive study with the implication of the experiments on polymer-based substrate flexible wearable device has been presented. There are indeed great prospects for continued development and device production in the direction this investigation has instigated for wearable flexible devices which are simultaneously applicable to general IoT applications.

References

[1] M. U. A. Khan, R. Raad, J. Foroughi, F. E. Tubbal, and J. Xi, "Novel Bow-Tie Chip-less RFID Tag for Wearable Applications," in *2019 19th International Symposium on Communications and Information Technologies (ISCIT)*, 2019: IEEE, pp. 10-13.

[2] M. U. A. Khan, R. Raad, J. Foroughi, F. Tubbal, P. I. Theoharis, and M. S. Raheel, "Effects of Bending Bow-Tie Chipless RFID Tag for Different Polymer Substrates," in *2019 13th International Conference on Signal Processing and Communication Systems (ICSPCS)*, 2019: IEEE, pp. 1-4.

[3] M. U. A. Khan, R. Raad, and J. Foroughi, "Transient Response & Electromagnetic Behaviour of Flexible Bow-Tie Shaped Chip-less RFID Tag for General IoT Applications," *Adv. Sci. Technol. Eng. Syst. J,* vol. 5, pp. 757-764, 2020.

[4] M. U. A. Khan, R. Raad, J. Foroughi, P. I. Theoharis, S. Liu, and J. Masud, "A Silver-Coated Conductive Fibre HC12 Sewed Chipless RFID Tag on Cotton Fabric for Wearable Applications," in *2020 IEEE 23rd International Multitopic Conference (INMIC)*, 2020: IEEE, pp. 1-5.

[5] M. U. A. Khan, R. Raad, and J. Foroughi, "A Fibre Embroidered Chipless RFID Tag on Cotton Fabrics for Wearable Applications," in *GLOBECOM 2020-2020 IEEE Global Communications Conference*, 2020: IEEE, pp. 1-6.

[6] M. U. A. Khan, R. Raad, J. Foroughi, M. S. Raheel, and S. Houshyar, "An octagonal-shaped conductive HC12 & LIBERATOR-40 thread embroidered chipless RFID for general IoT applications," *Sensors and Actuators A: Physical,* vol. 318, p. 112485, 2021.

[7] M. U. Ali Khan, R. Raad, F. Tubbal, P. I. Theoharis, S. Liu, and J. Foroughi, "Bending Analysis of Polymer-Based Flexible Antennas for Wearable, General IoT Applications: A Review," *Polymers,* vol. 13, no. 3, p. 357, 2021.

[8] F. Tubbal, R. Raad, P. I. Theoharis, S. Iranmanesh, S. Abulgase, and M. U. A. Khan, "Dual Band Slot Antenna with F-Shaped Slits for C-band and X-band Applications," in *2019 13th International Conference on Signal Processing and Communication Systems (ICSPCS)*, 2019: IEEE, pp. 1-4.

[9] S. Liu, R. Raad, P. I. Theoharis, F. Tubbal, M. U. A. Khan, and F. H. Malik, "A Dual Band Loop Antenna with Metal Frame for CubeSat Communication," in *2020 IEEE 23rd International Multitopic Conference (INMIC)*, 2020: IEEE, pp. 1-4.

[10] P. I. Theoharis, R. Raad, F. Tubbal, M. U. A. Khan, and S. Liu, "Software Defined Radios for CubeSat Applications: A Brief Review and Methodology," *IEEE Journal on Miniaturization for Air and Space Systems,* 2020.

[11] S. Abulgasem, F. Tubbal, R. Raad, P. I. Theoharis, S. Liu, and M. U. Ali Khan, "A Wideband Metal-Only Patch Antenna for CubeSat," *Electronics,* vol. 10, no. 1, p. 50, 2021.

[12] R. N. Region. "Flexible Electronics Market : Global Demand Analysis & Opportunity Outlook 2024." https://www.researchnester.com/reports/flexible-electronics-market-global-demand-analysis-opportunity-outlook-2024/270?utm_source=Market-Watch&utm_medium=DIG (accessed : 02-01-2020).

[13] J. Hu, "Overview of flexible electronics from ITRI's viewpoint," in *2010 28th VLSI Test Symposium (VTS)*, 2010: IEEE, pp. 84-84.

[14] C. P. Lin, C. H. Chang, Y. T. Cheng, and C. F. Jou, "Development of a flexible SU-8/PDMS-based antenna," (in English), *IEEE Antennas and Wireless Propagation Letters,* Article vol. 10, pp. 1108-1111, 2011, Art no. 6032064, doi: 10.1109/LAWP.2011.2170398.

[15] Y. Sun and J. A. Rogers, "Inorganic semiconductors for flexible electronics," *Advanced materials,* vol.

19, no. 15, pp. 1897-1916, 2007.

[16] S. Ahmed, F. A. Tahir, A. Shamim, and H. M. Cheema, "A Compact Kapton-Based Inkjet-Printed Multiband Antenna for Flexible Wireless Devices," *IEEE Antennas and Wireless Propagation Letters,* Article vol. 14, pp. 1802-1805, 2015, Art no. 7089213, doi: 10.1109/LAWP.2015.2424681.

[17] D. Giusto, "A. lera, G. Morabito, l. Atzori (Eds.) The Internet of Things," ed: Springer, 2010.

[18] P. S. Hall and Y. Hao, *Antennas and propagation for body-centric wireless communications*. Artech house, 2012.

[19] K. Finkenzeller and R. Handbook, "New York (NY)," ed: John Wiley & Sons, 2010.

[20] A. S. M. Sayem, R. B. Simorangkir, K. P. Esselle, and R. M. Hashmi, "Development of Robust Transparent Conformal Antennas Based on Conductive Mesh-Polymer Composite for Unobtrusive Wearable Applications," *IEEE Transactions on Antennas and Propagation,* vol. 67, no. 12, pp. 7216-7224, 2019.

[21] Z. Hamouda *et al.*, "Dual-band elliptical planar conductive polymer antenna printed on a flexible substrate," (in English), *IEEE Transactions on Antennas and Propagation,* Article vol. 63, no. 12, pp. 5864-5867, 2015, Art no. 7271007, doi: 10.1109/TAP.2015.2479643.

[22] N. J. Kirsch, N. A. Vacirca, E. E. Plowman, T. P. Kurzweg, A. K. Fontecchio, and K. R. Dandekar, "Optically transparent conductive polymer RFID meandering dipole antenna," in *RFID, 2009 IEEE International Conference on*, 2009: IEEE, pp. 278-282.

[23] P. Salonen, Y. Rahmat-Samii, H. Hurme, and M. Kivikoski, "Effect of conductive material on wearable antenna performance: A case study of WLAN antennas," in *IEEE Antennas and Propagation Society Symposium, 2004.*, 2004, vol. 1: IEEE, pp. 455-458.

[24] A. Verma *et al.*, "6 GHz microstrip patch antennas with PEDOT and polypyrrole conducting polymers," in *2010 International Conference on Electromagnetics in Advanced Applications*, 2010: IEEE, pp. 329-332.

[25] T. Kaufmann, A. Verma, V.-T. Truong, B. Weng, R. Shepherd, and C. Fumeaux, "Efficiency of a compact elliptical planar ultra-wideband antenna based on conductive polymers," *International Journal of Antennas and Propagation,* vol. 2012, 2012.

[26] S. J. Chen *et al.*, "A compact, highly efficient and flexible polymer ultra-wideband antenna," *IEEE Antennas and Wireless Propagation Letters,* vol. 14, pp. 1207-1210, 2015.

[27] A. Tsolis, W. G. Whittow, A. A. Alexandridis, and J. Vardaxoglou, "Embroidery and related manufacturing techniques for wearable antennas: challenges and opportunities," *Electronics,* vol. 3, no. 2, pp. 314-338, 2014.

[28] X. Huang *et al.*, "Binder-free highly conductive graphene laminate for low cost printed radio frequency applications," *Applied Physics Letters,* vol. 106, no. 20, p. 203105, 2015.

[29] M. Akbari, M. W. A. Khan, M. Hasani, T. Björninen, L. Sydänheimo, and L. Ukkonen, "Fabrication and characterization of graphene antenna for low-cost and environmentally friendly RFID tags," *IEEE Antennas and Wireless Propagation Letters,* vol. 15, pp. 1569-1572, 2015.

[30] L. Corchia, G. Monti, and L. Tarricone, "Durability of wearable antennas based on nonwoven conductive fabrics: Experimental study on resistance to washing and ironing," *International Journal of Antennas and Propagation,* vol. 2018, 2018.

[31] Z. Wang, L. Zhang, Y. Bayram, and J. L. Volakis, "Embroidered conductive fibers on polymer composite for conformal antennas," *IEEE Transactions on Antennas and Propagation,* vol. 60, no. 9, pp. 4141-4147, 2012.

[32] I. Locher and G. Troster, "Fundamental building blocks for circuits on textiles," *IEEE Transactions on advanced packaging,* vol. 30, no. 3, pp. 541-550, 2007.

[33] K. Koski, A. Vena, L. Sydänheimo, L. Ukkonen, and Y. Rahmat-Samii, "Design and implementation of electro-textile ground planes for wearable UHF RFID patch tag antennas," *IEEE Antennas and Wireless Propagation Letters,* vol. 12, pp. 964-967, 2013.

[34] C. Hertleer, A. Tronquo, H. Rogier, L. Vallozzi, and L. Van Langenhove, "Aperture-coupled patch antenna for integration into wearable textile systems," *IEEE antennas and wireless propagation letters,* vol. 6, pp. 392-395, 2007.

[35] L. Zhang, Z. Wang, and J. L. Volakis, "Textile antennas and sensors for body-worn applications," *IEEE Antennas and Wireless Propagation Letters,* vol. 11, pp. 1690-1693, 2012.

[36] C. Hertleer, H. Rogier, L. Vallozzi, and L. Van Langenhove, "A textile antenna for off-body communication integrated into protective clothing for firefighters," *IEEE Transactions on Antennas and Propagation,* vol. 57, no. 4, pp. 919-925, 2009.

[37] E. K. Kaivanto, M. Berg, E. Salonen, and P. De Maagt, "Wearable circularly polarized antenna for personal satellite communication and navigation," *IEEE Transactions on Antennas and Propagation,* vol. 59, no. 12, pp. 4490-4496, 2011.

[38] P. B. Samal, P. J. Soh, and G. A. Vandenbosch, "UWB all-textile antenna with full ground plane for off-body WBAN communications," *IEEE transactions on antennas and propagation,* vol. 62, no. 1, pp. 102-108, 2013.

[39] T. Kaufmann and C. Fumeaux, "Wearable textile half-mode substrate-integrated cavity antenna using embroidered vias," *IEEE Antennas and Wireless Propagation Letters,* vol. 12, pp. 805-808, 2013.

[40] L. Corchia *et al.*, "Fully-Textile, Wearable Chipless Tags for Identification and Tracking Applications," *Sensors,* vol. 20, no. 2, p. 429, 2020.

[41] F. Mokhtari *et al.*, "Wearable Electronic Textiles from Nanostructured Piezoelectric Fibers," *Advanced Materials Technologies,* vol. 5, no. 4, p. 1900900, 2020.

[42] F. Mokhtari, Z. Cheng, R. Raad, J. Xi, and J. Foroughi, "Piezofibers to smart textiles: a review on recent advances and future outlook for wearable technology," *Journal of Materials Chemistry A,* vol. 8, no. 19, pp. 9496-9522, 2020.

[43] L. Corchia *et al.*, "Radio-frequency Identification Based on Textile, Wearable, Chipless Tags for IoT Applications," in *2019 II Workshop on Metrology for Industry 4.0 and IoT (MetroInd4. 0&IoT)*, 2019: IEEE, pp. 1-5.

[44] S. Agneessens and H. Rogier, "Compact half diamond dual-band textile HMSIW on-body antenna," *IEEE Transactions on Antennas and Propagation,* vol. 62, no. 5, pp. 2374-2381, 2014.

[45] H. R. Khaleel, H. M. Al-Rizzo, and D. G. Rucker, "Compact polyimide-based antennas for flexible displays," *Journal of Display Technology,* vol. 8, no. 2, pp. 91-97, 2012.

[46] A. Constant *et al.*, "Development of thin film transistor based circuits on flexible polyimide substrates," in *Electrochem Soc Proc*, 1995, pp. 94-35.

[47] H. R. Khaleel, H. M. Al-Rizzo, D. G. Rucker, and S. Mohan, "A compact polyimide-based UWB antenna for flexible electronics," *IEEE Antennas and Wireless Propagation Letters,* vol. 11, pp. 564-567, 2012.

[48] S. Morris, A. R. Chandran, N. Timmons, and J. Morrison, "The fabrication and analysis of a polyimide based loop antenna for 2.45GHz WBAN applications," in *2016 Loughborough Antennas and Propagation Conference, LAPC 2016*, 2017, doi: 10.1109/LAPC.2016.7807510. [Online]. Available:

https://www.scopus.com/inward/record.uri?eid=2-s2.0-85014104267&doi=10.1109%2fLAPC.2016.7807510&partnerID=40&md5=f04422f58db706d839d9b447ad3c34d0 (accessed : 05-01-2020).

[49] S. Hong, Y. Kim, C. Lee, and C. W. Jung, "A flexible and transparent antenna on a polyimide substrate for laptop computers," in *Antennas and Propagation & USNC/URSI National Radio Science Meeting, 2015 IEEE International Symposium on*, 2015: IEEE, pp. 930-931.

[50] S. Beer, H. Gulan, C. Rusch, and T. Zwick, "Integrated 122-GHz antenna on a flexible polyimide substrate with flip chip interconnect," *IEEE Transactions on Antennas and Propagation,* vol. 61, no. 4, pp. 1564-1572, 2013.

[51] Y. Qiu *et al.*, "Compact parylene-c-coated flexible antenna for WLAN and upper-band UWB applications," (in English), *Electronics Letters,* Article vol. 50, no. 24, pp. 1782-1784, 2014, doi: 10.1049/el.2014.3647.

[52] H. R. Khaleel, "Design and fabrication of compact inkjet printed antennas for integration within flexible and wearable electronics," *IEEE transactions on components, packaging and manufacturing technology,* vol. 4, no. 10, pp. 1722-1728, 2014.

[53] J. Jung, H. Lee, and Y. Lim, "Broadband flexible comb-shaped monopole antenna," *IET microwaves, antennas & propagation,* vol. 3, no. 2, pp. 325-332, 2009.

[54] M. Boehme and C. Charton, "Properties of ITO on PET film in dependence on the coating conditions and thermal processing," *Surface and Coatings technology,* vol. 200, no. 1-4, pp. 932-935, 2005.

[55] H. K. Yoon, J. A. Park, Y. J. Yoon, and C.-H. Lee, "A CPW-fed polarization diversity antenna for UWB systems," in *Antennas and Propagation Society International Symposium, 2008. AP-S 2008. IEEE*, 2008: IEEE, pp. 1-4.

[56] D. Betancourt, K. Haase, A. Hübler, and F. Ellinger, "Bending and folding effect study of flexible fully printed and late-stage codified octagonal chipless RFID tags," *IEEE Transactions on Antennas and Propagation,* vol. 64, no. 7, pp. 2815-2823, 2016.

[57] A. T. Castro and S. K. Sharma, "Inkjet-Printed Wideband Circularly Polarized Microstrip Patch Array Antenna on a PET Film Flexible Substrate Material," *IEEE Antennas and Wireless Propagation Letters,* vol. 17, no. 1, pp. 176-179, 2018.

[58] R. Moro, M. Bozzi, A. Collado, A. Georgiadis, and S. Via, "Plastic-based substrate integrated waveguide (SIW) components and antennas," in *2012 42nd European Microwave Conference*, 2012: IEEE, pp. 1007-1010.

[59] S. M. Saeed, C. A. Balanis, and C. R. Birtcher, "Radiation characteristics of flexible reconfigurable antenna with curved cylindrical configurations," in *2016 IEEE International Symposium on Antennas and Propagation (APSURSI)*, 2016: IEEE, pp. 1433-1434.

[60] T. Kaufmann, D. C. Ranasinghe, M. Zhou, and C. Fumeaux, "Wearable quarter-wave folded microstrip antenna for passive UHF RFID applications," *International Journal of Antennas and Propagation,* vol. 2013, 2013.

[61] J. H. So, J. Thelen, A. Qusba, G. J. Hayes, G. Lazzi, and M. D. Dickey, "Reversibly deformable and mechanically tunable fluidic antennas," *Advanced Functional Materials,* vol. 19, no. 22, pp. 3632-3637, 2009.

[62] S. Cheng and Z. Wu, "A Microfluidic, Reversibly Stretchable, Large-Area Wireless Strain Sensor," *Advanced Functional Materials,* vol. 21, no. 12, pp. 2282-2290, 2011.

[63] M. Kubo *et al.*, "Stretchable microfluidic radiofrequency antennas," *Advanced materials,* vol. 22, no. 25, pp. 2749-2752, 2010.

[64] S. Hage-Ali *et al.*, "A millimeter-wave microstrip antenna array on ultra-flexible micromachined polydimethylsiloxane (PDMS) polymer," *IEEE Antennas and Wireless Propagation Letters,* vol. 8, pp. 1306-1309, 2009.

[65] S. Koulouridis, G. Kiziltas, Y. Zhou, D. J. Hansford, and J. L. Volakis, "Polymer–ceramic composites for microwave applications: fabrication and performance assessment," *IEEE Transactions on Microwave Theory and Techniques,* vol. 54, no. 12, pp. 4202-4208, 2006.

[66] M. L. Scarpello *et al.*, "Design of an implantable slot dipole conformal flexible antenna for biomedical applications," *IEEE Transactions on Antennas and Propagation,* vol. 59, no. 10, pp. 3556-3564, 2011.

[67] S. Cheng, A. Rydberg, K. Hjort, and Z. Wu, "Liquid metal stretchable unbalanced loop antenna," *Applied Physics Letters,* vol. 94, no. 14, p. 144103, 2009.

[68] G. J. Hayes, J.-H. So, A. Qusba, M. D. Dickey, and G. Lazzi, "Flexible liquid metal alloy (EGaIn) microstrip patch antenna," *IEEE Transactions on Antennas and Propagation,* vol. 60, no. 5, pp. 2151-2156, 2012.

[69] R. B. Simorangkir, Y. Yang, L. Matekovits, and K. P. Esselle, "Dual-band dual-mode textile antenna on PDMS substrate for body-centric communications," *IEEE Antennas and Wireless Propagation Letters,* vol. 16, pp. 677-680, 2016.

[70] M. Komeya and H. Shimasaki, "Studies on a cavity-backed slot antenna made of a conductive textile bent along a spherical surface," in *Electromagnetic Theory (EMTS), Proceedings of 2013 URSI International Symposium on*, 2013: IEEE, pp. 561-564.

[71] K. Fujiwara, H. Shimasaki, K. Morimoto, and N. Kuwahara, "Studies on a polyester fabric substrate of the feed line to a flexible slot antenna," in *Microwave Conference (APMC), 2014 Asia-Pacific*, 2014: IEEE, pp. 456-458.

[72] M. Sallam, S. Kandil, G. Vandenbosch, and E. Soliman, "Wideband CPW-fed Flexible Bow-tie Slot Antenna for WLAN/WiMax Systems," *IEEE Transactions on Antennas and Propagation,* 2017.

[73] A. C. Durgun, C. A. Balanis, C. R. Birtcher, and D. R. Allee, "Design, simulation, fabrication and testing of flexible bow-tie antennas," *IEEE Transactions on Antennas and Propagation,* vol. 59, no. 12, pp. 4425-4435, 2011.

[74] H.-L. Kao *et al.*, "Bending effect of an inkjet-printed series-fed two-dipole antenna on a liquid crystal polymer substrate," *IEEE Antennas and Wireless Propagation Letters,* vol. 13, pp. 1172-1175, 2014.

[75] J. Ni and J. Hong, "Compact varactor-tuned microstrip high-pass filter with a quasi-elliptic function response," *IEEE Transactions on Microwave Theory and Techniques,* vol. 61, no. 11, pp. 3853-3859, 2013.

[76] A. Rida, A. Margomeno, J. S. Lee, P. Schmalenberg, S. Nikolaou, and M. M. Tentzeris, "Integrated wideband 2-D and 3-D transitions for millimeter-wave RF front-ends," *IEEE Antennas and Wireless Propagation Letters,* vol. 9, pp. 1080-1083, 2010.

[77] A. Rida, S. Nikolaou, and M. M. Tentzeris, "Broadband UHF RFID/sensor modules for pervasive cognition applications," in *Antennas and Propagation, 2009. EuCAP 2009. 3rd European Conference on*, 2009: IEEE, pp. 2344-2347.

[78] D. L. Paul, L. Zhang, and L. Zheng, "Flexible dual-band LCP antenna for RFID applications," in *Electromagnetic Theory (EMTS), Proceedings of 2013 URSI International Symposium on*, 2013: IEEE, pp. 973-976.

[79] M. Venkateswara Rao, B. T. P. Madhav, T. Anilkumar, and B. Prudhvinadh, "Circularly polarized flexible antenna on liquid crystal polymer substrate material with metamaterial loading," *Microwave and Optical Technology Letters,* 2020.

[80] M. V. Rao, B. T. P. Madhav, T. Anilkumar, and B. Prudhvinadh, "Circularly polarized flexible antenna on liquid crystal polymer substrate material with metamaterial loading," *MICROWAVE AND OPTICAL TECHNOLOGY LETTERS,* 2019.

[81] G. DeJean, R. Bairavasubramanian, D. Thompson, G. Ponchak, M. Tentzeris, and J. Papapolymerou, "Liquid crystal polymer (LCP): A new organic material for the development of multilayer dual-frequency/dual-polarization flexible antenna arrays," *IEEE Antennas and Wireless Propagation Letters,* vol. 4, pp. 22-26, 2005.

[82] R. Vyas, A. Rida, S. Bhattacharya, and M. M. Tentzeris, "Liquid Crystal Polymer (LCP): The ultimate solution for low-cost RF flexible electronics and antennas," in *2007 IEEE Antennas and Propagation Society International Symposium*, 2007: IEEE, pp. 1729-1732.

[83] M. H. Sagor, Q. H. Abbasi, A. Alomainy, and Y. Hao, "Compact and conformal ultra wideband antenna for wearable applications," in *Proceedings of the 5th European Conference on Antennas and Propagation (EUCAP)*, 2011: IEEE, pp. 2095-2098.

[84] Y. Leterrier, "Mechanics of curvature and strain in flexible organic electronic devices," *Handbook of Flexible Organic Electronics: Materials, Manufacturing and Applications,* p. 1, 2014.

[85] N. L. Pira, "Smart integrated systems and circuits using flexible organic electronics: Automotive applications," *Handbook of Flexible Organic Electronics: Materials, Manufacturing and Applications,* p. 345, 2014.

[86] D. Evans, "The internet of things: How the next evolution of the internet is changing everything," *CISCO white paper,* vol. 1, no. 2011, pp. 1-11, 2011.

[87] E. Welbourne *et al.*, "Building the internet of things using RFID: the RFID ecosystem experience," *IEEE Internet computing,* vol. 13, no. 3, pp. 48-55, 2009.

[88] W. Zhou and S. Piramuthu, "Security/privacy of wearable fitness tracking IoT devices," in *2014 9th Iberian Conference on Information Systems and Technologies (CISTI)*, 2014: IEEE, pp. 1-5.

[89] L. Yan, Y. Zhang, L. T. Yang, and H. Ning, *The Internet of things: from RFID to the next-generation pervasive networked systems*. Crc Press, 2008.

[90] A. Bassi and G. Horn, "Internet of Things in 2020: A Roadmap for the Future," *European Commission: Information Society and Media,* vol. 22, pp. 97-114, 2008.

[91] M. Younan, E. H. Houssein, M. Elhoseny, and A. A. Ali, "Challenges and recommended technologies for the industrial internet of things: A comprehensive review," *Measurement,* vol. 151, p. 107198, 2020.

[92] J. N. Al-Karaki and A. E. Kamal, "Routing techniques in wireless sensor networks: a survey," *IEEE wireless communications,* vol. 11, no. 6, pp. 6-28, 2004.

[93] A. Al-Fuqaha, M. Guizani, M. Mohammadi, M. Aledhari, and M. Ayyash, "Internet of things: A survey on enabling technologies, protocols, and applications," *IEEE Communications Surveys & Tutorials,* vol. 17, no. 4, pp. 2347-2376, 2015.

[94] K. Aziz, S. Tarapiah, S. H. Ismail, and S. Atalla, "Smart real-time healthcare monitoring and tracking system using GSM/GPS technologies," in *2016 3rd MEC International Conference on Big Data and Smart City (ICBDSC)*, 2016: IEEE, pp. 1-7.

[95] G. Appelboom *et al.*, "Smart wearable body sensors for patient self-assessment and monitoring," *Archives of public health,* vol. 72, no. 1, p. 28, 2014.

[96] T. J. Webster, *Nanotechnology enabled in situ sensors for monitoring health*. Springer Science & Business Media, 2010.

[97] Y. J. Tan, J. Wu, H. Li, and B. C. Tee, "Self-healing electronic materials for a smart and sustainable future," *ACS applied materials & interfaces,* vol. 10, no. 18, pp. 15331-15345, 2018.

[98] H. Bahramiabarghouei, E. Porter, A. Santorelli, B. Gosselin, M. Popovíc, and L. A. Rusch, "Flexible 16 antenna array for microwave breast cancer detection," (in English), *IEEE Transactions on Biomedical Engineering,* Article vol. 62, no. 10, pp. 2516-2525, 2015, Art no. 2434956, doi: 10.1109/TBME.2015.2434956.

[99] J. Andreu-Perez, D. R. Leff, H. M. Ip, and G.-Z. Yang, "From wearable sensors to smart implants-–toward pervasive and personalized healthcare," *IEEE Transactions on Biomedical Engineering,* vol. 62, no. 12, pp. 2750-2762, 2015.

[100] J. R. Windmiller, A. J. Bandodkar, G. Valdés-Ramírez, S. Parkhomovsky, A. G. Martinez, and J. Wang, "Electrochemical sensing based on printable temporary transfer tattoos," *Chemical Communications,* vol. 48, no. 54, pp. 6794-6796, 2012.

[101] H. Khaleel, *Innovation in wearable and flexible antennas*. Wit Press, 2014.

[102] W. Tao, T. Liu, R. Zheng, and H. Feng, "Gait analysis using wearable sensors," *Sensors,* vol. 12, no. 2, pp. 2255-2283, 2012.

[103] H. R. Khaleel, H. M. Al-Rizzo, D. G. Rucker, and Y. Al-Naiemy, "Flexible printed monopole antennas for WLAN applications," in *Antennas and Propagation (APSURSI), 2011 IEEE International Symposium on*, 2011: IEEE, pp. 1334-1337.

[104] W. S. Wong and A. Salleo, *Flexible electronics: materials and applications*. Springer Science & Business Media, 2009.

[105] R. Cavallari, F. Martelli, R. Rosini, C. Buratti, and R. Verdone, "A survey on wireless body area networks: Technologies and design challenges," *IEEE Communications Surveys & Tutorials,* vol. 16, no. 3, pp. 1635-1657, 2014.

[106] I. S. Association, "IEEE Standard for Local and Metropolitan Area Networks—Part 15.6: Wireless Body Area Networks," *IEEE Standard for Information Technology, IEEE,* vol. 802, no. 6, pp. 1-271, 2012.

[107] B. Latré, B. Braem, I. Moerman, C. Blondia, and P. Demeester, "A survey on wireless body area networks," *Wireless Networks,* vol. 17, no. 1, pp. 1-18, 2011.

[108] J. Trajkovikj, J.-F. Zürcher, and A. K. Skrivervik, "PDMS, a robust casing for flexible W-BAN antennas [EurAAP corner]," *IEEE Antennas and Propagation Magazine,* vol. 55, no. 5, pp. 287-297, 2013.

[109] M. Ur-Rehman, Q. H. Abbasi, M. Akram, and C. Parini, "Design of band-notched ultra wideband antenna for indoor and wearable wireless communications," *IET Microwaves, Antennas & Propagation,* vol. 9, no. 3, pp. 243-251, 2014.

[110] F. Mustafa, U. A. Khan, M. Anjum, and S. Hussain, "Triple H-shaped multiple band frequency reconfigurable patch antenna," in *Innovative Computing Technology (INTECH), 2016 Sixth International Conference on*, 2016: IEEE, pp. 589-593.

[111] S. Hussain, U. A. Khan, M. Anjum, and M. Hayat, "Reconfigurable antenna parameters with the change in the position of switches," in *Innovative Computing Technology (INTECH), 2016 Sixth International Conference on*, 2016: IEEE, pp. 600-604.

[112] S.-J. Ha and C. W. Jung, "Reconfigurable beam steering using a microstrip patch antenna with a U-slot for wearable fabric applications," *IEEE Antennas and Wireless Propagation Letters,* vol. 10, pp. 1228-1231, 2011.

[113] T. F. Kennedy, P. W. Fink, A. W. Chu, N. J. Champagne, G. Y. Lin, and M. A. Khayat, "Body-worn E-textile antennas: the good, the low-mass, and the conformal," *IEEE Transactions on Antennas and Propagation,* vol. 57, no. 4, pp. 910-918, 2009.

[114] Y. Ouyang and W. J. Chappell, "High frequency properties of electro-textiles for wearable antenna applications," *IEEE Transactions on Antennas and Propagation,* vol. 56, no. 2, pp. 381-389, 2008.

[115] H. R. Raad, A. I. Abbosh, H. M. Al-Rizzo, and D. G. Rucker, "Flexible and compact AMC based antenna for telemedicine applications," (in English), *IEEE Transactions on Antennas and Propagation,* Article vol. 61, no. 2, pp. 524-531, 2013, Art no. 6327607, doi: 10.1109/TAP.2012.2223449.

[116] A. Nathan *et al.*, "Flexible electronics: the next ubiquitous platform," *Proceedings of the IEEE,* vol. 100, no. Special Centennial Issue, pp. 1486-1517, 2012.

[117] W. L. Stutzman and G. A. Thiele, *Antenna theory and design*. John Wiley & Sons, 2012.

[118] C. Balanis, "Antenna Theory Analysis and Design, ed., Hoboken, New Jersey: John Wilen & Sons," ed: Inc, 2005.

[119] A. B. Constantine, "Antenna theory: analysis and design," *MICROSTRIP ANTENNAS, third edition, John wiley & sons,* 2005.

[120] B. R. Mahafza, *Radar systems analysis and design using MATLAB*. CRC press, 2002.

[121] O. Rance, E. Perret, R. Siragusa, and P. Lemaitre-Auger, *RCS Synthesis for Chipless RFID*. Elsevier, 2017.

[122] B. Evenor, "Process for radiotelegraphic or radiotelephonic communication," ed: Google Patents, 1930.

[123] L. Brown, "A radar history of World War II," *J. Am. Hist. Res,* 1999.

[124] H. Stockman, "Communication by means of reflected power," *Proceedings of the IRE,* vol. 36, no. 10, pp. 1196-1204, 1948.

[125] R. Harrington, "Electromagnetic scattering by antennas," *IEEE Transactions on Antennas and Propagation,* vol. 11, no. 5, pp. 595-596, 1963.

[126] K. Finkenzeller, *RFID handbook: fundamentals and applications in contactless smart cards, radio frequency identification and near-field communication*. John wiley & sons, 2010.

[127] D. K. Klair, K.-W. Chin, and R. Raad, "A survey and tutorial of RFID anti-collision protocols," *IEEE Communications Surveys & Tutorials,* vol. 12, no. 3, pp. 400-421, 2010.

[128] R. Rezaiesarlak and M. Manteghi, *CHIPLESS RFID*. Springer, 2016.

[129] J. P. Vinding, "Interrogator-responder identification system," ed: Google Patents, 1969.

[130] O. E. Rittenbach, "Communication by radar beams," ed: Google Patents, 1969.

[131] R. M. Richardson, "Remotely actuated radio frequency powered devices," ed: Google Patents, 1963.

[132] R. F. Harrington, "Field measurements using active scatterers (correspondence)," *IEEE Transactions on Microwave Theory and Techniques,* vol. 11, no. 5, pp. 454-455, 1963.

[133] V. D. Hunt, A. Puglia, and M. Puglia, *RFID: a guide to radio frequency identification*. John Wiley & Sons, 2007.

[134] J. Foroughi, T. Mitew, P. Ogunbona, R. Raad, and F. Safaei, "Smart Fabrics and Networked Clothing: Recent developments in CNT-based fibers and their continual refinement," *IEEE Consumer*

Electronics Magazine, vol. 5, no. 4, pp. 105-111, 2016.

[135] N. C. Karmakar, R. Koswatta, P. Kalansuriya, and E. Rubayet, *Chipless RFID reader architecture*. Artech House, 2013.

[136] D. P. Morgan, "History of SAW devices," in *Proceedings of the 1998 IEEE International Frequency Control Symposium (Cat. No. 98CH36165)*, 1998: IEEE, pp. 439-460.

[137] B. A. Auld, *Acoustic fields and waves in solids*. Рипол Классик, 1973.

[138] R. Anwar, L. Mao, and H. Ning, "Frequency selective surfaces: a review," *Applied Sciences,* vol. 8, no. 9, p. 1689, 2018.

[139] A. Chamarti and K. Varahramyan, "Transmission delay line based ID generation circuit for RFID applications," *IEEE microwave and wireless components letters,* vol. 16, no. 11, pp. 588-590, 2006.

[140] J. Vemagiri, A. Chamarti, M. Agarwal, and K. Varahramyan, "Transmission line delay-based radio frequency identification (RFID) tag," *Microwave and optical technology letters,* vol. 49, no. 8, pp. 1900-1904, 2007.

[141] B. Shao, Q. Chen, Y. Amin, S. M. David, R. Liu, and L.-R. Zheng, "An ultra-low-cost RFID tag with 1.67 Gbps data rate by ink-jet printing on paper substrate," in *2010 IEEE Asian Solid-State Circuits Conference*, 2010: IEEE, pp. 1-4.

[142] C. S. Hartmann, "A global SAW ID tag with large data capacity," in *2002 IEEE Ultrasonics Symposium, 2002. Proceedings.*, 2002, vol. 1: IEEE, pp. 65-69.

[143] V. P. Plessky and L. M. Reindl, "Review on SAW RFID tags," *IEEE transactions on ultrasonics, ferroelectrics, and frequency control,* vol. 57, no. 3, pp. 654-668, 2010.

[144] L. Zhang, S. Rodriguez, H. Tenhunen, and L.-R. Zheng, "An innovative fully printable RFID technology based on high speed time-domain reflections," in *Conference on High Density Microsystem Design and Packaging and Component Failure Analysis, 2006. HDP'06.*, 2006: IEEE, pp. 166-170.

[145] S. Hu, Y. Zhou, C. L. Law, and W. Dou, "Study of a uniplanar monopole antenna for passive chipless UWB-RFID localization system," *IEEE Transactions on Antennas and Propagation,* vol. 58, no. 2, pp. 271-278, 2009.

[146] E. Moradi, T. Björninen, L. Ukkonen, and Y. Rahmat-Samii, "Characterization of embroidered dipole-type RFID tag antennas," in *2012 IEEE International Conference on RFID-Technologies and Applications (RFID-TA)*, 2012: IEEE, pp. 248-253.

[147] D. Betancourt *et al.*, "Square-shape fully printed chipless RFID tag and its applications in evacuation procedures," in *2015 9th European Conference on Antennas and Propagation (EuCAP)*, 2015: IEEE, pp. 1-5.

[148] S. Genovesi, F. Costa, M. Borgese, F. A. Dicandia, A. Monorchio, and G. Manara, "Chipless RFID sensor for rotation monitoring," in *2017 IEEE International Conference on RFID Technology & Application (RFID-TA)*, 2017: IEEE, pp. 233-236.

[149] R. Rezaiesarlak and M. Manteghi, "Identification of Chipless RFID tags in the reader," in *Chipless RFID*: Springer, 2015, pp. 95-126.

[150] A. Vena, E. Perret, and S. Tedjini, "Design of compact and auto-compensated single-layer chipless RFID tag," *IEEE Transactions on Microwave Theory and Techniques,* vol. 60, no. 9, pp. 2913-2924, 2012.

[151] M. A. Islam, Y. Yap, N. Karmakar, and A. Azad, "Orientation independent compact chipless RFID tag," in *2012 IEEE International Conference on RFID-Technologies and Applications (RFID-TA)*,

2012: IEEE, pp. 137-141.

[152] R. Nair *et al.*, "A novel fully printed 28-bits capacity chipless RFID tag based on open conical resonators," *Progress In Electromagnetics Research,* vol. 2219, 2014.

[153] L. Corchia, G. Monti, and L. Tarricone, "A frequency signature RFID chipless tag for wearable applications," *Sensors,* vol. 19, no. 3, p. 494, 2019.

[154] S. Preradovic, I. Balbin, N. C. Karmakar, and G. Swiegers, "A novel chipless RFID system based on planar multiresonators for barcode replacement," in *2008 IEEE International Conference on RFID*, 2008: IEEE, pp. 289-296.

[155] S. Preradovic and N. C. Karmakar, "Design of fully printable planar chipless RFID transponder with 35-bit data capacity," in *2009 European Microwave Conference (EuMC)*, 2009: IEEE, pp. 013-016.

[156] C. Nijas *et al.*, "Chipless RFID tag using multiple microstrip open stub resonators," *IEEE Transactions on Antennas and Propagation,* vol. 60, no. 9, pp. 4429-4432, 2012.

[157] A. T. Blischak and M. Manteghi, "Embedded singularity chipless RFID tags," *IEEE Transactions on Antennas and Propagation,* vol. 59, no. 11, pp. 3961-3968, 2011.

[158] R. Rezaiesarlak and M. Manteghi, "Complex-natural-resonance-based design of chipless RFID tag for high-density data," *IEEE Transactions on Antennas and Propagation,* vol. 62, no. 2, pp. 898-904, 2013.

[159] M. A. Riaz, H. Shahid, S. Z. Aslam, Y. Amin, A. Akram, and H. Tenhunen, "Novel T-shaped resonator based chipless RFID tag," *IEICE Electronics Express,* p. 14.20170728, 2017.

[160] M. Martinez and D. van der Weide, "Compact slot-based chipless RFID tag," in *2014 IEEE RFID Technology and Applications Conference (RFID-TA)*, 2014: IEEE, pp. 233-236.

[161] I. Jalaly and I. Robertson, "RF barcodes using multiple frequency bands," *IEEE MTT-S Digest,* vol. 4, 2005.

[162] A. Vena, E. Perret, and S. Tedjini, "High-capacity chipless RFID tag insensitive to the polarization," *IEEE Transactions on Antennas and Propagation,* vol. 60, no. 10, pp. 4509-4515, 2012.

[163] S. Dhupkariya, V. K. Singh, and A. Shukla, "A review of textile materials for wearable antenna," *J. Microw. Eng. Technol,* vol. 1, pp. 1-8, 2015.

[164] M. R. Islam and M. Ali, "A 900 MHz beam steering parasitic antenna array for wearable wireless applications," *IEEE transactions on antennas and propagation,* vol. 61, no. 9, pp. 4520-4527, 2013.

[165] B. S. Cook and A. Shamim, "Inkjet printing of novel wideband and high gain antennas on low-cost paper substrate," *IEEE Transactions on Antennas and Propagation,* vol. 60, no. 9, pp. 4148-4156, 2012.

[166] W. C. Hasz, V. S. Venkataramani, and C.-P. Lee, "Method for forming a channel on the surface of a metal substrate," ed: Google Patents, 2005.

[167] A. G. MacDiarmid, "Nobel Lecture:“Synthetic metals”: A novel role for organic polymers," *Reviews of Modern Physics,* vol. 73, no. 3, p. 701, 2001.

[168] I. Locher, M. Klemm, T. Kirstein, and G. Trster, "Design and characterization of purely textile patch antennas," *IEEE Transactions on advanced packaging,* vol. 29, no. 4, pp. 777-788, 2006.

[169] H. C. Ko *et al.*, "Curvilinear electronics formed using silicon membrane circuits and elastomeric transfer elements," *Small,* vol. 5, no. 23, pp. 2703-2709, 2009.

[170] M.-C. Choi, Y. Kim, and C.-S. Ha, "Polymers for flexible displays: From material selection to device applications," *Progress in Polymer Science,* vol. 33, no. 6, pp. 581-630, 2008.

[171] M. N. Srifi, S. K. Podilchak, M. Essaaidi, and Y. M. Antar, "Compact disc monopole antennas for current and future ultrawideband (UWB) applications," *IEEE Transactions on Antennas and Propagation,* vol. 59, no. 12, pp. 4470-4480, 2011.

[172] K. Myny *et al.*, "An inductively-coupled 64b organic RFID tag operating at 13.56 MHz with a data rate of 787b/s," in *Solid-State Circuits Conference, 2008. ISSCC 2008. Digest of Technical Papers. IEEE International*, 2008: IEEE, pp. 290-614.

[173] J.-K. Lee, Y.-S. Lim, C.-H. Park, Y.-I. Park, C.-D. Kim, and Y.-K. Hwang, "a-Si: H thin-film transistor-driven flexible color E-paper display on flexible substrates," *IEEE Electron Device Letters,* vol. 31, no. 8, pp. 833-835, 2010.

[174] S. H. Kim, C. Jang, K. J. Kim, S.-i. Ahn, and K. C. Choi, "Improvement of reliability of a flexible photoluminescent display using organic-based materials," *IEEE Transactions on Electron Devices,* vol. 57, no. 12, pp. 3370-3376, 2010.

[175] Q. Cao *et al.*, "Medium-scale carbon nanotube thin-film integrated circuits on flexible plastic substrates," *Nature,* vol. 454, no. 7203, p. 495, 2008.

[176] M. Jung *et al.*, "All-printed and roll-to-roll-printable 13.56-MHz-operated 1-bit RF tag on plastic foils," *IEEE Transactions on Electron Devices,* vol. 57, no. 3, pp. 571-580, 2010.

[177] D. J. Lipomi, B. C. K. Tee, M. Vosgueritchian, and Z. Bao, "Stretchable organic solar cells," *Advanced Materials,* vol. 23, no. 15, pp. 1771-1775, 2011.

[178] S. Bae *et al.*, "Roll-to-roll production of 30-inch graphene films for transparent electrodes," *Nature nanotechnology,* vol. 5, no. 8, p. 574, 2010.

[179] J. A. Rogers *et al.*, "like electronic displays: Large-area rubber-stamped plastic sheets of electronics and microencapsulated electrophoretic inks," *Proceedings of the National Academy of Sciences,* vol. 98, no. 9, pp. 4835-4840, 2001.

[180] F. Ilievski, A. D. Mazzeo, R. F. Shepherd, X. Chen, and G. M. Whitesides, "Soft robotics for chemists," *Angewandte Chemie International Edition,* vol. 50, no. 8, pp. 1890-1895, 2011.

[181] J. A. Rogers, T. Someya, and Y. Huang, "Materials and mechanics for stretchable electronics," *science,* vol. 327, no. 5973, pp. 1603-1607, 2010.

[182] T. P. Brody, "The birth and early childhood of active matrix—A personal memoir," *Journal of the society for information display,* vol. 4, no. 3, pp. 113-127, 1996.

[183] T. P. Brody, "The thin film transistor—A late flowering bloom," *IEEE Transactions on Electron Devices,* vol. 31, no. 11, pp. 1614-1628, 1984.

[184] H. Shirakawa, E. J. Louis, A. G. MacDiarmid, C. K. Chiang, and A. J. Heeger, "Synthesis of electrically conducting organic polymers: halogen derivatives of polyacetylene,(CH) x," *Journal of the Chemical Society, Chemical Communications,* no. 16, pp. 578-580, 1977.

[185] I.-C. Cheng and S. Wagner, "Overview of flexible electronics technology," in *Flexible Electronics*: Springer, 2009, pp. 1-28.

[186] H. Okaniwa, K. Nakatani, M. Asano, M. Yano, and Y. Hamakawa, "Production and properties of a-Si: H solar cell on organic polymer film substrate," in *16th Photovoltaic Specialists Conference*, 1982, pp. 1111-1116.

[187] S. Theiss and S. Wagner, "Amorphous silicon thin-film transistors on steel foil substrates," *IEEE*

Electron Device Letters, vol. 17, no. 12, pp. 578-580, 1996.

[188] "Philips Newscenter," *www.research.philips.com/newscenter/archieve/2005/050902-rolldisp.html,* 2005. (accessed : 02-05-2019).

[189] "Samsung Newscenter," *www.samsung.com/pressrelease/pressrelease.asp?seq=20051128_0000217879,* 2006. (accessed : 02-02-2019).

[190] "http://www.universaldisplay.com/press/press-2006-2-7.htm," *Universal Dispaly Coporation* 2006. (accessed : 22-06-2019).

[191] A. Poor, "Reformulating displays [Tools & Toys]," *IEEE Spectrum,* vol. 49, no. 9, 2012.

[192] H. Peng, X. Sun, W. Weng, and X. Fang, *Polymer Materials for Energy and Electronic Applications*. Academic Press, 2016.

[193] S.-C. Tjong, *Nanocrystalline materials: their synthesis-structure-property relationships and applications*. Newnes, 2013.

[194] H. Staudinger, "Uber Polymerisation," *Berichte der eutschen chemischen Gesellschaft (A and B series),* vol. 53, pp. 1073-1085, 1920.

[195] R. Crabb and F. Treble, "Thin silicon solar cells for large flexible arrays," *Nature,* vol. 213, no. 5082, pp. 1223-1224, 1967.

[196] K. A. Ray, "Flexible solar cell arrays for increased space power," *IEEE Transactions on Aerospace and Electronic Systems,* no. 1, pp. 107-115, 1967.

[197] R. M. Gelber and E. Small, "Liquid crystal display device with internal anti-reflection casting," ed: Google Patents, 1973.

[198] B. D'Andrade, A. Kattamis, and P. Murphy, "Flexible organic electronic devices on metal foil substrates for lighting, photovoltaic, and other applications, S," *Handbook of Flexible Organic Electronics: Materials, Manufacturing and Applications,* p. 315, 2014.

[199] C. Wronski, D. Carlson, and R. Daniel, "Schottky-barrier characteristics of metal–amorphous-silicon diodes," *Applied Physics Letters,* vol. 29, no. 9, pp. 602-605, 1976.

[200] G. Gustafsson, Y. Cao, G. Treacy, F. Klavetter, N. Colaneri, and A. Heeger, "Flexible light-emitting diodes made from soluble conducting polymers," *Nature,* vol. 357, no. 6378, pp. 477-479, 1992.

[201] N. Young, G. Harkin, R. Bunn, D. McCulloch, R. Wilks, and A. Knapp, "Novel fingerprint scanning arrays using polysilicon TFT's on glass and polymer substrates," *IEEE Electron Device Letters,* vol. 18, no. 1, pp. 19-20, 1997.

[202] P. Smith, P. Carey, and T. Sigmon, "Excimer laser crystallization and doping of silicon films on plastic substrates," *Applied physics letters,* vol. 70, no. 3, pp. 342-344, 1997.

[203] A. B. Chwang *et al.*, "Thin film encapsulated flexible organic electroluminescent displays," *Applied Physics Letters,* vol. 83, no. 3, pp. 413-415, 2003.

[204] M. Weaver *et al.*, "Organic light-emitting devices with extended operating lifetimes on plastic substrates," *Applied Physics Letters,* vol. 81, no. 16, pp. 2929-2931, 2002.

[205] J. Gartside, P. Mandlik, S. Wagner, T. Zhou, J. Silvernail, and M. Hack, "Material Characterisation of a Novel Permeation Barrier for Flexible Organic Displays," *MRS Online Proceedings Library Archive,* vol. 1007, 2007.

[206] F. So, J. Kido, and P. Burrows, "Organic light-emitting devices for solid-state lighting," *Mrs Bulletin,* vol. 33, no. 7, pp. 663-669, 2008.

[207] B. Lahey, A. Girouard, W. Burleson, and R. Vertegaal, "PaperPhone: understanding the use of bend gestures in mobile devices with flexible electronic paper displays," in *Proceedings of the SIGCHI Conference on Human Factors in Computing Systems*, 2011, pp. 1303-1312.

[208] D. Pierce, "Samsung introduces 'world's first' curved OLED TV 1," *Samsung Electronics,* 2013.

[209] D. Siegel and S. Shivakumar, *The Flexible Electronics Opportunity*. National Academies Press, 2014.

[210] D. D'Orazio, "Samsung shows off flexible OLED phone prototype (hands-on)," *he Verge. Retrieved 12 February 2013,* 2013. [Online]. Available: https://www.theverge.com/2013/1/9/3855960/samsung-flexible-oled-phone-prototype-hands-on (accessed : 02-01-2020).

[211] J. H. Raghu Das, Peter Harrop,, "IDTechEx Reports : 5G, RFID & The Internet of Things - IDTechEx Reports and Subscriptions," 2020. [Online]. Available: https://www.idtechex.com/. (accessed : 02-09-2019).

[212] J. Hayward, "IDTechEx : Wearable Technology Forecasts: 2020-2030," *IDtechEX,* 2020. [Online]. Available: https://www.idtechex.com/en/research-report/wearable-technology-forecasts-2020-2030/747. (accessed : 22-09-2020).

[213] K. Pretz, "The next evolution of the internet," *IEEE Magazine The institute,* vol. 50, no. 5, 2013.

[214] J. R. James and P. S. Hall, *Handbook of microstrip antennas*. IET, 1989.

[215] D. Kornek, E. Slottke, C. Orlob, and I. Rolfes, "Experimental investigation of bent patch antennas on MID substrate," in *Proceedings of the Fourth European Conference on Antennas and Propagation*, 2010: IEEE, pp. 1-3.

[216] O. Zinke and H. Brunswig, "Halbleiter, Halbleiterbauelemente und Elektronenröhren," in *Hochfrequenztechnik*: Springer, 1999, pp. 1-203.

[217] T. S. (ed.), *Stretchable Electronics* (Wiley-VCH). Weinheim, Germany: Wiley-VCH, 2013, pp. 484-485.

[218] R. Stewart *et al.*, "Rugged low-cost display systems," in *Proc SPIE–Int Soc Opt Eng*, 2002, vol. 4712, pp. 350-356.

[219] S. Inoue, S. Utsunomiya, T. Saeki, and T. Shimoda, "Surface-free technology by laser annealing (SUFTLA) and its application to poly-Si TFT-LCDs on plastic film with integrated drivers," *IEEE Transactions on Electron Devices,* vol. 49, no. 8, pp. 1353-1360, 2002.

[220] Y. Lee, H. Li, and S. J. Fonash, "High-performance poly-Si TFTs on plastic substrates using a nano-structured separation layer approach," *IEEE Electron Device Letters,* vol. 24, no. 1, pp. 19-21, 2003.

[221] W. Wong *et al.*, "Amorphous silicon thin-film transistors and arrays fabricated by jet printing," *Applied Physics Letters,* vol. 80, no. 4, pp. 610-612, 2002.

[222] H. Gleskova, S. Wagner, and D. Shen, "Electrophotographic patterning of thin-film silicon on glass foil," *IEEE Electron Device Letters,* vol. 16, no. 10, pp. 418-420, 1995.

[223] H. Sirringhaus *et al.*, "High-resolution inkjet printing of all-polymer transistor circuits," *Science,* vol. 290, no. 5499, pp. 2123-2126, 2000.

[224] F. Garnier, R. Hajlaoui, A. Yassar, and P. Srivastava, "All-polymer field-effect transistor realized by printing techniques," *Science,* vol. 265, no. 5179, pp. 1684-1687, 1994.

[225] T. Rai, P. Dantes, B. Bahreyni, and W. S. Kim, "A stretchable RF antenna with silver nanowires," *IEEE Electron Device Letters,* vol. 34, no. 4, pp. 544-546, 2013.

[226] C.-P. Lin, C.-H. Chang, Y. Cheng, and C. F. Jou, "Development of a flexible SU-8/PDMS-based antenna," *IEEE Antennas and wireless propagation letters,* vol. 10, pp. 1108-1111, 2011.

[227] L. Corchia, G. Monti, and L. Tarricone, "A fully-textile chipless tag," in *2018 48th European Microwave Conference (EuMC)*, 2018: IEEE, pp. 977-980.

[228] M. Stoppa and A. Chiolerio, "Wearable electronics and smart textiles: a critical review," *sensors,* vol. 14, no. 7, pp. 11957-11992, 2014.

[229] Z. Wang, L. Zhang, and J. L. Volakis, "Textile antennas for wearable radio frequency applications," *Textiles and Light Industrial Science and Technology,* vol. 2, no. 3, pp. 105-112, 2013.

[230] A. Dierck, F. Declercq, and H. Rogier, "Review of active textile antenna co-design and optimization strategies," in *RFID-Technologies and Applications (RFID-TA), 2011 IEEE International Conference on*, 2011: IEEE, pp. 194-201.

[231] E. Vandelle, T.-P. Vuong, G. Ardila, S. Hemour, and K. Wu, "Miniaturized Antenna on a Paper Substrate," in *2019 49th European Microwave Conference (EuMC)*, 2019: IEEE, pp. 73-76.

[232] H. I. Malik, M. Y. Ismail, and M. H. Mokhtar, "Design Optimization of Reflectarray Antenna Fabricated above Paper Based Substrate Materials," *International Journal of Integrated Engineering,* vol. 11, no. 6, pp. 151-158, 2019.

[233] H. F. Abutarboush and A. Shamim, "A reconfigurable inkjet-printed antenna on paper substrate for wireless applications," *IEEE Antennas and Wireless Propagation Letters,* vol. 17, no. 9, pp. 1648-1651, 2018.

[234] S. Moscato, R. Moro, M. Pasian, M. Bozzi, and L. Perregrini, "Innovative manufacturing approach for paper-based substrate integrated waveguide components and antennas," *IET Microwaves, Antennas & Propagation,* vol. 10, no. 3, pp. 256-263, 2016.

[235] S. Preradovic, S. M. Roy, and N. C. Karmakar, "RFID system based on fully printable chipless tag for paper-/plastic-ltem tagging," *IEEE Antennas and Propagation Magazine,* vol. 53, no. 5, pp. 15-32, 2011.

[236] V. Lakafosis, A. Rida, R. Vyas, L. Yang, S. Nikolaou, and M. M. Tentzeris, "Progress towards the first wireless sensor networks consisting of inkjet-printed, paper-based RFID-enabled sensor tags," *Proceedings of the IEEE,* vol. 98, no. 9, pp. 1601-1609, 2010.

[237] C.-z. Du, L.-x. Zhu, Z.-p. Yang, X. Wang, H.-y. Liu, and Y. Nie, "A CPW-fed UWB Flexible Antenna with Double Band-notched Characteristics," in *2019 IEEE 19th International Conference on Communication Technology (ICCT)*, 2019: IEEE, pp. 831-834.

[238] C.-Z. Du, "Compact Triple-Band Liquid Crystal Polymer Based Flexible Antenna for WiMAX/WLAN/5G Applications," in *2019 International Workshop on Electromagnetics: Applications and Student Innovation Competition (iWEM)*, 2019: IEEE, pp. 1-2.

[239] S. F. Jilani, Q. H. Abbasi, and A. Alomainy, "Inkjet-Printed Millimetre-Wave PET-Based Flexible Antenna for 5G Wireless Applications," in *2018 IEEE MTT-S International Microwave Workshop Series on 5G Hardware and System Technologies (IMWS-5G)*, 2018: IEEE, pp. 1-3.

[240] A. Timoshenko, K. Lomovskaya, A. Levanov, E. Borodulin, and E. Belousov, "Analysis and design of planar flexible antenna prototype," 2017: Institute of Electrical and Electronics Engineers Inc., doi: 10.1109/EWDTS.2016.7807741. [Online]. Available: https://www.scopus.com/inward/record.uri?eid=2-s2.0-85015256239&doi=10.1109%2fEWDTS.2016.7807741&partnerID=40&md5=01d648b0d9002d7807f4067d353d34ba (accessed : 18-01-2020).

[241] H. A. E. Elobaid, S. K. A. Rahim, M. Himdi, X. Castel, and M. A. Kasgari, "A Transparent and Flexible Polymer-Fabric Tissue UWB Antenna for Future Wireless Networks," *IEEE Antennas and Wireless Propagation Letters,* vol. 16, pp. 1333-1336, 2017.

[242] H. Zahir *et al.*, "Design fabrication and characterisation of polyaniline and multiwall carbon nanotubes composites-based patch antenna," (in English), *IET Microwaves, Antennas and Propagation,* Article vol. 10, no. 1, pp. 88-93, 2016, doi: 10.1049/iet-map.2015.0211.

[243] R. Lakshmanan and S. K. Sukumaran, "Flexible Ultra Wide Band Antenna for WBAN Applications," *Procedia Technology,* vol. 24, pp. 880-887, 2016.

[244] H. Bahrami, S. A. Mirbozorgi, R. Ameli, L. A. Rusch, and B. Gosselin, "Flexible, Polarization-Diverse UWB Antennas for Implantable Neural Recording Systems," (in English), *IEEE Transactions on Biomedical Circuits and Systems,* Article vol. 10, no. 1, pp. 38-48, 2016, Art no. 7061497, doi: 10.1109/TBCAS.2015.2393878.

[245] R. Quarfoth, Y. Zhou, and D. Sievenpiper, "Flexible Patch Antennas Using Patterned Metal Sheets on Silicone," (in English), *IEEE Antennas and Wireless Propagation Letters,* Article vol. 14, pp. 1354-1357, 2015, Art no. 7047785, doi: 10.1109/LAWP.2015.2406887.

[246] V. Fiore *et al.*, "An integrated 13.56-MHz RFID tag in a printed organic complementary TFT technology on flexible substrate," *IEEE Transactions on Circuits and Systems I: Regular Papers,* Article vol. 62, no. 6, pp. 1668-1677, 2015, Art no. 7108060, doi: 10.1109/TCSI.2015.2415175.

[247] H. Liu, S. Zhu, P. Wen, X. Xiao, W. Che, and X. Guan, "Flexible CPW-fed fishtail-shaped antenna for dual-band applications," (in English), *IEEE Antennas and Wireless Propagation Letters,* Article vol. 13, pp. 770-773, 2014, Art no. 6799246, doi: 10.1109/LAWP.2014.2317746.

[248] A. Kiourti and J. L. Volakis, "Stretchable and flexible E-fiber wire antennas embedded in polymer," (in English), *IEEE Antennas and Wireless Propagation Letters,* Article vol. 13, pp. 1381-1384, 2014, Art no. 6860296, doi: 10.1109/LAWP.2014.2339636.

[249] R. A. Liyakath, A. Takshi, and G. Mumcu, "Multilayer stretchable conductors on polymer substrates for conformal and reconfigurable antennas," (in English), *IEEE Antennas and Wireless Propagation Letters,* Article vol. 12, pp. 603-606, 2013, Art no. 6508851, doi: 10.1109/LAWP.2013.2260123.

[250] A. Kanso *et al.*, "Design and fabrication of EBG and CWP antennas using inkjet printing technology," *Microwave and Optical Technology Letters,* Article vol. 55, no. 7, pp. 1520-1526, 2013, doi: 10.1002/mop.27613.

[251] B. Gottel, S. Beer, H. Gulan, and T. Zwick, "Ultra broadband millimeter-wave antenna fabricated on flexible substrate," in *IEEE Antennas and Propagation Society, AP-S International Symposium (Digest)*, 2013, pp. 5-6, doi: 10.1109/APS.2013.6710663. [Online]. Available: https://www.scopus.com/inward/record.uri?eid=2-s2.0-84894161946&doi=10.1109%2fAPS.2013.6710663&partnerID=40&md5=27b6719b6b8019bd7ff4eb079e98de8a (accessed : 13-04-2020).

[252] G. A. Casula, G. Montisci, and G. Mazzarella, "A wideband PET inkjet-printed antenna for UHF RFID," *IEEE Antennas and Wireless Propagation Letters,* vol. 12, pp. 1400-1403, 2013.

[253] L. Wang, Y.-X. Guo, B. Salam, and C. W. A. Lu, "A flexible modified dipole antenna printed on PET film," in *Antennas and Propagation (APCAP), 2012 IEEE Asia-Pacific Conference on*, 2012: IEEE, pp. 239-240.

[254] K. Janeczek, M. Jakubowska, G. Kozioł, A. MŁozniak, and A. Araźna, "Investigation of ultra-high-frequency antennas printed with polymer pastes on flexible substrates," (in English), *IET Microwaves, Antennas and Propagation,* Article vol. 6, no. 5, pp. 549-554, 2012, doi: 10.1049/iet-map.2011.0351.

[255] K. Janeczek, G. Kozioł, T. Serzysko, and M. Jakubowska, "Investigation of RFID tag antennas printed on flexible substrates using two types of conductive pastes," in *Electronics System Integration Technology Conference, ESTC 2010 - Proceedings*, 2010, doi: 10.1109/ESTC.2010.5642844. [Online]. Available: https://www.scopus.com/inward/record.uri?eid=2-s2.0-78651265023&doi=10.1109%2fESTC.2010.5642844&partnerID=40&md5=61a52d76e1c92f2797a9cf691621bbec (accessed : 02-07-2018).

[256] S. H. Choi, H. J. Lee, and K. B. Lee, "Flexible antenna based on composite right/left-handed transmission line," (in English), *Electronics Letters,* Article vol. 46, no. 17, pp. 1181-1182, 2010, doi: 10.1049/el.2010.1464.

[257] S. K. Pavuluri, C. H. Wang, and A. J. Sangster, "A high-performance aperture-coupled patch antenna supported by a micromachined polymer ring," (in English), *IEEE Antennas and Wireless Propagation Letters,* Article vol. 7, pp. 283-286, 2008, Art no. 928468, doi: 10.1109/LAWP.2008.928468.

[258] D. Depret, H. Rogier, K. Dhaenens, and J. Vanfleteren, "Flexible-substrate low-cost construction of a coplanar-waveguide aperture-coupled microstrip patch antenna," *Microwave and Optical Technology Letters,* Article vol. 49, no. 5, pp. 1071-1074, 2007, doi: 10.1002/mop.22355.

[259] G. DeJean, R. Bairavasubramanian, D. Thompson, G. E. Ponchak, M. M. Tentzeris, and J. Papapolymerou, "Liquid Crystal Polymer (LCP): A new organic material for the development of multilayer dual-frequency/dual-polarization flexible antenna arrays," (in English), *IEEE Antennas and Wireless Propagation Letters,* Article vol. 4, no. 1, pp. 22-26, 2005, doi: 10.1109/LAWP.2004.841626.

[260] R. R. Muhammad Usman Ali Khan, Javad Froughi, Faisel Tubel, Panagiotis Ioannis Theoharis, Muhammad Salman Raheel, "Effects of Bending Bow-Tie Chipless RFID Tag for Different Polymer Substrates," *International Conference on Signal Processing and Communication Systems, ICSPCS'2019,* vol. 13, 2019.

[261] Y. Kim, H. Kim, and H.-J. Yoo, "Electrical characterization of screen-printed circuits on the fabric," *IEEE transactions on advanced packaging,* vol. 33, no. 1, pp. 196-205, 2009.

[262] G. Monti, L. Corchia, and L. Tarricone, "UHF wearable rectenna on textile materials," *IEEE Transactions on Antennas and Propagation,* vol. 61, no. 7, pp. 3869-3873, 2013.

[263] P. Macleod, *A review of flexible circuit technology and its applications*. PRIME Faraday Partnership, 2002.

[264] S. F. Sabri, S. M. Sam, K. Kamardin, and S. M. Daud, "Review of the Current Design on Wearable Antenna in Medical Field and its Challenges," *Jurnal Teknologi,* vol. 78, no. 6-2, 2016.

[265] J. Wang, E. Lim, M. Leach, Z. Wang, K. Man, and Y. Huang, "Review of wearable antennas for WBAN applications," *IAENG Int. J. Comput. Sci,* vol. 43, no. 4, pp. 16-19, 2016.

[266] S. Yan, P. J. Soh, and G. A. Vandenbosch, "Wearable ultrawideband technology—a review of ultrawideband antennas, propagation channels, and applications in wireless body area networks," *IEEE Access,* vol. 6, pp. 42177-42185, 2018.

[267] B. Mohamadzade, R. M. Hashmi, R. B. Simorangkir, R. Gharaei, S. Ur Rehman, and Q. H. Abbasi, "Recent advances in fabrication methods for flexible antennas in wearable devices: State of the art," *Sensors,* vol. 19, no. 10, p. 2312, 2019.

[268] A. Priya, A. Kumar, and B. Chauhan, "A review of textile and cloth fabric wearable antennas," *International Journal of Computer Applications,* vol. 116, no. 17, 2015.

[269] J. Virtanen, T. Bjorninen, L. Ukkonen, and L. Sydanheimo, "Passive UHF inkjet-printed narrow-line RFID tags," *IEEE Antennas and Wireless Propagation Letters,* vol. 9, pp. 440-443, 2010.

[270] J. A. Kreuz and C. M. Hawkins, "High speed etching of polyimide film," ed: Google Patents, 1984.

[271] R. Datasheet–RO, "Series High Frequency Circuit Materials," *Rogers Corporation,* 2010.

[272] R. Corporations, "RO3000 series high frequency circuit materials," *Internet, http://www. rogerscorporation. com/mwu/pdf/3000data. pdf,* 2005.

[273] H. F. Laminates, "RO3000® Series Circuit Materials," *RO3010, ROGERS corporation, USA,* 1998.

[274] R. C. A. C. Materials, "RT/Duroid 5870/5880 High Frequency Laminates," *Rogers Corporation*. [Online]. Available: https://www.google.com.au/url?sa=t&rct=j&q=&esrc=s&source=web&cd=4&cad=rja&uact=8&ved=0ahUKEwjj_9HdhdnWAhWEfrwKHes1DXUQFgg3MAM&url=http%3A%2F%2Fwww.itee.uq.edu.au%2Fetsg%2Fsystem%2Fstorage%2Fserve%2F2259%2FMss0142.pdf&usg=AOvVaw2ZmarBz9wLCzT78vPtAAms. (accessed : 02-11-2018).

[275] "Technical Data Sheet Teflon Laminated Plastics," *http://www.laminatedplastics.com/teflon.pdf*. (accessed : 02-11-2018).

[276] "PTFE Data sheet Hampshire Inc," *http://catalog.wshampshire.com/Asset/psg_teflon_ptfe.pdf*. (accessed : 02-11-2018).

[277] "PTFE general properties ATF Fluorotec," *http://www.fluorotec.com/blog/the-properties-and-advantages-of-polytetrafluoroethylene-ptfe/*. (accessed : 02-11-2018).

[278] "Data Sheet Sylgard 184," *http://research.engineering.ucdavis.edu/ncnc/wp-content/uploads/sites/11/2013/05/Sylgard_184_data_sheet.pdf*. (accessed : 02-11-2018).

[279] " Physical Properties of PTFE and Filled PTFE Products." [Online]. Available: https://www.srpco.com/wp-content/uploads/2017/07/Virgin-and-Filled-PTFE-Teflon.pdf. (accessed : 02-11-2018).

[280] D. Kapton, "HN, polyimide film Technical Data Sheet," *DuPont, editor,* 2011.

[281] Dupont, "Melinex 401 " 2015. [Online]. Available: http://www.cadillacplastic.co.uk/wp-content/uploads/2013/10/Melinex_401CW1.pdf. (accessed : 02-11-2018).

[282] G. Fellows, "Polyethylene Terephthalate Polyester (PET,PETP) Properties and Applications Supplier Data." [Online]. Available: https://www.azom.com/article.aspx?ArticleID=2047. (accessed : 07-11-2018).

[283] J. J. Heikkinen, T. T. Laine-Ma, and M. A. Kivikoski, "Flexible fabric-base patch antenna with protective coating," in *Antennas and Propagation Society International Symposium, 2007 IEEE*, 2007: IEEE, pp. 4168-4171.

[284] R. Moro, M. Bozzi, A. Collado, A. Georgiadis, and S. Via, "Plastic-based substrate integrated waveguide (SIW) components and antennas," in *Microwave Conference (EuMC), 2012 42nd European*, 2012: IEEE, pp. 1007-1010.

[285] A. D. Stroock and G. M. Whitesides, "Components for integrated poly (dimethylsiloxane) microfluidic systems," *Electrophoresis,* vol. 23, no. 20, pp. 3461-3473, 2002.

[286] A. Mata, A. J. Fleischman, and S. Roy, "Characterization of polydimethylsiloxane (PDMS) properties for biomedical micro/nanosystems," *Biomedical microdevices,* vol. 7, no. 4, pp. 281-293, 2005.

[287] H. Mao, T. Yang, and P. S. Cremer, "A microfluidic device with a linear temperature gradient for parallel and combinatorial measurements," *Journal of the American Chemical Society,* vol. 124, no. 16, pp. 4432-4435, 2002.

[288] M. U. Kopp, A. J. De Mello, and A. Manz, "Chemical amplification: continuous-flow PCR on a chip," *Science,* vol. 280, no. 5366, pp. 1046-1048, 1998.

[289] U. A. Khan, B. Tariq, K. Raza, S. Malik, and A. Muhammad, "Simulating Gradient Contour and Mesh of a Scalar Field," *International Journal of Physical and Mathematical Sciences,* vol. 5, no. 8, pp. 1138-1143, 2011.

[290] G. Wypych, *Handbook of polymers*. Elsevier, 2016.

[291] E. A. Campo, "The Complete Part Design Handbook," *Hanser, Munich,* 2006.

[292] T. A. Osswald, *International plastics handbook: the resource for plastics engineers*. Hanser Gardner Pubns, 2006.

[293] "Liquid Crystal Polymers (LCP) Properties " *Milton Plastics* [Online]. Available: http://www.miltonplastics.com/index.php/Picture/show/9.html. (accessed : 07-11-2018).

[294] A. Arif, M. Zubair, M. Ali, M. U. Khan, and M. Q. Mehmood, "A compact, low-profile fractal antenna for wearable on-body WBAN applications," *IEEE Antennas and Wireless Propagation Letters,* vol. 18, no. 5, pp. 981-985, 2019.

[295] S. H. Dar, J. Ahmed, and M. Raees, "Characterization of flexible wearable antenna based on rubber substrate," *Int. J. Adv. Comput. Sci. Appl,* vol. 7, pp. 190-5, 2016.

[296] D. d. P. L. Brandão, *Tecnologia da electricidade: materiais usados em electrotecnia*. 1983.

[297] J. Baker-Jarvis, M. D. Janezic, and D. C. DeGroot, "High-frequency dielectric measurements," *IEEE Instrumentation & Measurement Magazine,* vol. 13, no. 2, pp. 24-31, 2010.

[298] G. A. Conway and W. G. Scanlon, "Antennas for over-body-surface communication at 2.45 GHz," *IEEE Transactions on Antennas and Propagation,* vol. 57, no. 4, pp. 844-855, 2009.

[299] G. Catalogue, "Metals, Alloys, Compounds, Ceramics, Polymers," *Composites. Cambridge: GoodfellowMetals,* 1993.

[300] S. K. Pavuluri, C. Wang, and A. J. Sangster, "High efficiency wideband aperture-coupled stacked patch antennas assembled using millimeter thick micromachined polymer structures," (in English), *IEEE Transactions on Antennas and Propagation,* Article vol. 58, no. 11, pp. 3616-3621, 2010, Art no. 5559354, doi: 10.1109/TAP.2010.2071334.

[301] A. Michel *et al.*, "Design considerations on the placement of a wearable UHF-RFID PIFA on a compact ground plane," *IEEE Transactions on Antennas and Propagation,* vol. 66, no. 6, pp. 3142-3147, 2018.

[302] S. Yan, V. Volskiy, and G. A. Vandenbosch, "Compact dual-band textile PIFA for 433-MHz/2.4-GHz ISM bands," *IEEE Antennas and Wireless Propagation Letters,* vol. 16, pp. 2436-2439, 2017.

[303] P. Salonen, J. Kim, and Y. Rahmat-Samii, "Dual-band E-shaped patch wearable textile antenna," in *2005 IEEE antennas and propagation society international symposium*, 2005, vol. 1: IEEE, pp. 466-469.

[304] E. O. Hammerstad, "Equations for microstrip circuit design," in *1975 5th European Microwave Conference*, 1975: IEEE, pp. 268-272.

[305] H. Wang, Z. Zhang, Y. Li, and Z. Feng, "A dual-resonant shorted patch antenna for wearable application in 430 MHz band," *IEEE Transactions on Antennas and Propagation,* vol. 61, no. 12, pp. 6195-6200, 2013.

[306] F. Costa, S. Genovesi, and A. Monorchio, "A chipless RFID based on multiresonant high-impedance surfaces," *IEEE transactions on microwave theory and techniques,* vol. 61, no. 1, pp. 146-153, 2013.

[307] S. Rauf, M. A. Riaz, H. Shahid, M. S. Iqbal, Y. Amin, and H. Tenhunen, "Triangular loop resonator

based compact chipless RFID tag," *IEICE Electronics Express,* p. 14.20161262, 2017.

[308] X. Lin, J. Jia, N. Yousefi, X. Shen, and J.-K. Kim, "Excellent optoelectrical properties of graphene oxide thin films deposited on a flexible substrate by Langmuir–Blodgett assembly," *Journal of Materials Chemistry C,* vol. 1, no. 41, pp. 6869-6877, 2013.

[309] Y. Wang, L. Li, B. Wang, and L. Wang, "A body sensor network platform for in-home health monitoring application," in *Proceedings of the 4th International Conference on Ubiquitous Information Technologies & Applications*, 2009: IEEE, pp. 1-5.

[310] A. Čolaković, "Had? ialić M (2018) Internet of Things (IoT): a review of enabling technologies, challenges, and open research issues," *Comput Netw,* vol. 144.

[311] E. Jovanov, "Wearables Meet IoT: Synergistic Personal Area Networks (SPANs)," *Sensors,* vol. 19, no. 19, p. 4295, 2019.

[312] T. M. Fernández-Caramés and P. Fraga-Lamas, "Towards the Internet of smart clothing: A review on IoT wearables and garments for creating intelligent connected e-textiles," *Electronics,* vol. 7, no. 12, p. 405, 2018.

[313] R. Atakan *et al.*, "Protocol to assess the quality of transmission lines within smart textile structures," *Measurement,* vol. 152, p. 107194, 2020.

[314] P.-S. Kildal, *Foundations of antenna engineering: a unified approach for line-of-sight and multipath*. Artech House, 2015.

[315] R. Rezaiesarlak and M. Manteghi, "A space–time–frequency anticollision algorithm for identifying chipless RFID tags," *IEEE Transactions on Antennas and Propagation,* vol. 62, no. 3, pp. 1425-1432, 2014.

[316] A. Blischak and M. Manteghi, "Pole residue techniques for chipless RFID detection," in *2009 IEEE Antennas and Propagation Society International Symposium*, 2009: IEEE, pp. 1-4.

[317] C. E. Baum, "The singularity expansion method," in *Transient electromagnetic fields*: Springer, 1976, pp. 129-179.

[318] J.-M. Jin, *Theory and computation of electromagnetic fields*. John Wiley & Sons, 2011.

[319] I. Y. Immoreev, "-Signal Waveform Variations in Ultrawideband Wireless Systems: Causes and Aftereffects," *Ultrawideband Radar: Applications and Design,* pp. 71-104, 2012.

[320] W. Chen, S. Dols, S. B. Oetomo, and L. Feijs, "Monitoring body temperature of newborn infants at neonatal intensive care units using wearable sensors," in *Proceedings of the Fifth International Conference on Body Area Networks*, 2010, pp. 188-194.

[321] S. Sankaralingam and B. Gupta, "A circular disk microstrip WLAN antenna for wearable applications," in *2009 Annual IEEE India Conference*, 2009: IEEE, pp. 1-4.

[322] S. Talebian *et al.*, "Electrically Conducting Hydrogel Graphene Nanocomposite Biofibers for Biomedical Applications," *Frontiers in Chemistry,* vol. 8, 2020.

[323] N. Liu, Y. Lu, S. Qiu, and P. Li, "Electromagnetic properties of electro-textiles for wearable antennas applications," *Frontiers of Electrical and Electronic Engineering in China,* vol. 6, no. 4, pp. 563-566, 2011.

[324] E. Commission, "Smart Wearables Reflection and Orientation Paper; Technical Report," 2017. [Online]. Available: https://ec.europa.eu/digital-single-market/en/news/european-commission-seeks-inputreflection- (accessed : 02-11-2018).

[325] Z. Lu, R. Raad, F. Safaei, J. Xi, Z. Liu, and J. Foroughi, "Carbon Nanotube Based Fiber Supercapacitor as Wearable Energy Storage," *Frontiers in Materials,* vol. 6, p. 138, 2019.

[326] Y. Ouyang and W. J. Chappell, "Diversity characterization of body-worn textile antenna system at 2.4 GHz," in *2006 IEEE Antennas and Propagation Society International Symposium*, 2006: IEEE, pp. 2117-2120.

[327] T. Yang, W. A. Davis, and W. L. Stutzman, "Wearable ultra-wideband half-disk antennas," in *2005 IEEE Antennas and Propagation Society International Symposium*, 2005, vol. 3: IEEE, pp. 500-503.

[328] P. Salonen, Y. Rahmat-Samii, M. Schaffrath, and M. Kivikoski, "Effect of textile materials on wearable antenna performance: A case study of GPS antennas," in *IEEE Antennas and Propagation Society Symposium, 2004.*, 2004, vol. 1: IEEE, pp. 459-462.

[329] P. Salonen and L. Hurme, "A novel fabric WLAN antenna for wearable applications," in *IEEE Antennas and Propagation Society International Symposium. Digest. Held in conjunction with: USNC/CNC/URSI North American Radio Sci. Meeting (Cat. No. 03CH37450)*, 2003, vol. 2: IEEE, pp. 700-703.

[330] Y. Ouyang, E. Karayianni, and W. J. Chappell, "Effect of fabric patterns on electrotextile patch antennas," in *2005 IEEE Antennas and Propagation Society International Symposium*, 2005, vol. 2: IEEE, pp. 246-249.

[331] A. Vena *et al.*, "Design and realization of stretchable sewn chipless RFID tags and sensors for wearable applications," in *2013 IEEE International Conference on RFID (RFID)*, 2013: IEEE, pp. 176-183.

[332] T. Andriamiharivolamena, A. Vena, E. Perret, P. Lemaitre-Auger, and S. Tedjini, "Chipless identification applied to human body," in *2014 IEEE RFID Technology and Applications Conference (RFID-TA)*, 2014: IEEE, pp. 241-245.

[333] M. Jalil, N. A. Samsuri, M. K. A. Rahim, and R. Dewan, "Compact chipless RFID metamaterial based structure using textile material," in *2015 International Symposium on Antennas and Propagation (ISAP)*, 2015: IEEE, pp. 1-4.

[334] L. Corchia, G. Monti, and L. Tarricone, "Wearable antennas: Nontextile versus fully textile solutions," *IEEE Antennas and Propagation Magazine,* vol. 61, no. 2, pp. 71-83, 2019.

[335] S. Manzari, S. Pettinari, and G. Marrocco, "Miniaturized and tunable wearable RFID tag for body-centric applications," in *2012 IEEE International Conference on RFID-Technologies and Applications (RFID-TA)*, 2012: IEEE, pp. 239-243.

[336] G. Kim *et al.*, "Design of a UHF RFID fiber tag antenna with electric-thread using a sewing machine," in *2008 Asia-Pacific Microwave Conference*, 2008: IEEE, pp. 1-4.

[337] K. Koski *et al.*, "Practical read range evaluation of wearable embroidered UHF RFID tag," in *Proceedings of the 2012 IEEE International Symposium on Antennas and Propagation*, 2012: IEEE, pp. 1-2.

[338] B. A. Munk, "Frequency selective surfaces theory and design. john Wiley&Sons," *Inc,* 2000.

[339] J. Arnaud and F. Pelow, "Resonant-grid quasi-optical diplexers," *Bell System Technical Journal,* vol. 54, no. 2, pp. 263-283, 1975.

[340] C. Feng, W. Zhang, L. Li, L. Han, X. Chen, and R. Ma, "Angle-based chipless RFID tag with high capacity and insensitivity to polarization," *IEEE Transactions on Antennas and Propagation,* vol. 63, no. 4, pp. 1789-1797, 2015.

[341] M. UK, "MADEIRA INDUSTRIAL PRODUCTS," 28-03-2020 2020. [Online]. Available:

https://shop.madeira.co.uk/supertwist-30-1000m-rose-silver_st983-31-xxx-xxx.htm. (accessed : 02-11-2018).

[342] S. A. Materials, "LIBERATOR HC," 2020. [Online]. Available: http://www.metalcladfibers.com/liberator. (accessed : 02-11-2018).

[343] M. Ghebrebrhan *et al.*, "Textile frequency selective surface," *IEEE Microwave and Wireless Components Letters,* vol. 27, no. 11, pp. 989-991, 2017.

[344] Y. Kim, K. Lee, Y. Kim, and Y. C. Chung, "Wearable UHF RFID tag antenna design using flexible electro-thread and textile," in *2007 IEEE Antennas and Propagation Society International Symposium*, 2007: IEEE, pp. 5487-5490.

[345] G. Germany, "ZSK Technical Embroidery Systems," 2017. [Online]. Available: https://technicalembroidery.co.uk/download/ZSK-Technical-Embroidery-Systems_2017-07_EN_low.pdf (accessed : 02-11-2018).

[346] G. F. Carrier, M. Krook, and C. E. Pearson, *Functions of a complex variable: theory and technique*. Siam, 2005.